Bimetallic Group 4 Complexes as Olefin Polymerisation Catalysts

Richard A. Collins

Thesis submitted to the University of Oxford for the degree of

Doctor of Philosophy, June 2016.

Statement of confidentiality

Some of the work described in this Thesis is of a commercially sensitive nature. The examiners are requested to respect the confidentiality of this information and not to disclose the information to individuals outside the Board of Examiners.

The work described in this Thesis was carried out in the Chemistry Research Laboratory, University of Oxford from October 2012 to June 2016 under the supervision of Professor Philip Mountford. All work is my own unless stated to the contrary, and has not previously been submitted for any degree at this or any other university.

Richard A. Collins

June 2016

Abstract

Richard Anthony Collins Trinity 2016

Linacre College D.Phil. Thesis

This Thesis describes the synthesis and characterisation of half-sandwich bimetallic complexes supported by κ^1-amidinate ligands with different bridging moieties.

Chapter 1 introduces homogeneous polyolefin catalysis with a focus on Group 4 metals. The mechanism, catalyst development and the activation chemistry of metallocene and post-metallocene catalysts are discussed. The beneficial properties generated by bimetallic catalysts through cooperative interactions are introduced.

Chapter 2 describes the synthesis, structures and copolymerisation capabilities of cyclopentadienyl-amidinate phenylene bridged bimetallic titanium complexes. A series of monometallic cyclopentadienyl-amidinate dimethyl and dichloride titanium complexes are presented for comparison. A detailed description of their activation to form well-defined cationic species is presented.

Chapter 3 describes the synthesis, structures and copolymerisation capabilities of cyclopentadienyl-amidinate titanium bimetallic complexes with conformationally constrained and ferrocenyl covalent tethers. Alongside the ferrocenyl complexes introduced in Chapter one, an electrochemical analysis of all ferrocene based complexes will be discussed.

Chapter 4 details two different binuclear cocatalysts and their performances in a high temperature EPDM copolymerisation study. The form of the catalytic species is investigated through abstraction reactions with monometallic and bimetallic complexes previously introduced.

Chapter 5 describes the synthesis of a bimetallic zirconium complex and attempted synthesis of a Group 4 heterobimetallic complex. A parallel polymerisation reactor (PPR) experiment on *in situ* generated precatalysts is discussed, which is supported by synthetic and polymerisation experiments.

Chapter 6 presents full experimental procedures and characterising data for the new complexes reported in this Thesis.

CD Appendix contains .cif files for all new crystallographically characterised complexes described.

Contents

Acknowledgements

Firstly, I would like to thank my supervisor Prof. Philip Mountford. I have had the pleasure to know Philip for eight years and getting to this point would have been impossible without him. His dedication to everything he does is unmatched. Thank you so much for all the support and encouragement.

I would like to thank my collaborators LANXESS Elastomers. In particular Dr Gerard van Doremaele, Dr Alexandra Berthoud, Dr Richard Scott, Dr Raffaele Bernardo, Mr John van de Moosdijk, Mr Sander Niessen and Mr Hans Leduc. Their help and interest for my project as well as my time spent in Chemelot have been incredibly important for this Thesis.

A very important thank you must go to everyone in the Mountford group and friends across the CRL second floor. My Pt II and DPhil supervisors Drs Junjuda (Guun) Unruangsri and Adam Russell not only showed me so much, but also became two of my best friends and are the most creative and entertaining people I have ever met. In return I have been lucky to supervise Aidan Cooper, a Pt II who taught me so much and gave me my first foray into Group 5 hydrazides, and two DPhil students, Karen Gamero and Theresa Scharbert. I wish Karen and Theresa all the best with the rest of their studies. I have constantly been impressed by them and I hope they keep smiling and laughing throughout. Drs Laura (Stevie) Stevenson and Bryony Core have been great companions throughout my time in the science trenches, constantly inspiring and reassuring me. I am very thankful to them for my time in the group. A thank you to Dr Laura Groom, Dr Liban Saleh, (soon to be Dr) Helen Yin and other current and past group members who have all made coming to work, going to conferences and the activities out of labs a real pleasure. I have been lucky to receive wise scientific and life advice from 4 excellent postdocs in Drs Andrew Schwarz, Andrey Protchenko, Matthew Blake and Insun Yu. Thanks must also go to Dr Matthew Blake, Dr Insun Yu, Mr Ben Clough, Mr Ross Green and Miss Theresa Scharbert for the proof reading of this Thesis.

I am very grateful for all those who keep the CRL safe and operating. I would like to thank Drs Rémi Tirfoin and Sandy Kilpatrick for help with electrochemistry, Drs Nick Rees and Tim Claridge with NMR (and many a good uni-club pint with Nick) and Drs Amber Thompson and Richard Cooper with crystallography.

I am exceptionally lucky to have great friends who will never fail to keep life exciting and with whom I have shared the best memories. From friends who have been with me since school through to my Linacre family, your support is invaluable and I am very grateful to you all. I would like to thank Ruth for her help and support and I hope she always keeps her positive approach to life. During the DPhil I have had five amazing housemates in Boxey, Aidan, James, Sezgi and Becky. They have made every tough day a good one and every good day a great one. Thinking about my times in Jeune Street will always make me smile. This Thesis also comes with a big thank you to my person Claire, who has kept me going with so much happiness and enthusiasm. I cannot wait for all our adventures to come.

Finally, to my mum, dad and sister I want to give enormous thanks. I don't tell you anywhere near enough quite how important and reassuring your love and support is in every part of my life. To share any successes with you gives them meaning.

Abbreviations

General

Å	Ångstrom
avg.	average
ca.	*circa*, about
calcd.	calculated
Cp_{cent}	computed cyclopentadienyl ring carbon centroid
CSD	Cambridge Structural Database
CV	cyclic voltammetry
°C	degrees Celsius
°	degrees
d	day(s)
D	Diffusion coefficient
Da	Daltons
DFT	Density Functional Theory
Eq.	equivalent(s)
g	gram(s)
GPC	Gel Permeation Chromatography
η	hapticity
h	hour(s)
k	kilo
K	Kelvin
κ	denticity
kDa	kilodalton(s)
kJ	kilojoule(s)
l	litre(s)
mbar	millibar(s)
mg	milligram(s)
min	minute(s)

ml	millilitre(s)
mmol	millimole(s)
mV	millivolt(s)
psi	pounds per square inch
rpm	revolutions per minute
RT	room temperature
μ	bridging
μl	microlitre(s)
μmol	micromole(s)
V	volt(s)
vs.	*versus*

Chemical

Ar	aryl
Ar^{F_2}	$C_6H_3F_2$
BF_{15}	tris(pentafluorophenyl)borane, $B(C_6F_5)_3$
$[BF_{20}]^-$	tetra(pentafluorophenyl)borate, $[B(C_6F_5)_4]^-$
BHT	2,6-di-*tert*-butyl-4-methylphenol
Bn	benzyl
Bu	*n*-butyl
^{t}Bu	*tert*-butyl
CGC	constrained geometry catalyst
Cp	cyclopentadienyl
Cp^*	pentamethylcyclopentadienyl
DBF	1,1′-dibenzofuranyl
DME	1,2-dimethoxyethane
DMF	dimethylformamide
EP	ethylene-propylene
EPDM	ethylene-propylene-diene monomer
ENB	5-ethylidenebicyclo[2.2.1]hept-2-ene

Et	ethyl
Et_2O	diethyl ether
Fc	ferrocene
Fc′	1,1′-bis(1,4-phenyl)ferrocenyl
Ind	Indenyl, C_9H_7
L	a supporting ligand (set
M	metal or mol dm^{-3}
MAO	methylaluminoxane
Me	methyl
M_n	number average molecular weight
M_w	weight average molecular weight
PDI	polydispersity index
Ph	phenyl
PMH	pentamethylheptane
PPR	Parallel Polymerisation Reactor
^{i}Pr	*iso*-propyl
py	pyridine
R	generic alkyl group or hydrogen atom
TACN	triazacyclononane
TBF_{20}	trityl tetrakis(pentafluorophenyl)borate, $[Ph_3C][BF_{20}]$
TIBA	tri(isobutyl)aluminium
TMA	trimethylaluminium, $AlMe_3$
THF	tetrahydrofuran
Tp	tris(pyrazolyl)borate
TPM	tris(3,5-dimethylpyrazoyl)methane
TPMd	tris(3,5-dimethylpyrazoyl)methanide
VNB	5-vinylbicyclo[2.2.1]hept-2-ene
X	generic halide or alkyl ligand
Xanth	9,9-dimethyl-1,1′-xanthenyl

Xyl	2,6-$C_6H_3Me_2$

Nuclear Magnetic Resonance Spectroscopy

app.	apparent
br	broad
^{13}C-{^{1}H}	proton-decoupled ^{13}C
COSY	correlation spectroscopy
DOSY	Diffussion ordered spectroscopy
d	doublet
δ	chemical shift in ppm
HMBC	heteronuclear multiple bond correlation
HSQC	heteronuclear single quantum coherence
Hz	Hertz
i	*ipso*
J	coupling constant
m	*meta*
m	multiplet
MHz	Megahertz
NMR	Nuclear Magnetic Resonance
NOE	nuclear Overhauser effect
o	*ortho*
p	*para*
PGSE	Pulse Gradient Spin Echo
ppm	parts per million
q	quartet or quaternary
ROESY	rotating-frame nuclear Overhauser Effect spectroscopy
s	singlet
sept	septet
t	triplet
VT	variable temperature

Mass Spectrometry

EI	Electron Impact
ESI	Electrospray Ionisation
m/z	mass to charge ratio
MS	Mass spectrometry

Infrared Spectroscopy

cm^{-1}	wavenumbers
FT-IR	Fourier transform infrared
IR	Infrared
m	medium
s	strong
w	weak
ν	frequency

Notes

Literature compounds described in this Thesis are numbered **1.x**, **2.x**, **3.x**, **4.x**, **5.x** according to the Chapter in which they occur. The new compounds described in this Thesis are numbered **1-48**. X-ray data was collected, solved and refined by the author or by either Dr Andrew Schwarz (**1** and **3**) or Dr Matthew Blake (**47** and **13**). In all cases the molecular drawings were produced by Prof Philip Mountford. Polymerisations were carried out by LANXESS Elastomers under the supervision of Dr Alexandra Berthoud.

Chapter One

Introduction

1.1 General introduction

The pioneering discoveries by Karl Ziegler and Giulio Natta in the 1950s were the first steps in forming one of the most important industries in chemistry. In 2015, polyolefin materials such a polyethylene and polypropylene accounted for nearly half of the 300 million tons of global plastic production.[1] Apart from low-density polyethylene (LDPE), which is prepared *via* radical polymerisation, all other polyolefin products were formed by catalytic olefin insertion polymerisations. The majority is produced using heterogeneous Ziegler-Natta catalysis, but an ever increasing use of single-site homogeneous catalysis is being employed. Homogeneous catalysis has given the opportunity for highly tuned single-site catalysis and improved insight into the polymerisation mechanism. Research into homogeneous polyolefin catalysis has shifted from focusing on Group 4 metallocenes to widespread exploration of post-metallocene catalysts. This has been with the aim to better control polymer molecular weight, polydispersity, comonomer enchainment level and pattern, tacticity and synthesis of block copolymers. Since the early 1990s, research into well-defined homogeneous multimetallic olefin polymerisation catalysts has shown beneficial cooperative interactions that give rise to advantageous polymer properties. Both academic and industrial research continues to expand in this area.

This Thesis is concerned with the synthesis, characterisation and olefin polymerisation capabilities of covalently tethered bimetallic Group 4 half sandwich κ^1-amidinate supported complexes. This work builds upon the previously introduced monometallic variants which were shown to be very active in homo- and copolymerisation studies and for which the catalytically active cationic species have been studied.

In this Chapter, an overview of olefin polymerisation is carried out. This includes the early polyolefin history and subsequent catalyst evolution, the properties and analysis of the polymers, the mechanistic role and detailed understanding of the active species, and finally a discussion of the development and advantages of bimetallic catalysis. This project is carried out in collaboration with LANXESS Elastomers B.V and relevant research advancements will be highlighted throughout.

1.2 Ziegler-Natta catalysis

In 1953, Karl Ziegler submitted a patent in which the main claim was for "a method for preparing high-molecular polyethylene using aluminium trialkyls as catalysts, characterised by bringing together ethylene at pressures greater than 10 atmospheres and temperatures above 50 °C with mixture of aluminium trialkyls and compounds of the metals of Groups 4-6 of the periodic table with the atomic numbers 22 to 74 (namely titanium, zirconium, hafnium, niobium, tantalum, chromium, molybdenum and tungsten)". The initial patent and publication was closely followed by Natta's report on the stereoselective polymerisation of propene by the same system.[2] This work led them both to be awarded the Nobel Prize in 1963 "for their discoveries in the field of chemistry and technology of high polymers" and spawned one of the largest commercial ventures in chemistry in the 21st century. Heterogeneous Ziegler based catalysts remain the majority of those commercially employed to this day, progressive advancements have made them increasingly selective and efficient for both ethylene and higher α-olefins enchainment. However, these catalysts do not come without limitations, principle amongst them being the lack of well-defined active sites. This multi-site nature causes broad molecular weight distributions and prevented any mechanistic understanding of the polymerisation process.

1.3 Early homogeneous catalysis

In 1957, independent research by Natta and Breslow demonstrated how metallocene systems, specifically Cp_2TiBr_2 and Cp_2ZrBr_2, could polymerise ethylene when used in conjunction with Et_2AlCl or $AlEt_3$.[3, 4] Metallocene systems, or sandwich compounds, have a rich history in organometallic chemistry with Group 4 metallocenes first introduced by Wilkinson in 1953.[5] These systems were only moderately active compared to their heterogeneous counterparts, unable to polymerise propene and prone to reduction to inactive titanium(III) species.[6] However, the homogeneous nature of these systems gave the first opportunity for mechanistic insight into single-site molecular polyolefin catalysis, *vide infra*.

A significant advancement in homogeneous catalysis arose unexpectedly through the addition of water to the aluminium activated metallocene systems. Significant improvements in the productivity of ethylene and atactic propylene were proposed to be a result of the *in situ* formation of methyl aluminoxane (MAO).[7-11] MAO, formed

through the partial hydrolysis of trimethylaluminium (TMA), is a poorly defined substance thought to consist of oligomeric groups such as linear polymer, cyclics and cross-linked aggregates of the general formula $[Al(Me)O]_n$.[10] This species was shown to activate both neutral dihalide and dichloride compounds as well as act as a scavenger of impurities such as water.

1.4 Polymerisation mechanism

The exact form of the homogeneous catalytic pathway incurred a large amount of debate and it was widely assumed that a halide-bridged titanium-aluminium mixed-metal species was involved.[6] Shilov and co-workers first proposed a cationic active species of the form $[TiCp_2Me]^+$ in 1961, but without any direct evidence it did not reach widespread acceptance.[12, 13] An electrochemical experiment by Dyachkovskii gave support to this through evidence that the polymerisation was exclusively carried out within the cathode chamber.[13] Excellent evidence came in 1985 when Eisch and co-workers isolated and structurally characterised the insertion product of $PhC{\equiv}CSiMe_3$ into the Ti–Me bond of $[Cp_2TiMe]^+$.[14] Subsequently many Group 4 alkyl cations have been isolated and will be discussed in Section 1.9.

1.4.1 Proposed propagation mechanisms

In light of the suggested cationic species Cossee and Arlman proposed a mechanism for Ziegler-Natta polymerisation (Figure 1.1).[15, 16] Initial coordination of an olefin to an electron deficient metal centre results in formation of a π-adduct. This then undergoes alkyl migration to the unsaturated bond, which simultaneously propagates the polymeric chain and regenerates the active species. A modified model, proposed by Rooney and Green, generates a metal-alkylidene hydride through a 1,2-hydrogen shift from the α-carbon of the polymeric chain. This alkylidene then undergoes a [2+2] cycloaddition to form a metallacyclobutane, and reductive elimination completes the catalytic pathway.[17] Intermediate to these mechanisms is one termed the modified Green-Rooney mechanism in which a hydrogen atom on the growing polymeric chain interacts with the metal centre through a 3-centre 2-electron bond, also referred to as an agostic interaction.[18-20] The final mechanism displayed in Figure 1.1 is when the same stabilising agostic interaction only occurs during the transition state of the alkyl insertion.

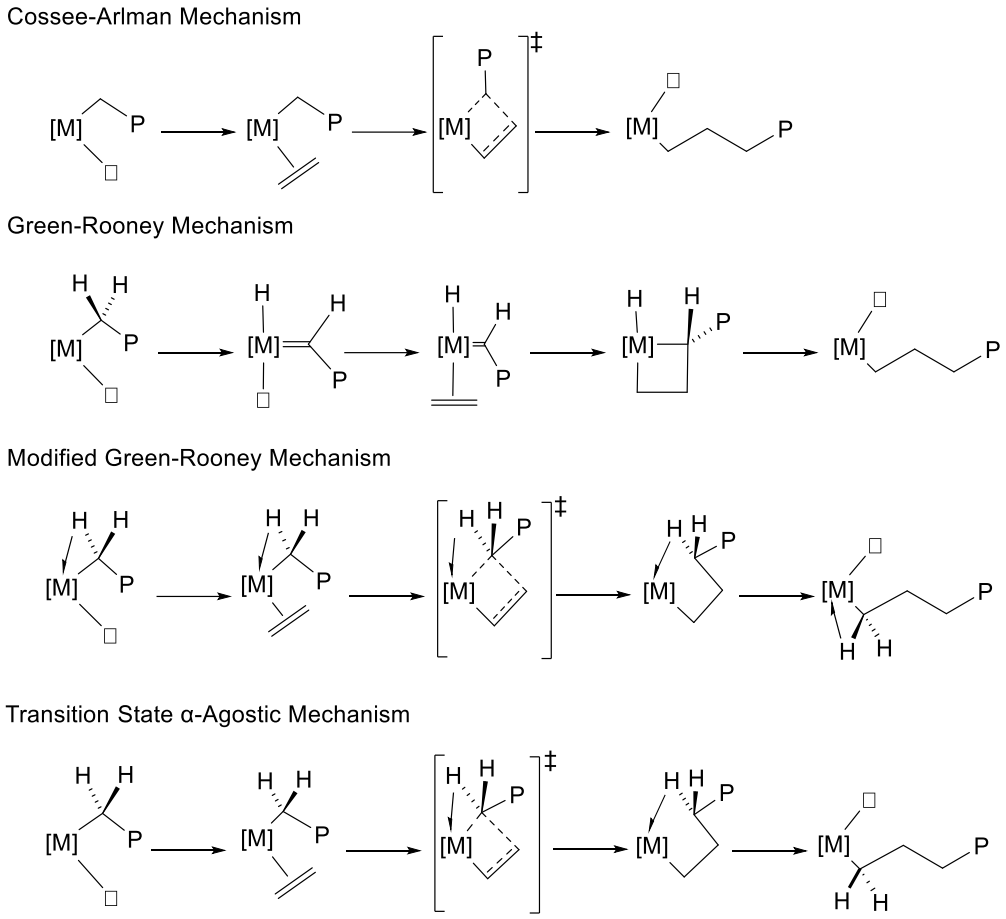

Figure 1.1 Proposed mechanisms for Ziegler-Natta catalysis.
P denotes a polymeryl chain.

The presence of an agostic interaction was effectively displayed in a study by Brintzinger and co-workers. The hydrodimerisation of *E*- and *Z*-BuCH=CHD resulted in an unequal distribution of *erythro* and *threo* products when a non-chiral catalyst is used. This was proposed to be a direct result of a favourable Zr---HC stabilising interaction over the deuterated counterpart.[21-23] This stabilising interaction was later confirmed in a theoretical study.[6] Many kinetic isotope and stereoselective studies have been carried out and do not give conclusive evidence as to a universal mechanism, instead it is presumed to be dependent on which step is rate determining and the overall reaction rate in each case.[24]

1.4.2 Chain transfer and termination pathways

The aforementioned propagation mechanisms can become terminated by one or more chain transfer pathways. These influence the polymeric end-group formation as well as the molecular weight values and distribution.

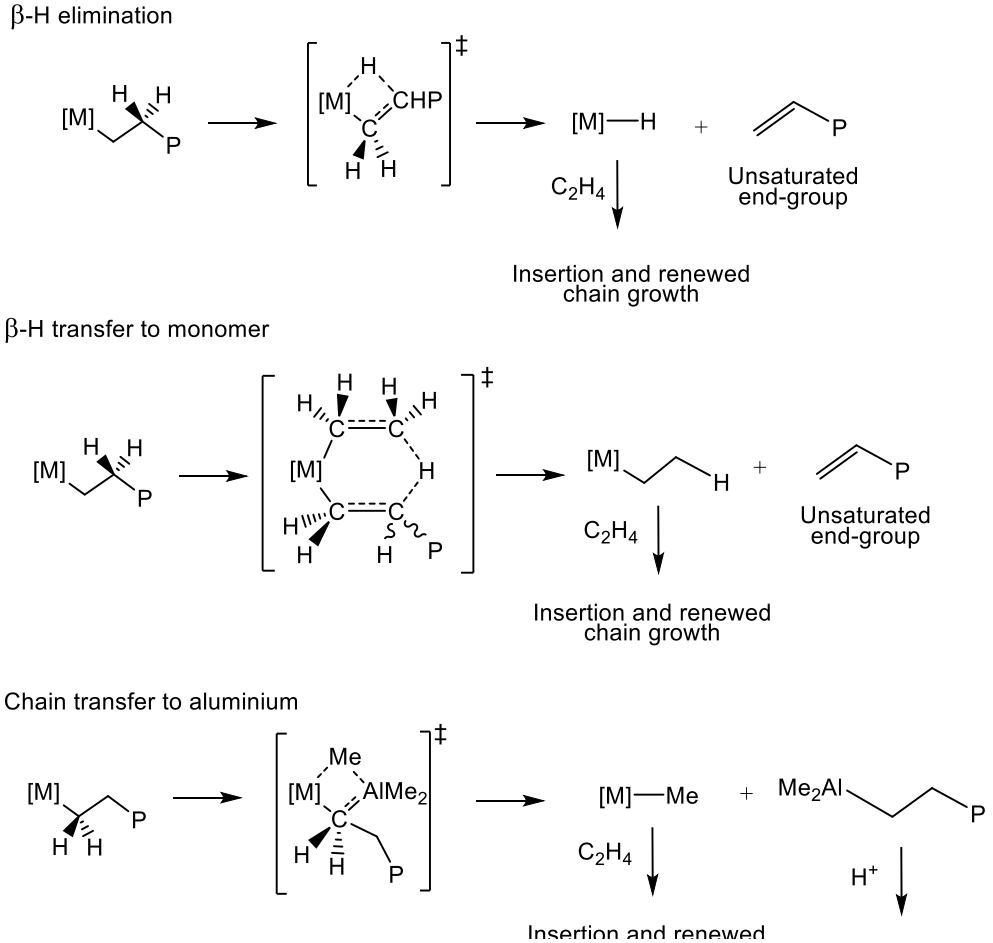

Figure 1.2 Termination pathways in olefin polymerisation.

P denotes a polymeryl chain.

Figure 1.2 highlights the mechanisms of the key termination pathways for a propagating chain. β-hydrogen elimination or transfer to monomer progress *via* a 4 or 6-membered ring transition state, respectively, and result in vinylic polymer end-groups.[25-29] An additional variation of β-methyl elimination can occur for branched polymers.[30] Both theoretical[31, 32] and experimental studies, displaying a molecular weight independence on monomer pressure, indicate that the chain transfer to monomer is the dominant mechanisms for Group 4 metallocenes and related catalysts.[33-35]

As discussed, aluminium agents are particularly effective as activating and scavenging species, however chain transfer to aluminium is another potential termination pathway. This has been observed for many early transition metal

systems[36-39] and the prevalence can be observed through the deviation from uniformity of vinylic end-groups per polymer chain. The post polymerisation protic workup causes Al–C_{Poly} bond cleavage and formation of saturated chain ends. Vinylic polymer end-groups can be indicated by NMR spectroscopy or C=C vibrational bands in the FT-IR spectrum. This metal-aluminium interaction and methods in overcoming it will be discussed in greater detail in Section 1.8. Chain transfer to other metal centres, typically but not limited to zinc species, have also been employed, either to control molecular weight or to facilitate end-group functionalisation.[40, 41] More recently, the use of excess inactive main-group-metal alkyl species have been shown to serve as "surrogate" chain growth sites, providing the rate of chain transfer far exceeds that of propagation.[42-44]

In cases where polymers with too higher molecular weights are formed, a result of the rate of propagation far exceeding the rate of termination for the pathways described above, hydrogen is often introduced as a chain transfer agent. The strong hydrogen affinity of a cationic metal alkyl species has a lower barrier to termination than the alternative pathways and can prevent reactor fouling and the formation of non-commercially desirable products. Saturated end-groups are exclusively observed and a metal hydride is believed to form and re-enter the catalytic cycle, as is depicted for β-hydrogen elimination.[45-49]

1.5 Polymer characterisation and steroselectivity

The composition, structure and stereo-regularity of the resultant polymer all give important properties. Polymers have been produced with varying strength, stability, flexibility and versatility. This Section will provide an introduction to polymer structure and analysis.

1.5.1 GPC analysis

The molecular weight properties of a polymer can be analysed by a type of size exclusion chromatography, known as Gel Permeation Chromatography (GPC). The polymer is dissolved in a solution and is passed through a column containing pores of varying size, the retention time is dependent on the hydrodynamic radius of the eluent. The resultant chromatogram displays the number average molecular weight (M_n) (Equation 1.1), the weight average molecular weight (M_w) (Equation 1.2) and the peak molecular weight (M_p) of the polymer. Although this technique gives good

relative molecular weights, absolute values require calibration, typically to polystyrene, and Mark-Houwink parameters (K and α) that are specific for each polymer type in solution and account for different relationships between a polymer's molecular weight and intrinsic viscosity.[50]

The number average molecular weight (M_n) is given by:

$$M_n = \frac{\sum N_i \times M_i}{\sum N_i} \qquad \textbf{Equation 1.1}$$

N_i is the number of molecules having molar mass of M_i. This quantity may therefore be interpreted straightforwardly as the total molar mass of the polymer molecules divided by the number of polymer molecules.

The weight average molecular weight (M_w) is given by:

$$M_w = \frac{\sum W_i \times M_i}{\sum W_i} \qquad \textbf{Equation 1.2}$$

W_i is the mass of polymers having a molar mass of M_i, hence $W_i = N_i \times M_i$.

The chromatogram can give insight into the polymerisation propagation and termination processes. If only one uniform active single-site is present then a monomodal trace will be observed, however if several active species are present than multiple molecular weight distributions will be observed. The molecular weight distributions will result in a distribution and the spread of this curve is indicative of the catalytic behaviour. This distribution is determined by the polydispersity index (PDI) calculated by M_w/M_n, which would give an ideal value of 1.0 if all chains are the same length.[51] This ideal value is the aim of 'living polymerisation', in which no termination pathways are present, however with chain transfer mechanisms in operation, the Schultz-Flory distribution predicts a single-site catalyst should give a polymer with PDI of 2.0.[52] Deviations above this can be a result of multi-site catalyst behaviour or competitive chain termination pathways.

1.5.2 Regio- and Stereochemistry

The polymerisation of alternative olefin monomers to ethylene gives additional structural considerations that have a large impact on the properties. Of note is the orientation of the monomer inserted and the relative stereochemistry of adjacent chiral centres, known as tacticity, in the polymeric chain. Taking propylene as the simplest

example the monomer can either insert with the methyl branch on the carbon β (1,2-insertion) or α (2,1-insertion) to the metal centre. Group 4 catalysed reactions end up with a majority 1,2 (primary) regiochemistry observed, this is a result of electronic and steric factors as has been supported theoretically[53] and experimentally.[54] Partial and nearly complete regioirregular polypropylene has been produced by select Group 4 catalysts,[55-57] but effective regioirregular insertion has been more commonly observed for vanadium[58] or iron based systems.[59, 60]

Unlike most catalytic systems the ancillary ligands of the active metal centre and the stereogenic centre of the last enchained monomer unit will both have an influence on the stereochemistry of monomer addition. The tacticity can be defined by the relative stereochemistry of the adjacent chiral centres within a macromolecule, *meso* is defined as the same and *rac* the alternate orientation. Figure 1.3 displays three extremes in polymer tacticities: when no repeating unit of stereochemistry is observed it is termed atactic, a series of exclusive *meso* units is defined as isotactic and a series of *racemic* units as syndiotactic. The tacticity has a large impact on the polymer properties; specifically the melting point, glass transition temperature and the friability. Variations between these tacticity limits are expected; of note are heterotactic enchainment, alternating *meso* and *rac* linkages, and isotactic stereoblock enchainment, alternating sections of opposing isotactic linkages, which give specific and diverse polymer properties.[23, 54, 61-63]

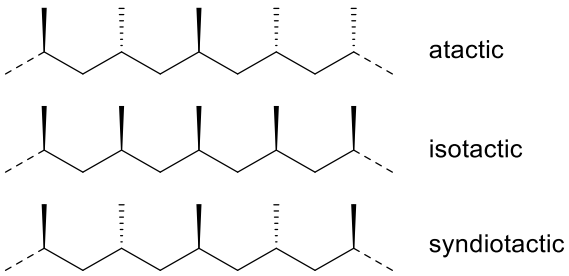

Figure 1.3 Examples of polymer tacticities.

The determination of a polymer's tacticity classification and quantifying the stereochemical purity is most effectively achieved using $^{13}C\{^{1}H\}$ NMR spectroscopy. Diagnostic shifts can be observed for a set of 5 stereocentres (a pentad) of which there are 10 variations.[64] Extensive research has gone into catalyst design for stereoselective olefin polymerisation and will be highlighted Section 1.7.

1.6 Specific monomer incorporation

The use of alkene monomer feedstocks beyond ethylene has already been highlighted above in the formation of polypropylene. This is not a limited field and a large number of alternative olefin monomers have been utilised varying from simple longer α-olefins, such as 1-hexene and styrene, through to more sophisticated monomers. Polyethylene, including HDPE, LLDPE and LDPE (HD = high density, LLD = linear low density and LD = low density), and polypropylene are the majority produced commercially.[65] The product of ethylene propylene diene monomer (EPDM) copolymerisation is an important class of polymer and is of specific note to this project. Alongside ethylene and propylene feedstocks bulky dienes are also introduced, these include 5-ethylidenebicyclo[2.2.1]hept-2-ene (ENB), 5-vinylbicyclo[2.2.1]hept-2-ene (VNB) and tricyclo[5.2.1.$0^{2,6}$]deca-3,8-diene (DCPD) (Figure 1.4). The unsaturated bond of the bicyclic ring system is preferentially incorporated into the polymer chain due to the relief of ring strain. The incorporation of these dienes produce a commercially viable synthetic rubber with high strength, flexibility and temperature resistance. The additional alkene gives excellent opportunities for post-polymerisation modifications including cross-linking and addition of functional groups.[66, 67] Typical applications include window gaskets, coolants hoses, O-rings and muffler mounts.[68] EPDM makes up *ca*. 10% of all synthetic rubbers and is projected to be worth $7.46 billion by 2019.[69] The degree of incorporation of comonomers can be identified *via* ^{1}H NMR spectroscopy for a soluble low molecular weight polymer. Alternatively, as described previously for end-group analysis, FT-IR can be utilised for detection of internal or terminal C=C bonds due to their different frequencies.

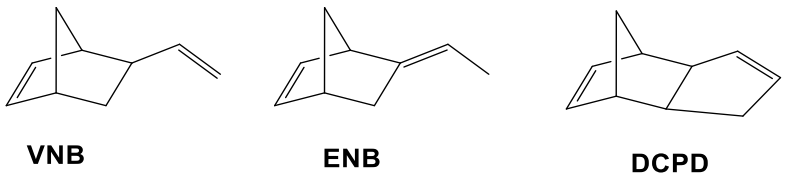

Figure 1.4 Example of diene monomers.

1.7 Homogeneous catalyst advancements

Metallocene systems activated with MAO are typically not very active for higher α-olefins, do not give any discernible stereotactic control and are not effective at high

temperatures due to a lack of stability. As a result of these limitations and extensive patenting a large amount of research has been performed in homogeneous catalyst design, in many cases with specific industrial ventures in mind. This Section will highlight many of the key ligand functional groups employed. For the purpose of this Thesis this Section will have a specific focus on early transition metal advancements, but it is important to note that an extensive range of coordination compounds across the periodic table have also been successfully developed and studied.[65, 70]

1.7.1 *Ansa*-metallocenes

Introducing bridging groups between cyclopentadienyl and indenyl metallocene complexes, termed *ansa*-metallocenes (*ansa* is a latin term meaning bent handle, attached at both ends), have been shown to have important effects on the activities of the catalysts and polymer properties. Catalysts of this form are the most successful for isospecific olefin polymerisation. Interest began when Ewen and co-workers showed that a mixture of the *meso* and *rac* (**1.01**) chiral *ansa*-(bis)indenyl-titanium dichloride with an ethylene bridge, initially prepared by Brintzinger and co-workers,[71] gave a mixture of atactic and isotactic polypropylene.[72] Subsequently the analogous isomerically pure C_2 symmetric *ansa*-(bis)indenyl zirconocene (**1.02**) produced exclusively isotactic polypropylene.[73] These advancements gave the origin of enantiomorphic site control, whereby the orientation of insertion is governed by the auxiliary ligands at the active site.[74, 75] However, these compounds displayed limited activity, temperature stability and high molecular weight capacity.[54]

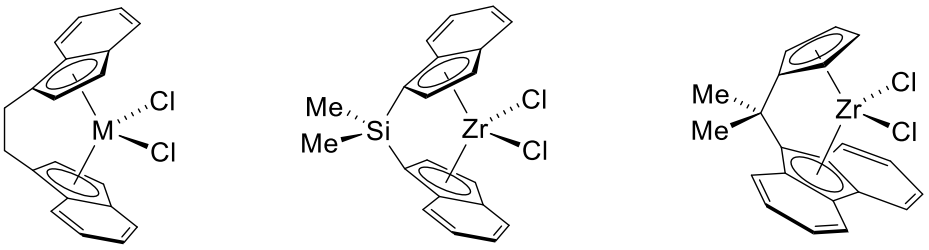

M = Ti (**1.01**) or Zr (**1.02**) **1.03** **1.04**

Figure 1.5 Example of *ansa*-metallocenes that exhibit tacticity control.

Replacement of the ethane bridge with a shorter dimethylsilyl linker and modification of the substituents promoted beneficial properties. The *ansa*-(bis)indenylzirconium compound with a dimethyl silyl linker (**1.03**) showed an increase in isotacticity and molecular weight than the ethane bridged analogue (**1.02**).[76] Variations of substituents

on the indenyl moiety were shown to have a large effect. The facile addition of a methyl group in the 2-position of the indenyl resulted in a five-fold increase in molecular weight[76] and subsequently substituents in varying positions on the indenyl ring, up to 9-phenanthryl in size, have been incorporated.[77-79]

Syndiotactic polypropylene has also been formed through the use of highly functionalised *ansa*-metallocenes. Ewen *et al.* introduced the C_s symmetric *ansa*-zirconocene **1.04**, regular alternation of olefins at the enantiotopic site gave highly syndiospecific polymerisation.[80]

1.7.2 Constrained geometry catalysts

In 1990, Bercaw and co-workers introduced an organoscandium compound with a silane bridged *ansa*-cyclcopentadienyl-amido ligand, which was suitable for olefin polymerisation.[81] Okuda *et al*. subsequently synthesised an analogous organotitanium compound[82] and modification of these constrained geometry catalysts (CGCs) were utilised by both Dow[83-86] and Exxon[87-90] with remarkable beneficial properties. Examples of organotitanium CGCs introduced by Dow are displayed in Figure 1.6.[91] The key feature of these systems is how the distance between the centroid of the π-system and additional ligand is smaller than the comparable unbridged complex. This leads to a much more open coordination sphere and in comparison to their metallocene analogues they have been shown to give superior activity, temperature stability and reduced propensity to undergo chain transfer.[92] Polymer products with advantageous long chain branches were also produced; this was a result of re-insertion of vinyl-terminated polymer macromonomers into the growing polymeric chain.[91, 93]

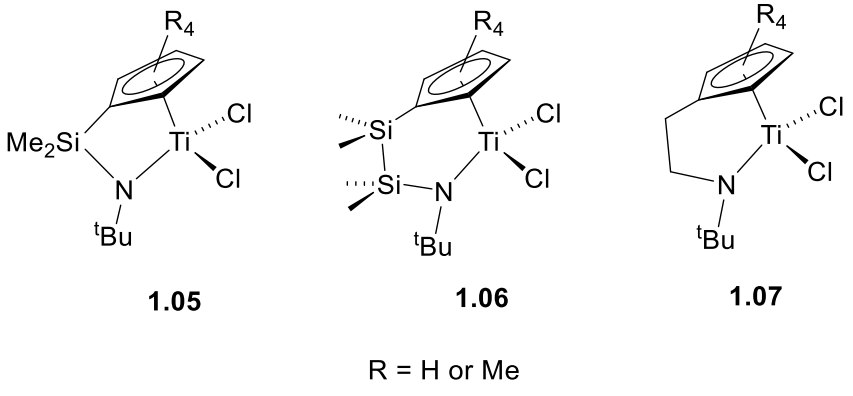

Figure 1.6 Constrained geometry pre-catalysts introduced by Dow.

The amido group acts at maximum as a three electron donor, which yields a highly electrophilic and consequently very active metal centre. An extensive number of studies have explored modifications on the general CGC structure through adjustments to the cyclopentadienyl moiety, the amido group or the *ansa*-bridge.[92] The use of CGCs are not limited to ethylene homopolymerisation, improved comonomer incorporation has allowed improvements with several different α-olefins and as previously highlighted the industrial relevance of these compounds is highly prevalent.[65] Of specific note to this project are the low-valency Ti(III) catalysts, Lovacat (**1.08**), disclosed by DSM[94, 95] and more recently the aryl-bridged cyclopentadienyl-amidinate titanium compounds (**1.09**) introduced by LANXESS Elastomers.[96] Both are used for the preparation of EPDM rubbers with reported excellent temperature stability, copolymer efficiency and molecular weight capacity. Outside of polyolefin chemistry CGCs are finding use in a multitude of catalytic organic transformations.[92]

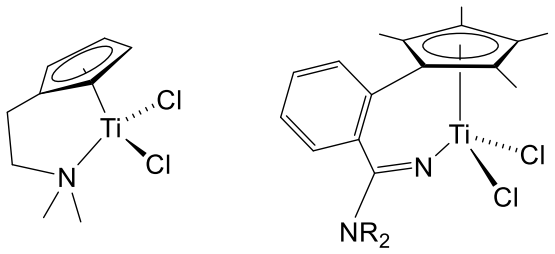

1.08 **1.09**

Figure 1.7 Chemical structures of DSM's Lovacat (left) and LANXESS Elastomers' CGC titanium amidinate (right).

1.7.3 Half-sandwich catalysts

The early success of Group 4 metallocenes in an industrial context resulted in extensive patenting. The frontier orbitals of a cyclopentadienyl moiety comprise of a single σ-donor and two π-donor orbitals, which can interact with the metal centre (Figure 1.8). The use of the isolobal analogy, introduced by Hoffmann,[97] can be a powerful tool in ligand design for new catalysts. Specific monoanionic functional groups with comparable electronic donation capacities can be used to replace one or two cyclopentadienyl groups with no other changes in coordination. Herein a series of half-sandwich compounds will be introduced, several of which invoke this isolobal

analogy for the secondary substituent, and their advantages in polymerisation discussed.

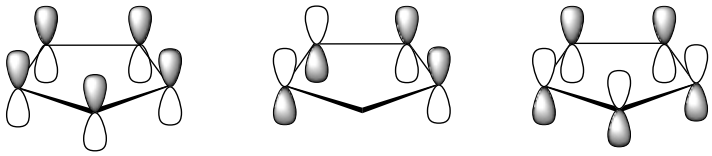

Figure 1.8 Frontier orbitals of monoanionic cyclopentadienyl (Cp^-) moiety.

A variety of half-sandwich Group 4 compounds with a phosphinimide group, general form $–NPR_3$ (**1.10**), were introduced by Stephan and co-workers (Figure 1.9).[98] These were shown to be electronically analogous[99, 100] and sterically similar[98, 101]to the cyclopentadienyl predecessor with binding in a linear fashion and a short (*ca.* 1.76 Å) Ti–N bond.[102] The complexes were shown to display a high level of thermal stability and steric interaction was shown to be the most important factor in polymerisation studies, with the *tert*-butyl substituted variant vastly outperforming the cyclohexyl or isopropyl analogues.[102, 103]

Group 4 non-*ansa*-amide complexes (**1.11**) have been investigated by both Okuda[104] and Nomura.[105, 106] $Cp^*Ti(NMe_2)(CH_2Ph)_2$ (where Cp^* = C_5Me_5) gave highly syndiotactic polystyrene when activated with $B(C_6F_5)_3$. This is in stark contrast to the dimethyl silyl bridged counterpart, which is inactive in the homopolymerisation of styrene. However, $Cp^*Ti(NMe_2)(CH_2Ph)_2$ only "sluggishly" polymerises ethylene when activated with MAO.[104] More recently Nomura reported a series of cyclopentadienyl-pyrrolide titanium complexes, the pyrrolide ligand bound in an exclusive η^1-fashion apart from when both *ortho* position contained a methyl group in which case an η^5-bonding interaction was observed. The unsubstituted pyrrolide ligand gave a high maximum activity of 990 kg mol^{-1} h^{-1} bar^{-1} upon MAO activation.[107]

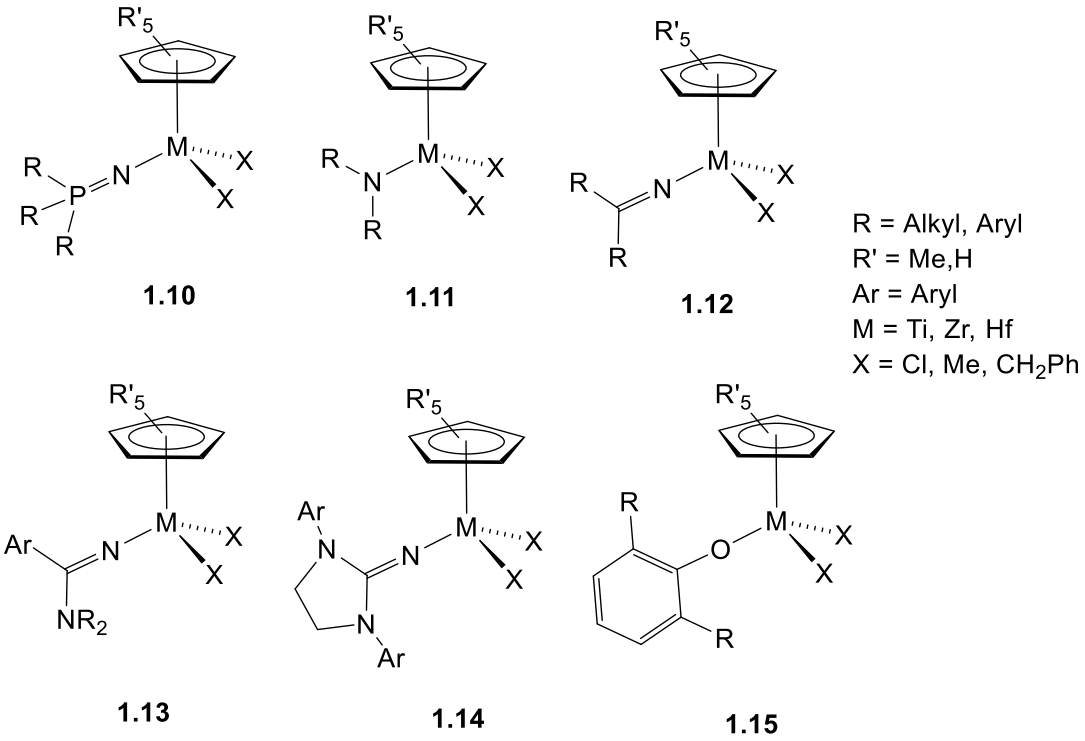

Figure 1.9 General forms of half-sandwich polyolefin catalysts.

Group 4 half-sandwich ketimide compounds, general form $–NCR_2$ (**1.12**), were disclosed by Nova Chemicals and are highly active olefin homo- and copolymerisation catalysts in gas phase, slurry and high-temperature solution polymerisation studies.[108] (indenyl)Ti(N=C^{t}Bu$_2$)Cl$_2$ was highly active in ethylene and 1-hexene copolymerisation study (greater than 10^6 kg mol^{-1} h^{-1} bar^{-1})[109] and Cp*Ti Ti(N=C^{t}Bu$_2$)Cl$_2$ was capable of catalysing the living copolymerisation of ethylene and styrene with MAO activation.[110] In 2016, Lamac and co-workers introduced a Group 4 CGC in which a ketimide bridges to the cyclopentadienyl group *via* an ethyl group. However, the polymerisation activity was considerably suppressed in comparison to the untethered counterpart.[111]

Replacement of one (amidinate) or both (guanidinate) of the ketimide alkyl substituents with a nitrogen donor results in greater ligand-to-metal dπ-pπ bonding. Proposed resonance forms displaying 3- or 5-electron donation capacity are depicted in Figure 1.10. These moieties are of specific interest to this Thesis and although κ^1- and κ^2-amidinate binding motifs are available only the κ^1-variant will be discussed at present. DSM licensed the half-sandwich ketimide catalyst from Nova Chemicals and went on to find further improvements with the amidinate moiety (**1.13**) in EPDM copolymerisation. This was marketed under the trade name Keltan ACE^{TM}

("advanced catalysis elastomers") and has been reported within the patent literature.[96, 112, 113]

In 2012, LANXESS acquired this enterprise from DSM and in 2015 built a plant in Changzhou, China, based upon this Keltan ACE^{TM} technology, securing its position as market leader in the production of EPDM.[114] Recently, a joint venture has been setup between LANXESS Elastomers and Saudi Aramco, called ARLANXEO.[115]

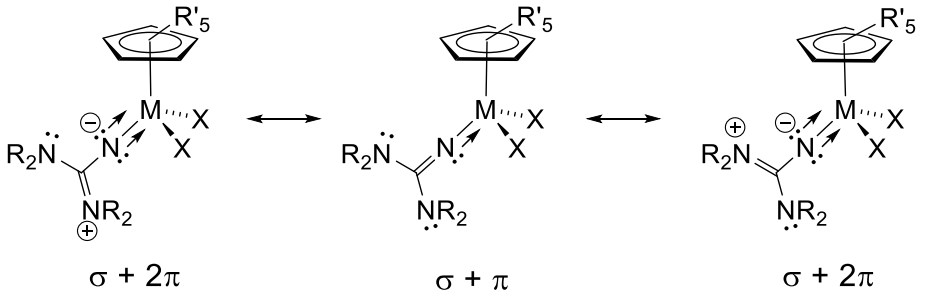

Figure 1.10 Resonance forms of a half-sandwich guanidinate compound.

In 2002, Hessen and co-workers reported the iminoimidazolide (cyclic guanidinate, **1.14**) complex CpTi{NC(NXylCH$_2$)$_2$}(CH$_2$Ph)$_2$ (where Xyl = xylyl). This was shown to have a large improvement in catalytic activity of ethylene in comparison to the equivalent ketimide species, CpTi(NC^{t}Bu$_2$)(CH$_2$Ph)$_2$ (1600 *vs.* 464 kg mol^{-1} h^{-1} bar^{-1}).[116] Subsequently several iminoimidazolide compounds have also been reported as polyolefin catalysts.[117-119] Recently Nomura and co-workers reported an extensive study on half-titanocenes containing 1,3-imidazolidin-2-iminato ligands, Cp*TiCl$_2$[1,3-R$_2$(CH$_2$N)$_2$C=N], which showed exceptionally high activity for ethylene and ethylene/1-hexene polymerisation studies. The bulky aromatic substituents (2,6-Me$_2$C$_6$H$_3$ and 2,6-^{i}Pr$_2$C$_6$H$_3$) gave the highest activity and also the Ti–N–C bond angles closest to linearity.[120] Non-cyclic guanidinates were reported by DSM again for their use in EPDM copolymerisation studies.[121]

The performance of bridged cyclopentadienyl-aryloxy complexes and their performance as polyolefin catalysts had been extensively explored before non-bridged variants were introduced.[70] At the end of the 20th century, Nomura introduced a series of complexes of the type CpTi(OAr)X$_2$ (**1.15**) which exhibited excellent activity for ethylene, propylene and 1-hexene when activated with MAO. It was found that Cp*Ti(O-2,6-^{i}Pr$_2$C$_6$H$_3$)Cl$_2$ gave the most notable activity and also the most linear Ti–O–C bond angle indicative of a greater π-donation and therefore a closer isolobal

analogy with cyclopentadienyl.[122, 123] Additional substituents into both the cyclopentadienyl and the aryloxy groups were subsequently targeted to different results with a range of α-olefins.[124-127]

This Section has so far only introduced neutral half-sandwich compounds with substituents binding in an η^1-mode, but several alternative monoanionic ligands with higher coordination modes have also been developed for olefin polymerisation.[70] Many face-capping ligands have been introduced as a replacement to cyclopentadienyl and will be discussed in the following Section, but some have also been used in conjunction with a cyclopentadienyl ligand to make unusual half-sandwich compounds. The hydrido(tripyrazolyl)borate (Tp) ligand was used to form a titanium or zirconium (**1.16**) mixed sandwich complex.[128, 129] Tp acts as a 6-electron donor cyclopentadienyl analogue *via* a single σ and two π orbitals. Complex **1.16** showed a lower activity than the zirconocene analogue in ethylene homopolymerisation and was inactive to propylene, this was proposed to be a result of the increased steric congestion around the metal centre.[130]

Half-sandwich zirconium complexes with a κ^2-amidinate supporting ligand (**1.17**) have also been introduced. Moderate activities were observed in ethylene polymerisation, this was much slower for propylene polymerisation and only gave an atactic product.[131-133] In addition to this Sita and co-workers synthesised a wide range of half-sandwich Group 4 complexes with an asymmetric κ^2-amidinate supporting ligand. The zirconium analogues were shown to be effective at ethylene polymerisation and able to catalyse the stereospecific living polymerisation of 1-hexene.[134-136] Other half-sandwich Group 4 complexes with monoanionic chelating rings including pyridylalkoxide, iminoindole, phenoxyimine and hydroxylamine substituents have also been synthesised.[137] Several of these chelating rings will be highlighted in Section 1.7.5.

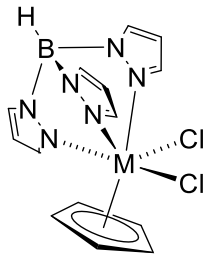

M = Ti or Zr

1.16

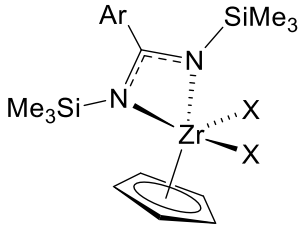

X = Cl or alkyl

1.17

Figure 1.11 Examples of Group 4 half-sandwich complexes.

1.7.4 Face-capping ligands

The monoanionic hydrido(tripyrazolyl)borate (Tp) ligand has found extensive use in organometallic chemistry.[138-142] Previous work within the Mountford group has explored the synthesis of a range of κ^1-amidinate titanium complexes with a supporting Tp ligand (**1.18**) and investigated their performance in ethylene polymerisation, which proved to be poorly active when activated with MAO.[143, 144] Tp-supported Group 4 polyolefin catalysts have been investigated by other groups.[130, 145-149]

Related neutral face-capping ligands tris(3,5-dimethylpyrazoyl)methane (TPM) and triazacyclononane (TACN) have also been employed with Group 4 and 5 polyolefin catalysts. A particularly well studied and relevant family of Group 4 catalysts are formed of these face-capping ligands in conjunction with an imido substituent.[150-156] The imido moiety, of general form –NR, is formally dianionic and is isolobal with cyclopentadienyl. It is reminiscent of the 5 electron donor resonance form of a guanidinate, observed in Figure 1.10. A Density Functional Theory (DFT) study has shown that the frontier molecular orbitals of the imido compound $[Ti(NMe)TACN]^{2+}$ are broadly similar to that of $[Cp_2Ti]^{2+}$.[153, 157] $(TPM)Ti(NR)Cl_2$ (**1.19**) and $(TACN)Ti(NR)Cl_2$ (**1.20**) have both been synthesised with a range of aryl and alkyl substituents as part of the imido moiety. These have been extensively screened as precatalysts for ethylene polymerisation and the results for **1.20** are summarised in Figure 1.12.[152, 154] It was found that bulky TACN and imido ligands give the best performance in both ethylene and styrene homopolymerisation studies.

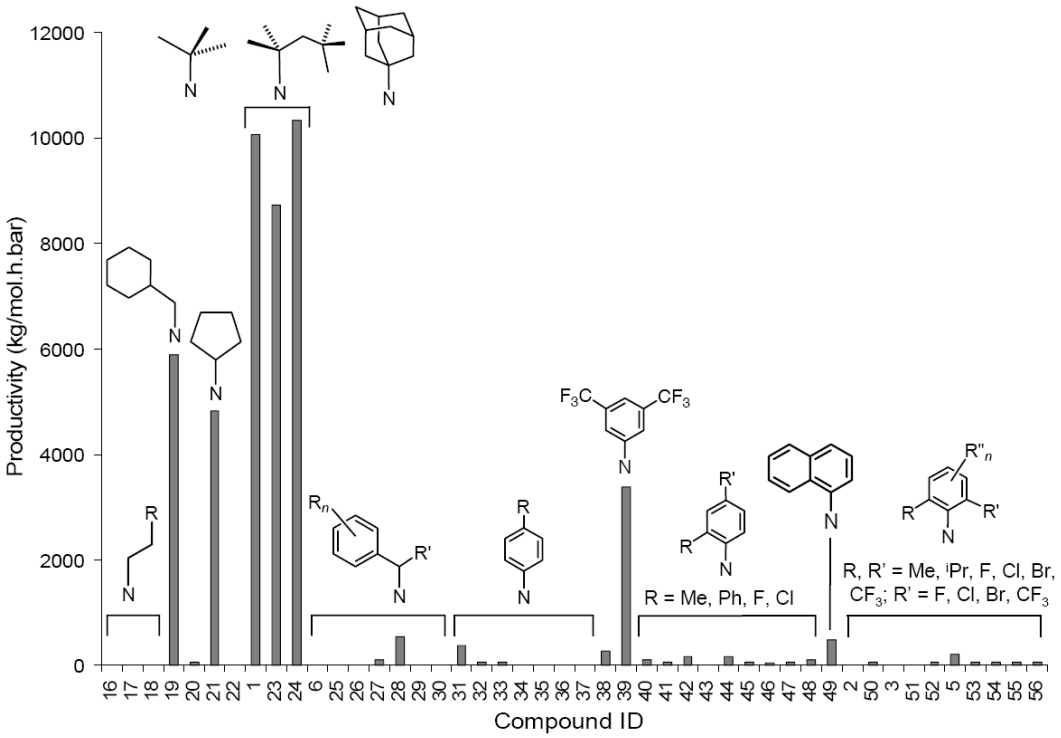

Figure 1.12 High throughput ethylene polymerisation screening with complex **1.20** activated with MAO.[154]

Extension of these neutral face-capping ligands to form cationic κ^1-amidinate complexes has also been investigated. The synthesis of these compounds will be introduced in Chapter Two. Abstraction of the TPM methane hydrogen gives rise to the zwitterionic compounds (TPMd)Ti(NR)Cl(py) (**1.21**, where TPMd = tris(3,5-dimethylpyrazoyl)methanide). The *ortho*-*tert*-butyl phenyl imide substituents proved to be highly active for ethylene homopolymerisation when MAO activated at 100 °C (131,000 kg mol^{-1} h^{-1} bar^{-1}).[152]

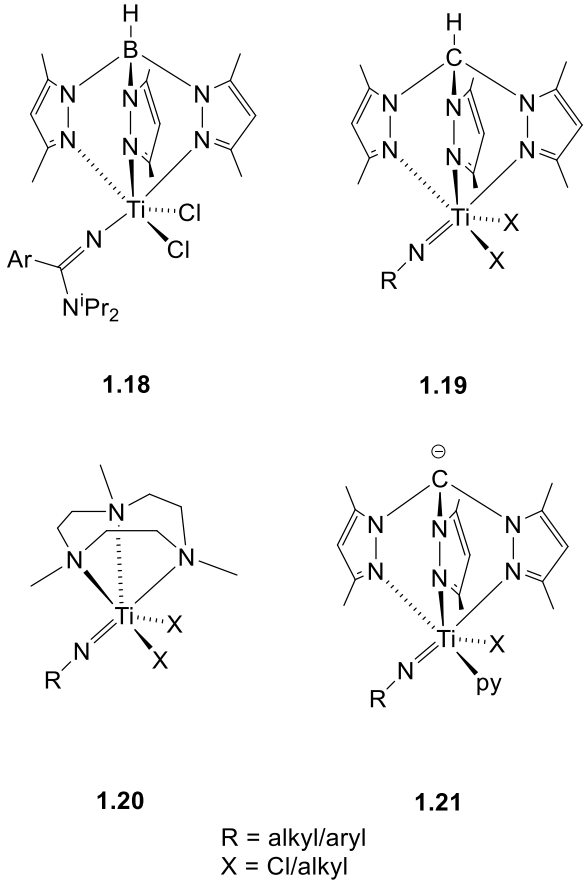

Figure 1.13 Group 4 complexes with face-capping ligands.

This Chapter has so far introduced the cyclopentadienyl moiety as 5-membered carbon ring, often containing different alkyl and aryl substituents. Alternative element incorporation into cyclopentadienyl has also been explored. The phosphacyclopentadienyl (C_4P) ligand maintains the same size and aromaticity. $(C_4P)_2ZrCl_2$ (**1.22**) afforded very high activities in ethylene polymerisation in comparison to the zirconocene analogue.[158] Incorporation of a boron atom into a cyclopentadienyl ring gives a boratobenzene (C_5B). The variation of the substituent on the boron atom of $(C_5BR)_2ZrCl_2$ (**1.23**) plays an important role; a reduced molecular weight is observed as the rate of β-H elimination increases upon changing from diisopropylamine to either phenyl or ethoxide substituents.[159-161]

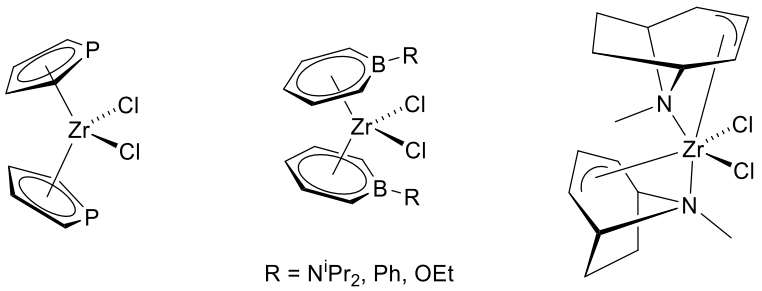

1.22 **1.23** **1.24**

Figure 1.14 Group 4 polyolefin catalysts with cyclopentadienyl analogues.

Lavoie and Bergmann introduced the tropidinyl (trop) ligand as a cyclopentadienyl replacement. This robust ligand has separate 2σ and 4π electron donor sites and does not deactivate by cyclometallation. Despite this, the $(trop)_2ZrCl_2$ (**1.24**) performs comparably to zirconocene under polymerisation conditions.[162, 163]

1.7.5 Chelating amide ligands

Outside of cyclopentadienyl or other face-capping coordination compounds a variety of other multidentate chelating species have been used as ligands with Group 4 metal polyolefin catalysts.[164] Diamido complexes of the form $(ArN(CH_2)_3NAr)TiR_2$ (Ar = 2,6-$Me_2C_6H_3$ and 2,6-$^{i}Pr_2C_6H_3$ (**1.25**)) were introduced by McConville and co-workers and achieved the room temperature living polymerisation of 1-hexene. These compounds are coordinatively unsaturated and were found to be sensitive to both the solvent and activator.[165, 166] A commonly employed chelating ligand is the imino-amido, which typically consists of a 5-membered metallacycle with one anionic and one neutral nitrogen donor.[164] Relative success with these ligands arose from the Klosin group with the trimethylethylidene-bridged Group 4 tribenzyl complex (**1.26**).[167] These complexes were very active and displayed an excellent 1-octene incorporation, but were shown to undergo a 1,2-methyl shift at high temperature. The isomer was found to be much less active and to exhibit multisite behaviour resulting in broader PDI values.[168] This was overcome through the use of an imino-enamido backbone (**1.27**) that proved to be more thermally robust to interconversion. Complex **1.27** was found to give highly active single site (PDI = 2.4) behaviour at temperature of 120 °C (7.2 x 10^5 kg mol^{-1} h^{-1} bar^{-1}) in the formation of an ultra-high-molecular weight ethylene/octene copolymer.[169, 170] Extending the backbone to aminotroponiminato catalysts, in which there is a complete delocalisation of the imine bond through the backbone, removed the importance of isomerisation but reduced the

catalytic activity in an ethylene/1-octene copolymerisation study and broad PDI values were observed.[171] Pyridyl-amido complexes with the general form of **1.28** have also been studied and were shown to polymerise propylene at high temperatures to form an isotactic high-molecular-weight product.[172, 173] It was found that the insertion of an olefin into the Hf–C_{aryl} bond is favoured over insertion into the Hf–C_{alkyl} bond. This gives formation of various isomeric cationic catalysts that can either induce stereocontrol or behave distinctly and give rise to broad molecular weights.[170, 174-176] Kempe and co-workers have introduced a range of aminopyridinato Group 4 complexes with a 4-membered metallacycle.[177-179] Titanium complexes (**1.29**) of this kind gave high regioselectivity in ethylene/propylene copolymerisation studies and were also of capable of incorporating cyclic monomers like the diene ENB.[178]

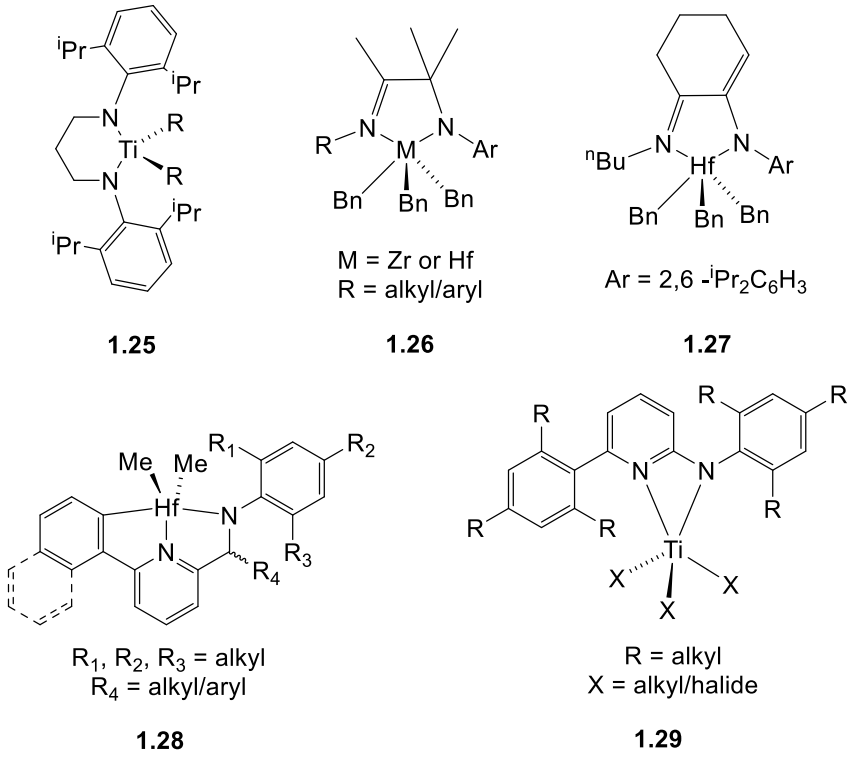

1.25 **1.26** **1.27** **1.28** **1.29**

Figure 1.15 Group 4 polyolefin catalysts with chelating N-donor ligands.

1.7.6 Chelating aryloxide ligands

The use of chelating ligands with oxygen donors has also been explored for the purpose of polyolefin catalyst design. Fujita and co-workers investigated phenoxyimine (FI) Group 4 complexes with a wide range of substituents on the backbone (**1.30**).[180] This work was carried out at Mitsui Chemicals and variations of the steric congestion imposed by the substituents were shown to have a strong

influence over the activity, molecular weight and temperature stability.[181, 182] The salicylaldiminato zirconium dichloride complex (**1.31**) is one of the most active ethylene polymerisation catalysts when activated with MAO (7.2 x 10^6 kg mol^{-1} h^{-1} bar^{-1}) and is stable at the industrially relevant temperature of 75 °C.[182] FI catalysts of this kind were also shown to polymerise propylene in a syndiospecific fashion by 2,1-insertion.[183] Inclusion of fluorine substituents resulted in living polymerisation; this was proposed and computationally verified to be a result of a hydrogen bond between the fluorine substituents and the β-hydrogen atoms of the polymer chain, which prevents termination pathways from occurring.[183-185] Kol and co-workers designed the C_2-symmetric Group 4 salan supported complexes (**1.32**), which have been shown to catalyse both the living and isospecific polymerisation of 1-hexene.[186]

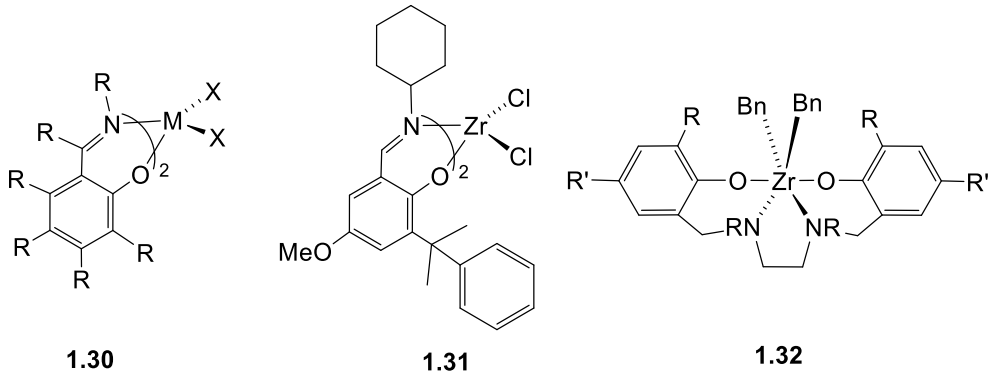

Figure 1.16 Group 4 polyolefin catalysts with chelating O-donor ligands.

1.8 Activators

The important discovery of MAO as a cocatalyst was introduced in Section 1.3 and to this day MAO is still predominantly used in commercial applications. MAO activates Group 4 dichloride species through ligand exchange, to generate the monomethylcomplex, and subsequent chloride abstraction to give a catalytically active ion-paired species. This process is inefficient and MAO is typically used in a large excess.[187, 188] MAO contains non-hydrolysed aluminium alkyls that have been proposed to generate the *in situ* monoalkylated compound, but also act as catalyst poisons. Trimethylaluminium (TMA) can beneficially scavenge oxygen and water from the reaction mixture and can be used as an activating species for zirconocene complexes, but significantly reduced productivities show that it is not the actual cocatalyst in MAO.[37, 189-191]

It was proposed that TMA can coordinate with a metal cation to form a resting state or act as a reducing agent.[41, 192, 193] The first TMA adduct with a Group 4 alkyl cation $[Cp_2Zr(\mu\text{-}Me)_2AlMe_2]^+$ was reported by Bochmann *et al.* (**1.33**),[194] and in 2006 Mountford *et al.* reported the first structurally authenticated cationic transition metal compound containing a $M(\mu\text{-}Me)_2AlMe_2$ moiety (**1.34**, Figure 1.17).[156] Synthetic modifications have been made to MAO since the initial introduction in order to enhance the activation efficiency.[65] 4-Methyl-2,6-di-*tert*-butylphenol (BHT) can preferentially react with TMA preventing this adduct from forming but still allowing it to operate as a scavenger. Synthetic and polymerisation studies specific to the inclusion of BHT will be discussed in Chapter Two.

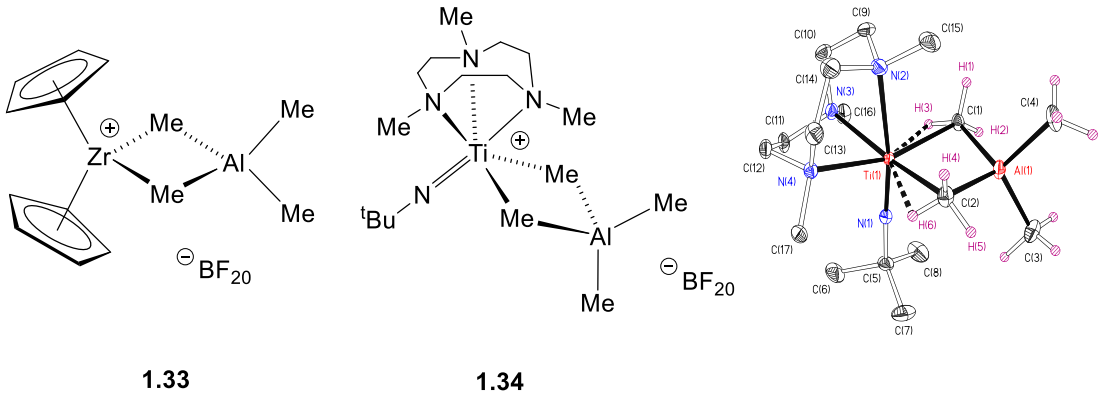

1.33 **1.34**

Figure 1.17 TMA adducts with Group 4 alkyl cations.[156, 194]

Formation of the active metal cation is not limited to the use of aluminium alkyl species. Several routes into the preparation of Group 4 monoalkyl cations have been developed and their influence in polymerisation studies examined. Unlike MAO many of the alternative cocatalysts operate with the same stoichiometry as that of the precatalyst, this gave the opportunity for more mechanistic studies to take place and also removed certain limitations associated with a large excess of aluminium alkyls.[195]

Tris(pentafluorophenyl)borane (BF_{15}) was first reported in 1964,[196] however the role it could play in polyolefin chemistry was not investigated until the early 1990s. BF_{15} is a strong Lewis acid and can therefore abstract a methyl group from a Group 4 dialkyl compound. Marks[197, 198] and Ewen[199] independently made use of this in conjunction with different zirconocenes. In 1991 the complex $[\{1,2\text{-}(CH_3)_2C_5H_3\}_2ZrCH_3][MeBF_{15}]$ (**1.35**) was isolated and crystallographically characterised to give the first example of an active metal cation (Figure 1.18).[197] Complex **1.35**, like many subsequent analogous compounds, displays an interaction

between the abstracted methyl group and the cationic metal centre acting through two agostic interactions.[197] This molecule can be considered as a zwitterionic complex with a bridging methyl group and is important concerning polymerisation studies as this bridging interaction must be overcome in order for an olefin monomer to approach and bind. A significant amount of research went into developing alternative strongly Lewis acidic boranes and diboranes.[195] The dinuclear analogue $\{B(C_6F_5)_2\}_2(\mu\text{-}C_6F_4)$ will be discussed both later in this Chapter and then extensively in Chapter Four.

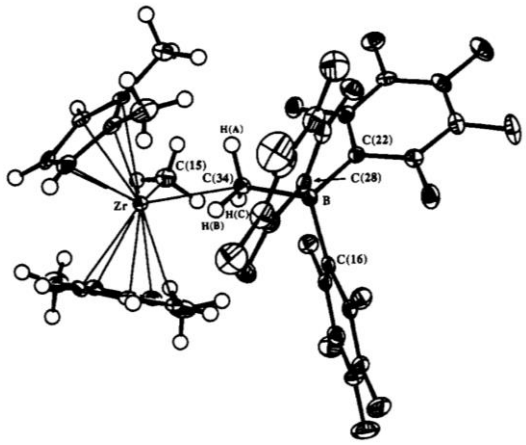

Figure 1.18 Molecular structure of $[\{1,2\text{-}(CH_3)_2C_5H_3\}_2ZrCH_3][MeBF_{15}]$ (**1.35**).[197]

Reprinted (adapted) with permission from X. Yang, C. L. Stern and T. J. Marks, *J. Am. Chem. Soc.*, 1991, **113**, 3623-3625. Copyright 1991 American Chemical Society.

Activation of Group 4 species has also been demonstrated by oxidative and abstractive cleavage of alkyl bonds by charged reagents,[200] protonolysis of metal alkyl bonds[201-205] and one-electron oxidation and reduction pathways.[206-208] Of note to this Thesis are alkyl abstractive cleavage pathways and in particular the use of trityl tetrakis(pentafluorophenyl)borate for this purpose, $[CPh_3][BF_{20}]$ (TBF_{20}). The trityl cation abstracts an alkyl anion to form an organic side-product, Ph_3CR, and the borate anion becomes associated to the active metal centre. The choice of anion is important in polymerisation; $[BPh_4]^-$ and $[C_2B_9H_{12}]^-$ have been shown to display fairly strong interactions with base-free cations, or be prone to C–H activation.[203, 209] However, $[BF_{20}]^-$ is non-coordinating and mostly innocent to reactions, which results in a very coordinatively open and correspondingly catalytically active metal centre. There are rare examples of a metal cation interacting with a $[BF_{20}]^-$ anion, these include a crystallographically characterised thorium cation displaying close contact through the

fluorine atoms of the anion and examples of $C_6F_5^-$ extraction and B–C bond cleavage with titanium cations.[210-212] Other non-coordinating anions have also been explored, including the dinuclear counterpart $[\{B(C_6F_5)_3\}_2(\mu\text{-}C_6F_4)][Ph_3C]_2$, these will be discussed in further detail in Chapter Four. The structure and reactivity of these naked cations will be discussed in the following Section.

1.9 Metal alkyl cations

1.9.1 Base Free metal alkyl cations

The coordinatively unsaturated nature of a cationic Group 4 metal cation results in prevalent stabilising interactions either from the substituents, the solvent or other neutral or cationic Group 4 complexes.[195]

The zirconium CGC, $[CGCZr(CH_2Ph)][BF_{20}]$ (where CGC = $Me_2Si(Me_4Cp)^tBuN$), is stabilised by an η^2-bound benzyl substituent (**1.36**) when activated with TBF_{20}.[200] This so called *ipso*-interaction has been regularly observed[213, 214] and this non-classical interaction can be identified through an upfield *ipso* carbon chemical shift in the ^{13}C NMR and a large $^1J_{CH}$ coupling constant for the methylene group.[213] Comparable agostic interactions from the substituents to the metal centre have been commonly observed, these include β-C–H[215, 216] and Si–Me[14, 153, 217, 218] interactions.

The analogous dimethyl complex of **1.36** forms an arene stabilised complex when activated in toluene (**1.37**),[219] hydrocarbon solvent interactions with transition metals have be on regularly observed.[220, 221] One relevant example that has been crystallographically characterised is the chlorobenzene stabilised zirconocene, $[Cp^*_2ZrCl(C_6H_5Cl)][BF_{20}]$ (**1.38**).[222]

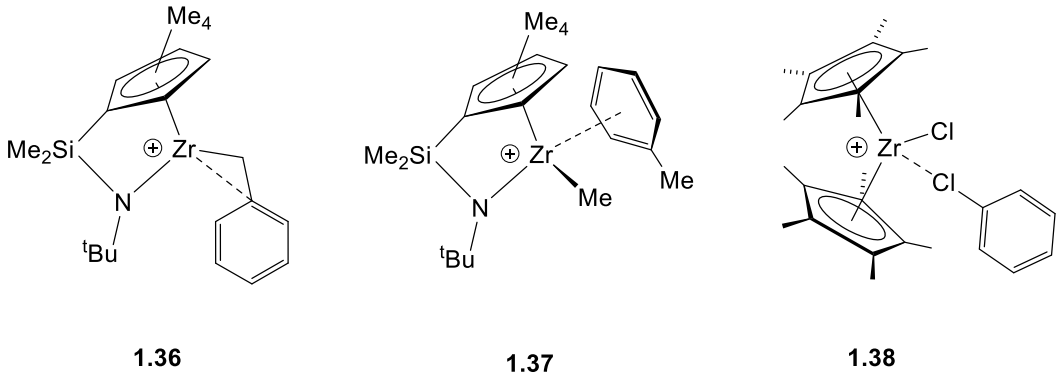

1.36 **1.37** **1.38**

Figure 1.19 Non-classical interactions with Group 4 metal cations.

Bochmann and co-workers reported that the addition of TBF_{20} to the metallocene Cp_2ZrMe_2 results in initial formation of $[Cp_2ZrMe(\mu\text{-}Me)MeZrCp_2][BF_{20}]$ (**1.39**) before onward formation of $[Cp_2ZrMe][BF_{20}]$. This monomethyl bridged monocation can be formed quantitatively by using 0.5 equiv. of TBF_{20}.[194]

In 2010, Mountford and co-workers in collaboration with DSM introduced a titanium half-sandwich κ^1-amidinate supported titanium complex, $Cp^*Ti\{NC(N^iPr_2)Ar^{F_2}\}Me_2$ (**1.40**, Ar^{F_2} = 2,6-$C_6H_3F_2$, Scheme 1.1).[223] Reaction of **1.40** with a stoichiometric amount of TBF_{20} resulted in the first example of a crystallographically characterised base-free Group 4 dimethyl-bridged dication $[Cp^*_2Ti_2\{NC(N^iPr_2)Ar^{F_2}\}_2Me_2][BF_{20}]_2$ (**1.41**). The molecular structure is displayed in Figure 1.20 and indicates that the bridging methyl groups interact *via* 3-centre-2-electron bonds and with two stabilising agostic interactions. Only one other Group 4 dication is known, $[Cp^*_2Zr_2\{MeC(N^tBu)(NEt)\}_2(\mu\text{-}Me)_2][BF_{20}]_2$, which again contains bridging methyl groups proposed to be in a trigonal bipyramidal geometry with an unprecedented doubly-bridging agostic C–H bond.[224] This has subsequently been contested in light of the crystallographically characterised complex **1.41** and using a DFT study.[223] The isolated complex **1.41** can be used as a catalyst in polymerisation studies and was shown to perform with the same capabilities as the analogous *in situ* generated catalyst.[223]

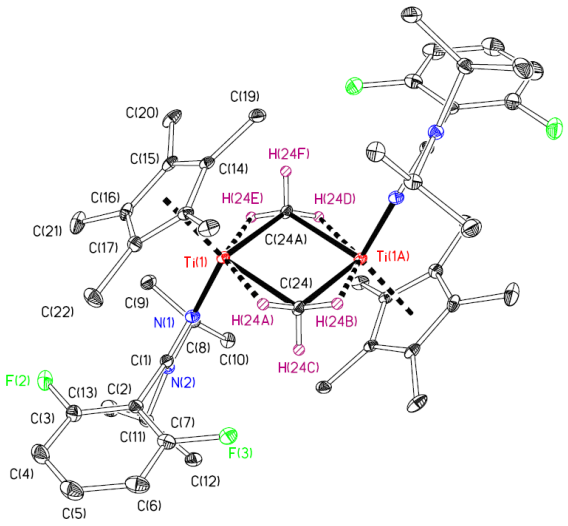

Figure 1.20 Molecular structure of $[Cp^*_2Ti_2\{NC(N^iPr_2)Ar^{F2}\}_2Me_2][BF_{20}]$ (**1.41**).[223]

If a sub-stoichiometric amount of TBF_{20} is present then a monomethyl bridged monocation, $[Cp^*_2Ti_2\{NC(N^iPr_2)Ar^{F_2}\}_2Me_2(\mu\text{-}Me)][BF_{20}]$ (**1.42**), comparable to complex **1.39** forms. The presence of $OPPh_3$ results in the monometallic Lewis base

stabilised cation [Cp*Ti{NC(N^{i}Pr$_2$)Ar^{F_2}}(OPPh$_3$)Me][BF$_{20}$] (**1.43**), this can be formed from **1.40**, **1.41** or **1.42** (Scheme 1.1).[223] Lewis base stabilised cations of this kind will be discussed further in Section 1.9.2.

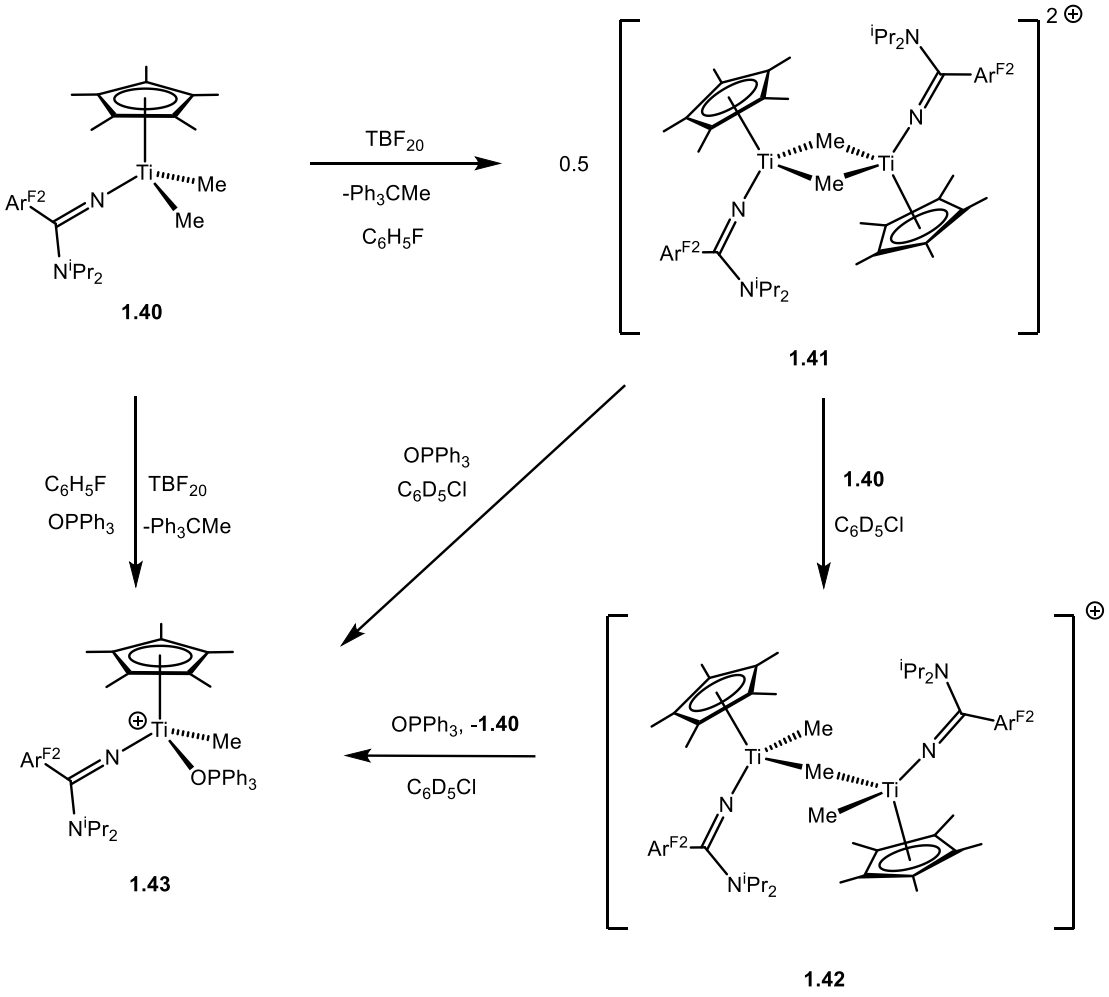

Scheme 1.1 Synthetic route to titanium cationic species. [BF$_{20}$]$^-$ anions omitted for clarity.[223]

1.9.2 Base stabilised metal alkyl cations

Unlike those highlighted above, in many cases the formation of extremely electron-deficient and highly coordinatively unsaturated Group 4 cationic species result in complicated oily mixtures of unstable and unidentifiable products.[195] The use of Lewis bases to form stabilised adducts has been routinely employed, these have included MeCN, PhCN, pyridine, THF, PMe$_3$, PMePh$_2$ and OPPh$_3$. Stronger donors, such as PMe$_3$ and OPPh$_3$, will displace moderately labile donors and the number of donors depends on the size of the ligand and ionic radii of the metal centre.[201, 225-227] Although easier to isolate and characterise the use of these isolated Lewis base

adducts in polymerisation unsurprisingly display both a suppressed catalytic activity and have also been shown to influence the resultant polymer properties.[195]

1.9.3 Reactivity of metal alkyl cations

Group 4 cationic species are highly reactive electron deficient metal centres. As was discussed in Section 1.8, these species can react with TMA to form a heterobimetallic species. This Section will explore their reactivity in forming insertion products with small unsaturated molecules and C-H activation products. The first insertion product was introduced in Section 1.4 with the insertion of $PhC{\equiv}CSiMe_3$ into the Ti–Me bond of $[Cp_2TiMe]^+$.[14] Subsequently, Bochmann *et al.* showed insertion of CO and ^{t}BuNC with the same cation.[201, 228] Jordan and co-workers extensively studied the insertion products of $[Cp_2ZrMe(THF)][BPh_4]$ (**1.44**) with CO, alkynes, ketones and nitriles (Scheme 1.2).[206, 229]

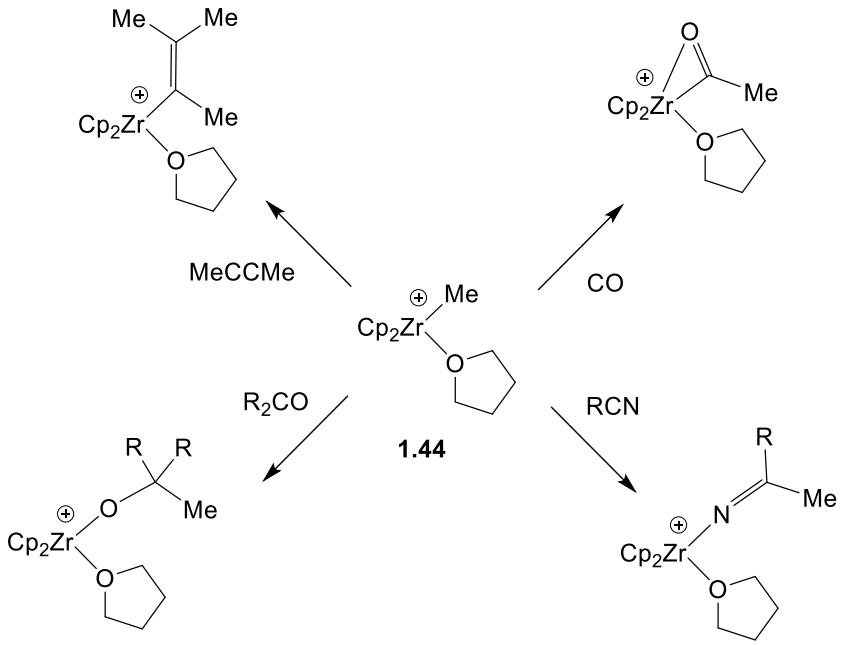

Scheme 1.2 Reaction of a Group 4 metallocene cation with unsaturated substrates.[206]

These isolated insertion compounds act as excellent mimics for the first propagation step in olefin polymerisation experiments. The isolation of compounds involving the insertion of alkenes across Group 4 M–C bonds has also been investigated. Reaction of the activated species $[Cp^*ZrBn_2][PhCH_2B(C_6F_5)_3)]$ (**1.45**), in which the abstracted benzyl group stabilises the cationic metal centre through an η^6-interaction from the phenyl ring, with propene resulted in the insertion product $[Cp^*ZrBn(CH_2CHMeCH_2Ph)][PhCH_2B(C_6F_5)_3)]$ (**1.46**) (Equation 1.3). The anion is

non-coordinating in this product as the metal centre is stabilised through a similar η^6-phenyl coordination, complex **1.46** was crystallographically characterised. Prior to this the activated product $[ZrBn_3\{(\eta^6\text{-}PhCH_2)B(C_6F_5)_3\}]$ had been shown to react with a variety of α-olefins in an analogous fashion, but no crystal structures were reported.[230-232] Other examples of alkene insertion reactions into a Group 4 M–C bond have subsequently been reported.[233-235]

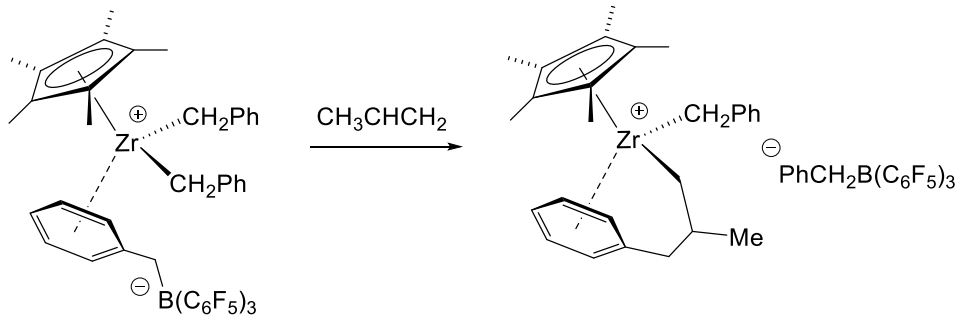

1.45 **1.46**

Equation 1.3

The first reported C–H activation by a Group 4 cation was observed through the interaction of $[Cp^*_2ZrMe]^+$ with the coordinating $[BPh_4]^-$ anion.[203] The aforementioned $[Cp_2ZrMe(THF)][BPh_4]$ (**1.44**) can react with α-picoline to initially displace THF and coordinate to the metal centre, this then undergoes a C–H activation with the extrusion of methane and subsequent re-coordination of THF to form the η^2-pyridyl species **1.47** as two isomers.[236, 237] If the *ortho* position is blocked then more remote positions can undergo C–H activation, it is interesting to note that the analogous titanium complex does not undergo the same reactivity.[201] Complex **1.47** was shown to rapidly react with ethylene or propylene to yield the corresponding insertion products (**1.48**, Scheme 1.3).[236]

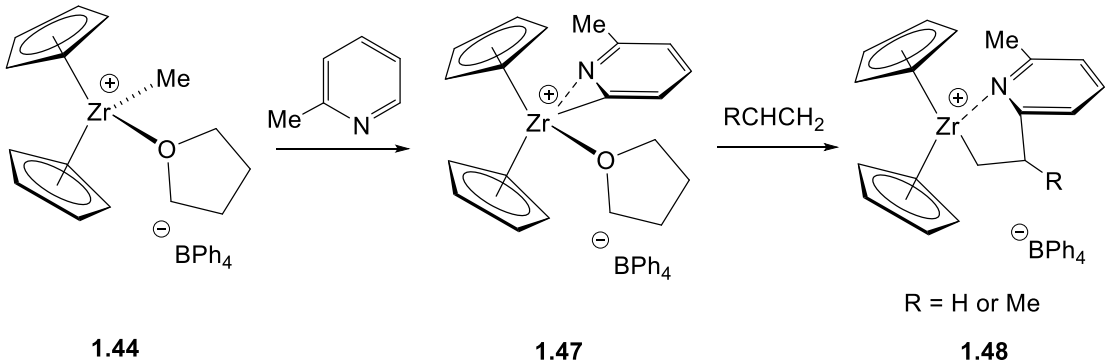

1.44 **1.47** **1.48**

Scheme 1.3 C–H activation and subsequent alkene insertion with a Group 4 cation.

1.10 Bimetallic catalysts

Since the early 1990s, multimetallic catalysts have been investigated for olefin polymerisation. Inspired by the role proximate metal centres play in increasing localised reagent concentration within enzymes, multimetallic species have been introduced to enhance several chemical transformations such as the Diels-Alder[238] and Strecker[239] reactions.[240, 241] Bimetallic catalysts can be linked either *via* a direct metal-metal bond, by a bridging atom or connected *via* a ligand. In olefin polymerisation a wide range of bimetallic catalysts tethered through their ligands have been employed. It took until the turn of the century for any advantageous properties to be seen, most notably, a higher molecular weight and superior chain branching. These properties arise from a complimentary interaction at the polymeric chain between adjacent metal centres, it is termed a cooperative effect.[241]

1.10.1 Group 4 bimetallic CGCs

A particularly successful and readily studied family of bimetallic catalysts are the covalently tethered *ansa*-amido-monocyclopentadienyl zirconium catalysts introduced by Li and Marks (Figure 1.21). [33, 242, 243]

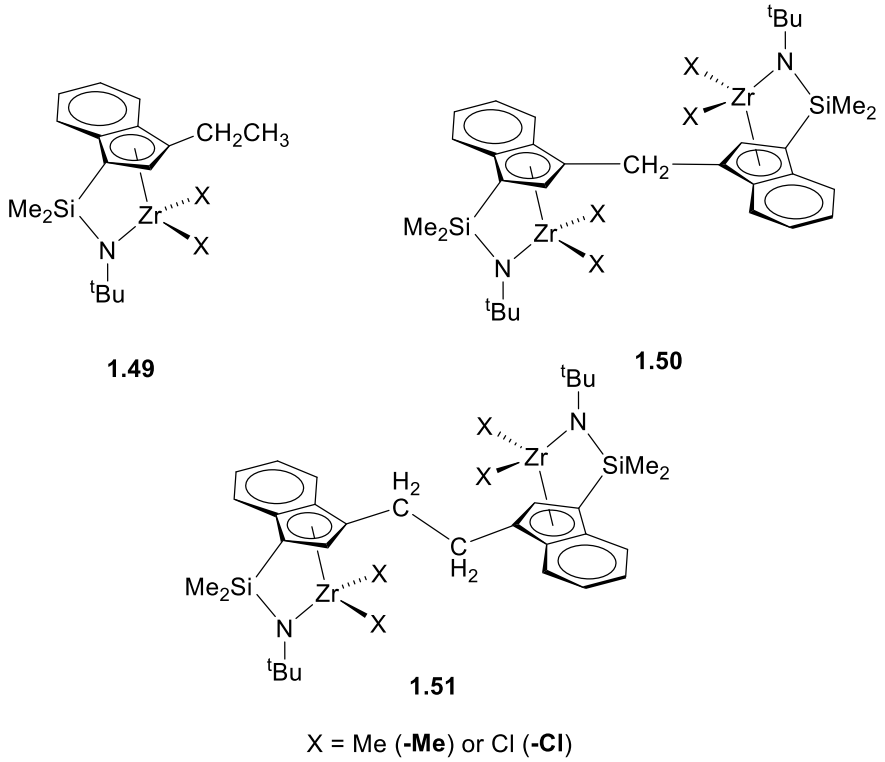

Figure 1.21 Covalently tethered group 4 bimetallic constrained geometry catalysts.

An MAO activated ethylene homopolymerisation study using precatalysts **1.49 – 1.51-Cl** displayed comparable activities (25-23 kg mol^{-1} h^{-1} bar^{-1}), but a very large increase in molecular weights for the bimetallic catalysts, 659 kg mol^{-1} (**1.50-Cl**) and 750 kg mol^{-1} (**1.51-Cl**), in comparison to their mononuclear counterpart, 1.2 kg mol^{-1} (**1.49-Cl**). For single-site polymerisations, which is indicated in this study by PDI values not exceeding 2.8, molecular weight is proportional to the ratio of the rate of propagation to the overall rate of termination. As the activities remain fairly consistent it is suggested that the termination kinetics must be substantially depressed.[243] This was proposed to be a result of a stabilising agostic interaction between the propagating polymeric chain and the proximate metal centre resulting in a higher barrier to termination.[242] A computational study was carried out by Fragala and co-workers on catalyst **1.51-Me** where n-octyl was used to represent a propagating chain and n-propyl was used to represent an oligomeric chain. The insertion and chain transfer transition states were analysed and similar energetic values were seen for ethylene insertion in both cases. A consistent destabilisation (2 kcal mol^{-1}) was seen for the β-hydrogen chain transfer of catalyst **1.51-Me** with an n-octyl chain, attributable to steric repulsions resulting from the constraints of the stabilising agostic interaction (Figure 1.22).[244]

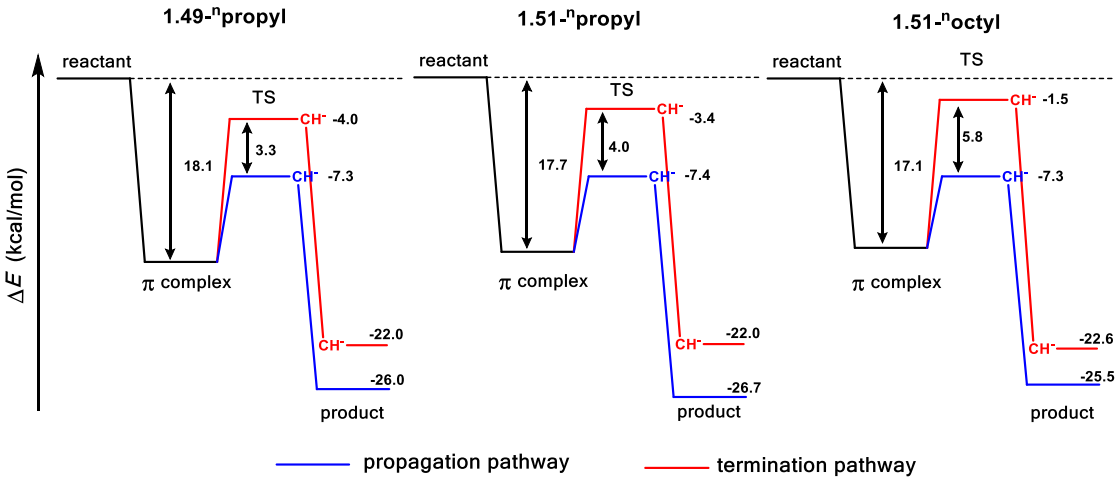

Figure 1.22 Reaction pathway describing the propagation and termination routes in ethylene homopolymerisation for complexes **1.49** and **1.51**.[244]

When the same precatalysts are activated with TBF_{20} a difference is observed. The activities decrease from the monometallic (**1.49-Me)** to the ethyl bridged bimetallic (**1.51-Me**) precatalyst and then again to the shorter methyl chain branched bimetallic

complex (**1.50-Me**) (127, 87 and 19 kg mol^{-1} h^{-1} bar^{-1}, respectively). The molecular weight displays a small increase from **1.49-Me** (610 g mol^{-1}) to **1.51-Me** (760 g mol^{-1}), but a very large increase for **1.50-Me** (49,500 g mol^{-1}). This study also gave data as to the number of ethyl branches per 1000 carbon atoms in the polymer chain of 1.1 (**1.49-Me**), 1.3 (**1.50-Me**) and 2.7 (**1.51-Me**), as the molecular weight increases then it can be concluded that the number of branches per polymeric chain dramatically increases.[33, 243] The increase in branching is proposed to arise from the recapture of the vinylic end of the polymer at the neighbouring metal centre after chain transfer. This process aids an intramolecular re-insertion into the growing polymeric chain. The computational study, introduced above, also refined the geometrical orientation of an oligomeric π-bonded vinyl terminated oligoethylene chain; a non-negligible (2 kcal mol^{-1}) stabilisation energy is observed with the second metal site, a pre-requisite for ethyl branching. The mechanism for this macromonomer is displayed in Scheme 1.3.

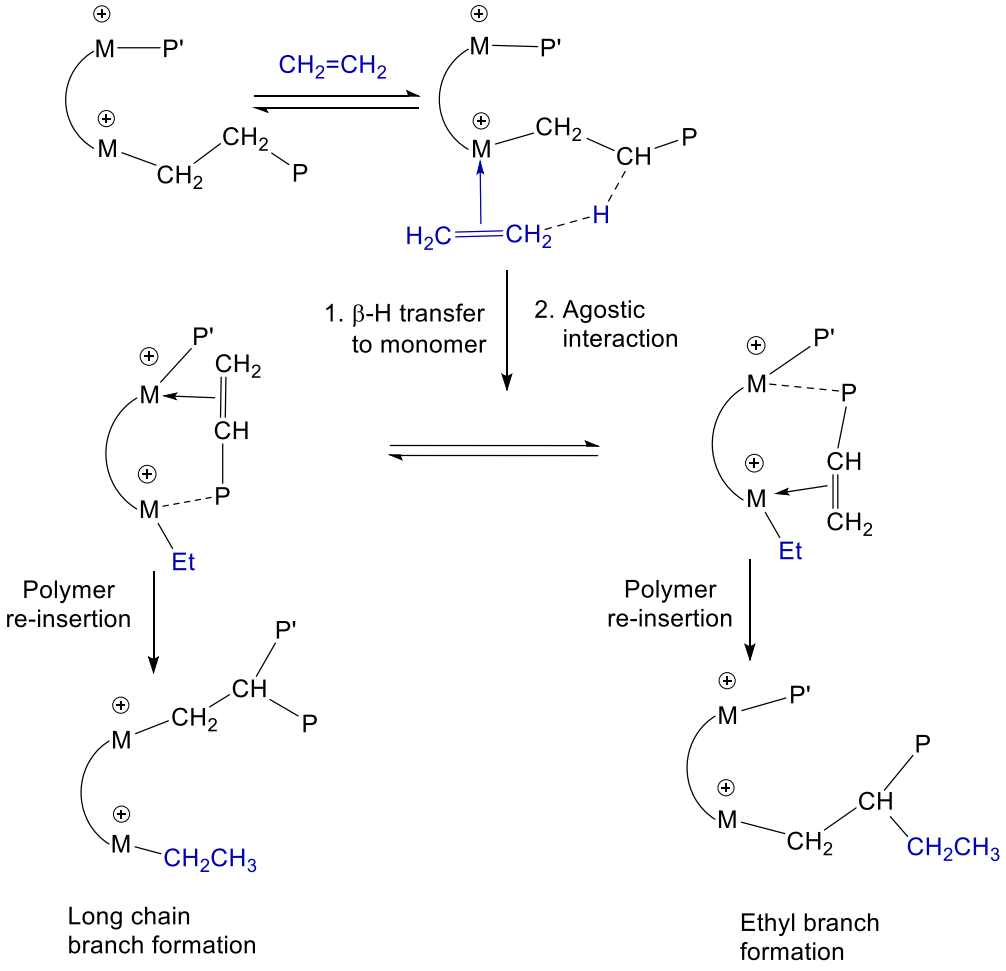

Scheme 1.3 Mechanism for macromonomer reinsertion.[243]

This favourable agostic interaction has been extended to other α-olefins. In the case of the styrene homopolymerisation with TBF_{20} activation the bimetallic catalysts **1.50-Me** and **1.51-Me** show an eight-fold and four-fold increase in activity compared to their mononuclear analogue **1.49-Me**, but the molecular weight capabilities follow the opposite trend. It was previously established that a strongly preferred 1,2-insertion of styrene is observed for organozirconium monometallic catalysts,[245] however in the case of **1.50-Me** and **1.51-Me** an increased percentage of 2,1-insertion regiochemistry is installed. The authors suggest this is a direct result of a favourable interaction with the proximate metal centre as is depicted in Equation 1.4.[246] An enhanced activity improvement is observed for the titanium analogues. The smaller coordination of the monometallic counterpart results in catalyst deactivation when a styrene monomer inserts in a 2,1-fashion, due to "backbiting". As a result the monometallic species incorporates styrene with a preferential 1,2-insertion regiochemistry, but when using the bimetallic species 1,2- and 2,1-insertion competes equally.[246, 247] These analogous titanium catalysts and further examples of preferential comonomer enchainment will be introduced in Chapter Two.

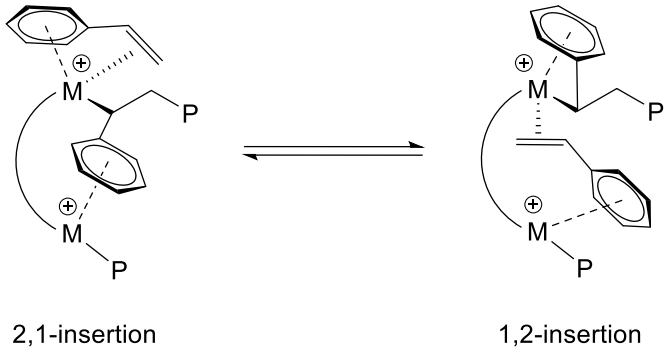

Equation 1.4 Proposed competing regiochemistry forms in the homopolymerisation of styrene.[247]

These precatalysts and their titanium analogues have also been used in conjunction with the dinuclear cocatalysts $[\{B(C_6F_5)_3\}_2(\mu\text{-}C_6F_4)][Ph_3C]_2$ and $\{B(C_6F_5)_2\}_2(\mu\text{-}C_6F_4)$, these will be introduced and discussed in Chapter Four.

The *ansa*-amido-monocyclopentadienyl catalysts introduced by Li and Marks gave the opportunity for excellent insight into the mechanism and potential of bimetallic catalysts. Research has gone into an extensive range of covalently bridged bimetallic olefin catalysts and these will be introduced in the following Section. Only Group 4

bimetallic catalysts will be discussed, but similar bridging moieties have been extended to a variety of different metal centres.[241]

1.10.2 Group 4 bimetallic catalysts tethered through a cyclopentadienyl moiety

Noh and co-workers reported a family of polymethylene-bridged zirconocene complexes with different bridge lengths (**1.52**) (Figure 1.23). It was found that the activity towards ethylene homopolymerisation varied in the order **1.52d** > **1.52c** > **1.52b** > **1.52a**, with all the catalysts, except **1.52a**, outperforming the mononuclear unsubstituted analogue. It was proposed that the increase in electron density provided by the bridge stabilises the active metal centre and increases activity relative to the mononuclear analogue. In the case of **1.52a** the chain is too short and steric clashes outweigh the improved electron density and limit the activity.[248] Silane bridged zirconocene species were first introduced by Green and co-workers[249] and Noh *et al*. subsequently developed a range of analogous siloxane bridged species to **1.52a-d** which were shown to have a decreased activity relative to the mononuclear and polymethylene-bridged species, but followed the same trend in activity with bridge length.[250] In 2002, Tian and co-workers introduced a range of silane and siloxane bridged zirconocenes **1.53a-e**, in MAO activated ethylene homopolymerisation both the activity and molecular weight were again both shown to increase with bridge length.[251]

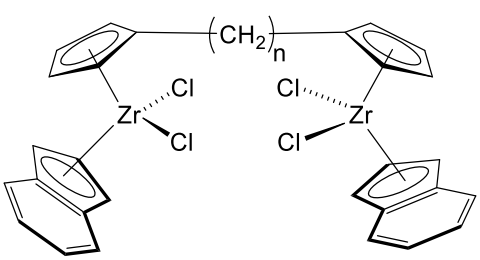

1.52a (n = 3)
1.52b (n = 5)
1.52c (n = 7)
1.52d (n = 9)

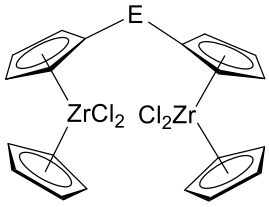

1.53a (E = Me_2Si)
1.53b (E = $Me_2SiSiMe_2$)
1.53d (E = $Me_2SiOSiMe_2$)
1.53e (E = $Me_2SiOSiMe_2OSiMe_2$)

Figure 1.23 Bimetallic zirconocene catalysts with polymethylene tethers.

Osakada and co-workers introduced a range of zirconocene complexes with a rigid alkene bridge **1.54a-c**, the complexes were synthesised *via* an intermolecular metathesis pathway with the use of a second generation Grubbs catalyst. Complex **1.54a** was synthesised as almost exclusively the trans isomer (99%). Hydrogenation

of the complexes affords the bimetallic complexes **1.55a-c** with a flexible polymethylene tether (Equation 1.5). Both series of complexes were used in MAO activated ethylene homopolymerisation and displayed the opposite trend to that observed for **1.52** and **1.53** in that the activity follows in the order **a** > **b** > **c**. The smaller chain branch was proposed to give a positive cooperative effect induced by effective separation of the active complex from the bulky anions. Both bimetallic series are more active than their monometallic counterparts and the flexible tethered series (**1.55a-c**) outperform the rigid alternative. A decrease in molecular weight was observed with the bimetallic catalysts than their monometallic, but no clear trend in chain length or flexibility was observed. The homopolymerisation of propylene under the same conditions were not as active, but followed the same trend in activity and no clear trend in molecular weight was apparent.[252]

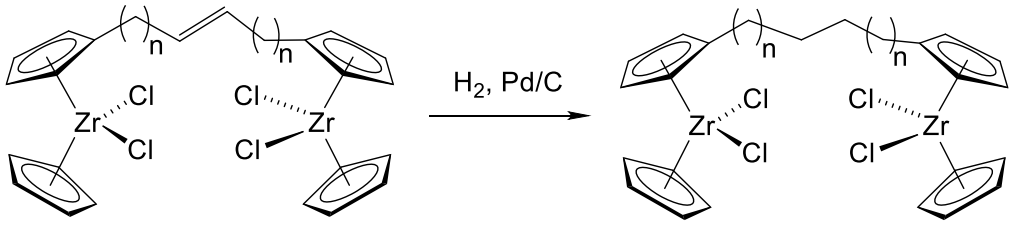

1.54a (n = 1)
1.54b (n = 2)
1.54c (n = 3)

1.55a (n = 1)
1.55b (n = 2)
1.55c (n = 3)

Equation 1.5

Erker and co-workers reported a similar system with an alkene bridged zirconocene (**1.56**), which was again synthesised *via* a metathesis pathway and a mixture of products was observed corresponding to the different stereoisomeric products. A preliminary polymerisation study of the homopolymerisation of ethylene and propylene was reported, but in both cases the bimetallic was reported as having poor activity.[253] A doubly bridged and therefore constrained bimetallic titanium catalyst (**1.57**) was shown to give excellent activity, molecular weight capacity and levels of syndiotacticity in the hompolymerisation of styrene. This is proposed to be a direct result of the metal centres being in close proximity and through ligand variation it was found that the bridge not connecting the cyclopentadienyl groups was more significant to the catalyst properties.[254] Further examples of conformationally locked bimetallic catalysts will be discussed in Chapter Four.

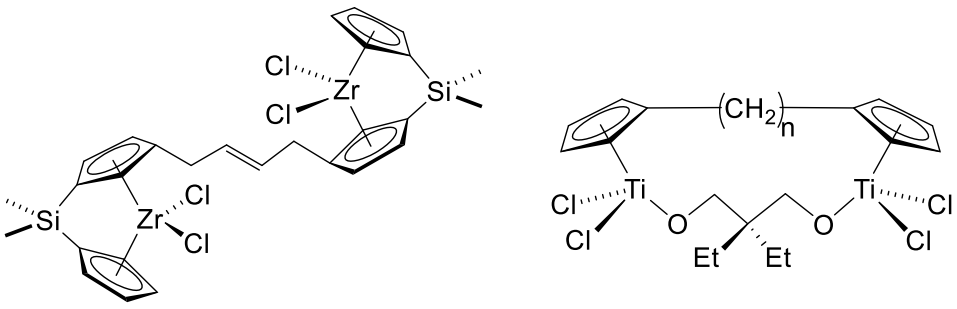

1.56 **1.57a** (n = 6)
1.57b (n = 9)

Figure 1.24 Group 4 bimetallic catalysts with rigid tethers.

Of specific note to this project, a recent patent was filed by LG chemicals for a large range of half-sandwich κ^1-amidinate Group 4 bimetallic complexes tethered through a bis-phenylene spacer connected to the cyclopentadienyl groups (**1.58**).[255] Limited polymerisation data was reported, but the high temperature copolymerisation gave active catalysts with excellent incorporation of propylene and the cyclic diene ENB.

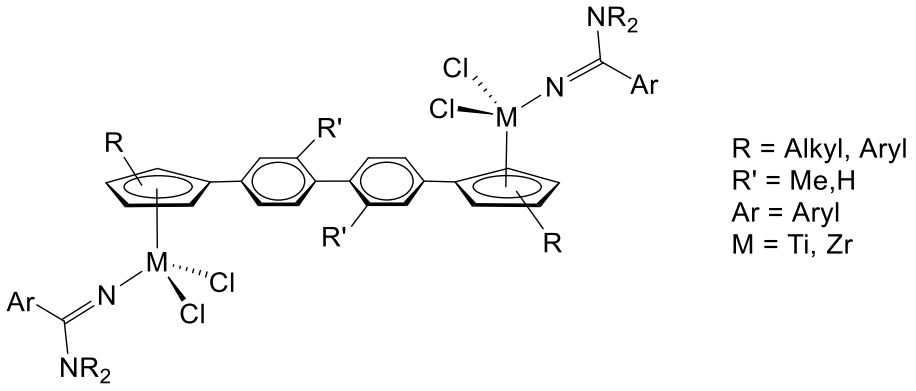

1.58

Figure 1.25 half-sandwich κ^1-amidinate Group 4 bimetallic complexes.

1.10.3 Alternative Group 4 bimetallic catalysts

Stephan and co-workers introduced a range of phenylene-tethered half-sandwich bimetallic phosphinimide titanium complexes (**1.59**). Although very active in the MAO activated homopolymerisation of ethylene, a bimodal polymer distribution was observed when using the bimetallic catalyst. This was proposed to be a result of MAO interfering with the catalyst to generate two or more active sites, no mechanistic investigations were reported.[256] In 2014, Radlauer and Agapie reported a family of bimetallic zirconium amine bis(phenolate) complexes (**1.60**). These were tested in the homopolymerisation of propylene and 1-hexene and exhibited very high activity and

stereocontrol. Polymers with >75% *meso* linkages were formed and activities exceeding 120 kg mol^{-1} h^{-1} bar^{-1} observed.[257]

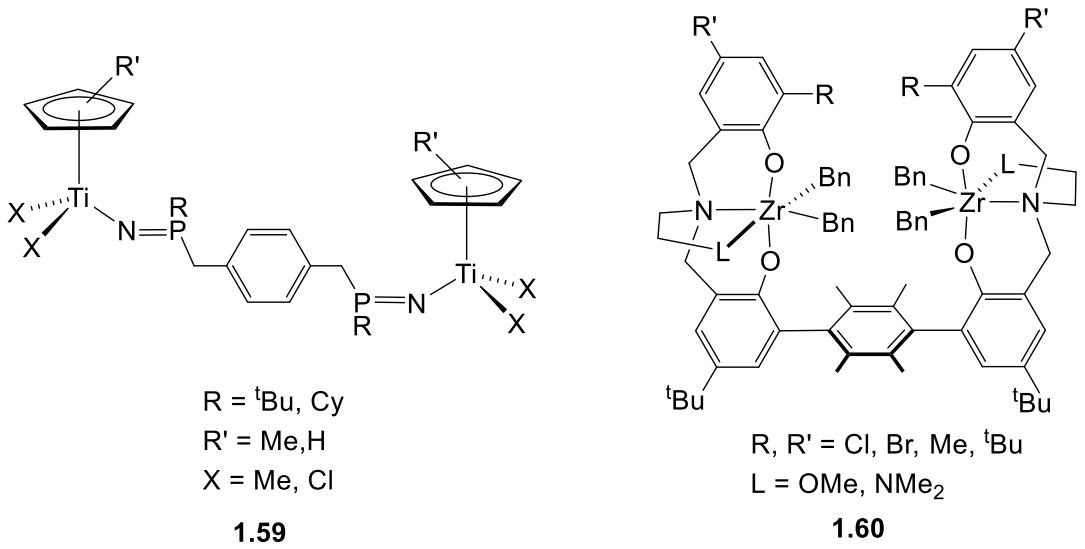

Figure 1.26 Group 4 bimetallic complexes.

1.10.4 Heterobimetallic catalysts

Different covalently tethered single site active metal centres sites have found a large advantage in homogeneous "tandem catalysis". One metal centre produces α-olefin oligomers, which are incorporated into high molecular weight polyethylene by the other metal centre. The advantages are that the branched polymer is formed from one ethylene gas feed and the spatial proximity of the metal centre improves the efficiency of α-olefin incorporation.[241] Marks and co-workers introduced the first covalently linked heterobimetallic constrained geometry polymerisation catalyst with a zirconium and titanium metal site (**1.61**), the monometallic zirconium CGC gives low molecular weight polymer and the titanium counterpart high molecular weight polymers. Long-chain branched polyethylene was produced in ethylene homopolymerisation using complex **1.61** when activated with TBF_{20}. If both monometallic species are present then a heterogeneous mixture of high and low molecular weight polymers are observed. This was proposed to be a result of the spatial proximity incurred by the tether giving rise to cooperative effects. The titanium metal centre is able to efficiently recapture the sizable oligomers produced at the zirconium centre.[258] Heterobimetallic complexes with a single silane bridge reminiscent of **1.53a** were synthesised with a variety of substituents on the untethered cyclopentadienyl ring (**1.62**). They were shown to exhibit a higher activity and

molecular weight capacity (29,000 – 124,000 g mol^{-1}) than their individual monometallic counterparts (25,000 g mol^{-1} for Cp_2ZrCl_2). It was observed that the trend in activities observed for the cyclopentadienyl substituents is the opposite for the molecular weight.[259, 260] Comparable silane bridged Zr/Ti and Zr/Hf heterobimetallic complexes were developed by Green *et al*. A small increase in molecular weight was again observed in ethylene homopolymerisation, but with reduced activities and broader PDI values.[249] Although outside of the scope of this project the use of a heterobimetallic complex in which a Group 4 metal centre is tethered to a metal from another group has been increasingly explored. Cobalt,[261-263] iron,[252] rhodium,[263] ruthenium,[263] manganese,[263] palladium,[262] nickel[262] and chromium[264, 265] have all been employed to varying successes.

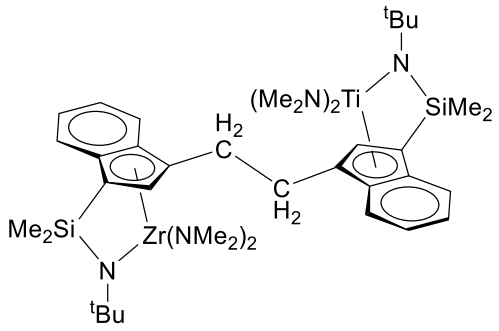

1.61

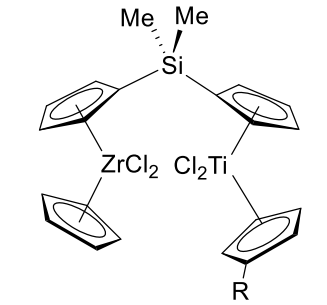

R = Me, benzyl, ^{i}Pr, Cy, allyl

1.62

Figure 1.27 Covalently tethered Group 4 heterobimetallic complexes.

1.11 Summary and objectives

This Chapter has introduced metal-catalysed olefin polymerisation with a specific interest into the post-metallocene catalyst development, the structure and reactivity of the catalytically active cationic species, and finally the more recent bimetallic advances. The progression of post-metallocene catalyst design has been both academically and industrially driven creating an extensively researched and heavily patented field with highly specialised commercially active catalysts produced. There is no evident recipe for what makes an improved bimetallic catalyst with a wide variety of covalently tethered systems employed to differing successes. There has been no comprehensive study for bimetallic catalysis in EPDM copolymerisation. The combinations of metals, substituents and cocatalysts have all been shown to be significant and further examples will be introduced throughout this Thesis. Chapter

Two will explore the synthesis and activation of new phenylene tethered half-sandwich κ^1-amidinate bimetallic precatalysts and appropriate monometallic analogues. In collaboration with LANXESS Elastomers all precatalysts will be investigated for EP and EPDM copolymerisation capabilities. The synthesis and copolymerisation capabilities of more conformationally restrained precatalysts as well as their EPDM copolymerisation capabilities will be discussed in Chapter Three. Chapter Four will introduce two dinuclear cocatalysts and discuss the activation of previously introduced monometallic and bimetallic precatalysts. Chapter Five will discuss Group 4 heterobimetallic complexes as well as a parallel polymerisation reactor (PPR) study to probe this further.

1.12 References

1. M. Stürzel, S. Mihan and R. Mülhaupt, *Chem. Rev.*, 2016, **116**, 1398-1433.
2. G. Natta, *Angew. Chem.*, 1956, **68**, 393-403.
3. D. S. Breslow and N. R. Newburg, *J. Am. Chem. Soc.*, 1957, **79**, 5072-5073.
4. G. Natta, P. Pino, G. Mazzanti and U. Giannini, *J. Am. Chem. Soc.*, 1957, **79**, 2975-2976.
5. G. Wilkinson, P. L. Pauson, J. M. Birmingham and F. A. Cotton, *J. Am. Chem. Soc.*, 1953, **75**, 1011-1012.
6. M. Bochmann, *J. Chem. Soc., Dalton Trans.*, 1996, 255-270.
7. K. H. Reichert and K. R. Meyer, *Makromol. Chem.*, 1973, **169**, 163-176.
8. W. P. Long and D. S. Breslow, *Justus Liebigs Ann. Chem.*, 1975, **1975**, 463-469.
9. A. Andresen, H.-G. Cordes, J. Herwig, W. Kaminsky, A. Merck, R. Mottweiler, J. Pein, H. Sinn and H.-J. Vollmer, *Angew. Chem. Int. Ed. Engl.*, 1976, **15**, 630-632.
10. H. Sinn, W. Kaminsky, F. G. A. Stone and W. Robert, in Adv. Organomet. Chem., Academic Press, 1980, vol. 18, pp. 99-149.
11. H. Sinn, W. Kaminsky, H.-J. Vollmer and R. Woldt, *Angew. Chem. Int. Ed. Engl.*, 1980, **19**, 390-392.
12. A. K. Zefirova and A. E. Shilov, *Dokl. Akad. Nauk*, 1961, **136**, 599-602.
13. F. S. Dyachkovskii, A. K. Shilova and A. E. Shilov, *J. Polym. Sci., Polym. Symp.*, 1967, **No. 16**, 2333-2339.

14. J. J. Eisch, A. M. Piotrowski, S. K. Brownstein, E. J. Gabe and F. L. Lee, *J. Am. Chem. Soc.*, 1985, **107**, 7219-7221.
15. P. Cossee, *J. Catal.*, 1964, **3**, 80-88.
16. E. J. Arlman and P. Cossee, *J. Catal.*, 1964, **3**, 99-104.
17. K. J. Ivin, J. J. Rooney, C. D. Stewart, M. L. H. Green and R. Mahtab, *J. Chem. Soc., Chem. Commun.*, 1978, 604-606.
18. Z. Dawoodi, M. L. H. Green, V. S. B. Mtetwa and K. Prout, *J. Chem. Soc., Chem. Commun.*, 1982, 1410-1411.
19. D. T. Laverty and J. J. Rooney, *J. Chem. Soc., Faraday Trans.*, 1983, **79**, 869-878.
20. M. Brookhart and M. L. H. Green, *J. Organomet. Chem.*, 1983, **250**, 395-408.
21. H. Krauledat and H.-H. Brintzinger, *Angew. Chem. Int. Ed. Engl.*, 1990, **29**, 1412-1413.
22. M. K. Leclerc and H. H. Brintzinger, *J. Am. Chem. Soc.*, 1995, **117**, 1651-1652.
23. H. H. Brintzinger, D. Fischer, R. Mülhaupt, B. Rieger and R. M. Waymouth, *Angew. Chem. Int. Ed. Engl.*, 1995, **34**, 1143-1170.
24. R. H. Grubbs and G. W. Coates, *Acc. Chem. Res.*, 1996, **29**, 85-93.
25. S. Hajela and J. E. Bercaw, *Organometallics*, 1994, **13**, 1147-1154.
26. S. Miya, T. Mise and H. Yamazaki, *Stud. Surf. Sci. Catal.*, 1990, **56**, 531-534.
27. L. Resconi, F. Piemontesi, G. Franciscono, L. Abis and T. Fiorani, *J. Am. Chem. Soc.*, 1992, **114**, 1025-1032.
28. L. Resconi, F. Piemontesi, I. Camurati, D. Balboni, A. Sironi, M. Moret, H. Rychlicki and R. Zeigler, *Organometallics*, 1996, **15**, 5046-5059.
29. Z. Guo, D. C. Swenson and R. F. Jordan, *Organometallics*, 1994, **13**, 1424-1432.
30. J. J. W. Eshuis, Y. Y. Tan, J. H. Teuben and J. Renkema, *J. Mol. Catal.*, 1990, **62**, 277-287.
31. P. Margl, L. Deng and T. Ziegler, *Top. Catal.*, 1999, **7**, 187-208.
32. M.-H. Prosenc and H.-H. Brintzinger, *Organometallics*, 1997, **16**, 3889-3894.
33. L. Li, M. V. Metz, H. Li, M.-C. Chen, T. J. Marks, L. Liable-Sands and A. L. Rheingold, *J. Am. Chem. Soc.*, 2002, **124**, 12725-12741.
34. Z. Liu, E. Somsook, C. B. White, K. A. Rosaaen and C. R. Landis, *J. Am. Chem. Soc.*, 2001, **123**, 11193-11207.

35. S. Lin, C. D. Tagge, R. M. Waymouth, M. Nele, S. Collins and J. C. Pinto, *J. Am. Chem. Soc.*, 2000, **122**, 11275-11285.
36. J. C. W. Chien and A. Razavi, *Journal of Polymer Science, Part A: Polymer Chemistry*, 1988, **26**, 2369-2380.
37. L. Resconi, S. Bossi and L. Abis, *Macromolecules*, 1990, **23**, 4489-4491.
38. N. Naga and K. Mizunuma, *Polymer*, 1998, **39**, 5059-5067.
39. M. G. Klimpel, J. Eppinger, P. Sirsch, W. Scherer and R. Anwander, *Organometallics*, 2002, **21**, 4021-4023.
40. M. van Meurs, G. J. P. Britovsek, V. C. Gibson and S. A. Cohen, *J. Am. Chem. Soc.*, 2005, **127**, 9913-9923.
41. G. J. P. Britovsek, S. A. Cohen, V. C. Gibson and M. van Meurs, *J. Am. Chem. Soc.*, 2004, **126**, 10701-10712.
42. J. Wei, W. Zhang and L. R. Sita, *Angew. Chem. Int. Ed.*, 2010, **49**, 1768-1772.
43. J. Wei, W. Hwang, W. Zhang and L. R. Sita, *J. Am. Chem. Soc.*, 2013, **135**, 2132-2135.
44. L. R. Sita, *Angew. Chem., Int. Ed.*, 2009, **48**, 2464-2472.
45. Y. V. Kissin, R. I. Mink and T. E. Nowlin, *J. Polym. Sci., Part A: Polym. Chem.*, 1999, **37**, 4255-4272.
46. Y. V. Kissin and A. J. Brandolini, *J. Polym. Sci., Part A: Polym. Chem.*, 1999, **37**, 4273-4280.
47. Y. V. Kissin, R. I. Mink, T. E. Nowlin and A. J. Brandolini, *J. Polym. Sci., Part A: Polym. Chem.*, 1999, **37**, 4281-4294.
48. S. W. Ewart, M. A. Parent and M. C. Baird, *J. Polym. Sci., Part A: Polym. Chem.*, 1999, **37**, 4386-4389.
49. H. Mori, M. Endo and M. Terano, *J. Mol. Catal. A: Chem.*, 1999, **145**, 211-220.
50. A. Rudin and H. L. W. Hoegy, *J. Polym. Sci., Part A: Polym. Chem.*, 1972, **10**, 217-235.
51. G. Odian, Principles of Polymerisation, Wiley-Interscience, 1992.
52. P. J. Flory, Principles of Polymer Chemistry, Cornell University Press, 1992.
53. H. Kawamura-Kuribayashi, N. Koga and K. Morokuma, *J. Am. Chem. Soc.*, 1992, **114**, 8687-8694.
54. G. W. Coates, *Chem. Rev.*, 2000, **100**, 1223-1252.

55. P. D. Hustad, J. Tian and G. W. Coates, *J. Am. Chem. Soc.*, 2002, **124**, 3614-3621.
56. T. Miyatake, K. Mizunuma and M. Kakugo, *Makromol. Chem.-M. Symp.*, 1993, **66**, 203-214.
57. L. Resconi and G. Moscardi, *Polym. Prepr. (Am. Chem. Soc., Div. Polym. Chem.)*, 1997, **38**, 832-833.
58. G. Natta, I. Pasquon and A. Zambelli, *J. Am. Chem. Soc.*, 1962, **84**, 1488-1490.
59. B. L. Small, M. Brookhart and A. M. A. Bennett, *J. Am. Chem. Soc.*, 1998, **120**, 4049-4050.
60. G. J. P. Britovsek, V. C. Gibson, B. S. Kimberley, P. J. Maddox, S. J. McTavish, G. A. Solan, A. J. P. White and D. J. Williams, *Chem. Commun.*, 1998, 849-850.
61. L. Resconi, L. Cavallo, A. Fait and F. Piemontesi, *Chem. Rev.*, 2000, **100**, 1253-1346.
62. K. Angermund, G. Fink, V. R. Jensen and R. Kleinschmidt, *Chem. Rev.*, 2000, **100**, 1457-1470.
63. V. Busico and R. Cipullo, *Prog. Polym. Sci.*, 2001, **26**, 443-533.
64. F. A. Bovey and P. A. Mirau, NMR of Polymers, Academic, 1996.
65. M. C. Baier, M. Zuideveld and S. Mecking, *Angew. Chem. Int. Ed.*, 2014, **53**, 9722-9744.
66. W. Kaminsky and M. Miri, *J. Polym. Sci.: Polym. Chem. Ed.*, 1985, **23**, 2151-2164.
67. A. Ostoja Starzewski, N. Steinhauser and B. S. Xin, *Macromolecules*, 2008, **41**, 4095-4101.
68. M. C. Haag, J. H. Z. Dos Santos, F. C. Stedile and J. Dupont, *J. Appl. Polym. Sci.*, 1999, **74**, 1997-2003.
69. http://www.marketsandmarkets.com/Market-Reports/epdm-rubber-market-483.html.
70. G. J. P. Britovsek, V. C. Gibson and D. F. Wass, *Angew. Chem. Int. Ed.*, 1999, **38**, 428-447.
71. F. R. W. P. Wild, L. Zsolnai, G. Huttner and H. H. Brintzinger, *J. Organomet. Chem.*, 1982, **232**, 233-247.
72. J. A. Ewen, *J. Am. Chem. Soc.*, 1984, **106**, 6355-6364.

73. W. Kaminsky, K. Külper, H. H. Brintzinger and F. Wild, *Angew. Chem. Int. Ed. Engl.*, 1985, **24**, 507-508.
74. M. C. Sacchi, E. Barsties, I. Tritto, P. Locatelli, H.-H. Brintzinger and U. Stehling, *Macromolecules*, 1997, **30**, 3955-3957.
75. P. Longo, A. Grassi, C. Pellecchia and A. Zambelli, *Macromolecules*, 1987, **20**, 1015-1018.
76. W. Spaleck, M. Antberg, J. Rohrmann, A. Winter, B. Bachmann, P. Kiprof, J. Behm and W. A. Herrmann, *Angew. Chem. Int. Ed. Engl.*, 1992, **31**, 1347-1350.
77. W. Spaleck, F. Kueber, A. Winter, J. Rohrmann, B. Bachmann, M. Antberg, V. Dolle and E. F. Paulus, *Organometallics*, 1994, **13**, 954-963.
78. W. Spaleck, M. Aulbach, B. Bachmann, F. Küber and A. Winter, *Macromol. Symp.*, 1995, **89**, 237-247.
79. U. Stehling, J. Diebold, R. Kirsten, W. Roell, H. H. Brintzinger, S. Juengling, R. Muelhaupt and F. Langhauser, *Organometallics*, 1994, **13**, 964-970.
80. J. A. Ewen, R. L. Jones, A. Razavi and J. D. Ferrara, *J. Am. Chem. Soc.*, 1988, **110**, 6255-6256.
81. P. J. Shapiro, E. Bunel, W. P. Schaefer and J. E. Bercaw, *Organometallics*, 1990, **9**, 867-869.
82. J. Okuda, *Chem. Ber.*, 1990, **123**, 1649-1651.
83. J. C. Stevens, F. J. Timmers, D. R. Wilson, G. F. Schmidt, P. N. Nickias, R. K. Rosen, G. W. Knight and S. Y. Lai, *EP416815A2*, 1991.
84. J. C. Stevens and D. R. Neithamer, *EP418044A2*, 1991.
85. R. K. Rosen, P. N. Nickias, D. D. Devore and F. J. Timmers, *WO9319104A1*, 1993.
86. R. K. Rosen, P. N. Nickias, D. D. Devore, J. C. Stevens and F. J. Timmers, *US5374696A*, 1994.
87. J. A. M. Canich, H. W. Turner and G. G. Hlatky, *US5621126A*, 1997.
88. J. A. M. Canich, *US5026798A*, 1991.
89. J. A. M. Canich, *EP420436A1*, 1991.
90. J. A. M. Canich, *US5096867A*, 1992.
91. J. C. Stevens and T. Kazuo Soga and Minoru, in Stud. Surf. Sci. Catal., Elsevier, 1994, vol. Volume 89, pp. 277-284.

92. H. Braunschweig and F. M. Breitling, *Coord. Chem. Rev.*, 2006, **250**, 2691-2720.
93. J. C. Stevens, in Stud. Surf. Sci. Catal., Elsevier, 1996, vol. 101, pp. 11-20.
94. G. J. M. Gruter, M. Kranenburg and M. Herklots, *EP919571A1,* 1999.
95. J. A. M. Van Beek, G. H. J. Van Doremaele, G. J. M. Gruter, H. J. Arts and G. H. M. R. Eggels, *WO9613529A1*, 1996.
96. A. Berthoud, V. Q. Norambuena, G. Van Doremaele, M. A. Zuideveld, R. T. W. Scott and P. Mountford, *EP2801578A1*, 2014.
97. R. Hoffmann, *Angew. Chem. Int. Ed.*, 1982, **21**, 711-724.
98. D. W. Stephan, *Organometallics*, 2005, **24**, 2548-2560.
99. T. Rübenstahl, F. Weller, S. Wocadlo, W. Massa and K. Dehnicke, *Z. Anorg. Allg. Chem.*, 1995, **621**, 953-958.
100. S. Anfang, K. Harms, F. Weller, O. Borgmeier, H. Lueken, H. Schilder and K. Dehnicke, *Z. Anorg. Allg. Chem.*, 1998, **624**, 159-166.
101. T. V. Lubben, P. T. Wolczanski and G. D. Van Duyne, *Organometallics*, 1984, **3**, 977-983.
102. D. W. Stephan, J. C. Stewart, F. Guerin, S. Courtenay, J. Kickham, E. Hollink, C. Beddie, A. Hoskin, T. Graham, P. Wei, R. E. v. H. Spence, W. Xu, L. Koch, X. Gao and D. G. Harrison, *Organometallics*, 2003, **22**, 1937-1947.
103. D. W. Stephan, J. C. Stewart, F. Guérin, R. E. v. H. Spence, W. Xu and D. G. Harrison, *Organometallics*, 1999, **18**, 1116-1118.
104. P.-J. Sinnema, T. P. Spaniol and J. Okuda, *J. Organomet. Chem.*, 2000, **598**, 179-181.
105. K. Nomura and K. Fujii, *Organometallics*, 2002, **21**, 3042-3049.
106. K. Nomura and K. Fujii, *Macromolecules*, 2003, **36**, 2633-2641.
107. I. Saeed, S. Katao and K. Nomura, *Organometallics*, 2009, **28**, 111-122.
108. J. McMeeking, X. Gao, H. S. R. E. von, S. J. Brown and D. Jeremic, *WO9914250A1*, 1999.
109. K. Nomura, K. Fujita and M. Fujiki, *J. Mol. Catal. A: Chem.*, 2004, **220**, 133-144.
110. H. Zhang and K. Nomura, *J. Am. Chem. Soc.*, 2005, **127**, 9364-9365.
111. M. Večeřa, V. Varga, I. Císařová, J. Pinkas, P. Kucharczyk, V. Sedlařík and M. Lamač, *Organometallics,* 2016, **35**, 785-798.

112. M. A. Grima, M. van Boggelen, M. Dees, G. van Doremaele, M. van Duin and P. Henricks-Knape, *Rubber World*, 2014, **250**, 37-43.
113. M. A. Zuideveld, R. T. W. Scott and P. Mountford, *EP2801579A1*, 2014.
114. http://www.keltan.com/en/home.
115. http://www.arlanxeo.com.
116. W. P. Kretschmer, C. Dijkhuis, A. Meetsma, B. Hessen and J. H. Teuben, *Chem. Commun.*, 2002, 608-609.
117. M. Tamm, S. Randoll, T. Bannenberg and E. Herdtweck, *Chem. Commun.*, 2004, 876-877.
118. M. Tamm, S. Randoll, E. Herdtweck, N. Kleigrewe, G. Kehr, G. Erker and B. Rieger, *Dalton Trans.*, 2006, 459-467.
119. K. Nomura, H. Fukuda, S. Katao, M. Fujiki, H. J. Kim, D.-H. Kim and S. Zhang, *Dalton Trans.*, 2011, **40**, 7842-7849.
120. K. Nomura, S. Patamma, H. Matsuda, S. Katao, K. Tsutsumi and H. Fukuda, *RSC Advances*, 2015, **5**, 64503-64513.
121. G. H. J. van Doremaele, M. A. Zuideveld, N. V. F. Quiroga and A. Leblanc, *WO2011054927A1*, 2011.
122. K. Nomura, N. Naga, M. Miki, K. Yanagi and A. Imai, *Organometallics*, 1998, **17**, 2152-2154.
123. K. Nomura, N. Naga, M. Miki and K. Yanagi, *Macromolecules*, 1998, **31**, 7588-7597.
124. K. Nomura, M. Tsubota and M. Fujiki, *Macromolecules*, 2003, **36**, 3797-3799.
125. Y. Qian, H. Zhang, X. Qian, J. Huang and C. Shen, *J. Mol. Catal. A: Chem.*, 2003, **192**, 25-33.
126. A. E. Fenwick, K. Phomphrai, M. G. Thorn, J. S. Vilardo, C. A. Trefun, B. Hanna, P. E. Fanwick and I. P. Rothwell, *Organometallics*, 2004, **23**, 2146-2156.
127. W. Wang, T. Tanaka, M. Tsubota, M. Fujiki, S. Yamanaka and K. Nomura, *Adv. Synth. Catal.*, 2005, **347**, 433-446.
128. D. L. Reger, R. Mahtab, J. C. Baxter and L. Lebioda, *Inorg. Chem.*, 1986, **25**, 2046-2048.
129. L. E. Manzer, *J. Organomet. Chem.*, 1975, **102**, 167-174.
130. H. Nakazawa, S. Ikai, K. Imaoka, Y. Kai and T. Yano, *J. Mol. Catal. A: Chem.*, 1998, **132**, 33-41.

131. A. N. Chernega, R. Gomez and M. L. H. Green, *J. Chem. Soc., Chem. Commun.*, 1993, 1415-1417.
132. R. Gomez, M. L. H. Green and J. L. Haggitt, *J. Chem. Soc., Chem. Commun.*, 1994, 2607-2608.
133. R. Gomez, R. Duchateau, A. N. Chernega, J. H. Teuben, F. T. Edelmann and M. L. H. Green, *J. Organomet. Chem.*, 1995, **491**, 153-158.
134. L. R. Sita and J. R. Babcock, *Organometallics*, 1998, **17**, 5228-5230.
135. L. A. Koterwas, J. C. Fettinger and L. R. Sita, *Organometallics*, 1999, **18**, 4183-4190.
136. K. C. Jayaratne and L. R. Sita, *J. Am. Chem. Soc.*, 2000, **122**, 958-959.
137. H. Tsurugi, K. Yamamoto, R. Rochat and K. Mashima, *Polym. J. (Tokyo, Jpn.)*, 2015, **47**, 2-17.
138. S. Trofimenko, *J. Am. Chem. Soc.*, 1966, **88**, 1842-1844.
139. S. Trofimenko, *J. Am. Chem. Soc.*, 1967, **89**, 3904-3905.
140. S. Trofimenko, *J. Am. Chem. Soc.*, 1967, **89**, 6288-6294.
141. S. Trofimenko, Scorpionates: The Coordination Chemistry of Polypyrazolylborate Ligands, 1999.
142. H. R. Bigmore, S. C. Lawrence, P. Mountford and C. S. Tredget, *Dalton Trans.*, 2005, 635-651.
143. H. Bigmore, DPhil Thesis, University of Oxford, 2007.
144. L. Clark, Part II Thesis, University of Oxford, 2008.
145. K. Michiue and R. F. Jordan, *Organometallics*, 2004, **23**, 460-470.
146. M. P. Gil, S. J. H. Z. Dos and O. L. Casagrande, Jr., *Macromol. Chem. Phys.*, 2001, **202**, 319-324.
147. M. P. Gil and O. L. Casagrande, *J. Organomet. Chem.*, 2004, **689**, 286-292.
148. M. P. Gil, S. J. H. Z. dos and O. L. Casagrande, *J. Mol. Catal. A: Chem.*, 2004, **209**, 163-169.
149. L. G. Furlan, M. P. Gil and O. L. Casagrande, Jr., *Macromol. Rapid Commun.*, 2000, **21**, 1054-1057.
150. N. Hazari and P. Mountford, *Acc. Chem. Res.*, 2005, **38**, 839-849.
151. H. R. Bigmore, M. A. Zuideveld, R. M. Kowalczyk, A. R. Cowley, M. Kranenburg, E. J. L. McInnes and P. Mountford, *Inorg. Chem.*, 2006, **45**, 6411-6423.

152. H. R. Bigmore, S. R. Dubberley, M. Kranenburg, S. C. Lawrence, A. J. Sealey, J. D. Selby, M. A. Zuideveld, A. R. Cowley and P. Mountford, *Chem. Commun.*, 2006, 436-438.

153. P. D. Bolton, E. Clot, N. Adams, S. R. Dubberley, A. R. Cowley and P. Mountford, *Organometallics*, 2006, **25**, 2806-2825.

154. N. Adams, H. J. Arts, P. D. Bolton, D. Cowell, S. R. Dubberley, N. Friederichs, C. M. Grant, M. Kranenburg, A. J. Sealey, B. Wang, P. J. Wilson, M. Zuideveld, A. J. Blake, M. Schroeder and P. Mountford, *Organometallics*, 2006, **25**, 3888-3903.

155. P. D. Bolton, N. Adams, E. Clot, A. R. Cowley, P. J. Wilson, M. Schroeder and P. Mountford, *Organometallics*, 2006, **25**, 5549-5565.

156. P. D. Bolton, E. Clot, A. R. Cowley and P. Mountford, *J. Am. Chem. Soc.*, 2006, **128**, 15005-15018.

157. J. C. Green, *Chem. Soc. Rev.*, 1998, **27**, 263-272.

158. C. Janiak, K. C. H. Lange, U. Versteeg, D. Lentz and P. H. M. Budzelaar, *Chem. Ber.*, 1996, **129**, 1517-1529.

159. G. C. Bazan, G. Rodriguez, A. J. Ashe, S. Al-Ahmad and C. Müller, *J. Am. Chem. Soc.*, 1996, **118**, 2291-2292.

160. G. C. Bazan, G. Rodriguez, A. J. Ashe, S. Al-Ahmad and J. W. Kampf, *Organometallics*, 1997, **16**, 2492-2494.

161. J. S. Rogers, G. C. Bazan and C. K. Sperry, *J. Am. Chem. Soc.*, 1997, **119**, 9305-9306.

162. S. J. Skoog, C. Mateo, G. G. Lavoie, F. J. Hollander and R. G. Bergman, *Organometallics* 2000, **19**, 1406-1421.

163. G. G. Lavoie and R. G. Bergman, *Angew. Chem. Int. Ed. Engl.*, 1997, **36**, 2450-2452.

164. J. Klosin, P. P. Fontaine and R. Figueroa, *Acc. Chem. Res.*, 2015, **48**, 2004-2016.

165. J. D. Scollard and D. H. McConville, *J. Am. Chem. Soc.*, 1996, **118**, 10008-10009.

166. J. D. Scollard, D. H. McConville, N. C. Payne and J. J. Vittal, *Macromolecules*, 1996, **29**, 5241-5243.

167. P. De Waele, B. A. Jazdzewski, J. Klosin, R. E. Murray, C. N. Theriault, P. C. Vosejpka and J. L. Petersen, *Organometallics*, 2007, **26**, 3896-3899.

168. R. D. J. Froese, B. A. Jazdzewski, J. Klosin, R. L. Kuhlman, C. N. Theriault, D. M. Welsh and K. A. Abboud, *Organometallics*, 2011, **30**, 251-262.

169. R. Figueroa, R. D. Froese, Y. He, J. Klosin, C. N. Theriault and K. A. Abboud, *Organometallics*, 2011, **30**, 1695-1709.

170. K. A. Frazier, R. D. Froese, Y. He, J. Klosin, C. N. Theriault, P. C. Vosejpka, Z. Zhou and K. A. Abboud, *Organometallics*, 2011, **30**, 3318-3329.

171. E. Szuromi, J. Klosin and K. A. Abboud, *Organometallics*, 2011, **30**, 4589-4597.

172. T. R. Boussie, G. M. Diamond, C. Goh, K. A. Hall, A. M. LaPointe, M. K. Leclerc, V. Murphy, J. A. W. Shoemaker, H. Turner, R. K. Rosen, J. C. Stevens, F. Alfano, V. Busico, R. Cipullo and G. Talarico, *Angew. Chem. Int. Ed.*, 2006, **45**, 3278-3283.

173. G. J. Domski, E. B. Lobkovsky and G. W. Coates, *Macromolecules*, 2007, **40**, 3510-3513.

174. R. D. J. Froese, P. D. Hustad, R. L. Kuhlman and T. T. Wenzel, *J. Am. Chem. Soc.*, 2007, **129**, 7831-7840.

175. C. Zuccaccia, A. Macchioni, V. Busico, R. Cipullo, G. Talarico, F. Alfano, H. W. Boone, K. A. Frazier, P. D. Hustad, J. C. Stevens, P. C. Vosejpka and K. A. Abboud, *J. Am. Chem. Soc.*, 2008, **130**, 10354-10368.

176. C. Zuccaccia, V. Busico, R. Cipullo, G. Talarico, R. D. J. Froese, P. C. Vosejpka, P. D. Hustad and A. Macchioni, *Organometallics*, 2009, **28**, 5445-5458.

177. M. Hafeez, W. P. Kretschmer and R. Kempe, *Eur. J. Inorg. Chem.*, 2011, **2011**, 5512-5522.

178. A. Noor, W. P. Kretschmer, G. Glatz and R. Kempe, *Inorg. Chem.*, 2011, **50**, 4598-4606.

179. M. Hafeez, W. P. Kretschmer and R. Kempe, *Z. Anorg. Allg. Chem.*, 2012, **638**, 324-330.

180. H. Makio, H. Terao, A. Iwashita and T. Fujita, *Chem. Rev.*, 2011, **111**, 2363-2449.

181. S. Matsui, M. Mitani, J. Saito, Y. Tohi, H. Makio, N. Matsukawa, Y. Takagi, K. Tsuru, M. Nitabaru, T. Nakano, H. Tanaka, N. Kashiwa and T. Fujita, *J. Am. Chem. Soc.*, 2001, **123**, 6847-6856.

182. H. Makio, N. Kashiwa and T. Fujita, *Adv. Synth. Catal.*, 2002, **344**, 477-493.

183. J. Tian, P. D. Hustad and G. W. Coates, *J. Am. Chem. Soc.*, 2001, **123**, 5134-5135.
184. J. Saito, M. Mitani, J.-I. Mohri, Y. Yoshida, S. Matsui, S.-I. Ishii, S.-I. Kojoh, N. Kashiwa and T. Fujita, *Angew. Chem. Int. Ed.*, 2001, **40**, 2918-2920.
185. M. Mitani, J.-i. Mohri, Y. Yoshida, J. Saito, S. Ishii, K. Tsuru, S. Matsui, R. Furuyama, T. Nakano, H. Tanaka, S.-i. Kojoh, T. Matsugi, N. Kashiwa and T. Fujita, *J. Am. Chem. Soc.*, 2002, **124**, 3327-3336.
186. E. Y. Tshuva, I. Goldberg and M. Kol, *J. Am. Chem. Soc.*, 2000, **122**, 10706-10707.
187. W. Kaminsky and R. Steiger, *Polyhedron*, 1988, **7**, 2375-2381.
188. D. Cam and U. Giannini, *Makromol. Chem.*, 1992, **193**, 1049-1055.
189. A. R. Siedle, R. A. Newmark, W. M. Lamanna and J. N. Schroepfer, *Polyhedron*, 1990, **9**, 301-308.
190. I. Tritto, S. Li, M. C. Sacchi and G. Zannoni, *Macromolecules*, 1993, **26**, 7111-7115.
191. I. Tritto, S. X. Li, M. C. Sacchi, P. Locatelli and G. Zannoni, *Macromolecules*, 1995, **28**, 5358-5362.
192. M. Bochmann, *J. Organomet. Chem.*, 2004, **689**, 3982-3998.
193. K. P. Bryliakov, N. V. Semikolenova, D. V. Yudaev, V. A. Zakharov, H. H. Brintzinger, M. Ystenes, E. Rytter and E. P. Talsi, *J. Organomet. Chem.*, 2003, **683**, 92-102.
194. M. Bochmann and S. J. Lancaster, *Angew. Chem. Int. Ed. Engl.*, 1994, **33**, 1634-1637.
195. E. Y.-X. Chen and T. J. Marks, *Chem. Rev.*, 2000, **100**, 1391-1434.
196. A. G. Massey and A. J. Park, *J. Organomet. Chem.*, 1964, **2**, 245-250.
197. X. Yang, C. L. Stern and T. J. Marks, *J. Am. Chem. Soc.*, 1991, **113**, 3623-3625.
198. X. Yang, C. L. Stern and T. J. Marks, *J. Am. Chem. Soc.*, 1994, **116**, 10015-10031.
199. M. J. Elder and J. A. Ewen, *Eur. Pat. Appl. 0 426 637*, 1991.
200. Y.-X. Chen and T. J. Marks, *Organometallics*, 1997, **16**, 3649-3657.
201. M. Bochmann, L. M. Wilson, M. B. Hursthouse and R. L. Short, *Organometallics*, 1987, **6**, 2556-2563.
202. H. W. Turner, *EP277004*, 1988.

203. G. G. Hlatky, H. W. Turner and R. R. Eckman, *J. Am. Chem. Soc.*, 1989, **111**, 2728-2729.

204. A. D. Horton, J. de With, A. J. van der Linden and H. van de Weg, *Organometallics*, 1996, **15**, 2672-2674.

205. J. S. J. McCahill, G. C. Welch and D. W. Stephan, *Dalton Trans.*, 2009, 8555-8561.

206. R. F. Jordan, W. E. Dasher and S. F. Echols, *J. Am. Chem. Soc.*, 1986, **108**, 1718-1719.

207. R. F. Jordan, R. E. LaPointe, C. S. Bajgur, S. F. Echols and R. Willett, *J. Am. Chem. Soc.*, 1987, **109**, 4111-4113.

208. M. Bochmann, A. J. Jaggar, L. M. Wilson, M. B. Hursthouse and M. Motevalli, *Polyhedron*, 1989, **8**, 1838-1843.

209. Manfred Bochmann, Andrew J. Jagger and J. C. Nicholls, *Angew. Chem. Int. Ed.*, 1990, **29**, 780-782.

210. X. Yang, C. Stern and T. J. Marks, *Organometallics*, 1991, **10**, 840-842.

211. F. Guerin, J. C. Stewart, C. Beddie and D. W. Stephan, *Organometallics*, 2000, **19**, 2994-3000.

212. J. D. Scollard, D. H. McConville and S. J. Rettig, *Organometallics*, 1997, **16**, 1810-1812.

213. M. Bochmann and S. J. Lancaster, *Organometallics*, 1993, **12**, 633-640.

214. X. Bei, D. C. Swenson and R. F. Jordan, *Organometallics*, 1997, **16**, 3282-3302.

215. R. F. Jordan, P. K. Bradley, N. C. Baenziger and R. E. LaPointe, *J. Am. Chem. Soc.*, 1990, **112**, 1289-1291.

216. L. H. Doerrer, M. L. H. Green, D. Haussinger and J. Sassmannshausen, *J. Chem. Soc., Dalton Trans.*, 1999, 2111-2118.

217. F. Song, S. J. Lancaster, R. D. Cannon, M. Schormann, S. M. Humphrey, C. Zuccaccia, A. Macchioni and M. Bochmann, *Organometallics*, 2005, **24**, 1315-1328.

218. P. D. Bolton, E. Clot, A. R. Cowley and P. Mountford, *Chem. Commun.*, 2005, 3313-3315.

219. L. Jia, X. Yang, C. L. Stern and T. J. Marks, *Organometallics*, 1997, **16**, 842-857.

220. M. D. Butts, B. L. Scott and G. J. Kubas, *J. Am. Chem. Soc.*, 1996, **118**, 11831-11843.

221. R. J. Kulawiec, J. W. Faller and R. H. Crabtree, *Organometallics*, 1990, **9**, 745-755.

222. F. Wu, A. K. Dash and R. F. Jordan, *J. Am. Chem. Soc.*, 2004, **126**, 15360-15361.

223. E. G. Ijpeij, B. Coussens, M. A. Zuideveld, G. H. J. van Doremaele, P. Mountford, M. Lutz and A. L. Spek, *Chem. Commun.*, 2010, **46**, 3339-3341.

224. R. J. Keaton, K. C. Jayaratne, J. C. Fettinger and L. R. Sita, *J. Am. Chem. Soc.*, 2000, **122**, 12909-12910.

225. R. F. Jordan, F. G. A. Stone and W. Robert, in Adv. Organomet. Chem., Academic Press, 1991, vol. 32, pp. 325-387.

226. L. Resconi, J. C. Chadwick and L. Cavallo, in Comprehensive Organometallic Chemistry III, ed. R. H. Crabtree, Elsevier, Oxford, 2007, pp. 1005-1166.

227. T. Fujita and H. Makio, in Comprehensive Organometallic Chemistry III, ed. R. H. Crabtree, Elsevier, Oxford, 2007, pp. 691-734.

228. M. Bochmann and L. M. Wilson, *J. Chem. Soc., Chem. Commun.*, 1986, 1610-1611.

229. Y. W. Alelyunas, R. F. Jordan, S. F. Echols, S. L. Borkowsky and P. K. Bradley, *Organometallics*, 1991, **10**, 1406-1416.

230. C. Pellecchia, A. Immirzi, A. Grassi and A. Zambelli, *Organometallics*, 1993, **12**, 4473-4478.

231. C. Pellecchia, A. Grassi and A. Zambelli, *Organometallics*, 1994, **13**, 298-302.

232. C. Pellecchia, A. Immirzi and A. Zambelli, *J. Organomet. Chem.*, 1994, **479**, c9-c11.

233. A. D. Horton and J. de With, *Organometallics*, 1997, **16**, 5424-5436.

234. M. Vatamanu, G. Stojcevic and M. C. Baird, *J. Am. Chem. Soc.*, 2007, **130**, 454-456.

235. F. Sauriol, J. F. Sonnenberg, S. J. Chadder, A. F. Dunlop-Brière, M. C. Baird and P. H. M. Budzelaar, *J. Am. Chem. Soc.*, 2010, **132**, 13357-13370.

236. R. F. Jordan, D. F. Taylor and N. C. Baenziger, *Organometallics*, 1990, **9**, 1546-1557.

237. R. F. Jordan and A. S. Guram, *Organometallics*, 1990, **9**, 2116-2123.

238. K. Yamatsugu, L. Yin, S. Kamijo, Y. Kimura, M. Kanai and M. Shibasaki, *Angew. Chem. Int. Ed.*, 2009, **48**, 1070-1076.
239. N. Kato, T. Mita, M. Kanai, B. Therrien, M. Kawano, K. Yamaguchi, H. Danjo, Y. Sei, A. Sato, S. Furusho and M. Shibasaki, *J. Am. Chem. Soc.*, 2006, **128**, 6768-6769.
240. H. Li and T. J. Marks, *Proc. Natl. Acad. Sci. U. S. A.*, 2006, **103**, 15295-15302.
241. M. Delferro and T. J. Marks, *Chem. Rev.*, 2011, **111**, 2450-2485.
242. H. Li, L. Li and T. J. Marks, *Angew. Chem. Int. Ed.*, 2004, **43**, 4937-4940.
243. H. Li, C. L. Stern and T. J. Marks, *Macromolecules*, 2005, **38**, 9015-9027.
244. A. Motta, I. L. Fragalà and T. J. Marks, *J. Am. Chem. Soc.*, 2009, **131**, 3974-3984.
245. L. Caporaso, L. Izzo, I. Sisti and L. Oliva, *Macromolecules*, 2002, **35**, 4866-4870.
246. N. Guo, C. L. Stern and T. J. Marks, *J. Am. Chem. Soc.*, 2008, **130**, 2246-2261.
247. N. Guo, L. Li and T. J. Marks, *J. Am. Chem. Soc.*, 2004, **126**, 6542-6543.
248. S. K. Noh, J. Kim, J. Jung, C. S. Ra, D.-h. Lee, H. B. Lee, S. W. Lee and W. S. Huh, *J. Organomet. Chem.*, 1999, **580**, 90-97.
249. T. Ushioda, M. L. H. Green, J. Haggitt and X. Yan, *J. Organomet. Chem.*, 1996, **518**, 155-166.
250. S. K. Noh, S. Kim, J. Kim, D.-H. Lee, K.-B. Yoon, H.-B. Lee, S. W. Lee and W. S. Huh, *J. Polym. Sci., Part A: Polym. Chem.*, 1997, **35**, 3717-3728.
251. G. Tian, B. Wang, S. Xu, X. Zhou, B. Liang, L. Zhao, F. Zou and Y. Li, *Macromol. Chem. Phys.*, 2002, **203**, 31-36.
252. J. Kuwabara, D. Takeuchi and K. Osakada, *Organometallics*, 2005, **24**, 2705-2712.
253. J. Cano Sierra, D. Hüerländer, M. Hill, G. Kehr, G. Erker and R. Fröhlich, *Chem. Eur. J.*, 2003, **9**, 3618-3622.
254. S. K. Noh, S. Kim, Y. Yang, W. S. Lyoo and D.-H. Lee, *Eur. Polym. J.*, 2004, **40**, 227-235.
255. S. C. Yoon, S. Y. Choi, S. H. Park, J. E. Kim and M. H. Lee, *KR2015081925A*, 2015.
256. E. Hollink, P. Wei and D. W. Stephan, *Can. J. Chem.*, 2004, **82**, 1304-1313.

257. M. R. Radlauer and T. Agapie, *Organometallics*, 2014, **33**, 3247-3250.

258. J. Wang, H. Li, N. Guo, L. Li, C. L. Stern and T. J. Marks, *Organometallics*, 2004, **23**, 5112-5114.

259. J. Huang, Z. Feng, H. Wang, Y. Qian, J. Sun, Y. Xu, W. Chen and G. Zheng, *J. Mol. Catal. A: Chem.*, 2002, **189**, 187-194.

260. M. Mitani, K. Oouchi, M. Hayakawa, T. Yamada and T. Mukaiyama, *Polym. Bull.*, 1995, **35**, 677-682.

261. J. Kuwabara, D. Takeuchi and K. Osakada, *J. Organomet. Chem.*, 2005, **690**, 269-275.

262. J. Kuwabara, D. Takeuchi and K. Osakada, *Chem. Commun.*, 2006, 3815-3817.

263. M. L. H. Green and N. H. Popham, *J. Chem. Soc., Dalton Trans.*, 1999, 1049-1059.

264. S. Liu, A. Motta, M. Delferro and T. J. Marks, *J. Am. Chem. Soc.*, 2013, **135**, 8830-8833.

265. S. Liu, A. Motta, A. R. Mouat, M. Delferro and T. J. Marks, *J. Am. Chem. Soc.*, 2014, **136**, 10460-10469.

Chapter Two

Bimetallic titanium catalysts with phenylene covalent tethers

2.1 Overview

As discussed in Chapter One bimetallic catalysts have been shown to impact the activity and polymer properties in olefin polymerisation. This Chapter describes the syntheses, structures and copolymerisation capabilities of three new bimetallic catalysts and four corresponding model monometallic complexes.

The main focus involves the ligand design of covalently tethered bis(protio-amidines) and their corresponding bimetallic precatalysts, which are fully characterised and compared using X-ray crystallography and variable-temperature NMR studies. High temperature EP and EPDM copolymerisation experiments were performed in collaboration with LANXESS Elastomers and, in light of these polymerisation experiments, a series of monometallic cyclopentadienyl-amidinate titanium complexes were prepared and studied. A detailed description of the synthesis and characterisation of these complexes is presented along with their reactions with $B(C_6F_5)_3$ and $[CPh_3][B(C_6F_5)_4]$ to form well-defined cationic species. Additional high temperature EPDM copolymerisation studies were performed and the productivities and resultant polymer composition are discussed.

2.2 Synthesis and characterisation of conjugated phenylene-bridged cyclopentadienyl-amidinate bimetallic complexes

Previous work in the Mountford group and by LANXESS Elastomers has generated a wide range of dialkyl and dichloro κ^1-amidinate titanium complexes (Figure 2.1). $Ti\{NC(Ar)NR_2\}Cl_3$ can be formed from the reaction of a silylated amidine and $TiCl_4$ with the elimination of Me_3SiCl. A large family of neutral complexes were formed from this synthon with a range of mono-anionic ligands *via* a salt elimination pathway, such as $Ti\{NC(NR_2)Ar\}\{R'C(NR)_2\}X_2$ (**2.01**)[1] and $Cp'Ti\{NC(NR_2)Ar\}X_2$ (**2.02**) where X = alkyl or halide.[2, 3] Alternatively, the displacement of chloride from this precursor by a neutral face-capping ligand can form analogous cationic amidinate complexes, for example $[Ti\{NC(NR_2)Ar\}\{HC(Me_2pz)_3\}X_2][A]$ (**2.03**)[4, 5] and $[Ti\{NC(NR_2)Ar\}(Me_3[9]aneN_3)X_2][A]$ (**2.04**).[5]

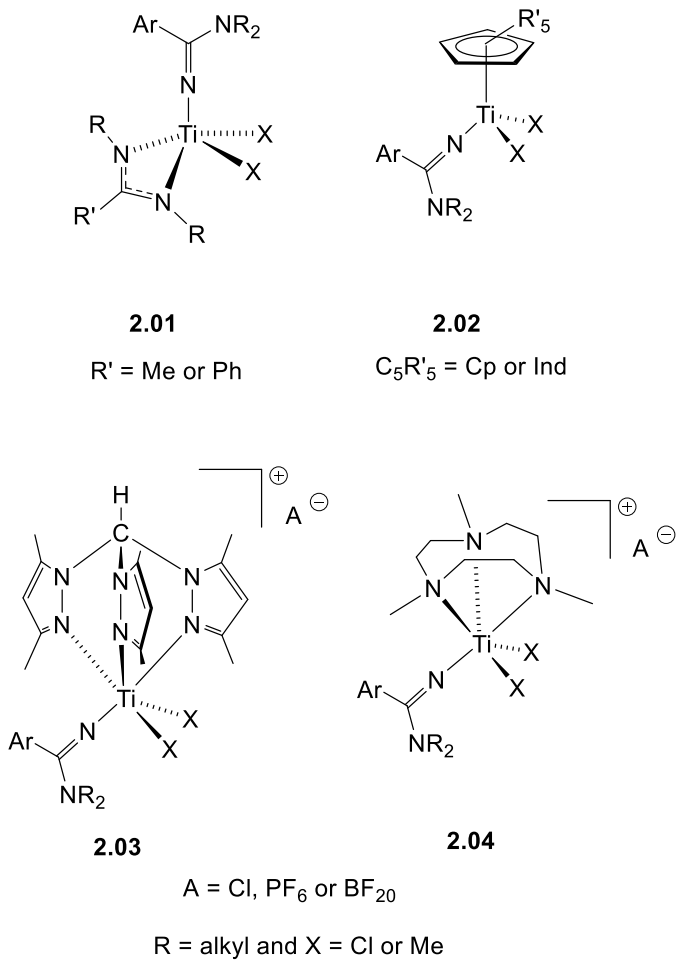

Figure 2.1 Previous examples of titanium κ^1-amidinate complexes.[1-5]

Introduction of a more sterically congested ligand, such as a C_5Me_5 (Cp^*), to form a neutral κ^1-amidinate titanium complex proved unsuccessful *via* this pathway. Reaction of $LiCp^*$ with $Ti\{NC(Ph)N^iPr_2\}Cl_3$ resulted in the unwanted formation of a Ti(III) species and no reaction was observed with the softer transmetallating agent Cp^*SiMe_3. An alternative methodology was established by reacting a protio-amidine with Cp^*TiCl_3 in the presence of an excess of triethylamine. This route was in turn shown to be higher yielding for the synthesis of $CpTi\{NC(Ph)N^iPr_2\}Cl_2$ (**2.05**) (Equation 2.1).[2, 3]

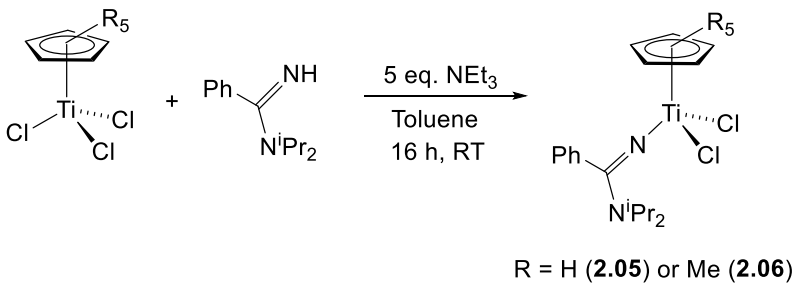

Equation 2.1

Both the silylated and protio amidines were synthesised in similar procedures. Nucleophilic attack on an aryl nitrile by an *in situ* generated magnesiated secondary amine, followed by quenching with either Me_3SiCl or methanol and water and purification by either crystallisation or distillation generated the desired products (Scheme 2.1). This synthetic route allowed for facile modification of either the secondary amine or aryl nitrile, except for the encumbered di-*tert*-butylamine.[6]

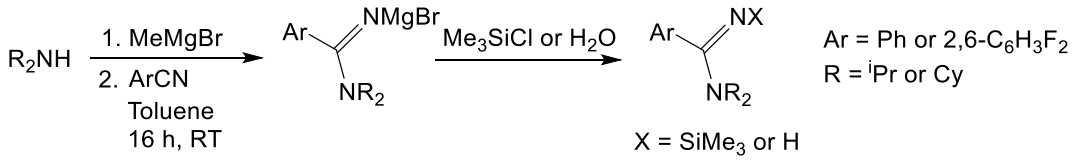

Scheme 2.1 Synthesis of silylated and protio-amidines.

2.2.1 Ligand synthesis

Copolymerisation studies involving $Cp^*Ti\{NC(Ph)N^iPr_2\}Me_2$ (**2.07**) proved it to be highly active as a precatalyst and stable under industrially relevant conditions. Catalyst systems based on **2.07** were shown to be effective at incorporating comonomers, in particular dienes, and will be discussed further in Section 2.5. An analogous bimetallic precatalyst containing a phenylene bridged moiety was the initial target of this work, with substituents in both the *meta* and *para* positions. The *ortho* substituted bis(protio-amidine), $1,2\text{-}C_6H_4\{C(NH)N^iPr_2\}_2$, was not targeted due to the well-established porphyrin ring formation that could form *via* cyclisation upon activation of one of the nitriles.[7]

The same ligand synthesis as described above was initially invoked to synthesise both $1,4\text{-}C_6H_4\{C(NH)N^iPr_2\}_2$ (**1**) and $1,3\text{-}C_6H_4\{C(NH)N^iPr_2\}_2$ (**2**). However, unlike their mono-substituted counterparts, vigorous conditions were required for both products. A large excess of the *in situ* generated amide, $^iPr_2NMgBr$, and additionally, in the case of **2,** a prolonged time period (24 h) under refluxing conditions were required. Both **1** and **2** were obtained in low yields (38 and 34% respectively), presumed to be a result of the difficulty in a nucleophilic attack on a nitrile conjugated to a deprotonated amidine. Whilst optimising the conditions towards the synthesis of **1** the mono-substituted analogue was produced, highlighting the difficulty of the second addition. This was subsequently isolated and the molecular structure is shown in Figure 2.2.

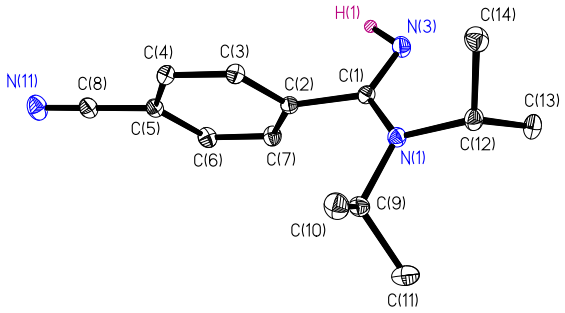

Figure 2.2 Displacement ellipsoid plot of 1,4-(NC)C_6H_4{C(NH)N^{i}Pr$_2$} (20% probability, C-bound H atoms omitted).

To overcome the need for a large excess of reagents and low isolated yields an alternative pathway, initially used by LANXESS Elastomers, was employed. Aluminium chloride was used as a Lewis acid catalyst, and, in the presence of an excess of diisopropylamine at high temperatures (120 °C), a successful disubstituted product was achieved. The reaction was initially attempted under melt conditions, but use of a minimum amount of xylene (15 mL) at 120 °C proved to be higher yielding. An acid-base extraction gave the pure compounds in high yields of 86 and 80% for **1** and **2**, respectively (Scheme 2.2). They were fully characterised by NMR and IR spectroscopy, ESI mass spectrometry and elemental analysis. Full characterising data for all new compounds are given in Chapter Six.

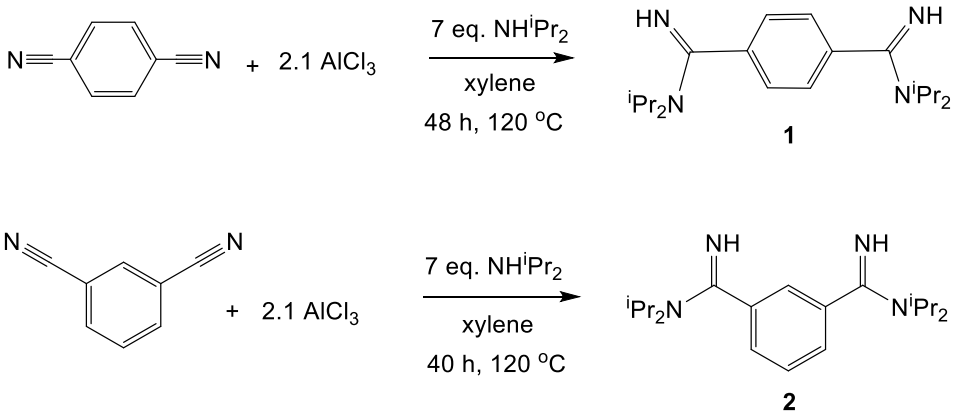

Scheme 2.2

Compounds **1** and **2** showed mass envelopes corresponding to both the $[M + H]^+$ (*m/z* = 331 g mol^{-1}) and $[M + 2H]^{2+}$ (*m/z* = 166 g mol^{-1}) in their ESI mass spectra. The ^{1}H NMR spectrum (298 K, $CDCl_3$) of **2** has a broad singlet corresponding to the N<u>H</u> proton at 5.67 ppm and a corresponding ν(N-H) absorption at 3283 cm^{-1} in its IR spectrum (Nujol mull). However, this was not observed for **1** in either the solid state

or solution. In both compounds fast rotation on the NMR timescale at room temperature about the C–N^{i}Pr$_2$ bond results in a single doublet resonance (1.29 and 1.37 ppm for **1** and **2**, respectively) along with a septet (3.59 and 3.65 ppm for **1** and **2**, respectively) corresponding to the methyl and methine protons of the isopropyl groups in their ^{1}H NMR spectra. The ^{13}C{^{1}H} NMR spectra showed the diagnostic central, C(NH)N^{i}Pr$_2$, carbon of the amidine moiety at 167.4 and 167.3 ppm for **1** and **2**, respectively.

Diffraction-quality crystals were grown at room temperature from saturated CH_2Cl_2 and pentane solutions for **1** and **2**. The molecular structures are shown in Figure 2.3 and full crystallographic data for these (and all structurally characterised) compounds can be found in the CD Appendix. For the crystallographic procedure used see Chapter Six. For comparison, the molecular structure of the previously synthesised HNC(Ph)N^{i}Pr$_2$ (**2.08**)[2] is also shown in Figure 2.3 and selected bond lengths and angles of **1**, **2** and **2.08** are compared in Table 2.1.

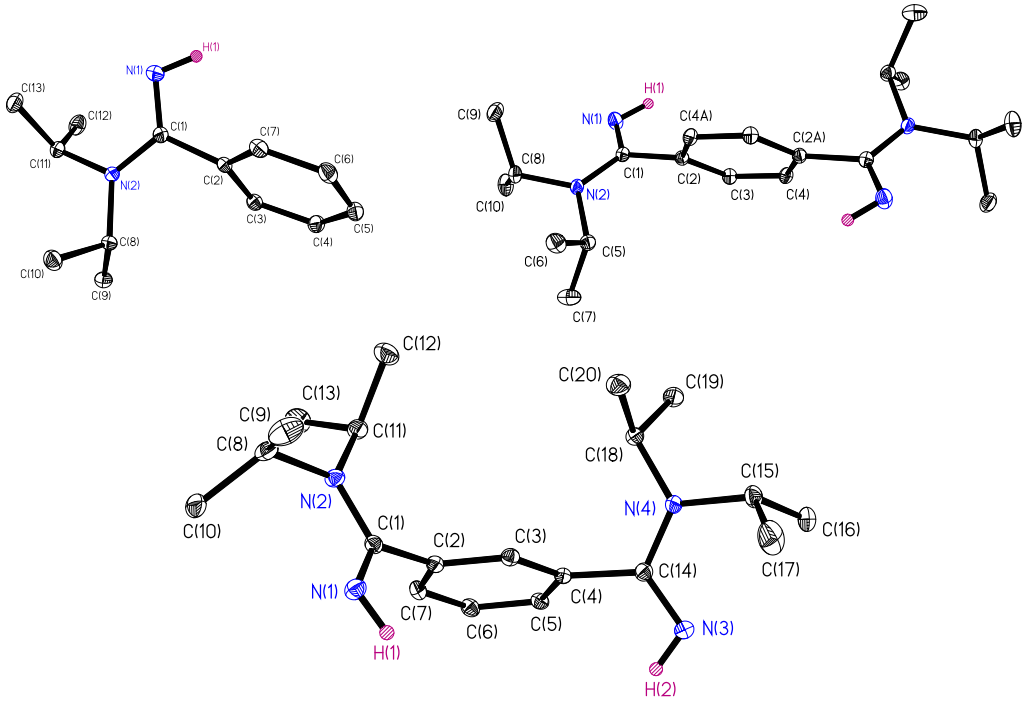

Figure 2.3 Displacement ellipsoid plots of HNC(Ph)N^{i}Pr$_2$ (**2.08**, above left), 1,4-C$_6$H$_4${C(NH)N^{i}Pr$_2$}$_2$ (**1**, above right) and 1,3-C$_6$H$_4${C(NH)N^{i}Pr$_2$}$_2$ (**2**, below) (20% probability, C-bound H atoms omitted). For compound **1** atoms carrying the suffix 'A' are related to their counterparts by the symmetry operator 1-x, 1-y, 1-z.

Table 2.1. Selected bond lengths (Å) and angles (°) for HNC(Ph)N^{i}Pr$_2$ (**2.08**), 1,4-C$_6$H$_4${C(NH)N^{i}Pr$_2$}$_2$ (**1**) and 1,3-C$_6$H$_4${C(NH)N^{i}Pr$_2$}$_2$ (**2**).

Parameter	**2.08**	**1**	**2**
C(1)-N(1)	1.2922(19)	1.2885(13)	1.288(2)
C(1)-N(2)	1.3627(17)	1.3682(13)	1.370(2)
C(1)-C(2)	1.5024(19)	1.5067(13)	1.501(2)
N(2)-C(8)	1.4767(17)	1.4793(12)	1.481(2)
N(1)-C(1)-C(2)	120.50(13)	120.87(9)	121.87(15)
N(1)-C(1)-N(2)	121.23(13)	121.98(9)	121.03(16)
C(2)-C(1)-N(2)	118.17(11)	116.99(8)	117.10(14)
C(8)-N(2)-C(x)†	116.37(11)	117.30(8)	116.19(13)

†x = 5 for **1** and 11 for **2** and **2.08**

The molecular structures are in agreement with the structure proposed based on NMR data. There are no significant differences observed in the bond lengths and angles across all three molecular structures. In all cases the aryl ring lies perpendicular to the N(1)=C(1)–N(2) plane, presumably to avoid unfavourable interactions with the isopropyl groups. Previously an extensive DFT study has demonstrated that the coplanar amidine moiety arises from an allylic-type-π-system, whereby the non-bonding and bonding π-system were successfully modelled.[2] The central carbon C(1) is *sp*^{2} hybridised and is planar in all cases, the sum of the angles subtended at C(1) are 359.9(2), 359.8(2) and 360.0(3)° for **2.08**, **1** and **2**, respectively.

2.2.2 Synthesis of 1,4-C$_6$H$_4${NCN^{i}Pr$_2$}$_2${Cp*TiMe$_2$}$_2$ (3) and 1,3-C$_6$H$_4${NCN^{i}Pr$_2$}$_2${Cp*TiMe$_2$}$_2$ (4)

As discussed above, an effective pathway to pentamethylcyclopentadienyl titanium amidinate complexes involves the reaction of a stoichiometric amount of a protio-amidine with Cp*TiCl$_3$ in the presence of an excess of triethylamine. The resultant dichloride species is subsequently alkylated to produce the desired precatalyst as a dialkyl species. This Thesis explored an alternate pathway, initial methylation and isolation of Cp*TiMe$_3$ by adding 3 equiv. MeLi solution dropwise at 0 °C to Cp*TiCl$_3$[8] followed by protonolysis with a protio-amidine with only methane evolving as a side-product. It was shown that Cp*Ti{NC(Ph)N^{i}Pr$_2$}Me$_2$ (**2.07**) can be produced quantitatively in 16 h *via* this pathway and that no additional purification steps were required.[2] This route was employed for the synthesis of 1,4-C$_6$H$_4${NCN^{i}Pr$_2$}$_2${Cp*TiMe$_2$}$_2$ (**3**) and 1,3-C$_6$H$_4${NCN^{i}Pr$_2$}$_2${Cp*TiMe$_2$}$_2$ (**4**) from

their respective bis(protio-amidines) **1** and **2** (Scheme 2.3). The route to **3** proved to be very facile with the pure product precipitating from a toluene solution after 15 h in 51% yield. Complex **4** was recrystallised from a saturated pentane solution at -30 °C in 46% yield.

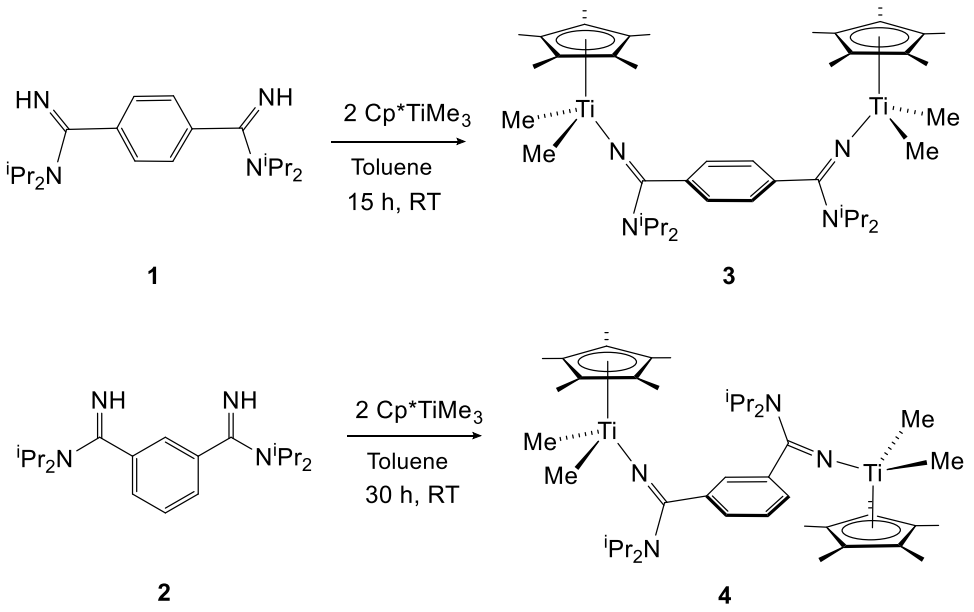

Scheme 2.3

The ^{1}H NMR spectrum (298 K, $CDCl_3$) of **3** is shown in Figure 2.4 and indicates a C_{2v}- or C_{2h}-symmetric molecule on the NMR timescale at room temperature. The broad nature of the resonances corresponding to the isopropyl group indicates that there are fluxional processes present at room temperature. A low temperature ^{1}H NMR study was carried out. At low temperature the CH<u>Me</u>$_2$ resonances decoalesced into a pair of doublets and the C<u>H</u>Me$_2$ resonances into a pair of septets arising from restricted rotation around the C–N partial double bond. At low temperature the upfield C<u>H</u>Me$_2$ proton is orientated towards the phenyl group and unlike its downfield counterpart the resonance is broad due to quadrupolar relaxation from the proximate nitrogen atom. The complex was fully characterised at 223 K. Single resonances are observed for the Cp* (1.64 ppm), Ti<u>Me</u>$_2$ (-0.19 ppm) and the aromatic region (7.13 ppm). This upfield resonance for Ti<u>Me</u>$_2$ is typical of a group bonded to an electropositive metal and corresponds to a ^{13}C NMR resonance at 45.9 ppm.

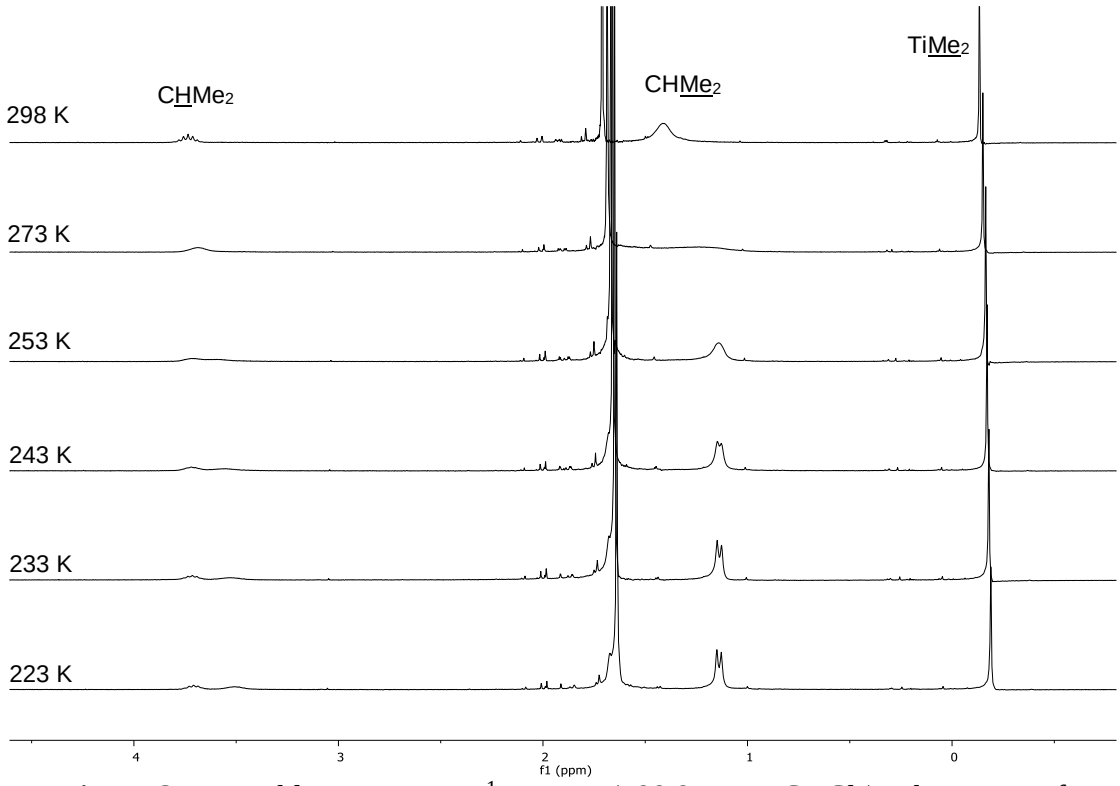

Figure 2.4 Variable temperature ^{1}H NMR (299.9 MHz, $CDCl_3$) sub-spectra of 1,4-$C_6H_4\{NCN^{i}Pr_2\}_2\{Cp^{*}TiMe_2\}_2$ (**3**).

A similar room temperature ^{1}H NMR spectrum (298 K, $CDCl_3$) was observed for **4** **(**Figure 2.6). However, at low temperatures a notable difference was observed, the isopropyl resonances decoalesced into 4 doublets and a pair of apparent septets, again due to restricted rotation around the C–N and C–phenyl bond. Unlike complex **3** absence of mirror symmetry causes all four methyl peaks to become inequivalent and the Ti<u>Me</u>$_2$ signal also decoalesed into two peaks. The apparently C_2-symmetric complex was again characterised at 223 K. This restricted rotation in both complexes is believed to be partially electronic in origin with a π-interaction from a lone pair of the amine nitrogen leading to a degree of double bond character across the conjugated amidinate moiety. This will be discussed further in Section 2.7.

The free energy of activation ($\Delta G^{\ddagger}$) for these exchange processes can be calculated by analysis of the NMR spectra at the low temperature limit and the coalescence temperature (T_c). Analysis of both the CH<u>Me</u>$_2$ and Ti<u>Me</u>$_2$ signals (T_c = 273 and 263 K, respectively) gave approximately the same value of $\Delta G^{\ddagger}$ (54.7 and 56.0 kJmol^{-1}, respectively) for **4** suggesting a geared process.[9] The gNMR programme was used to analyse the exchange process further using the Ti<u>Me</u>$_2$ resonances. An Eyring plot based on the derived exchange rate constants (*k*) afforded $\Delta H^{\ddagger}$, $\Delta S^{\ddagger}$ and thus $\Delta G_{263}^{\ddagger}$

of 96(3) kJmol^{-1}, 145(10) JK^{-1}mol^{-1} and 55(3) kJmol^{-1} (Figure 2.5). These values complement the value obtained using the coalescence temperature. The $\Delta S^{\ddagger}$ value is higher than expected for an intramolecular process and is proposed to be due to a transition state with greater rotational degrees of freedom.

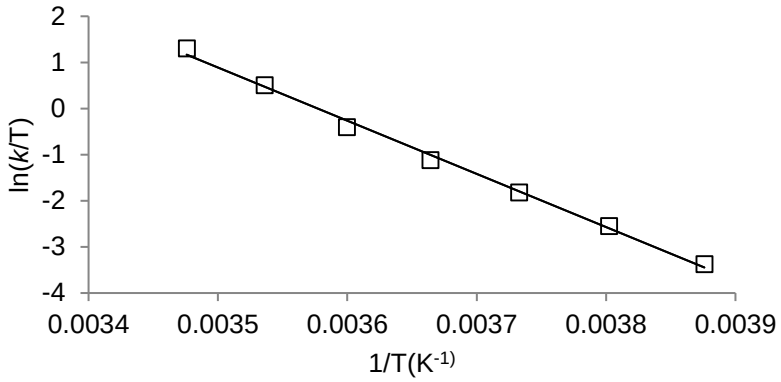

Figure 2.5 Eyring plot for Ti<u>Me</u>$_2$ group exchanging in 1,3-$C_6H_4\{NCN^iPr_2\}_2\{Cp^*TiMe_2\}_2$ (**4**). $\Delta H^{\ddagger}$ = 96(3) kJmol^{-1}, $\Delta S^{\ddagger}$ = 145(10) JK^{-1}mol^{-1} and $\Delta G_{263}^{\ddagger}$ = 55(3) kJmol^{-1}.

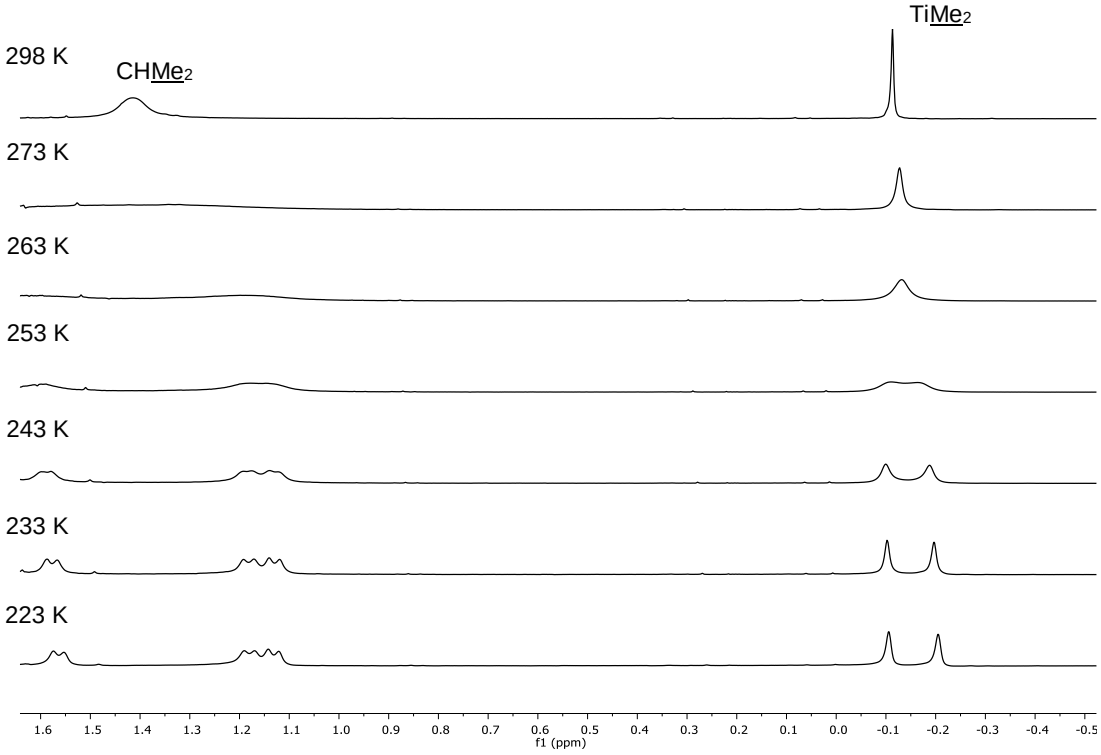

Figure 2.6 Variable temperature ^{1}H NMR (299.9 MHz, $CDCl_3$) sub-spectra of 1,3-$C_6H_4\{NCN^iPr_2\}_2\{Cp^*TiMe_2\}_2$ (**4**).

Diffraction-quality crystals of **3** were grown by slow cooling of a hot bromobenzene solution, and of **4** from a pentane solution at room temperature. The molecular

structures are shown in Figure 2.7 and possess approximate C_{2h} and C_2 symmetry, respectively consistent with the solution NMR data**.** Selected bond lengths and angles are compared in Table 2.2 along with those of their mononuclear analogue $Cp^*Ti\{NC(Ph)N^iPr_2\}Me_2$ (**2.07**).[2] The molecular structures are consistent with the low temperature NMR studies and both have the titanium metal centres facing in opposing directions to one another, presumably due to steric constraints. Unlike complex **3**, the lack of inversion centre through the phenylene ring in **4** gives the asymmetry observed at low temperature. Fast rotation around the C(11)–N(1) bond on the NMR timescale allows the $TiMe_2$ signals in the ^1H NMR spectrum to be equivalent even at low temperatures on the NMR experimental timescale in both **3** and **2.07**.

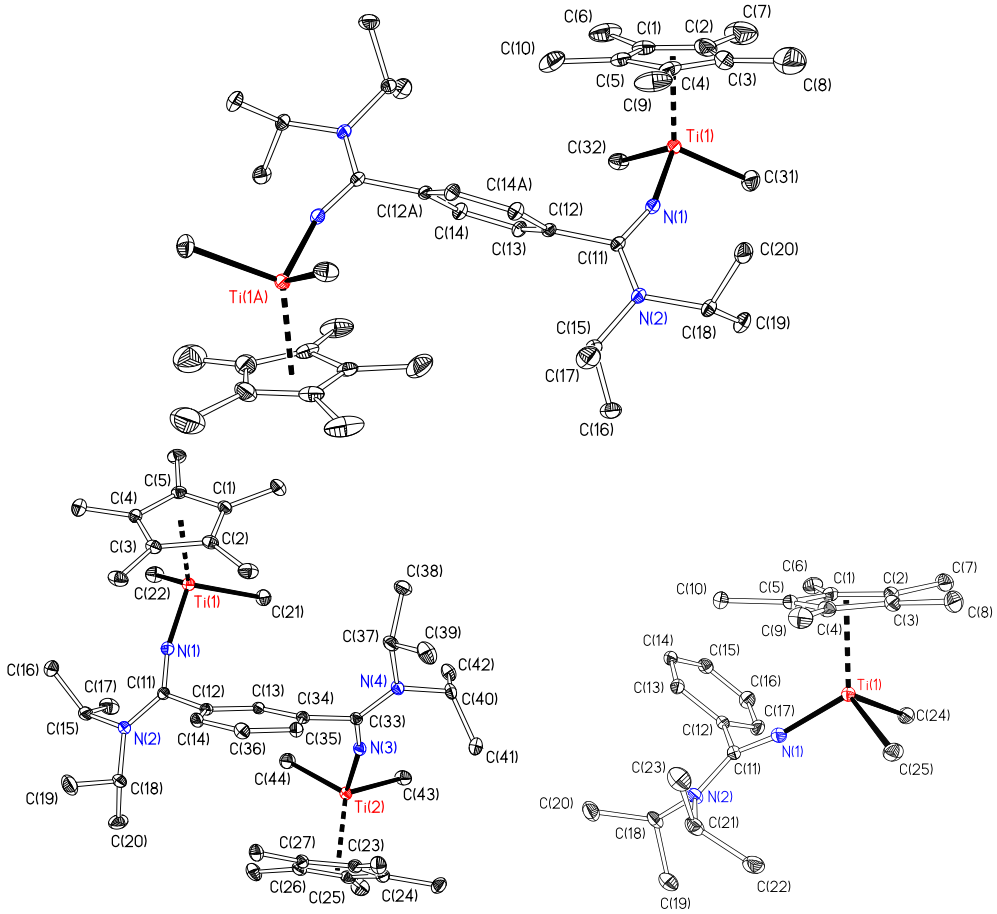

Figure 2.7 Displacement ellipsoid plots of 1,4-$C_6H_4\{NCN^iPr_2\}_2\{Cp^*TiMe_2\}_2$ (**3**, top), 1,3-$C_6H_4\{NCN^iPr_2\}_2\{Cp^*TiMe_2\}_2$ (**4**, bottom left) and $Cp^*Ti\{NC(Ph)N^iPr_2\}Me_2$ (**2.07**, bottom right). (20% probability, H atoms omitted). In complex **4** Cp^* disorder omitted and atoms carrying the suffix 'A' are related to their counterparts by the symmetry operator 2-x, 1-y, 1-z.

Table 2.2 Selected bond lengths (Å) and angles (°) for 1,4-$C_6H_4\{NCN^iPr_2\}_2\{Cp^*TiMe_2\}_2$ (**3**), 1,3-$C_6H_4\{NCN^iPr_2\}_2\{Cp^*TiMe_2\}_2$ (**4**) and $Cp^*Ti\{NC(Ph)N^iPr_2\}Me_2$ (**2.07**). Cp^*_{cent} is the computed Cp^* ring carbon centroid. For **4** the values in brackets are for the corresponding parameters for Ti(2).

Parameter	**2.07**	**3**	**4**
Ti(1)-Cp^*_{cent}	2.07	2.07	2.07, [2.06]
Ti(1)-N(1)	1.8452(1)	1.8491(17)	1.836(2), [1.845(2)]
N(1)-C(11)	1.290(2)	1.285(3)	1.288(3), [1.293(3)]
N(2)-C(11)	1.363(2)	1.363(2)	1.368(3), [1.364(3)]
C(11)-C(12)	1.502(2)	1.508(3)	1.502(3), [1.505(3)]
Ti(1)-Me(1)	2.1227(18)	2.133(3)	2.133(3), [2.124(3)]
Ti(1)-Me(2)	2.1326(19)	2.138(3)	2.125(3), [2.121(3)]
Cp^*_{cent}-Ti(1)-N(1)	120.8	119.1	119.6, [120.5]
Cp^*_{cent}-Ti(1)-Me(1)	113.9	119.1	113.9, [112.8]
Cp^*_{cent}-Ti(1)-Me(2)	113.9	111.0	114.6, [114.1]
C(11)-N(1)-Ti(1)	163.00(13)	159.64(15)	163.05(18), [163.55(17)]

The titanium centres (Figure 2.7) show the expected *pseudo*-tetrahedral three-legged piano stool arrangements. A near linear C(11)–N(1)–Ti(1) bond angle in both **3** (159.64(15)°) and **4** (163.05(18), 163.55(17)°) suggest a metal-amidinate dπ-pπ bonding contribution. The Ti(1)–N(1) bond lengths (1.8491(17) (**3**), 1.836(2) Å (**4**)) are intermediate between a Ti=N double bond (1.90 - 2.00 Å)[10] such as formed with amide (NR_2) ligands and longer than a formal triple Ti≡N bonds (as with imides, NR), which lie in the range 1.69 - 1.76 Å,[11, 12] suggesting a π-bonding contribution from the nitrogen between these two extremes. In all the molecular structures the aromatic ring is orthogonal to the amidinate moiety implying a negligible conjugation.

Table 2.2 shows that the respective bond lengths and angles are almost identical for the bimetallic structures and their mononuclear analogues; this demonstrates a similar electron donating ability for the two cases. Computational fragment analysis has been carried out within the Mountford group on titanium amidinate complexes; it has been shown that the nitrogen 2p-orbital which contributes to the C=N π-bond, contributes approximately half the amount of electrons to the metal centre compared to that of the orthogonal unconjugated p-orbital. This complements the bond length analysis and indicates that the donating capacity of the amidinate group lies between the 3 and 5

electron donor limits.[13] This is not reflected when comparing the bond lengths of the amidinate moiety in comparison to their protio-amidine counterparts, where no significant differences are observed.

2.3 Synthesis and characterisation of a non-conjugated diphenylene-bridged cyclopentadienyl-amidinate bimetallic complex

As discussed in Chapter One, bimetallic complexes with conjugated, unconjugated, restricted and flexible tethers have all been employed. Complexes **3** and **4** both maintain the conjugation to the metal centres through a phenylene tether. In order to probe the significance of this conjugation a non-conjugated bimetallic complex that still maintains a comparable structure to $Cp^{*}Ti\{NC(Ph)N^{i}Pr_2\}Me_2$ (**2.07**) was targeted.

2.3.1 Ligand synthesis

Introduction of a methylene spacer between two phenylene tethers was a proposed target. This would break the electronic conjugation and allow rotation, but a degree of proximity between the metal centres would still be maintained. 4,4′-dicyanodiphenylmethane (**2.09**, Scheme 2.4) was synthesised according to a literature procedure[14] and used in the formation of CH_2-1,4-$(C_6H_4)_2\{C(NH)N^{i}Pr_2\}_2$ (**5**). Unlike the conjugated systems, only 5 equiv. of the *in situ* generated amide reagent $^{i}Pr_2NMgBr$ were required to give formation of the di-substituted product **5** within 36 h at room temperature in a 71% yield (Scheme 2.4). The relative ease and improved yield of forming **5** in comparison to **1** and **2** can be attributed to a result of the methylene spacer; the activated amidine of the mono-substituted product does not electronically influence the unsubstituted nitrile group. The synthesis of **1** and **5** are both carried out in THF to enhance the solubility of the reagents and intermediate mono-substituted products.

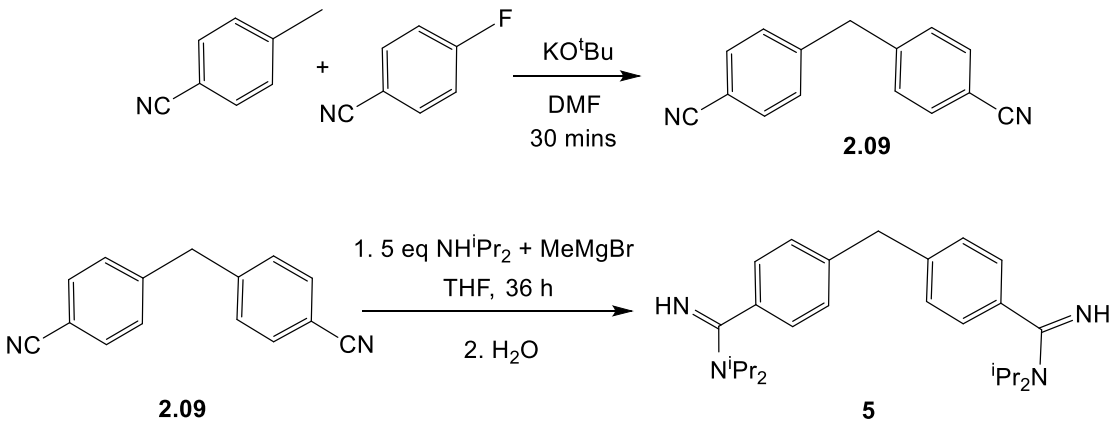

Scheme 2.4 Synthesis of CH_2-1,4-$(C_6H_4)_2\{C(NH)N^iPr_2\}_2$ (**5**)

The ^{1}H NMR spectrum (298 K, C_6D_6) of **5** is simple due to a low barrier to rotation around the C–N^{i}Pr$_2$ and C–phenylene bonds and is consistent with C_{2v} symmetry on the NMR timescale. Two doublets for the phenylene ring protons display roofing, and a diagnostic singlet methylene resonance is observed at 3.66 ppm for C<u>H</u>$_2$Ph$_2$ (Figure 2.8).[15] No N<u>H</u> signal was observed and, as was the case for **1** and **2,** mass envelopes corresponding to both the $[M + H]^+$ (421 g mol^{-1}) and $[M + 2H]^{2+}$ (*m/z* = 211 g mol^{-1}) in the ESI mass spectrum.

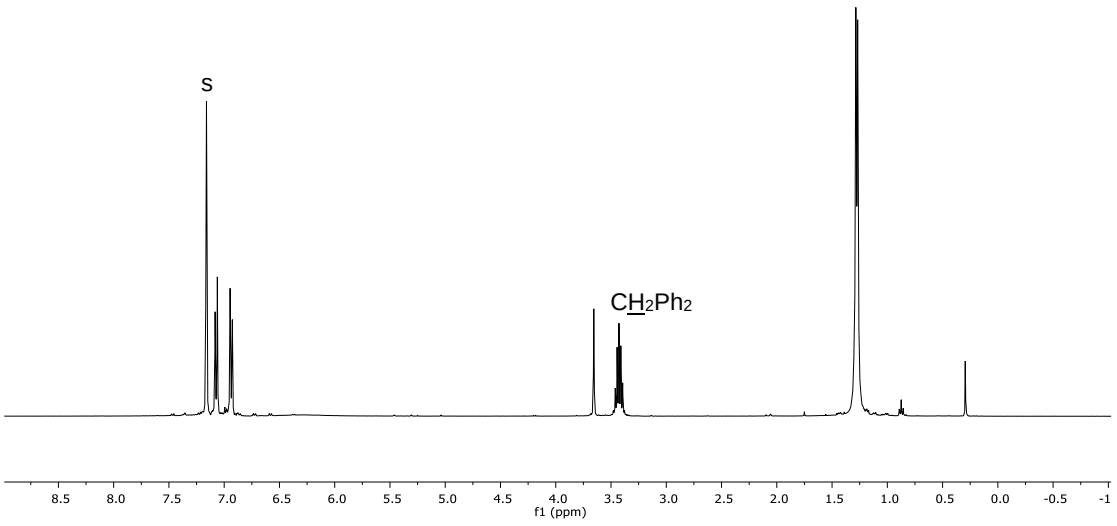

Figure 2.8 ^{1}H NMR (399.9 MHz, C_6D_6, 298 K) spectrum of CH_2-1,4-$(C_6H_4)_2\{C(NH)N^iPr_2\}_2$ (**5**). 's' denotes residual protio-solvent.

2.3.2 Synthesis of $CH_2\{1,4\text{-}C_6H_4\text{-}C(NH)N^iPr_2\}_2\{Cp^*TiMe_2\}_2$ (**6**)

Reaction of compound **5** with 2 equiv. of Cp^*TiMe_3 produced the desired bimetallic complex **6** *via* a protonolysis pathway as previously discussed (Equation 2.2).

$CH_2\{1,4\text{-}C_6H_4\text{-}NCN^iPr_2\}_2\{Cp^*TiMe_2\}_2$ (**6**) was isolated as a brown microcrystalline solid in 48% yield.

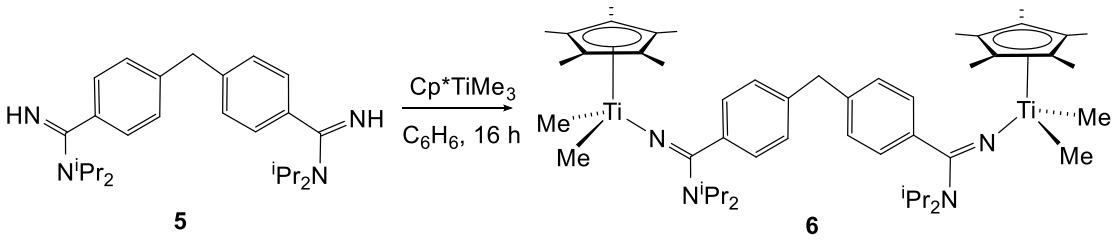

5 **6**

Equation 2.2

The ^{1}H NMR spectrum was consistent with fluxionality at room temperature, and a low temperature ^{1}H NMR study was carried out (Figure 2.9). Below 273 K the methyl and methine resonances for the isopropyl group decoalesced suggesting a similar rotational barrier to complexes **3** and **4** and the complex was fully characterised at 233 K. The chemical shifts corresponding to the ligand backbone in the ^{1}H NMR spectrum (298 K, C_6D_6) display minimal differences from the amidine precursor counterparts. The $C\underline{H}_2Ph_2$ resonance also has an identical chemical shift to that of **5** (3.66 ppm) and only the aromatic protons adjacent to the amidinate group shift downfield (7.21 ppm for **6** cf. 7.07 ppm for **5**). This is a result of the proximity to the amidinate group that has changed donation capacity through bonding to an electropositive metal centre.

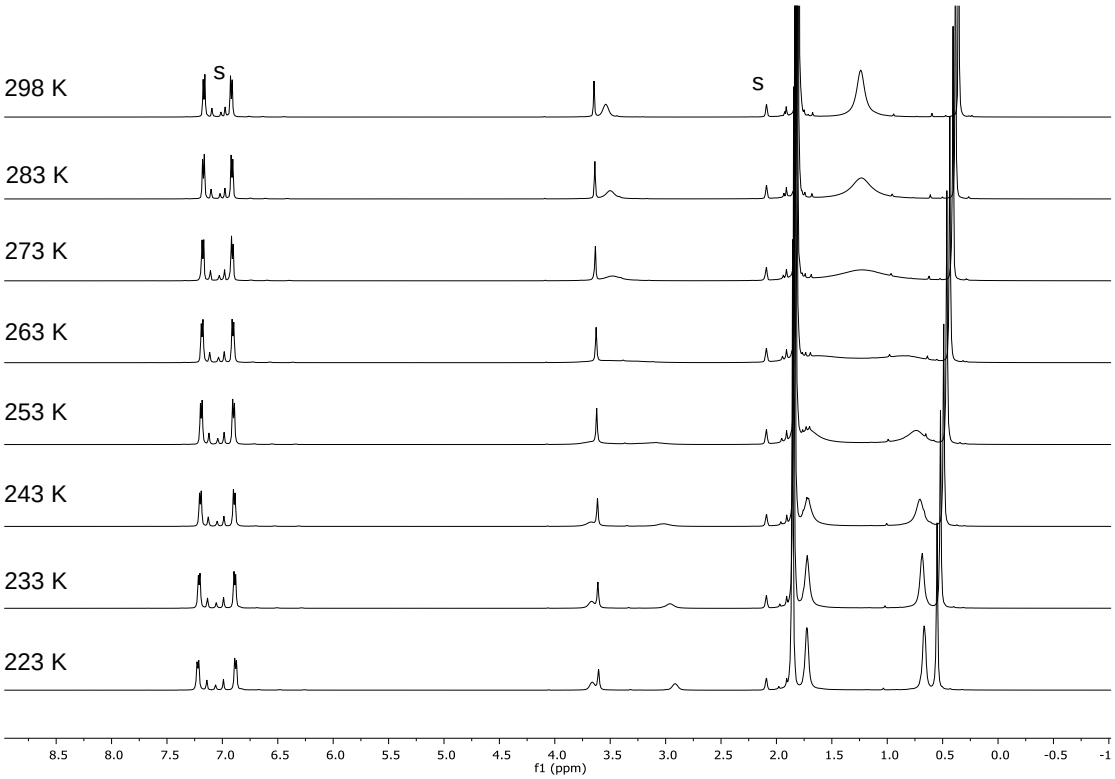

Figure 2.9 Variable temperature ^{1}H NMR (499.9 MHz, Tol-d_8) spectra of $CH_2\{1,4\text{-}C_6H_4\text{-}NCN^iPr_2\}_2\{Cp^*TiMe_2\}_2$ (**6**). 's' denotes residual protio-solvent.

2.4 Synthesis and characterisation of cationic bimetallic complexes

The properties and reactions of the catalytically active Group 4 mono-alkyl cations has been extensively investigated throughout the literature.[16-18] Of particular relevance to this Thesis is previous work within the Mountford group in collaboration with LANXESS Elastomers which has investigated the form of mononuclear cyclopentadienyl-amidinate titanium complexes as base-free alkyl cations, Lewis base adducts and alkyl insertion products. Some examples are given in Figure 2.10. The base-free cations proved to be a complicated mixture of monomethyl mono-cations or bimetallic species with different bridging moieties dictated by the ligand substituents.[13, 19] This is in keeping with previously explored systems discussed in Chapter One. Within the scope of this Thesis it was important to consider whether or not both titanium centres of a covalently tethered bimetallic catalyst could be simultaneously activated.

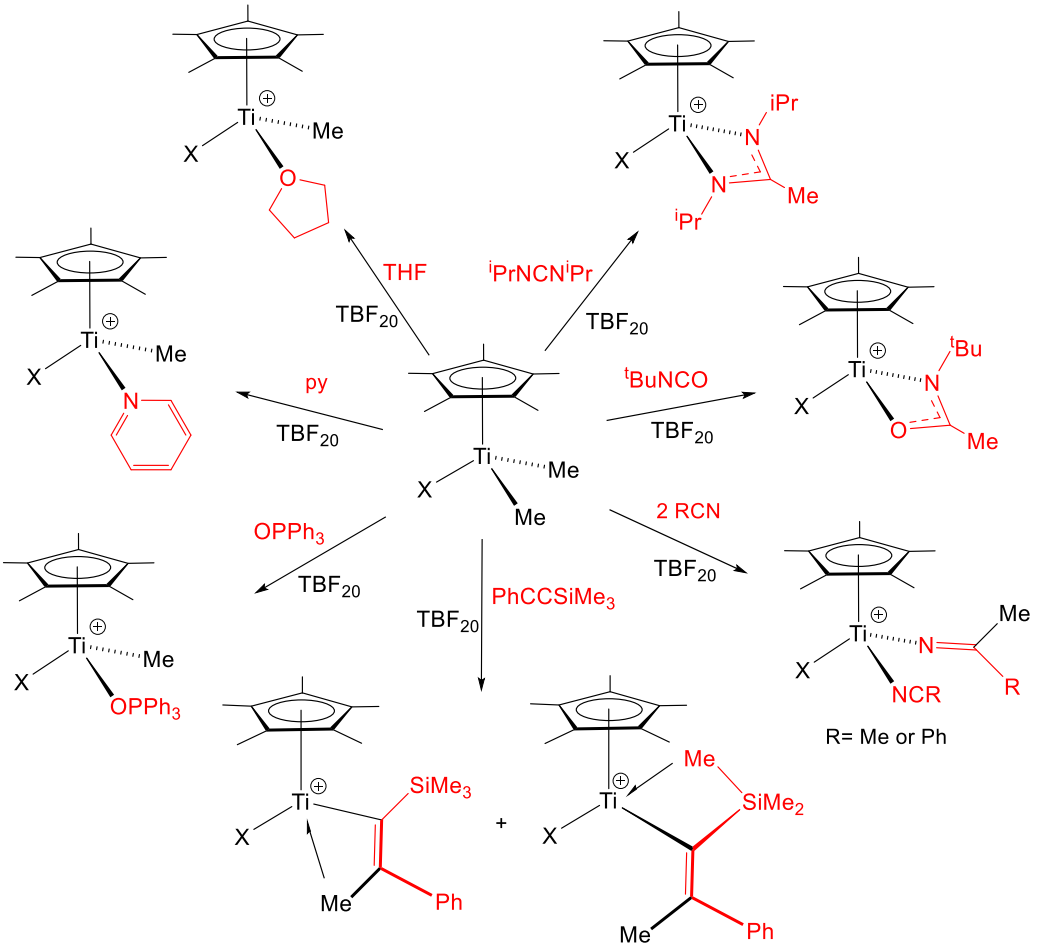

Figure 2.10 Syntheses of Lewis base adducts and insertion products of cyclopentadienyl titanium methyl cations. In all reactions the activation was carried out using a stoichiometric amount of TBF_{20}. X = amidinate group.[13]

NMR tube scale reactions were carried out in bromobenzene-d_5 as the solvent that provided the best solubility without reacting with the cationic titanium metal centre; fluorobenzene was employed as the solvent on larger scale reactions because it has a lower boiling point so could be more easily removed under vacuum. Despite these solvents being employed the reaction of **3** with either 1 or 2 equiv. of $B(C_6F_5)_3$ (BF_{15}) or $[CPh_3][B(C_6F_5)_4]$ (TBF_{20}) caused a dark oil to instantaneously form before any NMR data could be recorded. Instead an activation study was performed using 2 equiv. of TBF_{20} in the presence of 2 equiv. of *N*,*N*′-diisopropylcarbodiimide in fluorobenzene. This formed the insertion product [1,4-$C_6H_4\{NCN^iPr_2\}_2\{Cp^*Ti\{MeC(N^iPr)_2\}\}_2][BF_{20}]_2$ (**7**) in 60% isolated yield (Equation 2.3). The first migratory insertion product of this kind was introduced by Stephan and co-workers through a reaction of phosphinimide-supported zirconium and titanium cations, $[CpM(NP^tBu_3)Me][MeBF_{15}]$ (M = Ti or Zr), with *N*,*N*′-diisopropylcarbodiimide to yield $[CpM(NP^tBu_3)\{MeC(N^iPr_2)_2\}][MeBF_{15}]$.[20]

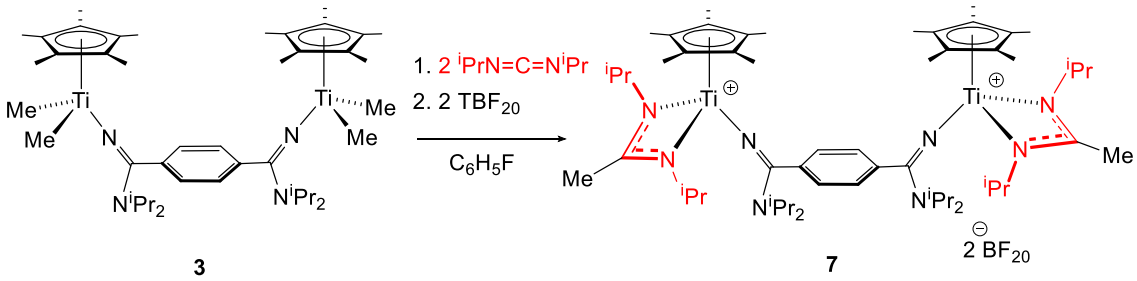

3 **7**

Equation 2.3

The ^1H NMR spectrum of complex **7** was recorded in THF-d_8 at room temperature for solubility and is shown in Figure 2.11. THF cannot usually be used as the solvent with Group 4 mono-methyl mono-cations due to the propensity for ring-opening polymerisation to take place. However, the more saturated insertion product is stable to this. The features of this spectrum are the Cp^* signal at 2.13 ppm, $\underline{Me}C(N^iPr)_2$ signal at 2.40 ppm, the $NCH\underline{Me}_2$ resonances at 0.92, 1.15 and 1.47 ppm and a singlet for the $C_6\underline{H}_4$ phenylene protons in the aromatic region at 7.56 ppm. The methine protons of both κ^1- and κ^2 -$NC\underline{H}Me_2$ are overlapping both with each other and the residual protio-solvent resonances and could not be distinguished. Overall **7** has effective C_{2v} symmetry on the NMR timescale which is indicative of fast rotation about the Ti–N (κ^1-amidinate) bond. The $^{13}C\{^1H\}$ NMR spectrum of **7** is consistent with the proposed structure. The ^{13}C NMR resonance of the migrated methyl group (13.9 ppm) is significantly upfield when compared to a Ti-$\underline{Me}$ in an alkyl cation (*ca.*

50-70 ppm) and a ^{1}H-^{13}C HMBC experiment shows a correlation between $\underline{Me}C(N^{i}Pr)_2$ and $MeC(N^{i}Pr)_2$ (171.5 ppm). The ^{19}F and ^{11}B NMR spectra are indicative of a non-coordinated $[B(C_6F_5)_4]^-$ anion.

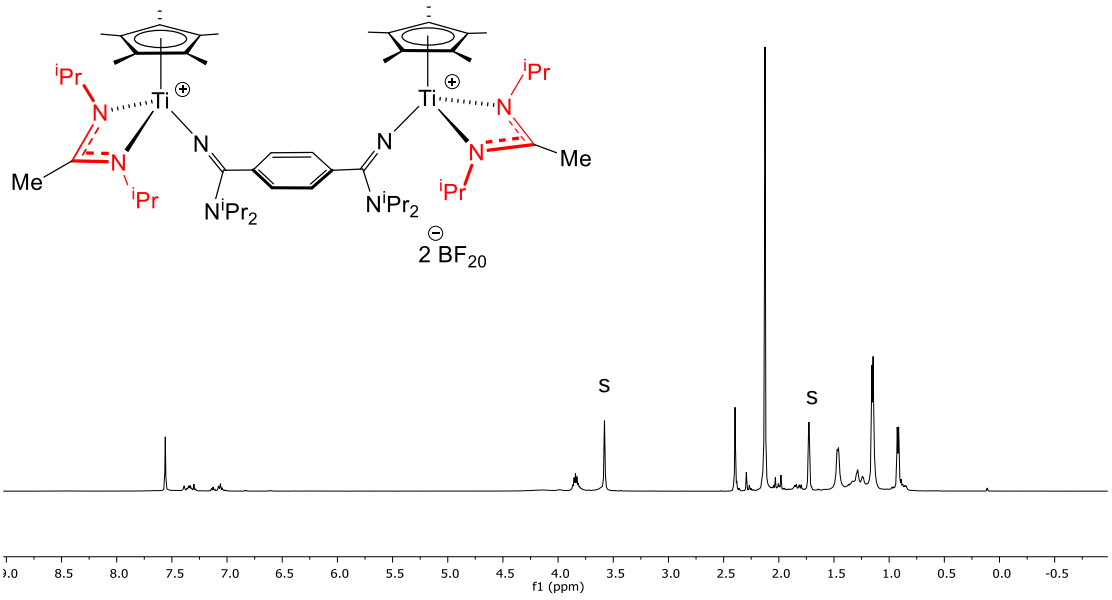

Figure 2.11 ^{1}H NMR (499.9 MHz, THF-d_8, 298 K) spectrum of [1,4-$C_6H_4\{NCN^{i}Pr_2\}_2\{Cp^{*}Ti\{MeC(N^{i}Pr)_2\}_2][BF_{20}]_2$ (**7**). 's' denotes residual protio-solvent.

The insertion product was also prepared on the NMR tube scale by using 2 equiv. of BF_{15}. The same ^{1}H NMR spectrum was observed in THF-d_8, but with an additional broad resonance at 0.53 ppm corresponding to the abstracted methyl, $\underline{Me}B(C_6F_5)_3$. Attempts to form the mono-activated insertion product by the addition of 1 equiv. of TBF_{20} in the presence of *N,N'*-diisopropylcarbodiimide only produced the disubstituted and unsubstituted products as a result of the poor solubility of **3**.

2.5 EPDM copolymerisation experiments using 2.07, 3, 4 and 6

EPDM (ethylene, propylene, dienes: 5-ethylidenebicyclo[2.2.1]hept-2-ene (ENB) and 5-vinylbicyclo[2.2.1]hept-2-ene (VNB)) copolymerisation testing of bimetallic complexes **3**, **4** and **6** were performed in a small-scale batch reactor under industrially relevant conditions at LANXESS Elastomers, The Netherlands. Comparison was made under the same conditions with the monometallic analogous complex, $Cp^{*}Ti\{NC(Ph)N^{i}Pr_2\}Me_2$ (**2.07**). Activation of the dimethyl precatalysts was achieved using methylaluminoxane (MAO-10T). A large excess of MAO was used ([Al]:[Cat] = 4500:1, where [Al] is the relative concentration of aluminium metal centres and

[Cat] is the precatalyst concentration) to ensure complete activation and with the addition of 2 equiv. of 4-methyl-2,6-di-*tert*-butylphenol (BHT) per aluminium centre the system can effectively scavenge any trace water in the reactor, protecting the catalyst without introducing chain-termination pathways.[21-26] Precatalysts were assessed using low (0.10 μmol) loadings in order to maintain isothermal conditions (exotherms < 3 °C) and to reduce the possibility of mass-transport limitations. Hydrogen was fed to the reactor together with the ethylene and propylene reactant gases in order to avoid the formation of higher molecular weight polymers, which result in reactor fouling.[27-29] Full experimental details are given in Chapter Six. The composition of the polymers was analysed using FT-IR and the molecular weight and polydispersity index (PDI) were obtained from GPC measurements, full polymer composition analysis procedures are given in Chapter Six. The results for the active catalysts are summarised in Table 2.3. It is important to note that both in this table and throughout this Thesis the productivity is calculated per metal centre not per catalyst where this differs.

Table 2.3. EPDM polymerisation results for $Cp^*Ti\{NC(Ph)N^iPr_2\}Me_2$ (**2.07**), 1,4-$C_6H_4\{NCN^iPr_2\}_2\{Cp^*TiMe_2\}_2$ (**3**), 1,3-$C_6H_4\{NCN^iPr_2\}_2\{Cp^*TiMe_2\}_2$ (**4**) and $CH_2\{1,4\text{-}C_6H_4\text{-}C(NH)N^iPr_2\}_2\{Cp^*TiMe_2\}_2$ (**6**).

Entry	Precatalyst	Cocatalyst	Productivity[a] (kg mol Ti^{-1} h^{-1} bar^{-1})	C_2 (wt%)	C_3 (wt%)	ENB (wt%)	VNB (wt%)	M_n (kDa)	M_w (kDa)	PDI
1	**2.07**	MAO	82,290	48.9	49.4	1.01	0.68	261	557	2.1
2	**3**	MAO	51,210	42.5	56.4	0.69	0.43	75	195	2.6
3	**4**	MAO	14,570	47.7	51.2	0.68	0.43	86	205	2.4
4	**6**	MAO	47,830	48.3	50.1	0.94	0.67	188	436	2.3
5	**3**	MAO	43,200	42.9	55.9	0.72	0.46	172	377	2.2
6	**6**	MAO	66,600	49.9	48.6	0.94	0.64	198	438	2.2

Polymerisation conditions. T = 90 °C, Pressure: 7 bar, [Cat] = 0.1 µmol, [Al]:[Cat] = 4500 (Entry 5: [Al]:[Cat] = 9000 and Entry 6: [Cat] = 0.05 µmol) [Al]:[BHT] = 0.5, 10 minute reaction time. Solvent pentamethylheptane (1L) C_3/C_2 =400/200 Nl h^{-1}, H_2 flow: 0.35 Nl h^{-1}, ENB: 0.7 mL, VNB: 0.7 mL. [a] Productivity per mol of transition metal centres.
Polymer characterisation. Polymer molecular weight and molecular weight distributions: the polymers have been analysed with the Freeslate Rapid GPC in 1,2,4 Trichlorobenzene against PS standards. *Average composition:* the polymers have been analysed via transmission IR spectroscopy on a pressed polymer film.

All the catalysts successfully produced sufficient polymer for analysis under the relevant polymerisation and activation conditions. Entries 1-4 detail the results of precatalysts **2.07**, **3**, **4** and **6** respectively. The productivities when using the bimetallic catalysts are all lower than their mononuclear analogue, with the more constrained complex **4** showing the lowest productivity. This is believed to be a result of the steric constraints that a proximate metal centre with a growing polymeric chain imposes upon the other and also the detrimental role a secondary neighbouring cationic species will have electronically on an active centre. The neighbouring cation could result in a direct influence on the electronic properties of the conjugated metal centre, an increase in the electrostatic ion-pairing that needs to be displaced for monomer insertion or the formation of highly aggregated species. A key feature of the resultant EPDM polymer is the incorporated dienes. The dienes give key physical polymer properties and opportunities for post polymer modifications as discussed in Chapter One. Unfortunately precatalysts **3** and **4** had a significant reduction and precatalyst **6** a minimal reduction in the amount of diene incorporated into the resultant polymer, suggesting no favourable cooperative interaction was taking place and that the increase in steric congestion around the metal centre increases the barrier to enchainment for a bulky monomer.

The two conjugated bimetallic precatalysts, **3** and **4** did, however, produce a polymer with a higher degree of propylene incorporation compared to **2.07**, in particular **3** which incurred a consistent increase (48.6 and 56.4%, respectively). A stabilising through-space interaction from the neighbouring metal centre is not believed to be present to facilitate this, particularly considering the greatest effect is observed from **3** when the metal centres are further removed. This increased affinity for propylene is therefore presumed to be electronic in origin. Mononuclear analogues were therefore also used as model systems to probe this effect as discussed in Section 2.7.

The molecular weight of the resultant polymers are decreased for **3**, **4** and **6** relative to **2.07**. This is indicative of the affinity for hydrogen as opposed to barriers to other competing termination pathways. As shown in Chapter One a common advantage observed from employing bimetallic catalysts is improved molecular weights. To investigate whether or not this phenomenon is found with these bimetallic systems a study without hydrogen in the gas feed was carried out and is discussed in Section 2.6. Entries 1-4 all display very similar narrow (PDI: 2.3-2.6) monomodal plots for

their molecular weight distribution, shown from the GPC chromatograms, see Figure 2.12 as example, consistent with single-site behaviour.[30, 31] The peak at lower molecular weight corresponds to BHT, which is introduced as an anti-oxidant to prevent degradation in high temperature GPC analysis and is also used as an internal flow-marker indicator. This single-site behaviour is in agreement with the formation of **7**, where both titanium centres can have an alkyl group abstracted and suggests that both metal centres perform comparably under the polymerisation conditions.

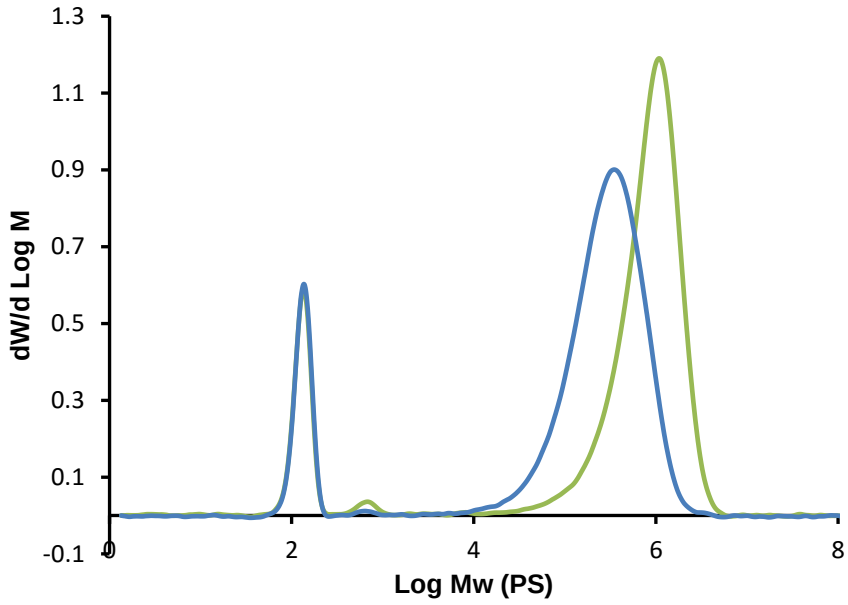

Figure 2.12 Example of monomodal GPCs for precatalyst **4** with EPDM (Entry 3 Table 2.3, blue) and EPM (Entry 3 Table 2.4, green). The low molecular weight peak corresponds to BHT.

There is no definitive trend concerning catalyst activity in the polymerisation of olefins when using bimetallic catalysts. As introduced in Chapter One electronic, steric and ion-pairing effects have all been cited as reasons to genereate a more stable and active catalytic site, which can enhance the rate of enchainment. However, sterically flexible and locked systems have also shown a reduced activity in both homo- and copolymerisation studies with α-olefins. Of specific note to the catalysts employed in this study is the work carried out by Mülhaupt and co-workers with their phenylene spaced zirconocene catalyst, 1,4-(η^5-3,4-$Me_2C_5H_2$-$ZrCpCl_2$)$_2C_6H_4$ (**2.10**), and by Noh and co-workers with their xylene-bridged binuclear titanocenes, {$(C_5H_4)TiCl_3$}$_2${$CH_2(C_6H_4)CH_2$}$_2$ (**2.11 – 2.13**), Figure 2.13.[32-34] A decreased productivity was reported for complex **2.10** and a lower molecular weight compared

to the mononuclear analogue, 1-(η^5-3,4-$Me_2C_5H_2$-$ZrCpCl_2$)-4-Me-C_6H_4 (**2.14**), in the MAO activated homopolymerisation of propylene (260 and 300 kg mol^{-1} h^{-1} bar^{-1} for **2.10** and **2.14**, respectively).[32] This was assumed to be a result of the neighbouring cationic site causing a lower electron density, and therefore Lewis basicity, of the cyclopentadienyl ring, which can therefore favour deactivation and termination pathways. Complexes **2.11 – 2.13** contain *ortho*-, *meta*- or *para*- xylene linkages between half-sanwich end groups and were used in a hompolymerisation study of styrene. It was shown that the activity increases in the order *para* > *meta* > *ortho,* which was hypothesised to be a result of a wider angle allowing for a larger active site. No obvious trend could be established for the molecular weights obtained for the polystyrenes formed.[33, 34]

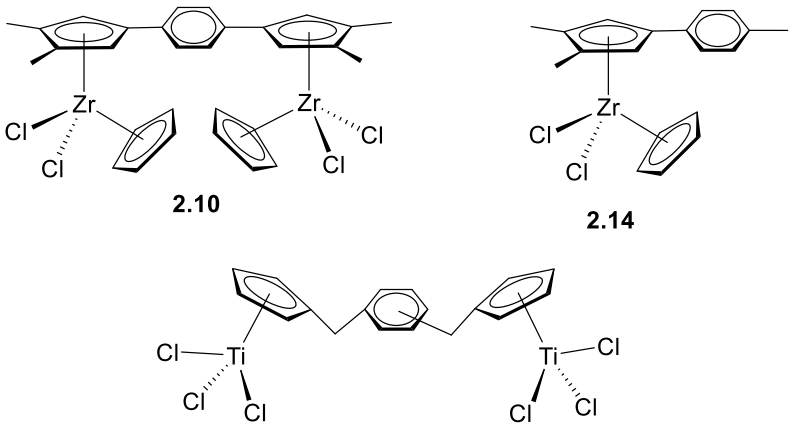

ortho (**2.11**), *meta* (**2.12**), *para* (**2.13**)

Figure 2.13 Related Group 4 bimetallic complexes.

Chapter One introduced the improved effect a bimetallic catalyst can have on comonomer incorporation in a variety of copolymerisation studies: propylene, pentene, hexene, octene, styrene and isoalkenes have all being employed as comonomers.[35] Precatalysts **3** shows a significant increase in propylene incorporation and will be explored in further detail in Section 2.7. There has been no comprehensive study for bimetallic catalysis for the copolymerisation of dienes or other very sterically encumbered monomers.

To avoid the presence of exotherms the use of **2.07** could not be carried out at higher loading conditions and due to the low productivity of **4** a lower loading could not be used without inadequate polymer being produced for analysis. Maintaining the catalyst concentration results in a different ratio between the aluminium and titanium

metal centres, although in both cases a large excess of MAO is employed. To probe the effect this may have 2 additional experiments were carried out (entries 5 and 6 in Table 2.3). Entry 5 maintained the concentration of **3** while doubling [Al] and as can be observed by the composition analysis an almost identical polymer was produced. An increase in molecular weight was observed in this case, this will be discussed further in Section 2.6. Entry 6 reduced the concentration of **6** to 0.05 μmol while maintaining the concentration of the activator and scavenger system. As can be observed the productivity increases by *ca.* 40%, the reason for this is unclear. The polymer composition shows a slight reduction in the incorporation of propylene, but is still very comparable with the polymer formed using **2.07**. This is unsurprising given the electronic similarity of **2.07** and **6**.

An additional study was carried out with precatalyst **2.07** to investigate whether the ratio of MAO to BHT had an impact when used in such large excesses compared to the metal centre. BHT has previously been proved to optimise the polymerisation when MAO is used as the activating species; this is because it can react with free trimethylaluminium (TMA) present to form non-coordinating $MeAl(BHT)_2$.[36, 37] This prevents the TMA from generating an inactive resting state through coordination to the cationic metal centre, as was discussed in Chapter One, or modifying the supporting ligand set.[23, 38-46] Studies have shown that increasing the level of BHT relative to aluminium caused an increase in productivity and vinylic end-groups on the polymeric chain.[21-26] The increased amount of vinylic end-groups are representative of more chain transfer to monomer as opposed to chain transfer to aluminium, which is consistent with "free" TMA being scavenged. Above a threshold the excess BHT showed detrimental effects on the polymerisation; this was proposed to be a result of either the BHT interacting with the active catalytic species, reacting with the Al–Me groups of MAO itself and therefore diminishing its ability in activation or reducing the efficiency of scavenging within the system.[26]

This additional study involved using only one equiv. of BHT per aluminium metal centre ([BHT]/[Cat] = 4500). This still leaves a very large excess relative to the "free" TMA in the MAO used (*ca.* 20%). This experiment displayed a very slight reduction in productivity (from 82,285 to 71,400 kg mol^{-1} h^{-1} bar^{-1}), but otherwise the polymer composition and molecular weight remained consistent. The slight reduction in productivity is within experimental error and the molecular weight remains the same.

It is therefore assumed that there is no influence on reducing the amount of BHT and the TMA is sufficiently scavenged. The complete data set can be seen in entry 1 of Table 2.9.

2.6 EP copolymerisation experiments using 2.07, 3, 4 and 6

In order to investigate the molecular weight capabilities of these systems an ethylene-propylene copolymerisation study was undertaken at LANXESS Elastomers. The same conditions were employed to those in Section 2.5 with the exception that no dihydrogen was included in the monomer gas feed and a lower catalyst dosing was used (0.05 μmol unless otherwise stated). EPDM experiments results in more branched and viscous polymer products which, without the presence of hydrogen gas to prevent high molecular weight formation, results in reactor fouling. The results are summarised in Table 2.4.

As is evident from Table 2.4, similar trends are observed for both the productivities and polymer composition. A stronger affinity for propylene for precatalysts **4** is again observed relative to **2.07** and this is exceeded by precatalyst **3**, which displays an unexplained relative increase without the presence of the dienes or dihydrogen. Without the use of dihydrogen the molecular weight is representative of the barrier to termination pathways described in Chapter One. The bimetallic catalysts all have similar molecular weight capacities, which is lower than the monometallic species. Molecular weight is proportional to the ratio of the rate of propagation to the overall rate of termination. The productivities when using precatalyst **2.07** are only slightly increased compared to those when using precatalysts **3** and **6**, but the molecular weights for the latter are significantly reduced. All these catalysts exhibit single-site behaviour as is evident by the GPC data in Figure 2.12.

The lower molecular weights for precatalyts **3** and **4** could be contributed by a lower rate of propagation, reflected in the reduced productivity, or increased rate of termination. The reduced rate of ethylene propagation in comparison to precatalysts **2.07** and **6** could be a result of an increased positive charge on the conjugated metal centres and the steric congestion of two proximate metal centres. It is important to note that the rate of incorporation of propylene is slower than that of ethylene. Considering different catalysts have different monomer affinities, and therefore polymers produced, the rates cannot be exactly compared.

In previous studies, monometallic κ^1-amidinate catalysts have been shown to have an ethylene concentration in solution dependence on the molecular weight, which suggest β-hydrogen elimination is the main termination pathway and therefore assumed to be prevalent here. An increased positive charge at the metal centre is expected to decrease the rate of β-hydrogen elimination and so maybe a larger molecular weight than is expected is observed for precatalysts **3** and **4**.

The use of precatalyst **4**, entry 3, has a significantly lower productivity but a comparable molecular weight and composition to precatalyst **3**. This suggests that both the rate of propagation and termination are reduced. The reduced propagation is assumed to be a result of steric proximity or a further increase in positive charge at the metal centres. The reduced termination may be a result of this increased positive charge at the metal centres or by an improved recapture of vinylic terminated polymers by the neighbouring metal centre, as was discussed in Chapter One.

Table 2.4. EP polymerisation results for $Cp^*Ti\{NC(Ph)N^iPr_2\}Me_2$ (**2.07**), 1,4-$C_6H_4\{NCN^iPr_2\}_2\{Cp^*TiMe_2\}_2$ (**3**), 1,3-$C_6H_4\{NCN^iPr_2\}_2\{Cp^*TiMe_2\}_2$ (**4**) and $CH_2\{1,4\text{-}C_6H_4\text{-}C(NH)N^iPr_2\}_2\{Cp^*TiMe_2\}_2$ (**6**).

Entry	Precatalyst	Cocatalyst	Productivity[a] (kg mol Ti^{-1} h^{-1} bar^{-1})	C_2 (wt%)	C_3 (wt%)	M_n (kDa)	M_w (kDa)	PDI
1	**2.07**	MAO	117,770	49.5	50.5	797	1451	1.8
2	**3**	MAO	83,830	43.2	56.8	488	1042	2.1
3	**4**	MAO	11,310	39.6	60.4	533	1031	1.9
4	**6**	MAO	95,830	47.7	52.3	553	1115	2.0

Polymerisation conditions. T = 90 °C, Pressure: 7 bar, [Cat] = 0.05 µmol (Entry 2: [Cat] = 0.03 µmol), [Al]:[Cat] = 4500, [Al]:[BHT] = 1, 10 minute reaction time. Solvent pentamethylheptane (1 L) C_3/C_2 =400/200 Nl h^{-1}. [a] Productivity per mol of transition metal centres.
Polymer characterisation. Polymer molecular weight and molecular weight distributions: the polymers have been analysed with the Freeslate Rapid GPC in 1,2,4 Trichlorobenzene against PS standards. *Average composition:* the polymers have been analysed via transmission IR spectroscopy on a pressed polymer film.

2.7 Synthesis and Characterisation of monometallic cyclopentadienyl-amidinate titanium complexes

As discussed in Chapter One, a key feature of the research by Marks and co-workers, involving *ansa*-amido-monocyclopentadienyl Ti and Zr bimetallic catalysts, involved the improved incorporation of α-olefins in copolymerisation studies. Using MAO as the cocatalyst the bimetallic titanium complex **2.16** (Figure 2.14) incorporated an increased amount of isobutene (6.2 compared to 2.9% for its mononuclear analogue (**2.15**)).[47] However, both the molecular weight and activity decreased when complex **2.16** was used in comparison to **2.15**.[48]

The analogous bimetallic zirconium catalysts **1.50-Cl** and **1.51-Cl** and their mononuclear analogue **1.49-Cl** introduced in Chapter One were used in MAO activated copolymerisation studies with ethylene and 1-hexene. The amount of 1-hexene incorporated increased in the bimetallic systems. 5.4 *n*-butyl branches were observed per 1000 carbon atoms for **1.49-Cl**, but this rose to 22.8 and 19.4 for **1.50-Cl** and **1.51-Cl**, respectively. As discussed in Chapter One these systems also showed a dramatic increase in molecular weight in homo- and copolymerisation studies with comparable activities (440, 328,000 and 253,000 g mol^{-1} for **1.49-Cl**, **1.50-Cl** and **1.51-Cl**, respectively, in an ethylene/hexene study).[49] To see if this effect was sterically-driven a modified version of **1.49-Cl** was synthesised with a napthyl substituent (**2.17**, Figure 2.14). Although no copolymerisation studies with α-olefins were carried out it was observed that in ethylene homopolymerisation a reduced molecular weight compared to the bimetallic counterparts was observed, and that therefore the improved molecular weight effect was not steric in origin.[50]

This Section has only discussed information involving MAO as the cocatalyst. The nuclearity of the cocatalyst can have a significant effect on α-olefin incorporation as will be discussed and experimentally explored in Chapter Four.

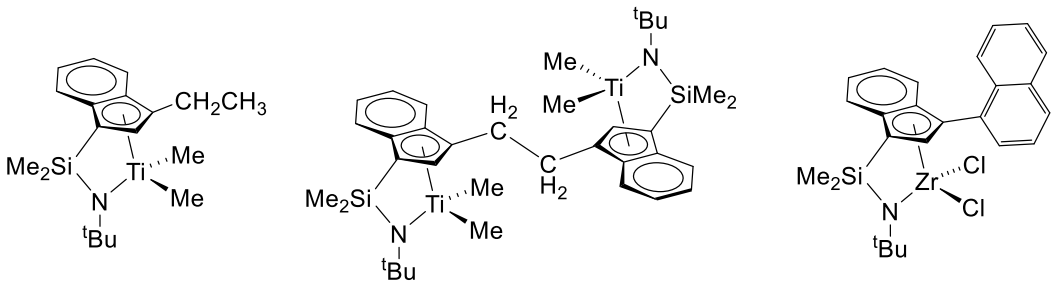

Figure 2.14 Monometallic and bimetallic constrained geometry catalysts.[48, 50]

As discussed in Chapter One, $Cp^{*}Ti\{NC(N^{i}Pr_2)Ar^{F_2}\}Me_2$ (Ar^{F_2} = 2,6-$C_6H_3F_2$) (**1.40**) forms a unique base-free dimeric methyl titanium dication in the solid state. This catalyst, with fluorine substituents in both *ortho* positions, also proved to have a higher affinity (C_3 = 52%, C_2 = 48%) than **2.07** (C_3 = 50.5%, C_2 = 49.5%) for propylene in an ethylene/propylene copolymerisation study with the same C_2:C_3 monomer molar ratio.[19]

An internal investigation from LANXESS Elastomers screened a range of metal amidinate complexes with different fluorine substituents on the aromatic ring (Figure 2.15).[51]

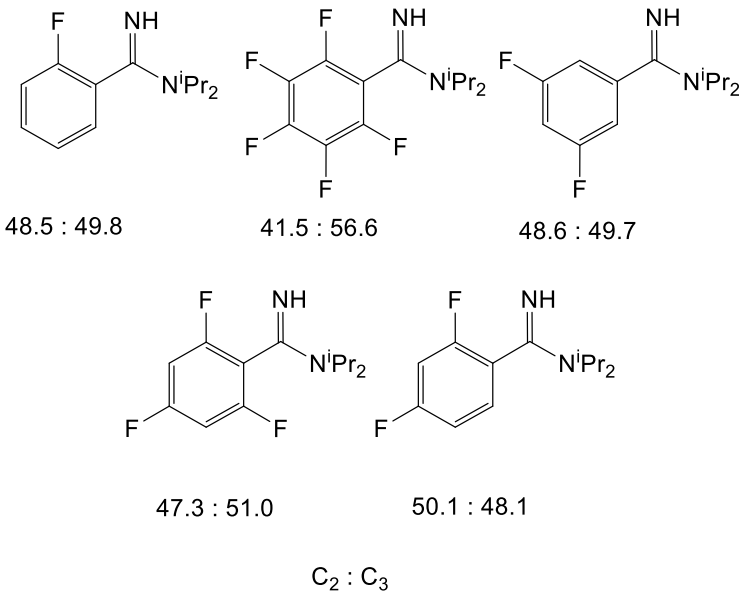

Figure 2.15 Amidines with fluorine substituents screened by LANXESS Elastomers. Included is C_2:C_3 composition for the resultant polymer of an EPDM copolymerisation with corresponding titanium complex used as the precatalyst.

The ligands with the most electron-withdrawing substituents resulted in the highest propylene affinities. In a comparable EPDM study to the one carried out in Section 2.5 the perfluorophenyl ring incorporated 56.6% propylene, whereas the complex with fluorine substituents exclusively in the *meta*-positions incorporated 49.7%. It was noted that the more electron-withdrawing perfluorophenyl ring resulted in a substantially lower activity and that no clear trend was observed for diene affinity.

From the copolymerisation results shown in Section 2.5 and 2.6 it was evident that the conjugated systems displayed an increased affinity for propylene over ethylene. To probe whether this was caused by electronic effects, a series of monometallic complexes, of the form $Cp^{*}Ti\{NC(Ar^{R})N^{i}Pr_2\}Me_2$, with a variety of substituents in the *para* position were synthesised and tested in EPDM copolymerisation studies. The different electron withdrawing or releasing substituent can be quantified by a Hammett parameter (σ), which have been used in a wide range of rate and equilibria analysis across organic and inorganic reactions.[52] Fluorine substituents are known to inductively withdraw electron density, but are also known to mesomerically donate; in the *para* position a σ_p value of 0.06 is reported, this is increased to 0.34 in the *meta* position due to unfavourable resonance forms. It is proposed that an electron-withdrawing group increases the electrophilicity of the metal centre and results in a relative increase in propylene incorporation, as observed for entry 2 in Table 2.3.

2.7.1 Ligand synthesis

Amidines comparable to **2.08** with the *para* substitution of CF_3 (**8**), Fc (**9**), ^{t}Bu (**10**) and NMe_2 (**11**) were all successfully synthesised. The substituents have σ_p values of 0.54, -0.18, -0.20 and -0.83, respectively. All the compounds were prepared *via* a nucleophilic attack on the nitrile precursors of the *in situ* generated amide reagent, $^{i}Pr_2NMgBr$, as previously discussed (Equation 2.4).

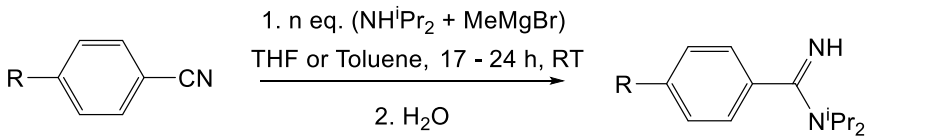

R = CF_3 (**8**, n= 1), Fc (**9**, n = 2),
^{t}Bu (**10**, n = 1) and NMe_2 (**11**, n = 2.5)

Equation 2.4

All of the benzonitrile precursors are commercially available apart from 4-ferrocenylbenzonitrile, which was prepared according to literature procedures. Ferrocene was first oxidised to ferrocenium using concentrated sulphuric acid and then reacted with an *in situ* generated diazonium salt in the presence of copper. This procedure was reported only with a 39% yield and this was not improved upon in this work.[53] Compounds **8** and **10** were both produced using a stoichiometric amount of amide reagents. In contrast, compounds **9** and **11** required 2 and 2.5 equiv. of the amide, respectively, and THF as the solvent to generate the desired products. This is presumed to be a result of the increased electron donation from the amine group for compound **11** and possibly increased steric bulk from the ferrocenyl group for compound **9.**

Heating the reaction mixture for **11** in toluene resulted in decomposition to an unknown side-product. Compound **8** formed as a colourless oil, the crude was purified by vacuum distillation (110 ^{o}C, 1 x 10^{-1} mbar) and dried by stirring over CaH_2 for 24 h at room temperature. Slow cooling of the oil caused crystallisation of the compound. The remaining compounds (**9** – **11**) were purified by washing or crystallisation and the overall yields are 55, 81, 81 and 84% for compounds **8** – **11**, respectively. The room temperature ^{1}H NMR (298 K, $CDCl_3$) spectra are displayed in Figure 2.16, and the only significant chemical shift differences occur for the phenyl protons. Minimal variation is observed for the ν(C=N) stretch in their IR spectra.

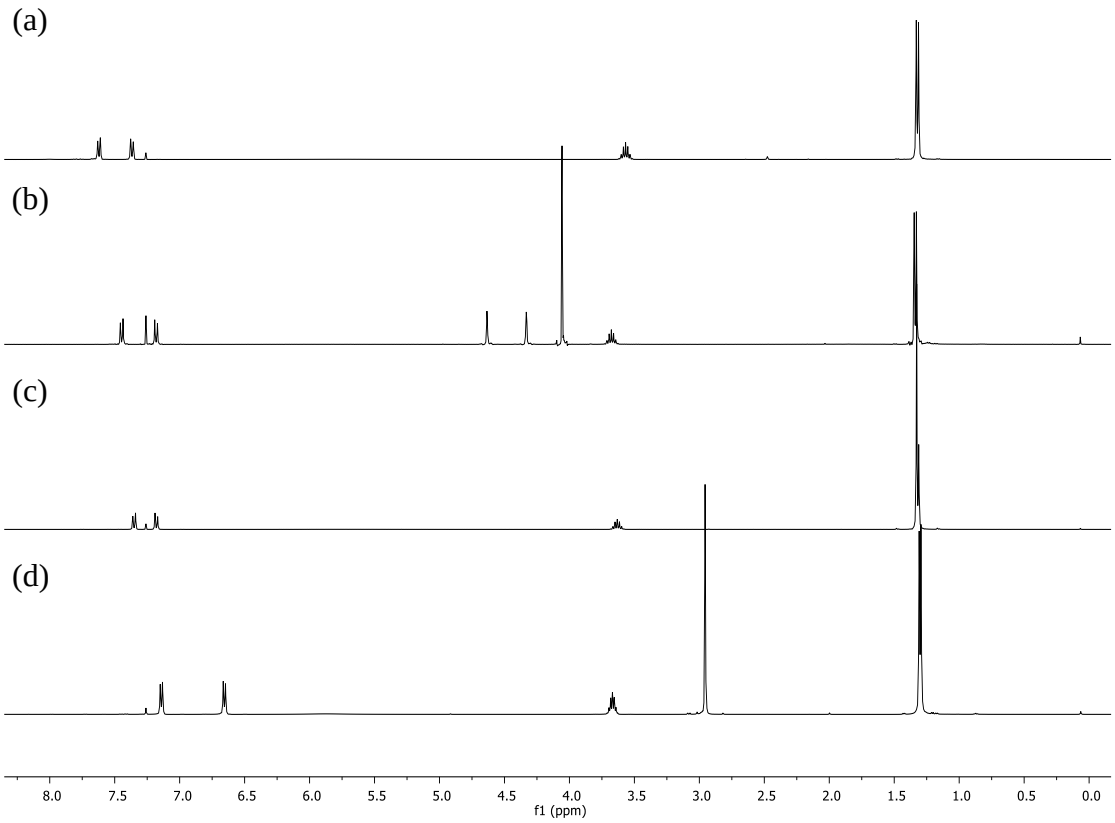

Figure 2.16 ^{1}H NMR (399.9 MHz, $CDCl_3$, 298 K) spectra of $HNC(Ar^{CF3})N^{i}Pr_2$ (**8**, a), $HNC(Ar^{Fc})N^{i}Pr_2$ (**9**, b), $HNC(Ar^{tBu})N^{i}Pr_2$ (**10**, c) and $HNC(Ar^{NMe2})N^{i}Pr_2$ (**11**, d).

Diffraction-quality crystals of **8** were grown *via* slow cooling of the neat compound, and of **9** from slow evaporation of a pentane solution. The molecular structures are shown in Figure 2.17, and selected bond lengths and angles of **8** and **9** are compared in Table 2.5.

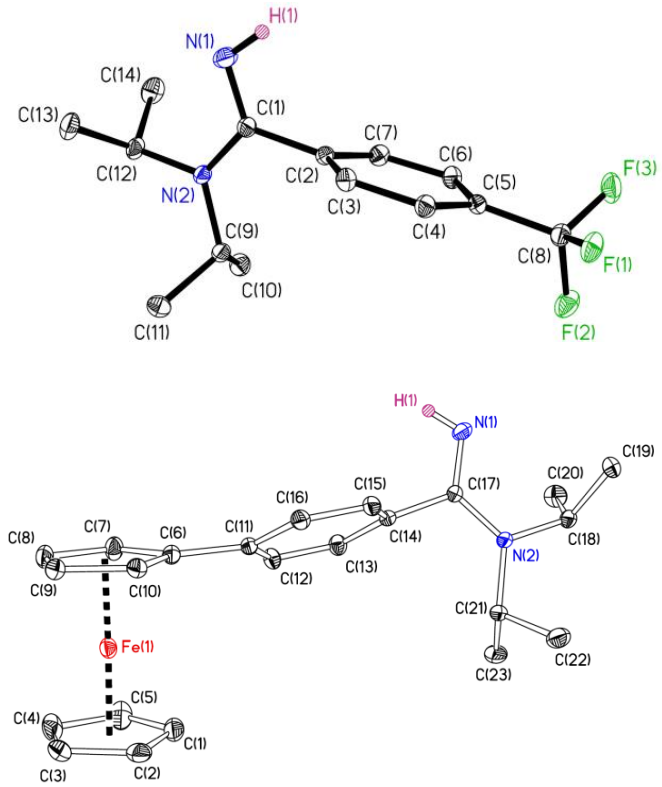

Figure 2.17 Displacement ellipsoid plots of HNC(Ar^{CF3})N^{i}Pr$_2$ (**8**, top) and HNC(Ar^{Fc})N^{i}Pr$_2$ (**9**, bottom; 2nd molecule in the asymmetric unit omitted) (20% probability, C-bound H atoms omitted).

Table 2.5. Selected bond lengths (Å) and angles (°) for HNC(Ar^{CF3})N^{i}Pr$_2$ (**8**, top) and HNC(Ar^{Fc})N^{i}Pr$_2$ (**9**, bottom). Two sets of values are shown for **9** for corresponding to the molecules in the asymmetric unit. Cp$_{cent}$ is the computed Cp ring carbon centroid.

Parameter		Parameter	
C(1)-N(1)	1.290(2)	N(1)-C(1)-C(2)	120.79(15)
C(1)-N(2)	1.361(2)	N(1)-C(1)-N(2)	121.88(15)
C(1)-C(2)	1.501(2)	C(2)-C(1)-N(2)	117.30(14)
N(2)-C(8)	1.475(2)	C(8)-N(2)-C(11)	116.64(13)

Parameter		Parameter	
C(17)-N(1)	1.285(3), 1.291(3)	N(1)-C(17)-C(14)	120.31(18), 121.67(19)
C(17)-N(2)	1.359(3), 1.363(3)	N(1)-C(17)-N(2)	121.37(19), 121.0(2)
C(17)-C(14)	1.511(3), 1.493(3)	C(14)-C(17)-N(2)	118.32(17), 117.36(18)
N(2)-C(18)	1.481(2), 1.471(3)	C(18)-N(2)-C(21)	116.81(16), 117.04(16)
Fe(1)-Cp$_{cent}$(1)	1.650, 1.649		
Fe(1)-Cp$_{cent}$(2)	1.643, 1.652		

There are no significant differences in the bond lengths and angles in common for either structure in comparison to one another or to **2.08**, **1** and **2** discussed in Section 2.2.1. As noted before, the phenyl ring lies perpendicular to N=C–N plane, and in the case of compound **9** it is in the same plane as the cyclopentadienyl ring of the ferrocene, allowing for conjugation. The ferrocenyl group adopts an eclipsed conformation and there is no discernible difference in bond length between the iron atom and the centroid of the substituted and unsubstituted cyclopentadienyl ring.

Compound **8** was considered to have the potential for intermolecular interactions in the supramolecular structure with the carbon-bound fluorines acting as a hydrogen bond acceptor and the amidinate moiety a donor. The occurence of F---H hydrogen bonds are contested within the literature, with Dunitz and Taylor entitling a paper "Organic Fluorine Hardly Ever Accepts Hydrogen Bonds" in 1997 based on a Cambridge Structural Database (CSD) review[54] and subsequent studies highlighting the persistence of a weak binding energy (1-4 kcal mol^{-1}) for these interactions. It is now, however, accepted that these hydrogen bonds do exist across a wide-range of chemical environments. The supramolecular structure of **8** shows no such interaction within the range previously reported for an F---H hydrogen bond or for other notable crystal packing intermolecular interactions, no H–F coupling is observed for the resonances in the ^{19}F NMR spectrum.[55, 56]

2.7.2 Attempted synthesis of a trimethylammonium *para* substituted amidine

A proposed target was the monometallic complex with a trimethylammonium ($-NMe_3^+$) substituent in the *para* position. This would not only represent an excellent inductively electron withdrawing substituent (σ_p = 0.82) even larger than $–CF_3$ (σ_p = 0.54), but a cationic group would be an excellent mimic of the active titanium centres in **3**. It has been previously shown that the anion employed can have a large influence on the polymerisation activity[57-59] and it is proposed that an anion exchange could occur between the trimethylammonium group and the monomethyl titanium cation. So as to negate this effect a trimethylammonium substituent with a $[BF_{20}]^-$ counterion was targeted, this would allow for TBF_{20} to be used as the activating species in a polymerisation study and result in only one type of anion being present.

[1,4-C_6H_4(CN)(NMe_3)]I (**2.18**) can be prepared according to literature procedure by reaction of 4-dimethylaminobenzonitrile with MeI at 50 °C for 24 h (Equation 2.5).[60]

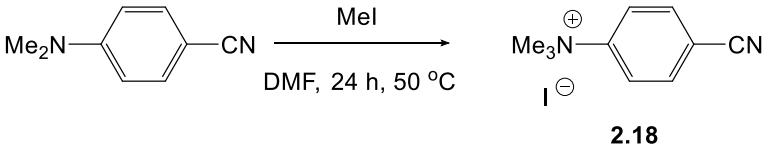

2.18

Equation 2.5

Reaction of **2.18** with KBF_{20} or $AgBF_{20}$, both prepared according to literature procedures,[61, 62] failed to give the anion exchange desired. A variety of solvents were attempted, but in all cases large amounts of the reagents remained not in solution. Reaction of **2.18** with 1 equiv. of TBF_{20} in THF gave a complicated mixture, a sub-stoichiometric amount of TBF_{20} was consumed and a distinctive colour change to dark purple was observed. The solid was washed with CH_2Cl_2, to remove the excess TBF_{20}, and the remaining red solid analysed. The ^{1}H NMR spectrum (298 K, acetone-d_6) showed one set of resonances comparable to **2.18**, the ^{11}B and ^{19}F NMR spectra corresponded to the $[BF_{20}]^-$ anion. Although these resonances are indicative of the desired product the elemental analysis was incorrect and the reaction is not in keeping with a sub-stoichiometric amount of TBF_{20} consumed. It was shown using X-ray diffraction analysis that the product is $[1,4\text{-}C_6H_4(CN)(NMe_3)][I_3]$ (Figure 2.18).

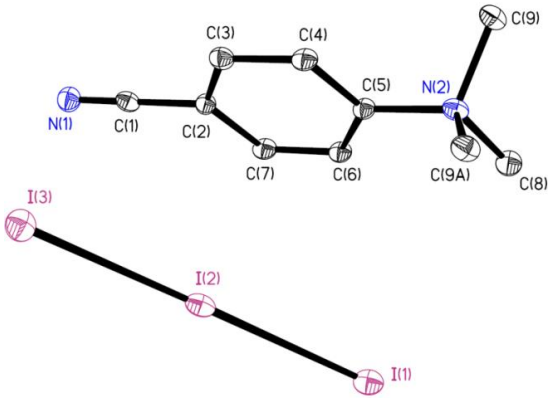

Figure 2.18 Displacement ellipsoid plot of $[1,4\text{-}C_6H_4(CN)(NMe_3)][I_3]$ (20% probability, C-bound H atoms omitted).

For this compound to form it suggests that triphenylmethyl iodide and the desired product, $[1,4\text{-}C_6H_4(CN)(NMe_3)][BF_{20}]$, are produced. However, the triphenylmethyl iodide allows for a redox pathway to take place forming iodine and the "Gomberg dimer" (3-triphenylmethyl-6-diphenylmethylidene-1,4-cyclohexadiene), through the dimerisation of two trivalent carbon species.[63, 64] The iodine can then react with **2.18** to form the triiodide product (Scheme 2.5). The colour observed is presumed to be a

result of the purple iodine and the red triiodide forming. Alternative solvent and reaction conditions were employed, but prevention of this product could not be achieved. The ^{1}H NMR spectrum only shows one set of resonances as expected.

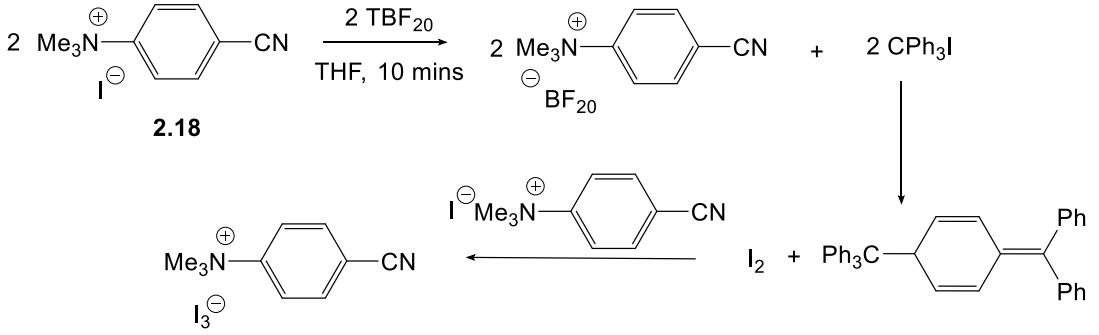

Scheme 2.5

To avoid this from taking place [1,4-C_6H_4(CN)(NMe_3)]Cl (**12**) was synthesised from the reaction of **2.18** with a freshly prepared sample of AgCl in acetonitrile. It was necessary for this reaction to be carried out in the dark. Compound **12** and AgI precipitated from acetonitrile, and extraction into distilled water afforded the desired product in a 75% yield, the AgI remained as an expected pale yellow precipitate. Compound **12** was fully characterised. The ^{1}H NMR spectrum (298 K, DMSO-d_6) gave three resonances at 8.25, 8.20 and 3.67 ppm for the two aromatic and trimethylammonium signals respectively, which are almost identical to those of **2.18**. A ^{1}H-^{13}C HSQC experiment indicated the resonance at 56.3 ppm in the ^{13}C{^{1}H} NMR spectra corresponds to the trimethylammonium group. Only the cation envelope was observed in the ESI mass spectrometry.

Reaction of **12** with a stoichiometric amount of TBF_{20} in acetonitrile produced the desired compound [1,4-C_6H_4(CN)(NMe_3)][BF_{20}] (**13**) in an 83% yield. The CPh_3Cl produced is harder to oxidise and it can be easily removed from **13** by extraction into CH_2Cl_2. Unlike **2.18** and **12**, compound **13** showed a greater degree of solubility and mass envelopes corresponding to both the cation and anion in ESI-mass spectrometry. Medium intensity bands corresponding to the ν(C≡N) were present at 2229 and 2236 cm^{-1} for **12** and **13**, respectively, in their IR spectra.

Diffraction-quality crystals of **13** were grown at room temperature from an acetone solution and the molecular structure is shown in Figure 2.19. The bond lengths and

angles shows no discernible differences between the cations in [1,4-$C_6H_4(CN)(NMe_3)$][I_3] and **13**.

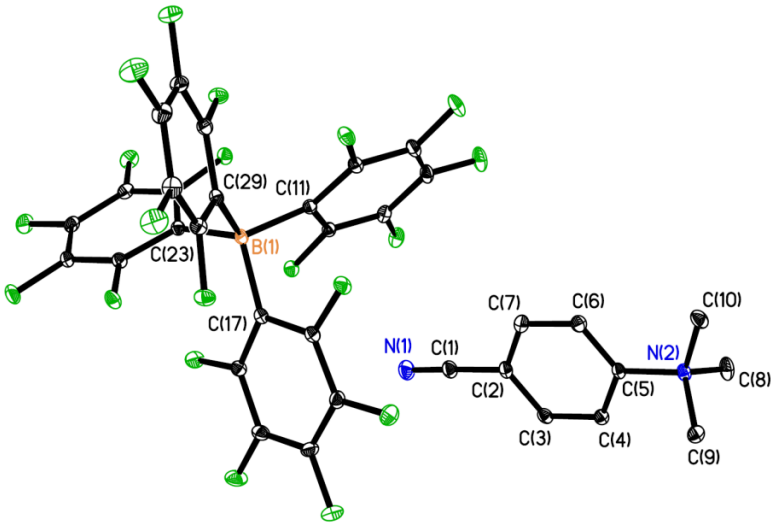

Figure 2.19 Displacement ellipsoid plot of [1,4-$C_6H_4(CN)(NMe_3)$][BF_{20}] (**13**) (20% probability, C-bound H atoms omitted).

Reaction of **13** with either the *in situ* generated amide, $^{i}Pr_2NMgBr$, or $^{i}Pr_2NH$ in the presence of aluminium trichloride generated a mixture of products. There was no evidence of the desired amidine product being formed by either NMR spectroscopy or mass spectrometry. Quenching of the reaction mixture by water or Me_3SiCl was carried out without success.

Reaction of **2.18** with 2 equiv. of $^{i}Pr_2NMgBr$ in THF and subsequent quenching with Me_3SiCl produced the desired amidine, [$SiMe_3NC(Ar^{NMe3})N^{i}Pr_2$]I, as determined by ^{1}H NMR spectroscopy and elemental analysis (Equation 2.6). A yield above 10% could not be achieved and as a result this route was not further pursued.

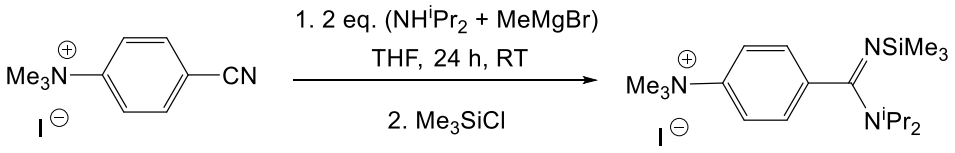

Equation 2.6

Formation of [$HNC(Ar^{NMe3})N^{i}Pr_2$]I from the amidine **11** was also attempted. However, compound **11** showed no reactivity with MeI in either diethyl ether or DMF at room temperature or elevated temperatures.

2.7.3 Synthesis of cyclopentadienyl-amidinate monometallic complexes

The synthesis of the target complexes was attempted *via* the previously described protonolysis pathway but using compounds **8 – 11**.

Reaction of **8** and **9** with Cp^*TiMe_3 proved straightforward and generated the desired products, $Cp^*Ti\{NC(Ar^{CF3})N^iPr_2\}Me_2$ (**14**) and $Cp^*Ti\{NC(Ar^{Fc})N^iPr_2\}Me_2$ (**15**), at room temperature within 17 h (Equation 2.7). Purification was achieved by washing with hexane, at low temperature (-30 °C) in the case of **14**, and the final products were obtained in 40 and 64% yields, respectively. Complexes **14** and **15** were fully characterised and the analysis will be discussed in Section 2.7.5. The corresponding reaction of Cp^*TiMe_3 with **10** and **11** was unsuccessful at room temperature, with no reaction taking place. Heating a reaction mixture of **10** with Cp^*TiMe_3 to 70 °C also resulted in no reaction, and at higher temperatures decomposition products were observed. This limited reactivity results from the more electron-donating substituents decreasing the Brønsted acidity.

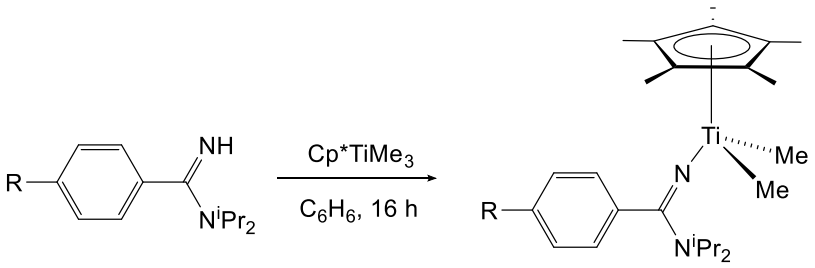

R = CF_3 (**8**) or Fc (**9**) — R = CF_3 (**14**) or Fc (**15**)

Equation 2.7

This synthetic limitation was overcome by reaction of **10** or **11** with Cp^*TiCl_3 in the presence of an excess of triethylamine as an external base, resulting in the desired dichloride complexes $Cp^*Ti\{NC(Ar^{tBu})N^iPr_2\}Cl_2$ (**16**) and $Cp^*Ti\{NC(Ar^{NMe2})N^iPr_2\}Cl_2$ (**17**). Both reactions were completed after 20 h at room temperature (Equation 2.8). Extraction away from the ammonium chloride salt using benzene, and purification by washing with hexane or crystallisation afforded the complexes in 48 and 79% yields, respectively.

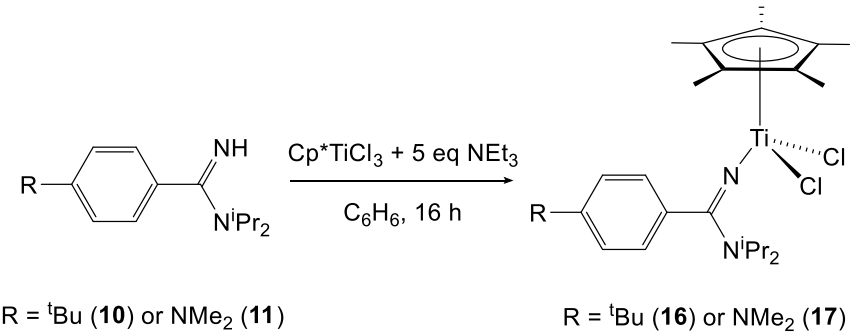

Equation 2.8

The ^{1}H NMR spectra of complexes **14** and **15** both indicate fluxionality at room temperature as judged by the resonances corresponding to the isopropyl groups, and also show the same trend in aromatic resonances as observed in their amidine counterparts. As shown before, variable temperature NMR data can be used to probe this and the complexes were fully characterised at a temperature where the resonances are separate and distinguishable, namely 243 and 213 K respectively. The variable temperature NMR spectra for complex **16** are shown in Figure 2.20.

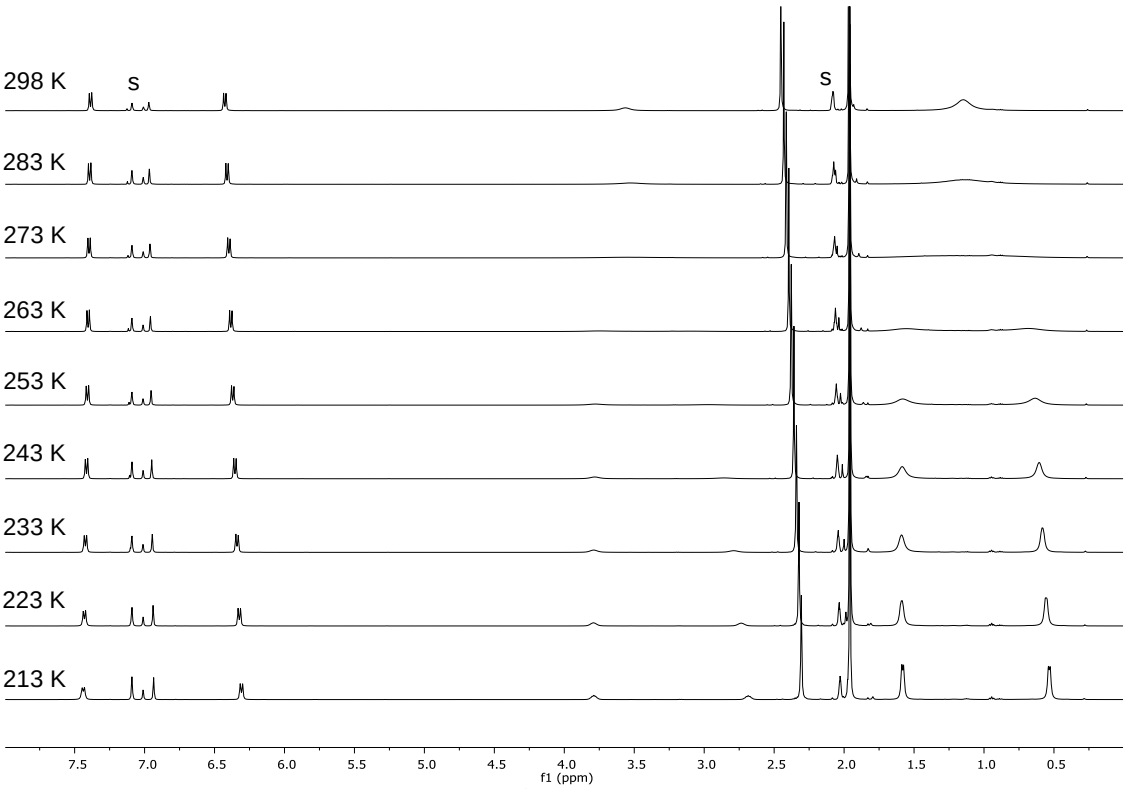

Figure 2.20 variable temperature ^{1}H NMR (499.9 MHz, Tol-d_8) spectra of Cp*Ti{NC(Ar^{NMe2})N^{i}Pr$_2$}Cl$_2$ (**15**). 's' denotes residual protio-solvent.

The rates of isopropyl group exchange are different for **16** and **17**. The temperature of coalescence is approximately 273 K for **17**, whereas the resonances had not coalesced at 298 K for **16**. This is despite the comparable frequency separations in the low temperature regime. As discussed in Chapter One the amidinate moiety can act as up to a 5-electron which lead to a partial double bond character between the central carbon and amine nitrogen, $\underline{N}^{i}Pr_2$. It is restricted rotation around this bond which leads to the fluxionality observed (*cf.* Figure 2.16). The extent of the double bond character will influence the coalescence temperature. Since **17** has a lower barrier to activation, this implies less double bond character bought upon by the presence of a dimethylamino group as opposed to a *para-tert*-butyl group. This is due to the capacity for the dimethylamino substituent to both inductively and mesomerically donate into the phenyl ring, providing a competing resonance form as denoted in Figure 2.21.

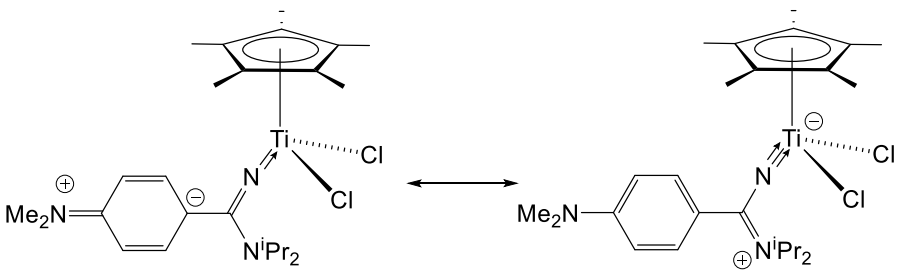

Figure 2.21 Proposed resonance forms of $Cp^{*}Ti\{NC(Ar^{NMe2})N^{i}Pr_2\}Cl_2$ (**17**)

To probe this further a variable temperature NMR study was carried out comparing $Cp^{*}Ti\{NC(Ar^{NMe2})N^{i}Pr_2\}Cl_2$ (**17**) and the previously synthesised $Cp^{*}Ti\{NC(Ph)N^{i}Pr_2\}Cl_2$ (**2.06**), which has a coalescence temperature of 313 K. Exchange rate constants were calculated at various temperatures using gNMR and were used to construct an Eyring plot (Figure 2.22).

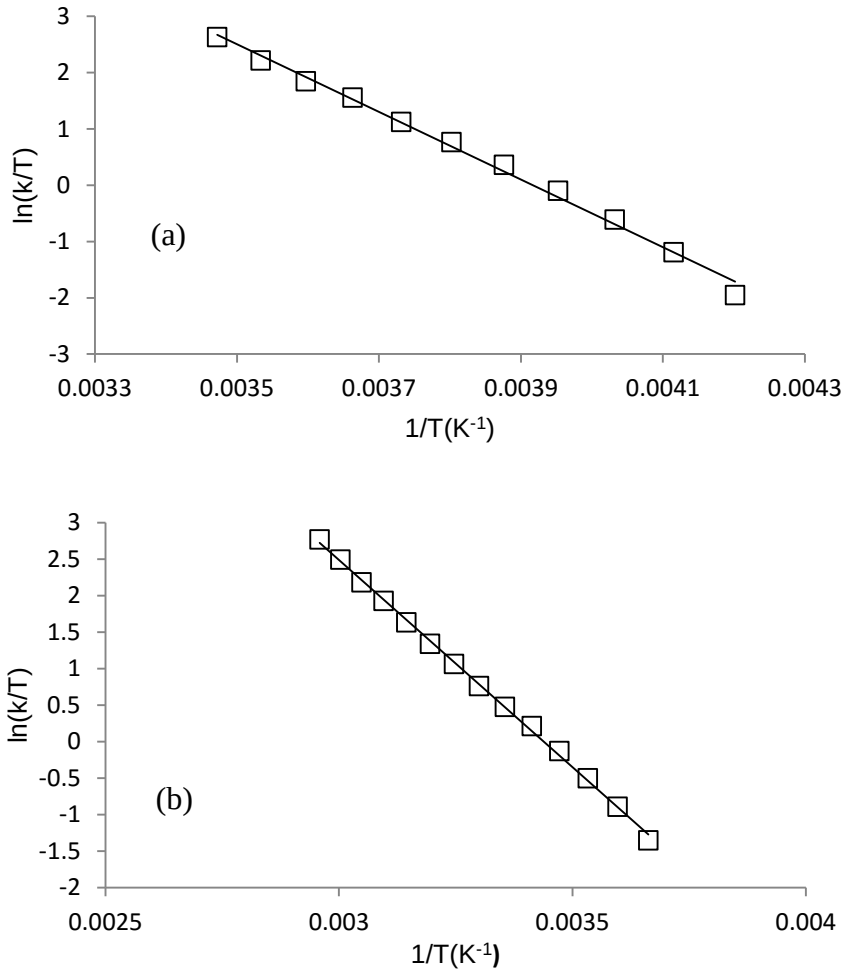

Figure 2.22 Eyring plots for N^{i}Pr$_2$ group exchanging in Cp*Ti{NC(Ar^{NMe2})N^{i}Pr$_2$}Cl$_2$ (**17**, a) ($\Delta H^{\ddagger}$ = 50(1) kJmol^{-1}, $\Delta S^{\ddagger}$ = -2(5) JK^{-1}mol^{-1} and $\Delta G_{285}^{\ddagger}$ = 51(1) kJmol^{-1}) and Cp*Ti{NC(Ph)N^{i}Pr$_2$}Cl$_2$ (**2.06**, b) ($\Delta H^{\ddagger}$ = 47.1(5) kJmol^{-1}, $\Delta S^{\ddagger}$ = -36(2) JK^{-1}mol^{-1} and $\Delta G_{285}^{\ddagger}$ = 57.3(4) kJmol^{-1}).

From the Eyring plots barriers of $\Delta G_{285}^{\ddagger}$ = 57.3(4) kJmol^{-1} for **2.06** and $\Delta G_{285}^{\ddagger}$ = 51(1) kJmol^{-1} for **17** were calculated. This decreased barrier to rotation is in keeping with the above discussion concerning a decreased amount of double bond character within the amine bond of the amidinate moiety. The Gibbs free energy calculated from the coalescence temperatures ($\Delta G_{273}^{\ddagger}$ = 50.6 and $\Delta G_{313}^{\ddagger}$ = 58.3 kJmol^{-1} for **17** and **2.06**, respectively) are in good agreement with those calculated from the values extracted from the Eyring plots ($\Delta G_{273}^{\ddagger}$ = 50.5 and $\Delta G_{313}^{\ddagger}$ = 58.4 kJmol^{-1} for **17** and **2.06**, respectively). The reason for the difference in the entropy values obtained ($\Delta S^{\ddagger}$ = -2 and -36(2) JK^{-1}mol^{-1} for **17** and **2.06**, respectively) is unclear.

2.7.4 X-ray structures of $Cp^*Ti\{NC(Ar^{tBu})N^iPr_2\}Cl_2$ (16) and $Cp^*Ti\{NC(Ar^{NMe2})N^iPr_2\}Cl_2$ (17)

Diffraction-quality crystals were grown from hexane solutions at 0 and -30 °C for **16** and **17**, respectively. The molecular structures are shown in Figure 2.23. Selected bond lengths and angles of **16** and **17** are compared in Table 2.6 along with these for previously synthesised $Cp^*Ti\{NC(Ph)N^iPr_2\}Cl_2$ (**2.06**)[2] for comparison.

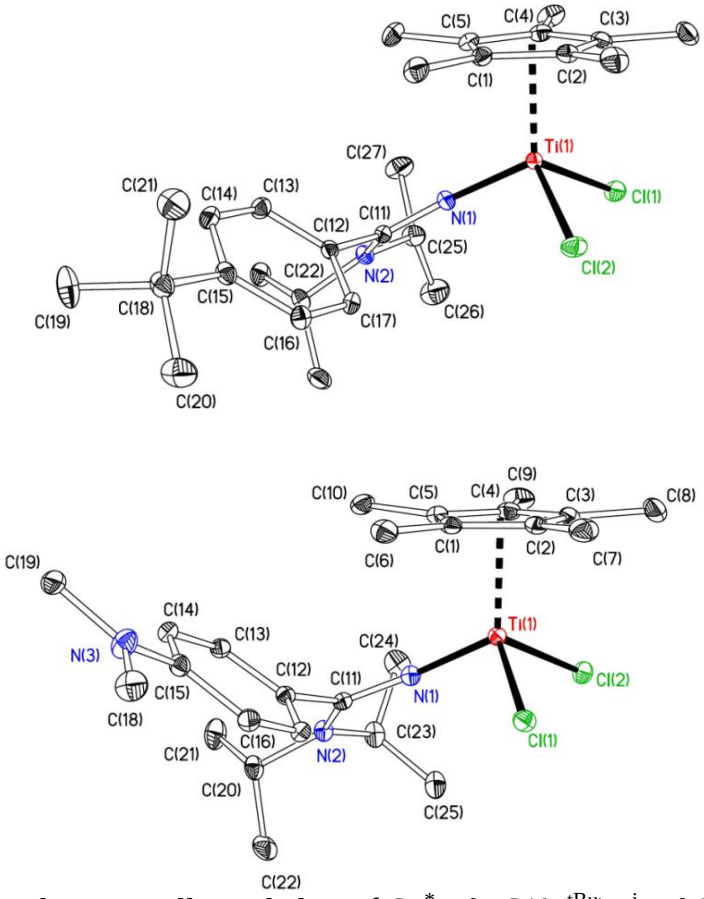

Figure 2.23 Displacement ellipsoid plots of $Cp^*Ti\{NC(Ar^{tBu})N^iPr_2\}Cl_2$ (**16**, top) and $Cp^*Ti\{NC(Ar^{NMe2})N^iPr_2\}Cl_2$ (**17**, bottom) (20% probability, C-bound H atoms omitted).

Table 2.6 Selected bond lengths (Å) and angles (°) for $Cp^*Ti\{NC(Ph)N^iPr_2\}Cl_2$ (**2.06**), $Cp^*Ti\{NC(Ar^{tBu})N^iPr_2\}Cl_2$ (**16**) and $Cp^*Ti\{NC(Ar^{NMe2})N^iPr_2\}Cl_2$ (**17**). Cp^*_{cent} is the computed Cp^* ring carbon centroid.

Parameter	**2.06**	**16**	**17**
Ti(1)-Cp^*_{cent}	2.05	2.04	2.05
Ti(1)-N(1)	1.800(3)	1.798(2)	1.7920(17)
N(1)-C(11)	1.310(4)	1.302(3)	1.310(2)
N(2)-C(11)	1.340(4)	1.355(3)	1.344(2)
C(11)-C(12)	1.509(5)	1.499(3)	1.499(3)
Ti(1)-Cl(1)	2.3137(11)	2.2965(8)	2.2927(6)
Ti(1)-Cl(2)	2.3051(11)	2.3066(7)	2.3266(6)
Cp^*_{cent}-Ti(1)-N(1)	118.0	116.0	117.8
Cp^*_{cent}-Ti(1)-Cl(1)	113.5	115.1	116.2
Cp^*_{cent}-Ti(1)-Cl(2)	115.0	115.1	112.9
C(11)-N(1)-Ti(1)	165.2(3)	168.25(19)	164.28(14)

The molecular structures of **16** and **17** show the expected *pseudo*-tetrahedral three-legged piano stool titanium centre. The linear C(11)–N(1)–Ti(1) bond angle in **2.06** (165.2(3)°), **16** (168.25(19)°) and **17** (164.28(14)°) suggests a Ti(1)–N(1) dπ-pπ contribution to the bonding. In **17** the NMe_2 *para*-phenyl substituent has a trigonal planar sp^2 conformation (the sum of the angles subtended at N(3) is 359.95(32)°) to allow for conjugation of the nitrogen lone-pair and the phenyl π-system, as proposed in Figure 2.21. Despite the different NMR activation parameters for **2.06** and **17**, there are no significant differences for Ti(1)–N(1), N(2)–C(11) and N(1)–C(11) bond length of **2.06**, **16** or **17**. In all the molecular structures the aromatic ring is orthogonal to the amidinate moiety implying a negligible conjugation. This results in a limited influence of the *para*-phenyl substituents in the solid state. A comprehensive comparison with their dimethyl counterparts will be carried out in Section 2.7.6

2.7.5 Synthesis and characterisation of cyclopentadienyl-amidinate monometallic dimethyl complexes

The synthesis of $Cp^*Ti\{NC(Ar^{tBu})N^iPr_2\}Me_2$ (**18**) and $Cp^*Ti\{NC(Ar^{NMe2})N^iPr_2\}Me_2$ (**19**) was achieved by a cold (5 °C) dropwise addition of 2 equiv. of MeLi to a solution of **16** or **17** in benzene (Equation 2.9). In both cases an immediate colour

change from red to yellow was observed. Isolated yields of 48 and 58% were obtained for **16** and **17**, respectively.

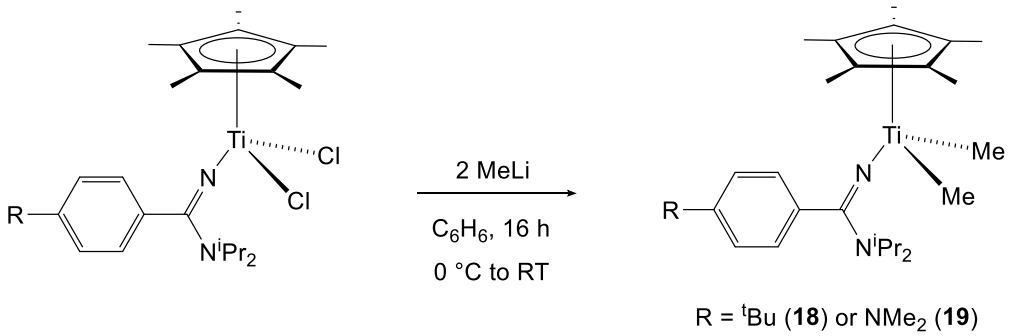

Equation 2.9

The ^{1}H NMR spectra of complexes **14**, **15**, **18** and **19** are shown in Figure 2.24. A similar trend is observed across this series as was seen for the protio-amidines. A distinctive upfield chemical shift of 6.47 ppm is observed for **19** corresponding to the aromatic protons *meta* to the *para*-phenyl substituent. In the ^{1}H NMR spectrum of **15** characteristic resonances corresponding to a mono-substituted ferrocenyl moiety are observed at 4.78, 4.33 and 4.01 ppm in a 1:1:2 ratio. All the complexes displayed fluxionality at room temperature as judged by the resonances corresponding to the isopropyl groups and were subsequently characterised at low temperature, as has been previously discussed. The spectra of **18** and **19** at 298 K show sharper resonance corresponding to the isopropyl group than their dichloride analogues and a variable temperature study established lower coalescence temperatures.This is indicative of a reduced double bond character within the N=C–N^{i}Pr$_2$ of the amidinate moiety bought about by methyl being a stronger σ-donor than chloride. This will be discussed further in the following section.

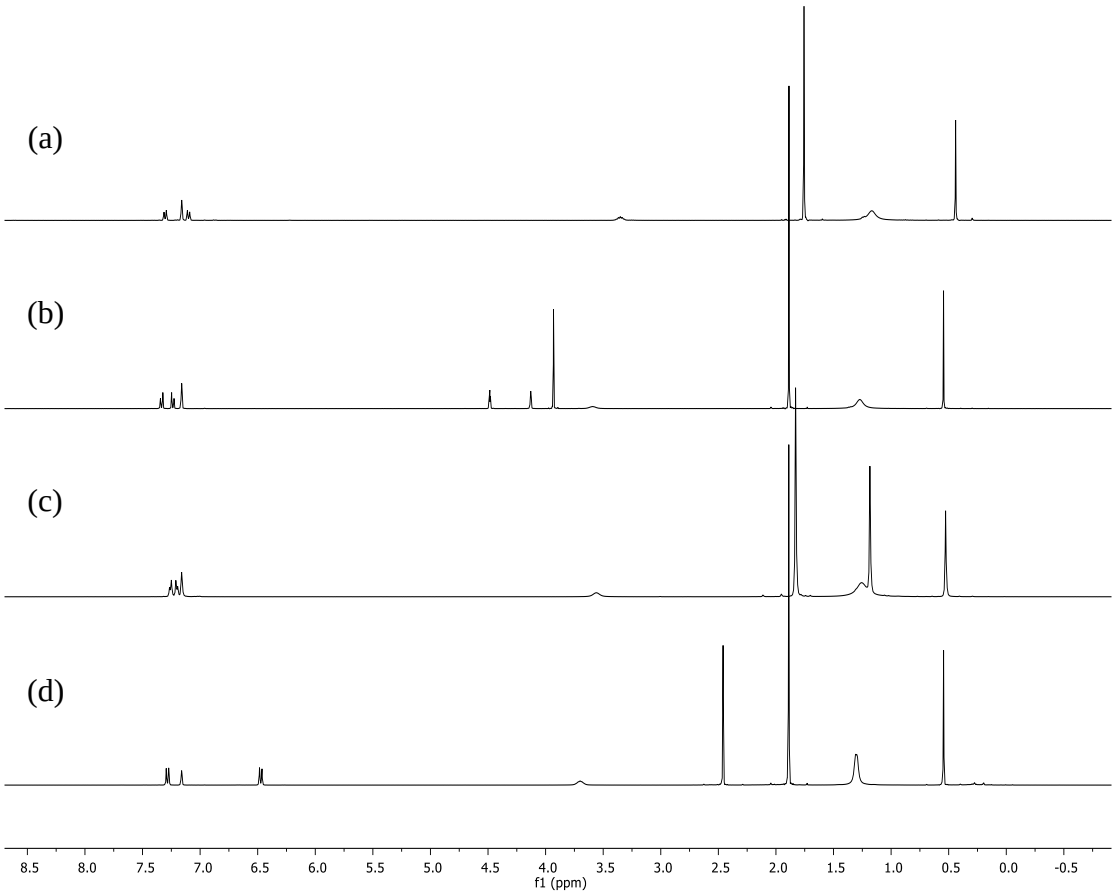

Figure 2.24 ^{1}H NMR (399.9 MHz, C_6D_6, 298 K) spectra of $Cp^{*}Ti\{NC(Ar^{CF3})N^{i}Pr_2\}Me_2$ (**14**, a), $Cp^{*}Ti\{NC(Ar^{Fc})N^{i}Pr_2\}Me_2$ (**15**, b), $Cp^{*}Ti\{NC(Ar^{tBu})N^{i}Pr_2\}Me_2$ (**18**, c) and $Cp^{*}Ti\{NC(Ar^{NMe2})N^{i}Pr_2\}Me_2$ (**19**, d).

Bent's rule states "atomic s-character concentrates in orbitals directed toward electropositive substituents".[65] An example of this is the difference in the $^{1}J_{CH}$ coupling constants in the compounds CH_4 (125 Hz) and MeCN (136 Hz) that can be attributed to the increased 2s orbital contribution to the C–H bonds of MeCN due to the introduction of the electronegative CN group. In 1988 Grubbs and co-workers investigated the effect of different ring-substituents on $^{1}J_{CH}$ for a series of titanocene methyl chloride complexes. It was shown that the methyl group in $Cp_2Ti(Me)Cl$ has $^{1}J_{C\text{-}H}$ = 128.9 Hz, which decreases with increased amount of methyl substitution on the cyclopentadienyl rings, and increases with electron-withdrawing substituents (126.5 and 129.9 Hz for $Cp^{*}{}_2Ti(Me)Cl$ and $CpCp^{CF3}Ti(Me)Cl$ respectively).[66] This is a result of the electon-withdrawing substituents lowering the energy level of the titanium orbitals. The 2s orbital character of the carbon is concentrated more in a bond to a more electropositive substituent. Table 2.7 shows selected $^{1}J_{CH}$ values and associated chemical shifts for complexes **2.07**, **14**, **15**, **18** and **19**. The coupling

constants were calculated from the proton-coupled 125 MHz ^{13}C spectra in C_6D_6. Zero-point filling was employed to improve the resolution and reduce error. The chemical shifts of the central carbon of the amidine moiety, N<u>C</u>(N^iPr_2), and of the aromatic carbon *ipso* to the amidinate moiety, <u>C</u>$_i$CN(N^iPr_2), in C_6D_6 are also shown for all compounds.

Table 2.7 Coupling constants and chemical shift of methyl groups attached to titanium and chemical shift of N<u>C</u>(N^iPr_2) and <u>C</u>$_i$CN(N^iPr_2) in complexes $Cp^*Ti\{NC(Ph)N^iPr_2\}Me_2$ (**2.07**), $Cp^*Ti\{NC(Ar^{CF3})N^iPr_2\}Me_2$ (**14**), $Cp^*Ti\{NC(Ar^{Fc})N^iPr_2\}Me_2$ (**15**), $Cp^*Ti\{NC(Ar^{tBu})N^iPr_2\}Me_2$ (**18**) and $Cp^*Ti\{NC(Ar^{NMe2})N^iPr_2\}Me_2$ (**19**).

	Substituent	$^1J_{CH}$ Ti<u>Me</u> (Hz)	δ Ti<u>Me</u> (ppm)	δ N<u>C</u>(N^iPr_2) (ppm)	δ <u>C</u>$_i$CN(N^iPr_2) (ppm)
14	CF_3	118.8	49.0	158.7	144.6
2.07	H	118.6	47.9	160.7	141.7
15	Fc	118.5	47.8	161.0	139.2
18	^{t}Bu	118.6	47.7	161.0	139.3
19	NMe_2	118.4	46.7	162.2	137.2

A similar trend as observed by Grubbs and co-workers is apparent in Table 2.7, with the more electron-withdrawing group in the amidinate phenyl ring results in the largest coupling constant and chemical shift for the titanium methyl groups. The change in coupling constant is minimal compared to the previously study; suggesting that the *para*-phenyl substituent has a limited effect on the metal centre. The spacing between data points in the spectra is approximately 0.1 Hz, suggesting that the difference in coupling constants is not significant within error. The Ti<u>Me</u> chemical shift shows a significant downfield trend with more electron-withdrawing substituents which is a result of the increased donation from the methyl group causing an apparent deshielding effect and larger chemical shift. The same trend is more pronounced with <u>C</u>$_i$CN(N^iPr_2) due to the increased proximity and electronic conjugation to the *para*-substituent. The chemical shifts for the central amidinate carbon show the opposite trend, this is a result of an enhanced donation from the amine nitrogen when conjugated to a more withdrawing aryl substituent. The chemical shifts for the central amidinate carbons in the amidines are therefore downfield compared to their parent titanium methyl counterparts (eg. 167.6 (**10**) *vs.* 161.0 (**18**) ppm).

2.7.6 X-ray structures of $Cp^*Ti\{NC(Ar^{Fc})N^iPr_2\}Me_2$ (15), $Cp^*Ti\{NC(Ar^{tBu})N^iPr_2\}Me_2$ (18) and $Cp^*Ti\{NC(Ar^{NMe2})N^iPr_2\}Me_2$ (19)

Diffraction-quality crystals of **15** were grown from a toluene solution at 0 °C, and of **18** and **19** from hexane solutions at 0 and -30 °C, respectively. The molecular structures are shown in Figure 2.25 and selected bond lengths and angles of **2.07**, **15**, **18** and **19** are compared in Table 2.8.

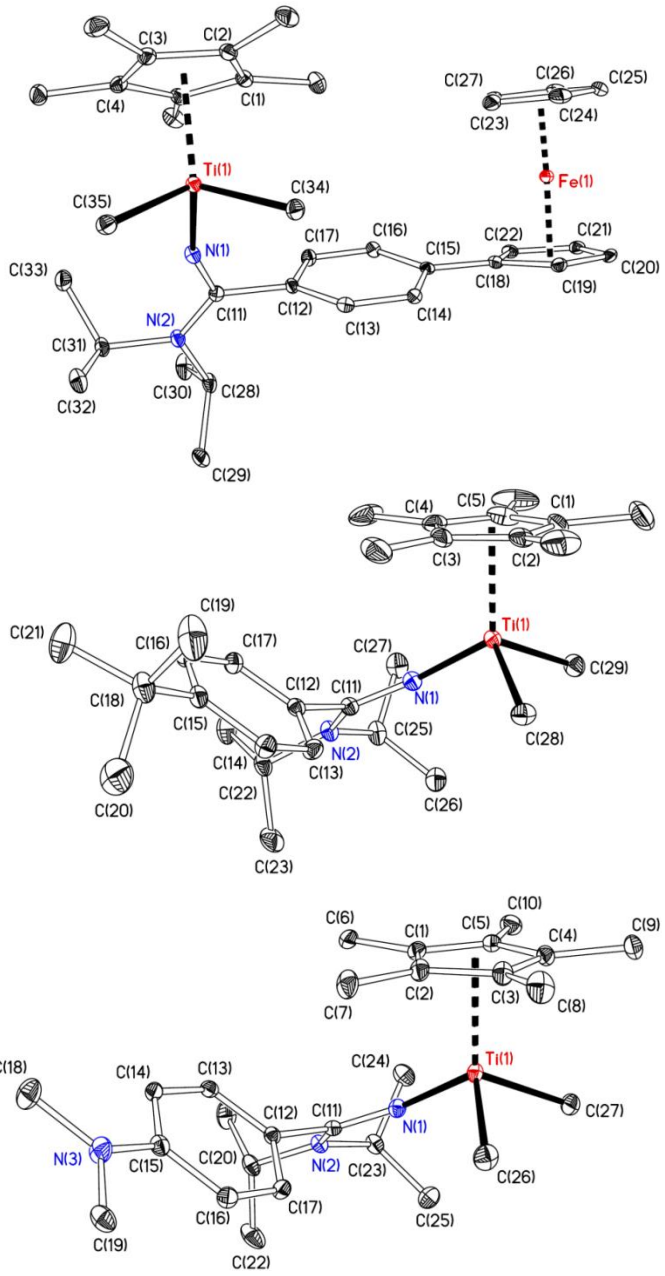

Figure 2.25 Displacement ellipsoid plots of $Cp^*Ti\{NC(Ar^{Fc})N^iPr_2\}Me_2$ (**15**, top) $Cp^*Ti\{NC(Ar^{tBu})N^iPr_2\}Me_2$ (**18**, middle) and $Cp^*Ti\{NC(Ar^{NMe2})N^iPr_2\}Me_2$ (**19**, bottom) (20% probability, H atoms omitted).

Table 2.8 Selected bond lengths (Å) and angles (°) for $Cp^*Ti\{NC(Ph)N^iPr_2\}Me_2$ (**2.06**), $Cp^*Ti\{NC(Ar^{Fc})N^iPr_2\}Me_2$ (**15**) $Cp^*Ti\{NC(Ar^{tBu})N^iPr_2\}Me_2$ (**18**) and $Cp^*Ti\{NC(Ar^{NMe2})N^iPr_2\}Me_2$ (**19**). Cp^*_{cent} is the computed Cp^* ring carbon centroid.

Parameter	**2.07**	**15**	**18**	**19**
Ti(1)-Cp^*_{cent}	2.07	2.07	2.06	2.07
Ti(1)-N(1)	1.8452(1)	1.851(3)	1.847(2)	1.8352(14)
N(1)-C(11)	1.290(2)	1.290(4)	1.290(3)	1.297(2)
N(2)-C(11)	1.363(2)	1.366(4)	1.357(3)	1.356(2)
C(11)-C(12)	1.502(2)	1.515(4)	1.507(4)	1.503(2)
Ti(1)-Me(1)	2.1227(18)	2.114(4)	2.108(3)	2.116(2)
Ti(1)-Me(2)	2.1326(19)	2.120(4)	2.127(3)	2.1392(18)
Cp^*_{cent}-Ti(1)-N(1)	120.8	118.7	120.3	119.7
Cp^*_{cent}-Ti(1)-Me(1)	113.8	113.9	114.1	114.1
Cp^*_{cent}-Ti(1)-Me(2)	113.9	115.1	113.3	114.4
C(11)-N(1)-Ti(1)	163.00(13)	158.5(3)	161.1(2)	163.05(18)

Complexes **15**, **18** and **19** are all structural analogues with the titanium centre residing in a *pseudo*-tetrahedral three-legged piano stool arrangement as was observed for their unsubstituted analogue **2.07**. Despite the range of substituents employed no structural differences were observed within the amidinate moiety or in the bonding interaction with titanium. This is in agreement with the NMR observations made in Section 2.7.5. In both **15** and **19** the *para*-phenyl substituents are aligned within the same plane as the phenyl to allow for conjugation. Complex **15** shows that the ferrocene substituent is orientated to the same side as the titanium centre, a ROESY experiment displayed a through-space NOE between the Cp^* and Cp rings. In comparison to their dichloride counterparts, **16** and **17**, the Ti(1)–N(1) bond lengths in **18** and **19** are significantly longer (1.847(2) (**18**) and 1.8352(14) (**19**) compared to 1.798(2) (**16**) and 1.7920(17) (**17**) Å). Increased σ-donation from methyl compared to chloride ligands results in a reduction in dπ-pπ bonding character in the Ti(1)–N(1) bond. A similar trend is observed in the molecular structure comparison of **2.06** and **2.07**.

2.7.7 Oxidation of $Cp^*Ti\{NC(Ar^{Fc})N^iPr_2\}Me_2$ (15)

Redox-active ligands have found extensive use throughout chemistry.[67] The ability to switch between two useful states of reactivity *via* an oxidative or reductive pathway within the ancillary ligand has found extensive applications.[67] Gibson and co-workers

have shown that the redox switching of ferrocenyl moieties tethered to a catalytically active titanium centre in the ring-opening polymerisation of *rac*-lactide can effectively supress and re-establish the catalytic activity.[68] In 2014, a study by Diaconescu and co-workers showed that redox switching of a zirconium precatalyst, which contains a ferrocenyl group embedded in close proximity in the ancillary ligand, can give substrate selectivity between L-lactide and ε-caprolactone.[69] Recently, this redox switching effect was again shown to be present in the ring-opening polymerisation of cyclic esters when using a series of lanthanide complexes with a ferrocenyl group embedded in the ligand backbone.[70]

More relevant to this project is the redox-control of olefin polymerisation. Gibson *et al.* introduced ferrocenyl-containing pyridine-imine Ni and Pd complexes and ferrocenyl-substituted bis(imino)pyridine Fe and Co polyolefin. Neither system showed any discernible difference between the neutral and oxidised form of their ancillary ligands under the relevant polymerisation conditions.[71, 72] In 2015, Chen and co-workers synthesised a series of palladium complexes with ferrocenyl-containing phosphine sulphonate ligands. The neutral and oxidised forms provided markedly different activities in the homopolymerisation of ethylene, which was thought to be a result of the oxidised form not being stable at the temperature required for polymerisation. However the oxidised form was shown to be active in the oligomerisation of norborene, unlike its neutral counterpart, and that this control could take place *in situ*.[73]

The oxidised form of **15** would give both an electron-withdrawing substituent comparable to **14 (**σ_p value of -0.18 for Fc and 0.29 for Fc^+) and the presence of a cationic group also would provide an electronic mimic of the active titanium centres in **3**, as discussed in Section 2.7.2. A cyclic voltammetry (CV) study was carried out on **9** and **15** to both observe any differences from the presence of a conjugated titanium metal centre and to identify a suitable oxidising agent to form ferrocenium. The cyclic voltammograms revealed *quasi*-reversible oxidation and reduction waves for the ferrocene/ferrocenium couple with a standard potential of 0.01 V relative to ferrocene for both complexes in the same conditions. A full discussion on this study including cyclic voltammograms is given in Chapter Three and experimental details can be found in Chapter Six. The same standard potential indicates a limited influence that the titanium has on the ferrocenyl group. This result is in keeping with the

previously discussed molecular structure and NMR analysis, from which it is apparent that there is minimal deviation on the complexes as the *para*-phenyl substituent is varied.

In 1987 Jordan *et al.* found that $[Cp_2Fe][BPh_4]$ can cause abstraction of an alkyl group from a dialkyl zirconocene species with the reduction of ferrocenium species to ferrocene (Equation 2.10).[74] This gives the opportunity for an internal abstraction and extrusion of ethane to take place from the oxidised form of **15**. Although the electrochemical reversibility of **15** indicates that this is not happening on the time scale of the cyclic voltammetry study scan-rate an investigation prior to oxidation was required.

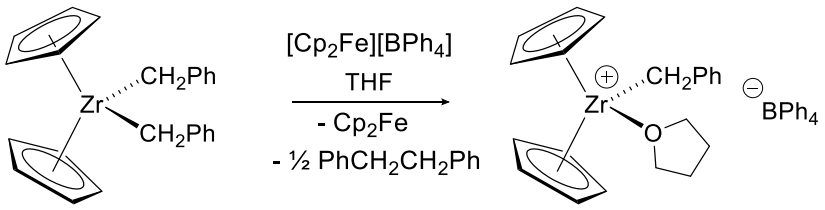

Equation 2.10

As was discussed in Section 2.7.2 it is important that only relatively non-coordinating anions are present in polymerisation, therefore the oxidised form of **15** with a $[BF_{20}]^-$ anion was targeted, $[Cp^*Ti\{NC(Ar^{Fc+})N^iPr_2\}Me_2][BF_{20}]$. A reaction between **2.07** and $[Cp_2Fe][BF_{20}]$ was carried out to see if the abstraction described by Jordan *et al.* was possible with these cyclopentadienyl titanium amidinate dialkyl species. No change was observed over several hours, with the same broad paramagnetic resonance in the ^1H NMR spectra and the distinctive blue-green colour of $[Cp_2Fe][BF_{20}]$ persisting. In light of this the oxidised form of **15** was proposed to be stable and oxidation reactions were carried out.

The CV study showed that an oxidising agent with a positive standard reduction potential relative to ferrocene was required.[75] The oxidising agent must not interfere with the titanium alkyl end group, and it must contain the desired $[BF_{20}]^-$ anion; the commonly employed silver cation oxidants have previously been shown to abstract metal alkyl groups.[74] $[N(4\text{-}C_6H_4Br)_3][BF_{20}]$ has a standard potential of 0.70 V and has been shown to oxidise ferrocene.[76] The oxidising agent was prepared according to literature procedures,[76] but upon addition to **15** no reaction was observed. The reason for this is unclear, it has previously been reported that a pendant electrophilic metal

centre can make oxidation of a ferrocene problematic.[72] However, it has been established that there is very limited communication between the titanium centre and *para*-substituent in these complexes. No further avenues were pursued. Complex **14** contains a -CF_3 group (σ_p = 0.54), which will give an excellent representation of a ferrocenium group in a polymerisation study.

2.8 Synthesis and characterisation of cationic monometallic catalysts

As was discussed in Section 2.4, extensive investigations into the catalytically active titanium species have been carried out. This has involved studies of the base-free alkyl cations, Lewis base adducts and Ti–Me insertion products. As was introduced in Chapter One, the Lewis acid BF_{15} is an effective methyl anion abstraction agent, generating $[MeBF_{15}]^-$ anion. This anion has been shown to remain often partially coordinated to the cationic titanium centre through a weak Ti---Me---BF_{15} interaction.[77] The comparative effectiveness of this activator and others in polymerisation studies will be analysed and discussed in Chapter Four.

In 1996 Horton *et al.* found that the separation (denoted $\Delta(m,p)$) between the *meta*- and *para*- C_6F_5 ^{19}F chemical shifts in $[MeB\underline{F}_{15}]^-$ is a good probe of the degree of anion association to cationic d^0 metals. Values of 3-6 ppm indicate "coordination", and those below 3 ppm indicate the free anion is present in solution.[78] It has previously been shown within the Mountford group that cyclopentadienyl titanium dialkyl complexes with different κ^1-amidinate or κ^1-guanidinate supporting ligands show a range of values for the $\Delta(m,p)$ in the ^{19}F NMR spectra upon activation with BF_{15}. Activation of $Cp^*Ti\{NC(NMe_2)_2\}Me_2$ (**2.19**) displayed a $\Delta(m,p)$ of 2.65 ppm and in comparison activation of $Cp^*Ti\{NC(N^iPr_2)Ar^{F_2}\}Me_2$ (Ar^{F_2} = 2,6-$C_6H_3F_2$) (**1.40**) generated a $\Delta(m,p)$ of 5.18 ppm. This result highlights the electronic differences that can observed with this spectroscopic probe. It has also previously been shown that the reaction of $Cp^*Ti\{NC(Ph)N^iPr_2\}Me_2$ (**2.07**) with BF_{15} forms $[Cp^*Ti\{NC(Ph)N^iPr_2\}Me][MeBF_{15}]$ (**2.20**) with a single resonance at 1.76 ppm for the Cp^* group and a broad resonance at 0.72 for the $[\underline{Me}BF_{15}]^-$ in the ^1H NMR spectrum. A $\Delta(m,p)$ of 4.69 ppm was observed in the ^{19}F NMR spectra. This value is slightly smaller than that observed with **1.40** and indicates how only a minimal change of substituents within the amidinate group can have a significant influence on the coordination of $[MeBF_{15}]^-$.

To investigate whether the phenyl ring *para*-substituents of the amidinate moiety influence the catalytically-active species, a series of activation studies with BF_{15} were performed. An NMR tube scale reaction of **14** or **19** with BF_{15} in C_6D_5Br resulted in an immediate colour change from yellow to dark brown. However, in both cases a brown oil formed before any NMR data could be recorded. This has been observed for a variety of cyclopentadienyl monometallic titanium complexes upon activation with either BF_{15} or TBF_{20}.

Insertion reaction products of **14** and **19** were synthesised to prevent this from occurring in solution and to confirm that alkyl abstraction can occur. NMR tube scale reaction of **14** or **19** with BF_{15} in the presence of 1 equiv. of $^{i}PrNCN^{i}Pr$ in C_6D_5Br formed $[Cp^{*}Ti\{NC(Ar^{CF3})\}\{MeC(N^{i}Pr)_2\}][MeB(C_6F_5)_3]$ (**20**) and $[Cp^{*}Ti\{NC(Ar^{NMe2})\}\{MeC(N^{i}Pr)_2\}][MeB(C_6F_5)_3]$ (**21**) (Equation 2.11). In both cases the ^{19}F NMR spectra gave a $\Delta(m,p)$ value of 2.4 ppm, which is indicative of an uncoordinated $[MeBF_{15}]^{-}$ anion. The inserted *N*,*N*′-diisopropylcarbodiimide coordinates in a bidentate fashion as a κ^2-amidinate, resulting in no vacant coordination sites.

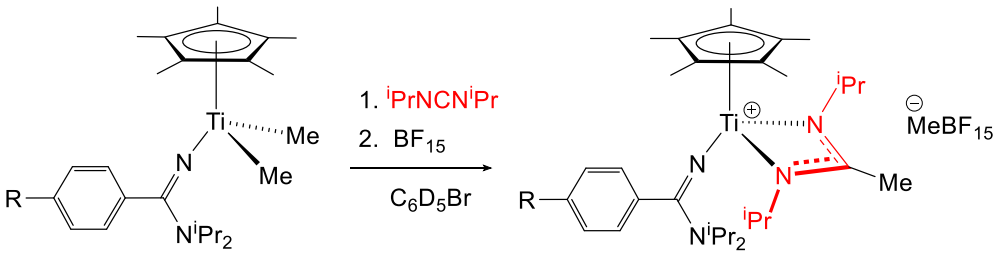

R = CF_3 (**14**) or NMe_2 (**19**)

R = CF_3 (**20**) or NMe_2 (**21**)

Equation 2.11

The ^{1}H NMR spectra of both **20** and **21** show similar resonances, with the only major difference arising in the aromatic region and resonance specific for their substituents. The carbodiimide inserts into the Ti–Me bond to give a C_s symmetric structure and the corresponding methyl resonance in the ^{1}H NMR spectra occur at 2.10 ppm in **20** and **21**, as anticipated this is significantly downfield compared to a methyl group directly bonded to an electropositive metal centre. The ^{11}B NMR spectra show a sharp resonance at -14.2 ppm for both complexes. This is characteristic of a tetra-coordinated anionic boron.

NMR tube scale reaction of **15** or **18** with BF_{15} in C_6D_5Br again resulted in an immediate colour change from yellow to dark brown. However, in these cases no precipitation was observed and spectroscopic data could be recorded. ^{1}H, ^{19}F and ^{11}B NMR spectra of these two reactions revealed single products identifiable as the ion pairs $[Cp^{*}Ti\{NC(Ar^{tBu})N^{i}Pr_2\}Me][MeBF_{15}]$ (**22**) and $[Cp^{*}Ti\{NC(Ar^{Fc})N^{i}Pr_2\}Me][MeBF_{15}]$ (**23**).

The ^{1}H NMR spectra and proposed complexes are shown in Figure 2.26. The features of these spectra are the Cp^{*} signal at 1.77 and 1.82 ppm, Ti<u>Me</u> at 1.11 and 1.12 ppm and a broad signal for the $[\underline{Me}BF_{15}]^{-}$ at 0.68 and 0.73 ppm, for **22** and **23** respectively. As can be observed in the top spectrum a sharp singlet in observed at 1.43 ppm for the C<u>Me</u>$_3$ group in **22** and in the bottom spectrum resonances at 4.79, 4.45 and 4.19 ppm in a 1:1:2 ratio correspond to the mono-substituted ferrocene moiety. There are two resonances corresponding to the NCH<u>Me</u>$_2$ group in both **22** and **23**, in both cases one appears as very broad and the other much sharper; the same result is observed for the methine protons within the isopropyl group, with both broad and sharp resonances apparent. This is believed to be a result of an increased donation from the amidinate moiety to the now cationic metal centre and the proximity of a large coordinated anion causing steric impositions on the complex. Increased π-interaction from lone pair of the amine nitrogen results in a greater amount of double bond character and subsequent restricted rotation as has been previously discussed. The steric imposition is also observed in the aromatic region with broadening of the aromatic protons *ortho* to the zwitterionic substituent, unlike their analogous *meta* resonances. Further suggestion of a coordinated anion is evidenced in the ^{19}F and ^{11}B NMR spectra. A $\Delta(m,p)$ value of 4.66 ppm is observed for both **22** and **23** in the ^{19}F NMR spectra, as discussed above this is indicative of coordination. Compared to complexes **20** and **21**, the resonances for the boron environment shift downfield, -13.8 and -13.7 ppm for **22** and **23** respectively. This is a result of some electron density still residing in the titanium-methyl bond as opposed to exclusively in the boron-methyl bond.

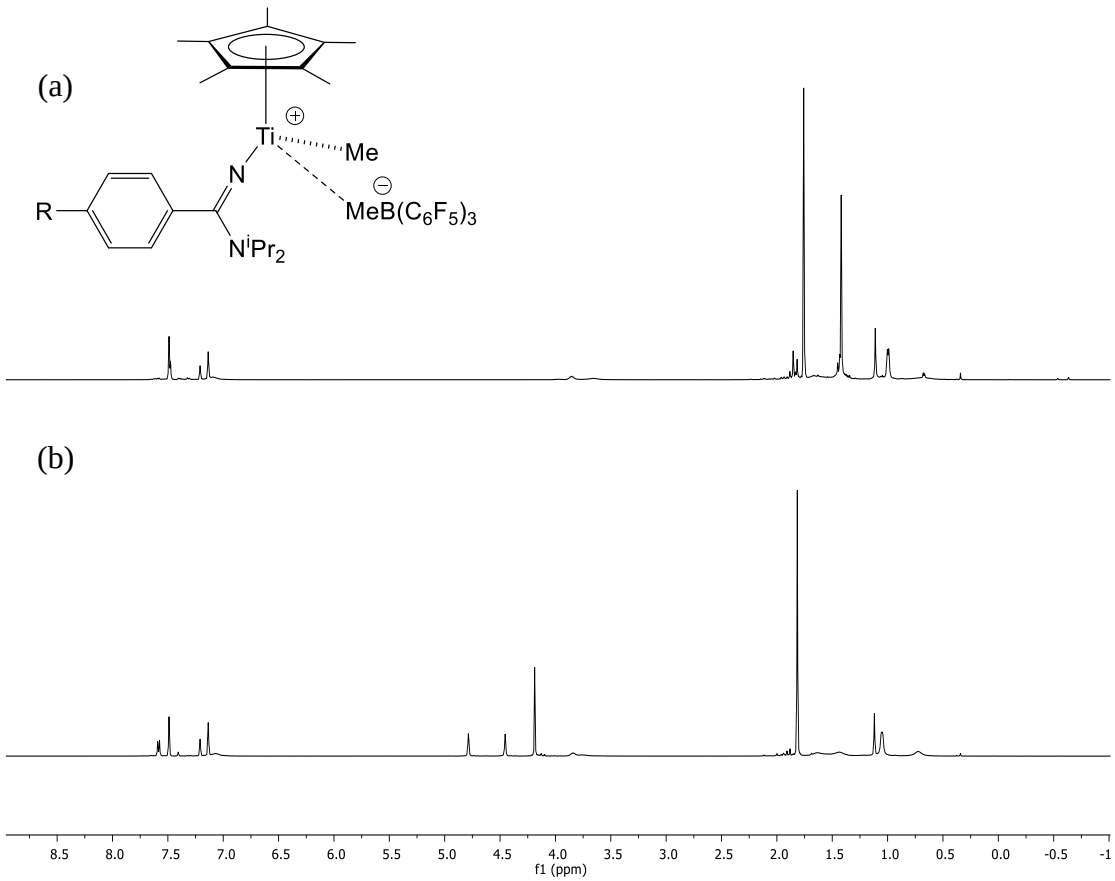

Figure 2.26 ^{1}H NMR (499.9 MHz, C_6D_5Br, 298 K) spectra of [Cp*Ti{NC(Ar^{tBu})N^{i}Pr$_2$}Me][MeBF$_{15}$] (**22**, a) and [Cp*Ti{NC(Ar^{Fc})N^{i}Pr$_2$}Me][MeBF$_{15}$] (**23**, b).

As was discussed previously, the Δ(*m*,*p*) value in the ^{19}F NMR spectrum can give a spectroscopic probe on any electronic differences exhibited by the cationic species. Complexes **22** and **23** have identical Δ(*m*,*p*) values and only differed by 0.03 ppm from **2.20** (4.69 ppm). This suggests that very limited electronic differences occur across these three cations, which complements the studies on the neutral complexes in Section 2.7.

2.9 EPDM copolymerisation experiments using 14, 15, 18 and 19

Analogous EPDM copolymerisation experiments to those carried out in Section 2.5 were undertaken using precatalysts **14**, **15**, **18** and **19** at LANXESS Elastomers. The results are summarised in Table 2.9. Due to the setup and in-house preference at the time of testing either one or two equiv. of BHT relative to the number of aluminium centres was employed, indicated in Table 2.9. This may have a minimal impact on productivities, but has been shown not to influence composition, molecular weight or

PDI of the resultant polymer under the relevant conditions. Chapter Four includes a consistent data set with non-aluminium based activating species and indicates a similar trend in productivities as will be discussed below.

All of the catalysts successfully produced sufficient polymer for analysis, and all proved to be less active than the unsubstituted counterpart **2.07**. Precatalyst **14** generated the least active species and **19** also gave a less active species. Concerning the composition of the resultant polymer there are no significant differences irrelevant of the *para*-phenyl substituent present. This is in agreement with the limited spectroscopic variations of the neutral and cationic species that have been previously discussed. The increased propylene affinity observed in the EPDM copolymerisation experiments with complexes **3** and **4** (Table 2.4) is therefore thought not to be a result of the presence of an electron-withdrawing metal centre conjugated through the amidinate group. This affinity could be the result of the electrostatic impact of a spatially proximate metal centre. However, this would also be expected to be observed when complex **6** is used as the precatalyst, which shows comparable composition to that of the monometallic analogue. The molecular weights also remain consistent in the presence of dihydrogen as a chain transfer agent.

The cause of the enhanced propylene affinity observed in the EPDM copolymerisation experiments with complexes **3** and **4** remains unknown. The most pronounced effect arises with complex **3** in which the metal centres are the furthest removed. Further investigations into maintaining spatial proximity between the metal centres through either catalyst ligand design or electrostatically with dinuclear cocatalysts will be explored in Chapters Two and Three.

Table 2.9 EPDM polymerisation results for $Cp^*Ti\{NC(Ph)N^iPr_2\}Me_2$ (**2.07**), $Cp^*Ti\{NC(Ar^{CF3})N^iPr_2\}Me_2$ (**14**), $Cp^*Ti\{NC(Ar^{Fc})N^iPr_2\}Me_2$ (**15**), $Cp^*Ti\{NC(Ar^{tBu})N^iPr_2\}Me_2$ (**18**) and $Cp^*Ti\{NC(Ar^{NMe2})N^iPr_2\}Me_2$ (**19**).

Entry	*para*-R	Precatalyst	Cocatalyst	Productivity (kg mol Ti^{-1} h^{-1} bar^{-1})	C_2 (wt%)	C_3 (wt%)	ENB (wt%)	VNB (wt%)	M_n (kDa)	M_w (kDa)	PDI
1	H	**2.07**	MAO	71,400	48.2	50.0	1.10	0.72	256	586	2.3
2[a]	CF_3	**14**	MAO	19,371	47.9	50.5	0.92	0.62	211	476	2.3
3[a]	Fc	**15**	MAO	59,657	48.2	50.1	1.07	0.72	236	497	2.1
4	^{t}Bu	**18**	MAO	54,257	49.8	48.3	1.11	0.75	235	569	2.4
5	NMe_2	**19**	MAO	34,028	49.5	48.8	1.01	0.71	234	520	2.2

Polymerisation conditions. T = 90 °C, Pressure: 7 bar, [Cat] = 0.1 µmol, [Al]:[Cat] = 4500, [Al]:[BHT] = 1([a] [Al]:[BHT] = 0.5), 10 minute reaction time. Solvent pentamethylheptane (1 L) C_3/C_2 =400/200 Nl h^{-1}, H_2 flow: 0.35 Nl h^{-1}ENB: 0.7 mL, VNB: 0.7 mL.
Polymer characterisation. Polymer molecular weight and molecular weight distributions: the polymers have been analysed with the Freeslate Rapid GPC in 1,2,4 Trichlorobenzene against PS standards. *Average composition:* the polymers have been analysed via transmission IR spectroscopy on a pressed polymer film.

2.10 Summary

This Chapter has described the synthesis and characterisation of three new bimetallic catalysts and four analogous model monometallic complexes. This has included a comprehensive discussion of their structures in both the solid state and solution phase through variable temperature NMR studies and where applicable X-ray crystal structure analysis. The synthetic limitations when targeting additional cationic monometallic models were also introduced. Reactions of both monometallic and bimetallic complexes with $B(C_6F_5)_3$ and $[CPh_3][B(C_6F_5)_4]$ to form well-defined cationic titanium species have been performed and discussed.

High temperature EP and EPDM copolymerisation experiments were performed in collaboration with LANXESS Elastomers. Overall these studies showed no evidence of cooperativity invoked from a secondary metal centre in the bimetallic systems and that an unexpected enhancement of propylene affinity in certain examples could not be rationalised through the presence of a conjugated electron withdrawing group.

2.11 References

1. L. Clark, Part II Thesis, University of Oxford, 2008.
2. R. Scott, DPhil Thesis, University of Oxford, 2013.
3. M. A. Zuideveld, R. T. W. Scott and P. Mountford, *EP2801579A1*, 2014.
4. H. Bigmore, DPhil Thesis, University of Oxford, 2007.
5. A. Heath, DPhil Thesis, University of Oxford, 2011.
6. E. G. Ijpeij, P. J. H. Windmuller, H. J. Arts, F. Van der Burgt, G. H. J. Van Doremaele and M. A. Zuideveld, *WO/2005/090418*, 2005.
7. B. I. Kharisov, U. Ortiz Mendez and J. Rivera de la Rosa, *Russ. J. Coord. Chem*, 2006, **32**, 617-631.
8. M. Mena, P. Royo, R. Serrano, M. A. Pellinghelli and A. Tiripicchio, *Organometallics*, 1989, **8**, 476-482.
9. P. J. Hore, Nuclear Magnetic Resonance, Oxford University Press, 2015.
10. J. R. Hagadorn and J. Arnold, *Organometallics*, 1998, **17**, 1355-1368.
11. F. H. Allen, O. Kennard, J. J. Galloy, O. Johnson and D. G. Watson, *Chem. Des. Autom. News*, 1993, **8**, 1 & 31.
12. D. A. Fletcher, R. F. McMeeking and D. Parkin, *J. Chem. Inf. Comput. Sci.*, 1996, **36**, 746 (The UK Chemical database Service: CSD updated May 2015).

13. A. F. Russell, DPhil Thesis, University of Oxford, 2014.
14. J. Doiron, A. H. Soultan, R. Richard, M. M. Touré, N. Picot, R. Richard, M. Čuperlović-Culf, G. A. Robichaud and M. Touaibia, *Eur. J. Med. Chem.*, 2011, **46**, 4010-4024.
15. T. Mahdi and D. W. Stephan, *Angew. Chem. Int. Ed.*, 2015, **54**, 8511-8514.
16. E. Y.-X. Chen and T. J. Marks, *Chem. Rev.*, 2000, **100**, 1391-1434.
17. M. Bochmann, *Organometallics*, 2010, **29**, 4711-4740.
18. R. A. Collins, A. F. Russell and P. Mountford, *Appl. Petrochem. Res.*, 2015, **5**, 153-171.
19. E. G. Ijpeij, B. Coussens, M. A. Zuideveld, G. H. J. van Doremaele, P. Mountford, M. Lutz and A. L. Spek, *Chem. Commun.*, 2010, **46**, 3339-3341.
20. L. Cabrera, E. Hollink, J. C. Stewart, P. Wei and D. W. Stephan, *Organometallics*, 2005, **24**, 1091-1098.
21. V. C. Williams, C. Dai, Z. Li, S. Collins, W. E. Piers, W. Clegg, M. R. J. Elsegood and T. B. Marder, *Angew. Chem. Int. Ed.*, 1999, **38**, 3695-3698.
22. V. C. Williams, G. J. Irvine, W. E. Piers, Z. Li, S. Collins, W. Clegg, M. R. J. Elsegood and T. B. Marder, *Organometallics*, 2000, **19**, 1619-1621.
23. R. Vollmerhaus, M. Rahim, R. Tomaszewski, S. Xin, N. J. Taylor and S. Collins, *Organometallics*, 2000, **19**, 2161-2169.
24. R. A. Metcalfe, D. I. Kreller, J. Tian, H. Kim, N. J. Taylor, J. F. Corrigan and S. Collins, *Organometallics*, 2002, **21**, 1719-1726.
25. V. Busico, R. Cipullo, F. Cutillo, N. Friederichs, S. Ronca and B. Wang, *J. Am. Chem. Soc.*, 2003, **125**, 12402-12403.
26. N. Adams, H. J. Arts, P. D. Bolton, D. Cowell, S. R. Dubberley, N. Friederichs, C. M. Grant, M. Kranenburg, A. J. Sealey, B. Wang, P. J. Wilson, M. Zuideveld, A. J. Blake, M. Schroeder and P. Mountford, *Organometallics*, 2006, **25**, 3888-3903.
27. S. W. Ewart, M. A. Parent and M. C. Baird, *J. Polym. Sci., Part A: Polym. Chem.*, 1999, **37**, 4386-4389.
28. Y. V. Kissin, R. I. Mink, T. E. Nowlin and A. J. Brandolini, *J. Polym. Sci., Part A: Polym. Chem.*, 1999, **37**, 4281-4294.
29. H. Mori, M. Endo and M. Terano, *J. Mol. Catal. A: Chem.*, 1999, **145**, 211-220.
30. P. J. Flory, Principles of Polymer Chemistry, Cornell University Press, 1992.

31. G. Odian, Principles of Polymerisation, Wiley-Interscience, 1992.
32. S. Jungling, R. Mullhaupt and H. Plenio, *J. Organomet. Chem.*, 1993, **460**, 191-195.
33. S. K. Noh, W. Jung, H. Oh, Y. R. Lee and W. S. Lyoo, *J. Organomet. Chem.*, 2006, **691**, 5000-5006.
34. N. T. B. Linh, N. T. D. Huyen, S. K. Noh, W. S. Lyoo, D.-H. Lee and Y. Kim, *J. Organomet. Chem.*, 2009, **694**, 3438-3443.
35. M. Delferro and T. J. Marks, *Chem. Rev.*, 2011, **111**, 2450-2485.
36. A. P. Shreve, R. Mulhaupt, W. Fultz, J. Calabrese, W. Robbins and S. D. Ittel, *Organometallics*, 1988, **7**, 409-416.
37. M. D. Healy, D. A. Wierda and A. R. Barron, *Organometallics*, 1988, **7**, 2543-2548.
38. M. Bochmann and S. J. Lancaster, *Angew. Chem. Int. Ed. Engl.*, 1994, **33**, 1634-1637.
39. M. Bochmann and S. J. Lancaster, *J. Organomet. Chem.*, 1995, **497**, 55-59.
40. V. C. Gibson and S. K. Spitzmesser, *Chem. Rev.*, 2003, **103**, 283-315.
41. G. J. P. Britovsek, S. A. Cohen, V. C. Gibson and M. van Meurs, *J. Am. Chem. Soc.*, 2004, **126**, 10701-10712.
42. K. P. Bryliakov, E. P. Talsi and M. Bochmann, *Organometallics*, 2004, **23**, 149-152.
43. K. P. Bryliakov, D. E. Babushkin, E. P. Talsi, A. Z. Voskoboynikov, H. Gritzo, L. Schröder, H.-R. H. Damrau, U. Wieser, F. Schaper and H. H. Brintzinger, *Organometallics*, 2005, **24**, 894-904.
44. R. A. Petros and J. R. Norton, *Organometallics*, 2004, **23**, 5105-5107.
45. D. W. Stephan, *Organometallics*, 2005, **24**, 2548-2560.
46. P. D. Bolton, E. Clot, A. R. Cowley and P. Mountford, *Chem. Commun.*, 2005, 3313-3315.
47. T. D. Shaffer, J. A. M. Canich and K. R. Squire, *Macromolecules*, 1998, **31**, 5145-5147.
48. H. Li, L. Li, T. J. Marks, L. Liable-Sands and A. L. Rheingold, *J. Am. Chem. Soc.*, 2003, **125**, 10788-10789.
49. H. Li, C. L. Stern and T. J. Marks, *Macromolecules*, 2005, **38**, 9015-9027.
50. H. Li, L. Li and T. J. Marks, *Angew. Chem. Int. Ed.*, 2004, **43**, 4937-4940.
51. J. van de Moosdjik, LANXESS Elastomers B.V., personal communication.

52. C. Hansch, A. Leo and R. W. Taft, *Chem. Rev.*, 1991, **91**, 165-195.
53. B. J. Coe, C. J. Jones, J. A. McCleverty, D. Bloor and G. Cross, *J. Organomet. Chem.*, 1994, **464**, 225-232.
54. J. D. Dunitz and R. Taylor, *Chem. Eur. J.*, 1997, **3**, 89-98.
55. P. A. Champagne, J. Desroches and J.-F. Paquin, *Synthesis*, 2015, **47**, 306-322.
56. D. A. Smith, T. Beweries, C. Blasius, N. Jasim, R. Nazir, S. Nazir, C. C. Robertson, A. C. Whitwood, C. A. Hunter, L. Brammer and R. N. Perutz, *J. Am. Chem. Soc.*, 2015, **137**, 11820-11831.
57. M.-C. Chen, J. A. S. Roberts and T. J. Marks, *Organometallics*, 2004, **23**, 932-935.
58. M.-C. Chen, J. A. S. Roberts, A. M. Seyam, L. Li, C. Zuccaccia, N. G. Stahl and T. J. Marks, *Organometallics*, 2006, **25**, 2833-2850.
59. J. A. S. Roberts, M.-C. Chen, A. M. Seyam, L. Li, C. Zuccaccia, N. G. Stahl and T. J. Marks, *J. Am. Chem. Soc.*, 2007, **129**, 12713-12733.
60. L.-G. Xie and Z.-X. Wang, *Angew. Chem. Int. Ed.*, 2011, **50**, 4901-4904.
61. P. Romanato, S. Duttwyler, A. Linden, K. K. Baldridge and J. S. Siegel, *J. Am. Chem. Soc.*, 2010, **132**, 7828-7829.
62. M. Santiago Cintrón, O. Green and J. N. Burstyn, *Inorg. Chem.*, 2012, **51**, 2737-2746.
63. M. Gomberg, *J. Am. Chem. Soc.*, 1902, **24**, 597-628.
64. K. M. Harmon and F. E. Cummings, *J. Am. Chem. Soc.*, 1965, **87**, 539-542.
65. H. A. Bent, *Chem. Rev.*, 1961, **61**, 275-311.
66. W. C. Finch, E. V. Anslyn and R. H. Grubbs, *J. Am. Chem. Soc.*, 1988, **110**, 2406-2413.
67. A. M. Allgeier and C. A. Mirkin, *Angew. Chem. Int. Ed.*, 1998, **37**, 894-908.
68. C. K. A. Gregson, V. C. Gibson, N. J. Long, E. L. Marshall, P. J. Oxford and A. J. P. White, *J. Am. Chem. Soc.*, 2006, **128**, 7410-7411.
69. X. Wang, A. Thevenon, J. L. Brosmer, I. Yu, S. I. Khan, P. Mehrkhodavandi and P. L. Diaconescu, *J. Am. Chem. Soc.*, 2014, **136**, 11264-11267.
70. C. Hermans, W. Rong, T. P. Spaniol and J. Okuda, *Dalton Trans.*, 2016, **45**, 8127-8133.
71. V. C. Gibson, C. M. Halliwell, N. J. Long, P. J. Oxford, A. M. Smith, A. J. P. White and D. J. Williams, *Dalton Trans.*, 2003, 918-926.

72. V. C. Gibson, N. J. Long, P. J. Oxford, A. J. P. White and D. J. Williams, *Organometallics*, 2006, **25**, 1932-1939.
73. M. Chen, B. Yang and C. Chen, *Angew. Chem. Int. Ed.*, 2015, **54**, 15520-15524.
74. R. F. Jordan, R. E. LaPointe, C. S. Bajgur, S. F. Echols and R. Willett, *J. Am. Chem. Soc.*, 1987, **109**, 4111-4113.
75. N. G. Connelly and W. E. Geiger, *Chem. Rev.*, 1996, **96**, 877-910.
76. A. R. O'Connor, C. Nataro, J. A. Golen and A. L. Rheingold, *J. Organomet. Chem.*, 2004, **689**, 2411-2414.
77. R. Hoff and R. T. Mathers, Handbook of Transition Metal Polymerization Catalysts, Wiley, 2010.
78. A. D. Horton, J. de With, A. J. van der Linden and H. van de Weg, *Organometallics*, 1996, **15**, 2672-2674.

Chapter Three

Bimetallic titanium catalysts with conformationally constrained covalent tethers

3.1 Overview

Following on from the work described in Chapter Two, this Chapter describes the synthesis, structures and copolymerisation capabilities of cyclopentadienyl-amidinate titanium bimetallic complexes with conformationally constrained and ferrocenyl covalent tethers. The preparation of bimetallic systems with dibenzofuran, xanthene and ferrocenyl covalent tethers will be discussed, along with their bis(amidine) precursors. Mono-substituted xanthene complexes were also synthesised and "self-trapping" activation experiments with TBF_{20} were performed. Alongside the ferrocenyl complexes introduced in Chapter One, an electrochemical analysis of all ferrocene based complexes will be discussed. High temperature EPDM copolymerisation experiments were performed on all precatalysts in collaboration with LANXESS Elastomers.

3.2 Introduction to Group 4 bimetallic polyolefin catalysts with rigid covalent tethers

Chapter Two introduced a series of cyclopentadienyl-amidinate titanium complexes with phenylene bridged covalent tethers. As was evident in the molecular structures of the precatalysts the metal centres are not in close proximity. The polymerisation studies revealed an enhanced propylene affinity for the conjugated bimetallic systems, but the reason for this is unclear. Bimetallic complexes with rigid bridges, which conformationally lock the metal centres in a close spatial proximity, have been shown to give advantageous properties in olefin polymerisation experiments.[1] An early notable example of a conformationally locked Group 4 bimetallic catalyst was the doubly bridged complex **1.57** introduced in Chapter One. In 2008, Salata and Marks reported a binuclear phenoxyiminato zirconium catalyst (**3.01**), which was calculated to reduce the distance between zirconium centres to ~5.9 Å as opposed to ~7.4 – 8.7 Å in the previously described CGCs (**1.50** and **1.51**).[2, 3] This distance was also shown to be shorter than the optimised computed geometries of the CGC when activated with a bis(borate) system, discussed further in Chapter Four (**1.50** ~6.0 and **1.51** ~6.6 Å).[1-3] Complex **3.01** and the analogous titanium complex **3.02** both showed a greater activity and degree of comonomer enchainment than their mononuclear counterparts (**3.03** and **3.04**) in MAO activated ethylene/1-hexene and ethylene/1-octene copolymerisation studies.[2, 3] This was proposed to be a result of an improved coordination environment, improving the enchainment efficiency, and a bimetallic

cooperative effect. Lee and co-workers introduced bimetallic complexes where two metal centres are bound to the nitrogen atom of a bridging anilide moiety (**3.05** and **3.06**). Complexes **3.05** and **3.06** were shown to be inactive for ethylene homopolymerisation or ethylene/1-hexene copolymerisation.[4]

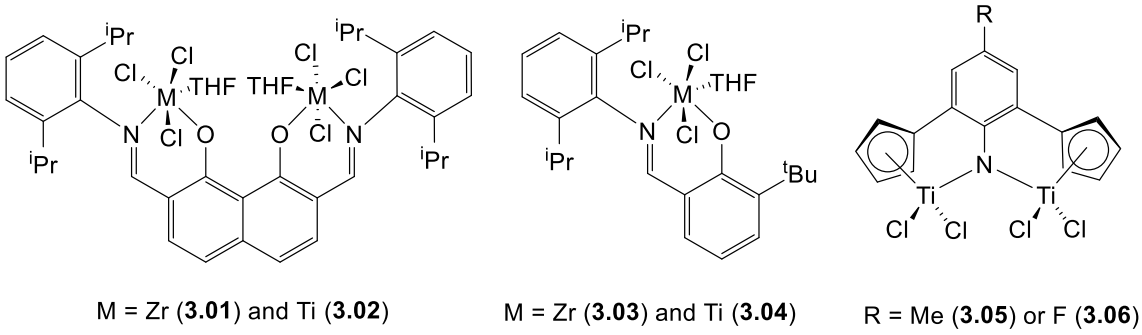

Figure 3.1 Bimetallic Group 4 complexes with rigid tethers and the appropriate mononuclear analogues with a phenoxyiminato ligand.

3.3 Synthesis and characterisation of a dibenzofuran bridged cyclopentadienyl-amidinate bimetallic complex

Dibenzofuran has been used extensively as a rigid pre-organised planar ligand backbone, for example to bridge chelating diphosphines or in the form of 4,5-bis(2-oxazidinyl)dibenzofuran (DBF-Box) which have been used for a variety of organometallic complexes and catalytic processes.[5-12] This ligand has not been used extensively in conjunction with early transition metals, but both monometallic pincer complexes and bimetallic compounds are known.[13-16]

The bis(amidine) DBF(C(NH)N^{i}Pr$_2$)$_2$ (**24**) (where DBF = 1,1′-dibenzofuranyl) was synthesised *via* the previously described nucleophilic attack of the *in situ* generated amide, ^{i}Pr$_2$NMgBr, on DBF(CN)$_2$ (**3.07**). Compound **3.07** was synthesised in a two-step literature procedure. DBF(I)$_2$ (**3.08**) is firstly synthesised by lithiation of the commercially available unsubstituted dibenzofuran, through addition of *sec*-BuLi in conjunction with tetramethylethylenediamine (TMEDA), and reaction with iodine. Compound **3.08** is then reacted with copper cyanide at high temperatures to generate **3.07** (Scheme 3.1).[17]

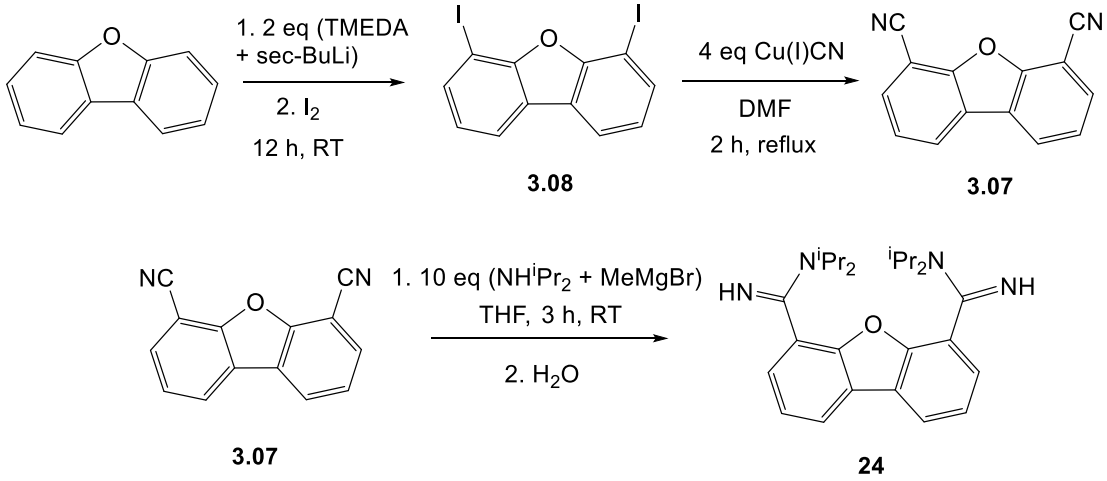

Scheme 3.1 Synthesis of DBF(C(NH)N^{i}Pr$_2$)$_2$ (**24**).

Compound **24** was isolated in a 42% yield and was fully characterised. The ^{1}H NMR spectrum (298 K, C_6D_6) displayed a single doublet and a septet resonance at 1.42 and 3.49 ppm, respectively, corresponding to the methyl and methine region of the isopropyl groups, and two doublets and an apparent triplet signal in the aromatic region. This is indicative of a symmetric molecule with free rotation about the C–N^{i}Pr$_2$ bond. Mass envelopes corresponding to both the $[M + H]^+$ (*m/z* = 421 g mol^{-1}) and $[M + 2H]^{2+}$ (*m/z* = 211 g mol^{-1}) molecular ions were observed in the ESI-MS spectrum. Diffraction-quality crystals were grown at room temperature from a saturated pentane solution (Figure 3.2).

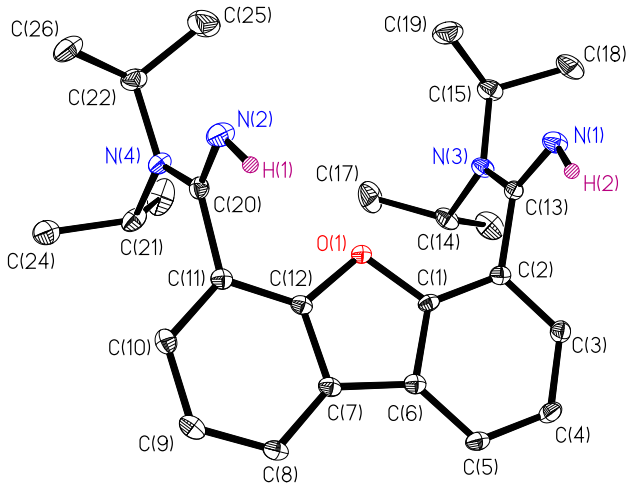

Figure 3.2 Displacement ellipsoid plot of DBF(C(NH)N^{i}Pr$_2$)$_2$ (**24**) (20% probability, C-bound H atoms omitted).

The molecular structure is consistent with the room temperature ^{1}H NMR spectrum. The dibenzofuran backbone is planar and lies perpendicular to the amidine moieties, which are orientated in the same direction. The supramolecular structure shows no hydrogen-bonding deriving from the imine nitrogen (N(1) and N(2)) atoms. The parallel orientation is believed to be a result of minimising steric congestion between molecules in the close-packed molecular structure. Within the amidine moiety the central carbon is sp^2 hybridised and the N(1)–C(13) (1.283(3) Å) and N(3)–C(13) (1.362(3) Å) bond lengths are not significantly different to the amidines introduced in Chapter Two.

The precatalyst DBF{NCN^{i}Pr$_2$}$_2${Cp*TiMe$_2$}$_2$ (**25**) was synthesised from **24** *via* a protonolysis pathway with 2 equiv. of Cp*TiMe$_3$ and was isolated in a 53% yield (Equation 3.1).

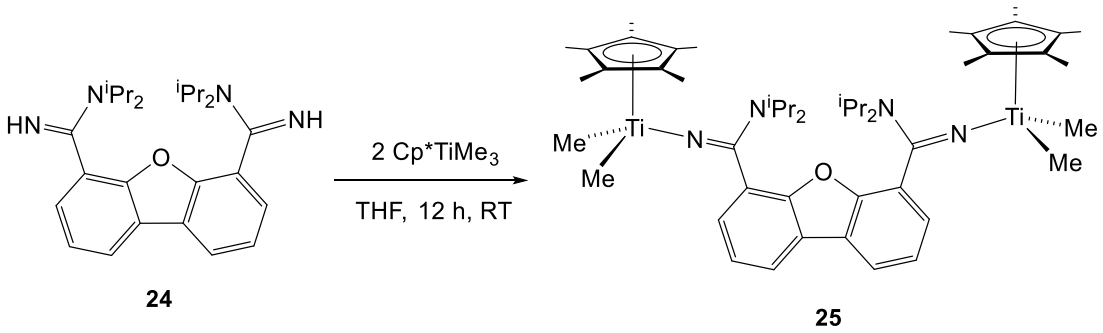

24 **25**

Equation 3.1

The ^{1}H NMR spectrum (298 K, C_6D_6) of **25** is shown in Figure 3.3. The isopropyl resonances are resolved at room temperature into four doublet and two septet signals and the Ti<u>Me</u>$_2$ signal also appears as two signals, reminiscent of the low temperature regime seen for 1,3-C$_6$H$_4${NCN^{i}Pr$_2$}$_2${Cp*TiMe$_2$}$_2$ (**4**) (Figure 2.6). This suggests a more sterically congested structure with a higher barrier to rotation caused by the proximate metal centres.

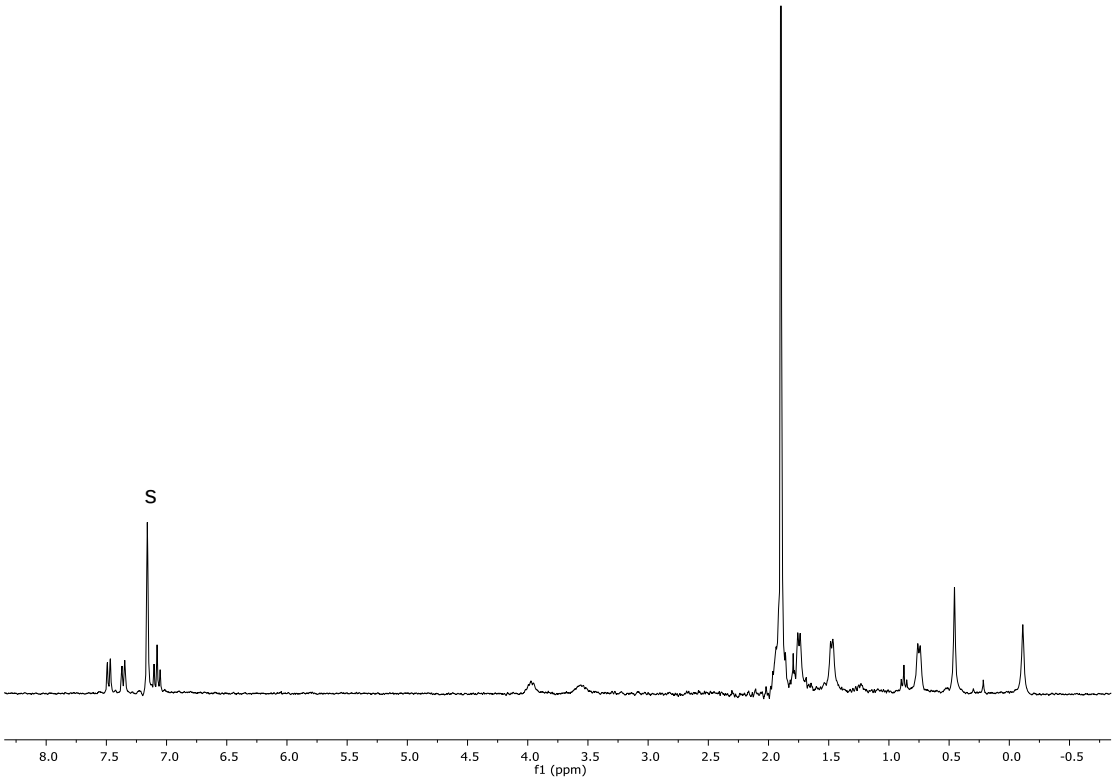

Figure 3.3 ^{1}H NMR (299.9 MHz, C_6D_6, 298 K) spectrum of DBF{NCN^{i}Pr$_2$}$_2${Cp*TiMe$_2$}$_2$ (**25**). 's' denotes residual protio-solvent.

3.4 Synthesis and characterisation of a xanthene-bridged cyclopentadienyl-amidinate bimetallic complex

3.4.1 Ligand synthesis

Xanthene only differs from dibenzofuran through the presence of a phenylene bridging six-membered ring as opposed to a five-membered ring. This additional carbon results in a smaller bond angle between the 1 and 1′ substituents, which would result in a closer metal-metal distance in the resultant bimetallic catalyst.[15] Xanth(CN)$_2$ (**26**) (where Xanth = 9,9-dimethyl-1,1′-xanthenyl) was synthesised *via* an analogous procedure to the dibenzofuran counterpart; synthesis of Xanth(I)$_2$ was prepared according to literature procedures[18] and reaction with an excess of Cu(I)CN in DMF under reflux conditions gave compound **26** in an isolated 80% yield after recrystallisation (Scheme 3.2). An alternative synthetic route was attempted by initial formation of Xanth(CHO)$_2$[19] and onward reaction with hydroxylamine hydrochloride in the presence of 2 equiv. of potassium iodide and zinc oxide.[20] This resulted in exclusive formation of the oxime and as such was not further investigated. Compound

26 displayed a strong ν(C≡N) stretch at 2230 cm^{-1} in its IR spectrum and the $^{13}C\{^{1}H\}$ NMR spectrum showed the diagnostic nitrile carbon at 101.9 ppm.

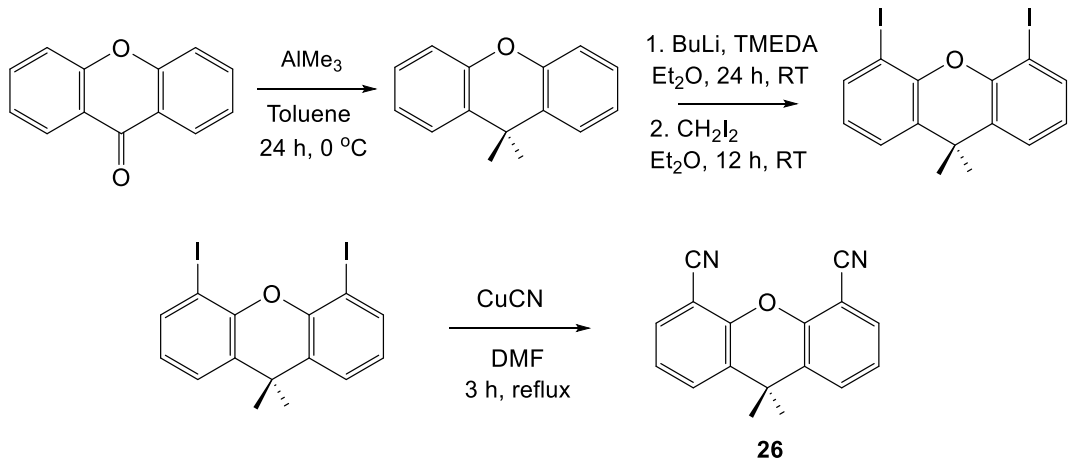

Scheme 3.2 Synthesis of Xanth$(CN)_2$ (**26**).

Diffraction-quality crystals of **26** were grown from a saturated chloroform solution at room temperature and the molecular structure is shown in Figure 3.4. The molecular structure displays the expected symmetric structure with a planar backbone. The nitrile groups are coplanar with the aromatic groups with C(1)–N(1) bond lengths of 1.1473(18) Å.

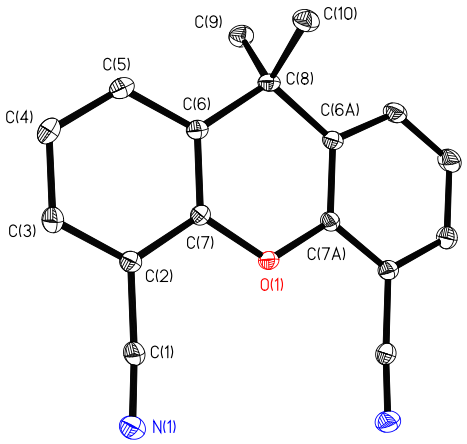

Figure 3.4 Displacement ellipsoid plot of Xanth$(CN)_2$ (**26**) (20% probability, H atoms omitted). Atoms carrying the suffix 'A' are related to their counterparts by the symmetry operator x, -y + ½, z.

The formation of the bis(amidine) from compound **26** proved not to be at all facile. The reaction with 2 or more equivalents of the *in situ* generated amide, $^{i}Pr_2NMgBr$, in THF exclusively resulted in the formation of the mono-substituted product at reaction temperatures varying from room temperature to that of reflux conditions. This mono-

substituted product will be discussed further in the following section. The same reaction in toluene proved more complex; if an excess of 2 equiv. of reagent, with immediate heating of the reaction mixture or a hot addition was employed then an unidentifiable complicated mixture of products was observed. Instead, it was found that upon amide addition the mixture must be stirred at room temperature for a minimum of 16 h, followed by subsequent heating to 100 °C for 3 h to achieve complete conversion (Equation 3.2).

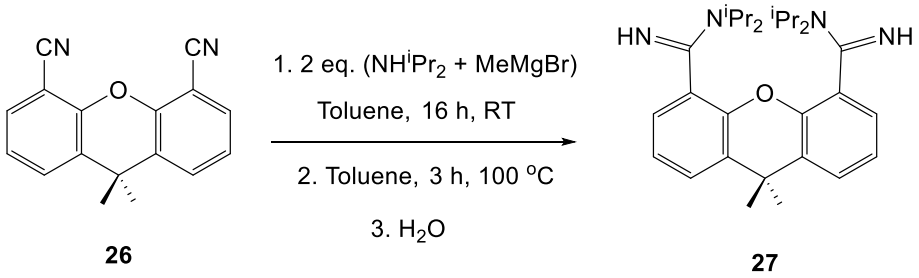

26 **27**

Equation 3.2

The product, Xanth(C(NH)N^{i}Pr$_2$)$_2$ (**27**), was initially isolated as a HBr (**27·HBr**) salt, which forms upon quenching with water. This was confirmed by X-ray crystallography and the molecular structure is displayed in Figure 3.5. The HBr forms a templating interaction between the two amidine groups. The molecular structure is disordered over two positions in which one imine nitrogen becomes protonated, an equivalent position of the bromide ion is found on the opposing side of the amidine moiety with a corresponding proton on the other unsubstituted imine nitrogen (only one form is depicted in Figure 3.5). The formal positive charge is equally distributed across both amidine moieties, which corresponds to the bromide anion residing centrally between them. There is no significant difference in bond lengths between the imine bond lengths (1.323(5) and 1.313(4) Å for N(1)–C(1) and N(2)–C(2), respectively) or amine bond lengths (1.323(5) and 1.329(4) Å for N(3)–C(1) and N(4)–C(2), respectively). The imine bond is longer than those previously introduced in the unsubstituted protio-amidine molecular structures, which is a result of a greater degree of electron density donating into the hydrogen bond interaction. An increase in π-donation from the amine nitrogen helps stabilise this and results in the shorter bond lengths observed.

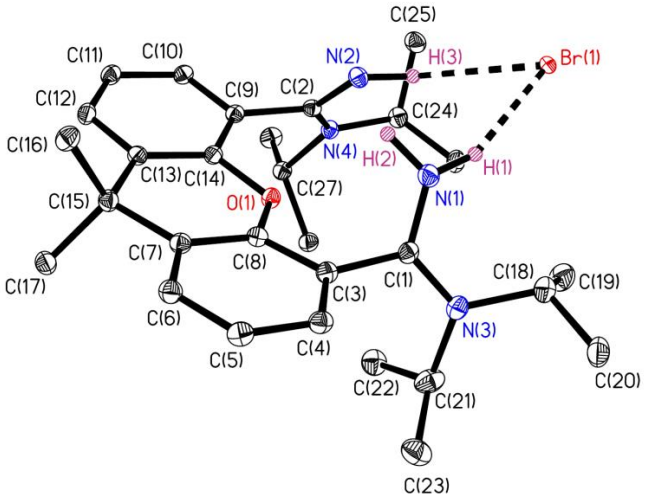

Figure 3.5 Displacement ellipsoid plot of [Xanth(C(NH$_2$)N^{i}Pr$_2$)(C(NH)N^{i}Pr$_2$)]Br (**27·HBr**) (20% probability, C-bound H atoms omitted).

A salt product always forms in the generation of protio-amidines *via* this pathway and typically the HBr is removed through washing with a concentrated NaOH solution. However, the isolation of **27** required extensive stirring with a concentrated NaOH solution for over 24 h to fully remove the HBr. This is presumed to be a result of the stability of the salt formed through this templating interaction. Removal of the HBr through reaction with organic bases, such as Et$_3$N, or by stirring over CaH$_2$ proved unsuccessful.

The neutral compound **27** was isolated without the HBr salt in a 62% yield and was fully characterised. The room temperature ^{1}H NMR (298 K, CD$_2$Cl$_2$) spectrum indicates a C_s molecule, and the features are a doublet and a septet resonance for the methyl and methine resonances at 1.29 and 3.60 ppm respectively, the C<u>Me</u>$_2$ signal at 1.64 ppm, and two doublet of doublets and an apparent triplet in the aromatic region at 7.41, 6.99 and 7.06 ppm respectively. Again, mass envelopes corresponding to both the $[M + H]^+$ (*m/z* = 463 g mol^{-1}) and $[M + 2H]^{2+}$ (*m/z* = 232 g mol^{-1}) molecular ions were observed in the ESI-MS spectrum.

In the process of synthesising **27** several alternative syntheses were unsuccessfully carried out. The use of AlCl$_3$ as a Lewis acid catalyst in the presence of an excess of diisopropylamine, as was described in the synthesis of **1** and **2** in Chapter Two, only resulted in formation of the mono-substituted product. It has been reported that ^{i}Pr$_2$NLi (LDA) will undergo nucleophilic addition to aromatic nitriles with halogen substituents, as opposed to aromatic substitution or benzyne formation, if carried out

in controlled conditions.[21] However, in this case this procedure formed an insoluble mixture despite thermodynamically controlled conditions being employed. Previous work within the Mountford group has found that amidines and guanidines can be formed through the reaction of carboxamides or ureas with a reactive acyl chloride, such as oxalyl chloride, followed by ammonia, or alternatively with ammonium chloride in the presence of triflic anhydride and pyridine.[22-24] Xanth(C(O)N^{i}Pr$_2$)$_2$ (**3.09**) was prepared according to literature procedures,[25] but no onward reaction was observed *via* either route.

To overcome the difficulties in removing HBr, which unavoidably forms when aromatic nitriles are reacted with an *in situ* generated amide, ^{i}Pr$_2$NMgBr, and quenched with either water or methanol, an alternative quenching reagent was developed. The addition of Me$_3$SiCl formed the bis(silylated) product Xanth(C(NSiMe$_3$)N^{i}Pr$_2$)$_2$ (**28**), however this could only be isolated in a 16% yield after recrystallisation (Equation 3.3).

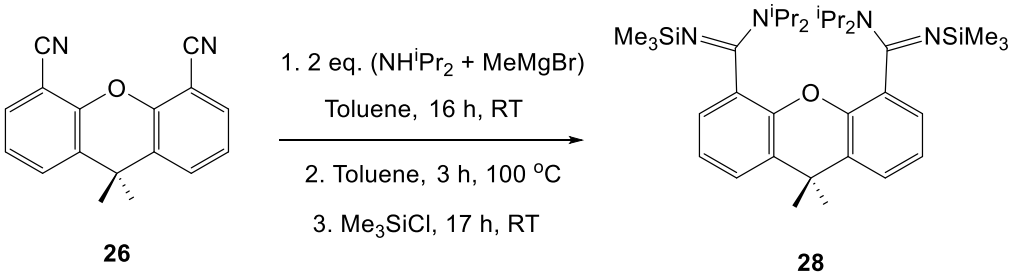

26 **28**

Equation 3.3

The ^{1}H NMR spectrum (298 K, C$_6$D$_6$) displays four distinct doublet resonances and two septet resonances for the methyl and methine resonances of the isopropyl groups respectively (Figure 3.6). This is in direct contrast to the room temperature ^{1}H NMR spectrum of compound **27,** in which the isopropyl methyl groups are equivalent on the NMR timescale. This is a result of the steric constraints imposed by the trimethylsilyl groups. The xanthene backbone remains planar and symmetric as indicated by a single resonance for C<u>Me</u>$_2$ and three signals for the aromatic region.

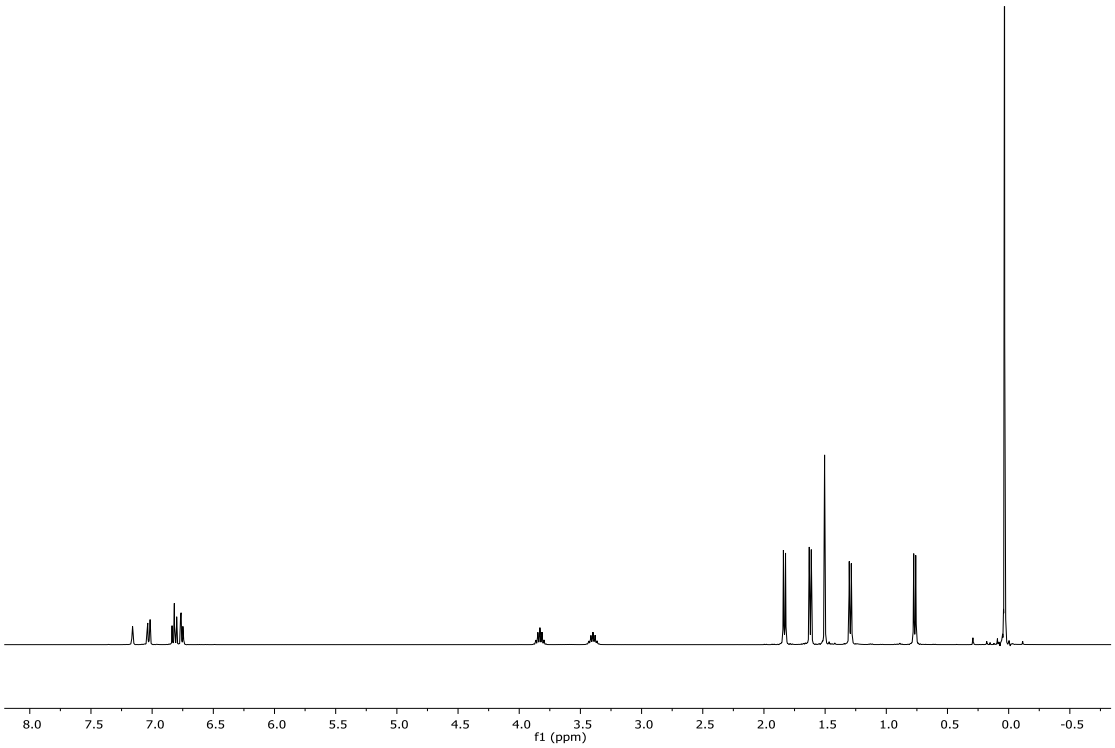

Figure 3.6 ^{1}H NMR (399.9 MHz, C_6D_6, 298 K) spectrum of Xanth(C(NSiMe$_3$)N^{i}Pr$_2$)$_2$ (**28**).

Diffraction-quality crystals of **28** were grown from a saturated pentane solution at -30 °C and the molecular structure is shown in Figure 3.7. For comparison, the molecular structure of the previously synthesised compound Me$_3$SiNC(Ph)N^{i}Pr$_2$ (**3.10**) is also shown in Figure 3.7, and selected bond lengths and angles of **28** and **3.10** are compared in Table 3.1.

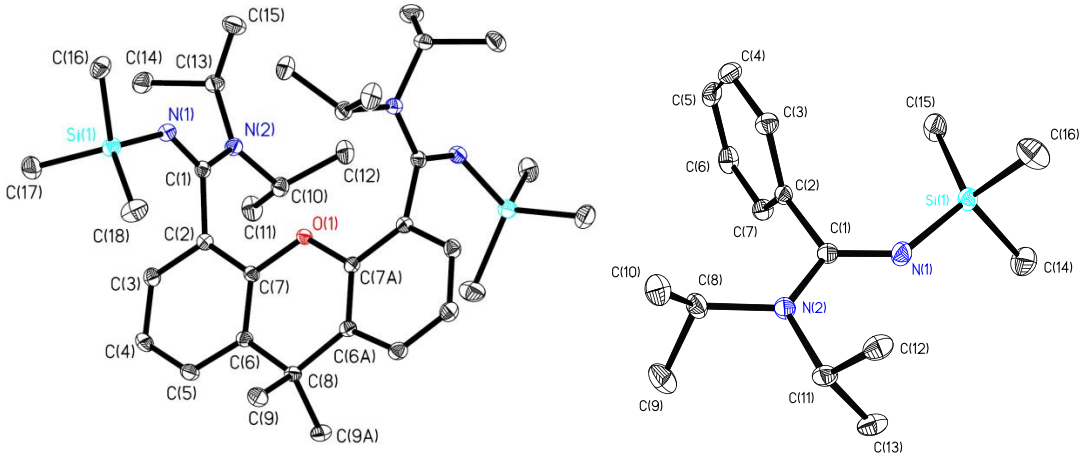

Figure 3.7 Displacement ellipsoid plots of Xanth(C(NSiMe$_3$)N^{i}Pr$_2$)$_2$ (**28**, left) and Me$_3$SiNC(Ph)N^{i}Pr$_2$ (**3.10**, right) (20% probability, C-bound H atoms omitted). Atoms carrying the suffix 'A' are related to their counterparts by the symmetry operator 1-x, y, ½-z.

Table 3.1. Selected bond lengths (Å) and angles (°) for Xanth(C(NSiMe$_3$)N^{i}Pr$_2$)$_2$ (**28**) and Me$_3$SiNC(Ph)N^{i}Pr$_2$ (**3.10**).

Parameter	**28**	**3.10**†
N(1)-Si(1)	1.7131(13)	1.705(3), 1.705(3)
C(1)-N(1)	1.2841(19)	1.285(4), 1.275(4)
C(1)-N(2)	1.3612(19)	1.361(4), 1.367(4)
C(1)-C(2)	1.512(2)	1.508(4), 1.505(4)
N(2)-C$_{alkyl}$	1.4761(19) 1.4782(19)	1.476(4), 1.477(4) 1.478(4), 1.481(4)
Si(1)-N(1)-C(1)	133.66(11)	136.4(2), 134.8(2)
N(1)-C(1)-C(2)	120.41(13)	121.2(3), 120.6(3)
N(1)-C(1)-N(2)	122.05(13)	122.5(3), 122.1(3)
C$_{alkyl}$-N(2)-C$_{alkyl}$	117.10(12)	116.9(2), 116.6(2)

†2 molecules in the asymmetric unit

The molecular structure of **28** is in agreement with the room temperature NMR data. The aryl backbone is forced perpendicular to the conjugated N(1)=C(1)–N(2) plane to avoid unfavourable steric interactions. In both cases the Me$_3$Si group is directed away from the alkyl substituents and in the case of **28** the Me$_3$Si groups are orientated in opposite directions to minimise the steric congestion. The bond lengths and angles show no significant differences between each other or the amidines previously discussed with the N(1)–Si(1) being σ-only in character and the amidine perpendicular to the aromatic substituents. The C=N–Si bond angles are larger than that of the analogous protio-amidine C=N–H angle, **2.08** (105.3(13)°), **1** (108.0(9)°) and **2** (110.2(13)°), presumably as a result of the steric constraints.

3.4.2 Metal complex synthesis

Reaction of compound **28** with 2 equiv. of Cp*TiCl$_3$ showed no reaction at room temperature or temperatures up to 60 °C. At reaction temperatures above this the monometallic pincer complex Xanth{NCN^{i}Pr$_2$}$_2${Cp*TiCl} (**29**) forms, with the extrusion of 2 equiv. of Me$_3$SiCl (Equation 3.4). The desired bimetallic complex was not observed even with an excess of Cp*TiCl$_3$. Complex **29** was isolated in a 40% yield after reaction with 1 equiv. of Cp*TiCl$_3$ at 90 °C in toluene.

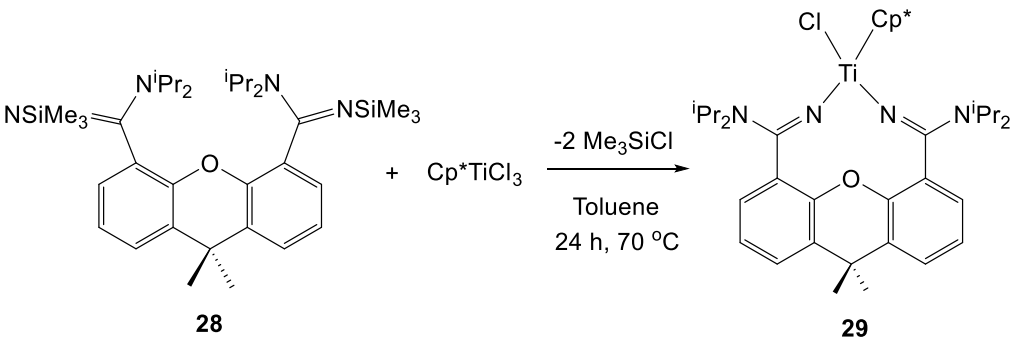

Equation 3.4

The room temperature ^{1}H NMR (298 K, C_6D_6) spectrum show that the symmetry previously observed in the xanthene ligand has been disrupted (Figure 3.8). The C<u>Me</u>$_2$ now exists as two distinct signals (1.27 and 1.55 ppm) suggesting that the backbone is puckered, rather than planar. A 2D ROESY NMR experiment displayed a through-space interaction between signals corresponding to the aromatic region and only the downfield C<u>Me</u>$_2$ signal. It is therefore assumed that one methyl group lies in the same plane as the xanthene aromatic rings and the other perpendicular to the rings. The perpendicular methyl observes an increase in shielding as a result of the aromatic ring currents and is correspondingly shifted upfield. The steric congestion induced by forming this pincer complex results in distinct resonances for the methyl and methine protons of the isopropyl group. A variable temperature NMR study revealed that all the signals have decoalesced at room temperature, but are unidentifiable through overlap with either the Cp^* resonance or each other. At low temperatures the C<u>Me</u>$_2$ signals remain unchanged suggesting that there is only one orientation to this puckering, which is concurrent with how only one methyl group sees a through-space correlation with the aromatic protons.

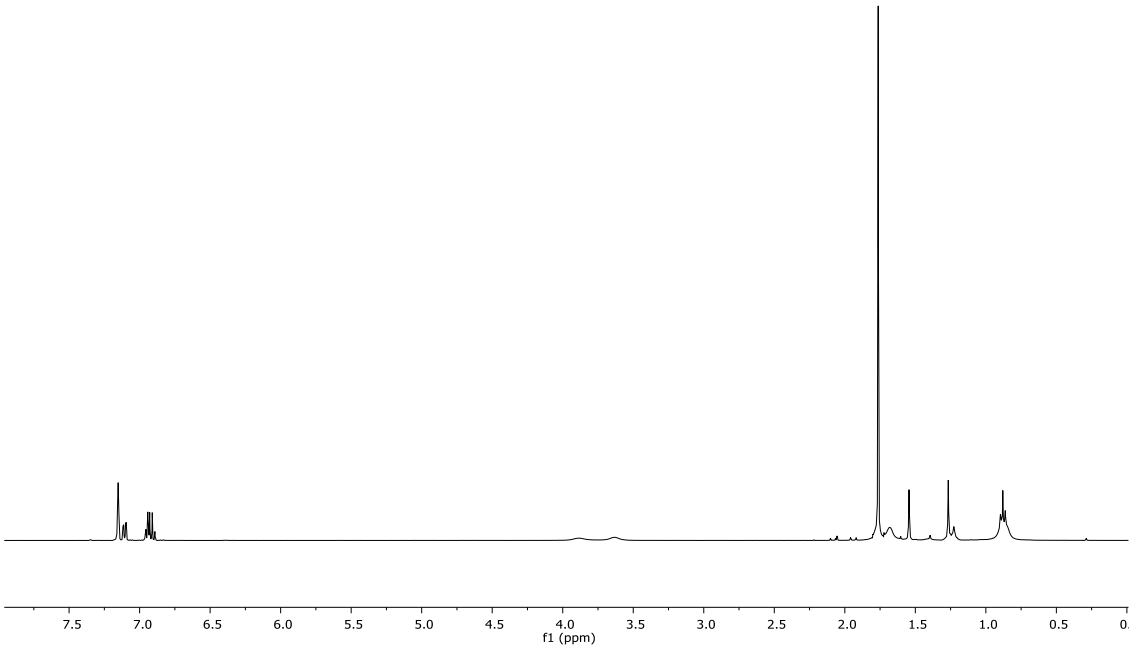

Figure 3.8 ^{1}H NMR (399.9 MHz, C_6D_6, 298 K) spectrum of Xanth{NCN^{i}Pr$_2$}$_2${Cp*TiCl} (**29**).

Diffraction-quality crystals of **29** were grown from a saturated hexane solution at -30 °C and the molecular structure is shown in Figure 3.9. Selected bond lengths and angles are displayed in Table 3.2. There are no significant differences between the bond lengths and angles of the two amidinate groups so parameters from only one group will be discussed. The molecular structure of **29** shows the titanium centre resides in the expected *pseudo*-tetrahedral three-legged piano stool arrangement, surrounded by η^5-cyclopentadienyl, two κ^1-amidinate ligands and a chloride substituent. The backbone is puckered with C(26) perpendicular to the aromatic plane, which is in agreement with the NMR data, and the hinge angle defined by the two aromatic rings is *ca.* 19°. This puckering is presumed to relieve ring-strain while maintaining the allylic-type-π-system within the κ^1-amidinate moieties. The Ti(1)–N(1) bond is significantly longer than that of Cp*Ti{NC(Ph)N^{i}Pr$_2$}Cl$_2$ (**2.06**) (1.7855(13) Å) as a chloride substituent has been replaced by a κ^1-amidinate, which reduces the amount of electron-density withdrawn from the metal centre and competes for π-donation. This competitive donation lengthens the Ti(1)–Cl(1) and N(2)–C(1) bond within the amidinate moiety (2.3095(5) *vs.* 2.3751(8) Å and 1.3279(19) *vs.* 1.375(4) Å for **2.06** and **29** respectively). There is no bonding interaction from the oxygen in the xanthene backbone (Ti(1)---O(1) = 3.82 Å).

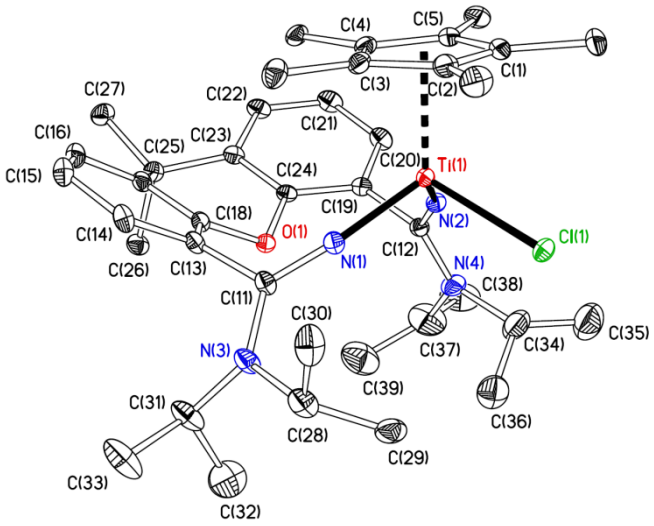

Figure 3.9 Displacement ellipsoid plot of Xanth{NCN^{i}Pr$_2$}$_2${Cp*TiCl} (**29**) (20% probability, H atoms omitted).

Table 3.2. Selected bond lengths (Å) and angles (°) for Xanth{NCN^{i}Pr$_2$}$_2${Cp*TiCl} (**29**). Cp$^*_{cent}$ is the computed Cp* ring carbon centroid.

Parameter		Parameter	
Ti(1)-Cp$^*_{cent}$	2.08	Cp$^*_{cent}$-Ti(1)-N(1)	116.7
Ti(1)-N(1)	1.860(3)	Cp$^*_{cent}$-Ti(1)-Cl(1)	110.7
Ti(1)-Cl(1)	2.3751(8)	C(11)-N(1)-Ti(1)	161.7(2)
N(1)-C(11)	1.280(4)	C(13)-C(11)-N(1)	119.8(3)
N(3)-C(11)	1.375(4)	N(1)-C(11)-N(3)	125.0(3)
C(11)-C(13)	1.506(4)		

The most closely related literature complexes that have been crystallographically characterised are **3.11**[26] and **3.12**,[16] shown in Figure 3.10. Complex **3.11** has a bonding interaction from the oxygen in the backbone and is also puckered with an aromatic hinge angle of *ca*. 15°. Unlike **29** this puckered rigidity is not maintained in solution and a C_{2v} structure is observed with equivalent C<u>Me</u>$_2$ and dimethylamido environments on the NMR timescale.[26] Complex **29** is presumed to remain puckered in solution due to the steric constraints imposed by the Cp* group. Complex **3.12** displays significant ring strain with the κ^2-amidinate bent towards the metal centre, however no puckering is observed in the backbone.

The bis(amidine) backbone of **3.12**, Xanth(^{i}PrNCN^{i}Pr)$_2$H$_2$ (**3.13**), is prepared *via* reaction of *N*,*N*′-diisopropylcarbodiimide with doubly deprotonated 9,9-

dimethylxanthene. Compound **3.13** was reacted with 1 equiv. of $Zr(CH_2Ph)_4$ to give **3.12** and it was shown that reaction with 2 equiv. gave the bimetallic analogue, Xanth{^{i}PrNCN^{i}Pr}{$Zr(CH_2Ph)_3$})$_2$ (**3.14**). Hagadorn and co-workers also went on to synthesise analogous bimetallic zirconium complexes with different substituents, as well as their titanium counterparts, of the form Xanth({^{i}PrNCN^{i}Pr}{$MR^1R^2R^3$})$_2$ (M = Ti or Zr; $R^1 = R^2 = R^3 = NMe_2$, R^1 = Cp $R^2 = R^3$= alkyl or halide (**3.15**)).[15, 16, 27, 28] As discussed previously, the bimetallic counterpart to **29** was unable to be formed presumably due to the steric constraints imposed by the Cp* group.

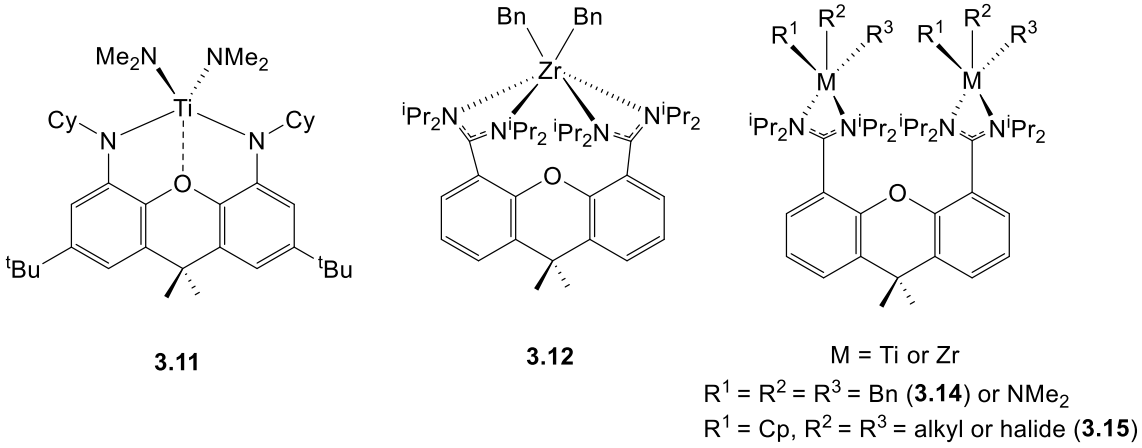

3.11 **3.12**

Figure 3.10 Group 4 xanthene pincer and bimetallic complexes.

Dialkyl or dihalide titanium complexes with two κ^1-amidinate substituents have previously been prepared within the Mountford group,[23] although at the time covalent tethers between the two amidinate moieties proved elusive. The complexes Ti{NC(Ph)N^{i}Pr$_2$}$_2$Cl$_2$ (**3.13**) and Ti{NC(Ph)N^{i}Pr$_2$}$_2$Me$_2$ (**3.14**) were tested as catalysts for the polymerisation of ethylene at both ambient and high temperatures with MAO as an activating species. The results showed the catalytic species to be poorly active and very unstable under the relevant polymerisation conditions.[23]

Reaction of **27·HBr** with 2 equiv. of Cp*TiMe$_3$ at room temperature gave a complicated mixture of products, however co-crystallisation of the pincer complexes Xanth{NCN^{i}Pr$_2$}$_2${Cp*TiBr} and Xanth{NCN^{i}Pr$_2$}$_2${Cp*TiMe} was achieved. Xanth{NCN^{i}Pr$_2$}$_2${Cp*TiBr} was confirmed by X-ray crystallography and the molecular structure is shown in Figure 3.11. Reaction of the co-crystalline product with a MeLi solution exclusively formed Xanth{NCN^{i}Pr$_2$}$_2${Cp*TiMe}, which was

confirmed by elemental analysis and a variable temperature NMR study. Surprisingly no reaction was observed between **29** and 1 equiv. of a MeLi solution. There are no discernible differences in bond lengths and angles between Xanth{NCN^{i}Pr$_2$}$_2${Cp*TiBr} and that of **29**, apart from an increased Ti–X (where X = Cl or Br) bond length for the bromide analogue (2.5430(13) *vs.* 2.3751(8) Å).

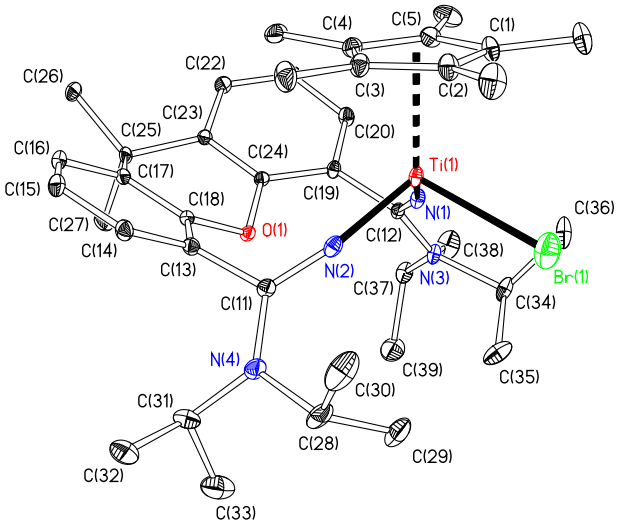

Figure 3.11 Displacement ellipsoid plot of Xanth{NCN^{i}Pr$_2$}$_2${Cp*TiBr} (20% probability, H atoms omitted).

An NMR tube scale reaction of **27** with 2 equiv. of Cp*TiMe$_3$ formed the mono-substituted product, Xanth(HNCN^{i}Pr$_2$){(NCN^{i}Pr$_2$)(Cp*TiMe$_2$)}, after 48 h at room temperature. At elevated temperatures a mixture of the bimetallic complex, Xanth{NCN^{i}Pr$_2$}$_2${Cp*TiMe$_2$}$_2$ (**30**), and the methyl pincer Xanth{NCN^{i}Pr$_2$}$_2${Cp*TiMe} was observed. On the preparative scale, addition of **27** to a small excess of Cp*TiMe$_3$ at 60 ^{o}C exclusively formed **30** after 72 h, which was isolated in a low yield of 27% and fully characterised (Equation 3.5).

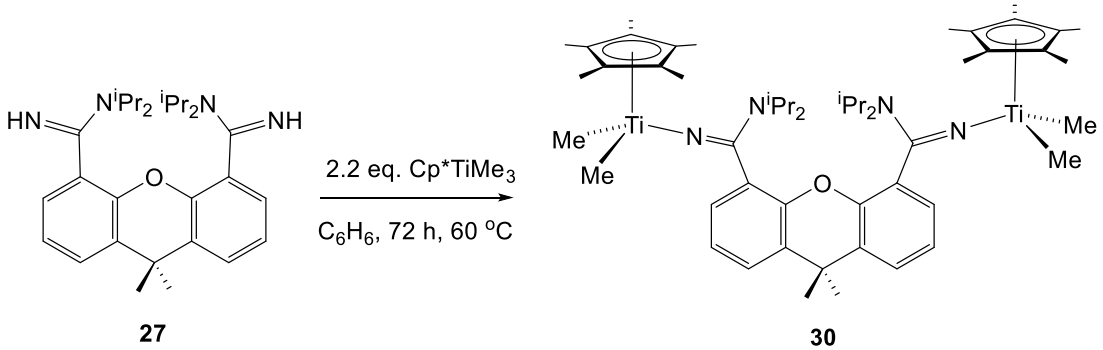

27 **30**

Equation 3.5

The room temperature ^{1}H NMR (298 K, C_6D_6) spectrum of **30** shows comparable resonances to those of **25** and suggests a C_2-symmetric species where the isopropyl resonances are resolved into four doublet and two septet signals and the Ti<u>Me</u>$_2$ signal also appears as two signals. The xanthene backbone is planar with the aromatic region consisting of two doublet of doublets and an apparent triplet (6.96, 6.85 and 6.72 ppm respectively). A single resonance corresponding to the C<u>Me</u>$_2$ is observed suggesting a planar ligand backbone with an overall molecular C_2 symmetry.

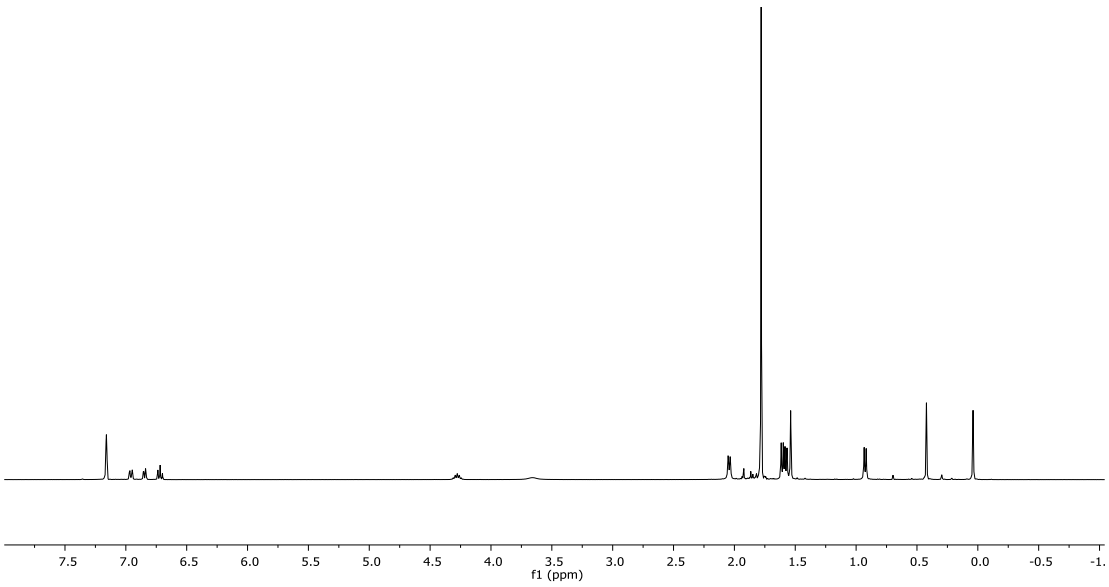

Figure 3.12 ^{1}H NMR (399.9 MHz, C_6D_6, 298 K) spectrum of Xanth{NCN^{i}Pr$_2$}$_2${Cp*TiMe$_2$}$_2$ (**30**).

Diffraction-quality crystals of **30** were grown from a saturated benzene solution at room temperature and the molecular structure is shown in Figure 3.13. Selected bond lengths and angles are displayed in Table 3.3. The molecular structure is in good agreement with the NMR data. In this structure the titanium methyl groups are positioned above or away from the xanthene backbone, and with restricted rotation around C(11)–C(12) and N(2)–C(11), as is evident from the distinct isopropyl resonances even if there is free rotation to the metal centre the methyl groups will remain inequivalent on the NMR timescale. In Figure 3.9 C(26) is orientated above the xanthene backbone and is therefore presumed to be shifted upfield relative to C(27) due to the presence of aromatic ring currents (0.04 and 0.42 ppm respectively). The methyl groups in the xanthene backbone of complex **30**, C(19), are symmetric and therefore only one corresponding resonance is observed in the ^{1}H and ^{13}C{^{1}H}

NMR spectra. The molecule overall has C_2 symmetry, although there is a small amount of distortion across the xanthene backbone with a torsion angle between the amidinate substituents of *ca.* 36°. The titanium centres again reside in a *pseudo*-tetrahedral three-legged piano stool arrangement with *trans* orientation to minimise steric interaction. There are no significant differences in the bond lengths and angles observed here as was discussed previously for other monometallic and bimetallic dimethyl species discussed in Chapter Two.

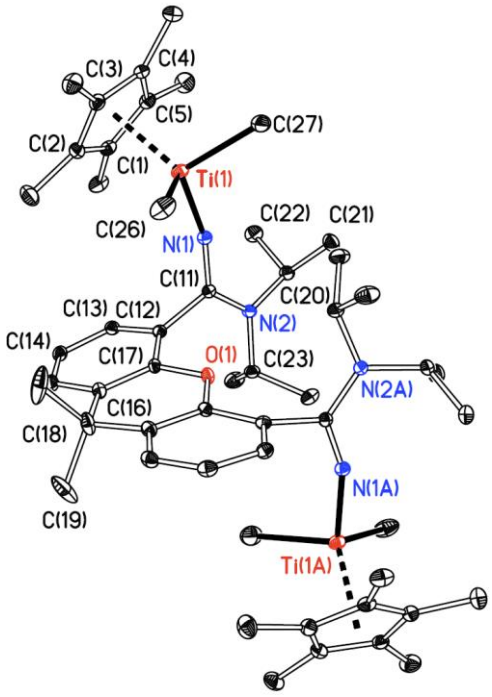

Figure 3.13 Displacement ellipsoid plot of Xanth{NCN^{i}Pr$_2$}$_2${Cp*TiMe$_2$}$_2$ (**30**) (20% probability, H atoms omitted). Atoms carrying the suffix 'A' are related to their counterparts by the symmetry operator 1-*x*, *y*, -*z*+$^1/_2$.

Table 3.3. Selected bond lengths (Å) and angles (°) for Xanth{NCN^{i}Pr$_2$}$_2${Cp*TiMe$_2$}$_2$ (**30**). Cp$^*_{cent}$ is the computed Cp* ring carbon centroid.

Parameter		Parameter	
Ti(1)-Cp$^*_{cent}$	2.08	Cp$^*_{cent}$-Ti(1)-N(1)	124.2
Ti(1)-N(1)	1.8464(17)	Cp$^*_{cent}$-Ti(1)-Me(1)	113.9
N(1)-C(11)	1.295(2)	Cp$^*_{cent}$-Ti(1)-Me(2)	110.9
N(2)-C(11)	1.354(3)	C(11)-N(1)-Ti(1)	159.50(15)
C(11)-C(12)	1.512(3)		
Ti(1)-Me(1)	2.101(3)		
Ti(1)-Me(2)	2.131(3)		

3.5 Synthesis, characterisation and activation studies of xanthene bridged cyclopentadienyl-amidinate monometallic complexes

3.5.1 Ligand synthesis

As discussed in Section 3.4.1, in the process of synthesising compound **27** the mono-substituted product was formed. Reaction with 2 or more equivalents of the *in situ* generated amide, $^{i}Pr_2NMgBr$, in THF exclusively resulted in the formation of the mono-substituted product. Quenching the reaction mixture with water or Me_3SiCl allowed the products Xanth(CN)(C(NH)N^{i}Pr$_2$) (**31**) and Xanth(CN)(N(SiMe$_3$)CN^{i}Pr$_2$) (**32**) to be formed (Equation 3.6).

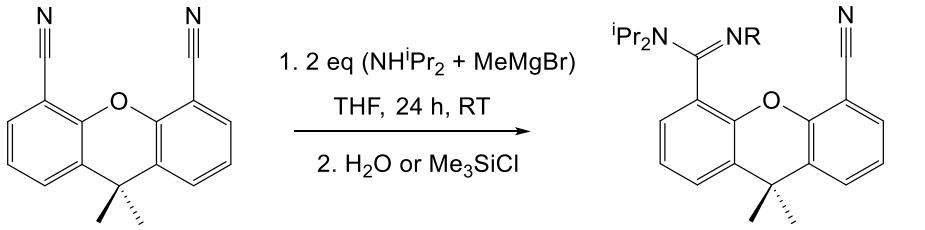

Equation 3.6

Compounds **31** and **32** were isolated in 68 and 59% yields respectively and fully characterised. The room temperature ^{1}H NMR spectra show very different characteristics; the sterically demanding Me_3Si group of **32** prevents free rotation and results in four distinct methyl doublet resonances and two distinct methine septet resonances for the isopropyl groups, whereas the comparable environments appear equivalent at room temperature for **31**. This steric imposition also results in the xanthene-bound methyl groups becoming inequivalent, a smaller chemical shift difference is observed here than for the puckered pincer compound **29** (0.02 and 0.27 ppm, respectively) (Figure 3.14). Compounds **31** and **32** both displayed strong ν(C≡N) (2231 and 2235 cm^{-1}) and ν(C=N) (1575 and 1616 cm^{-1}) stretches in the IR spectra with no discernible differences between the two compounds.

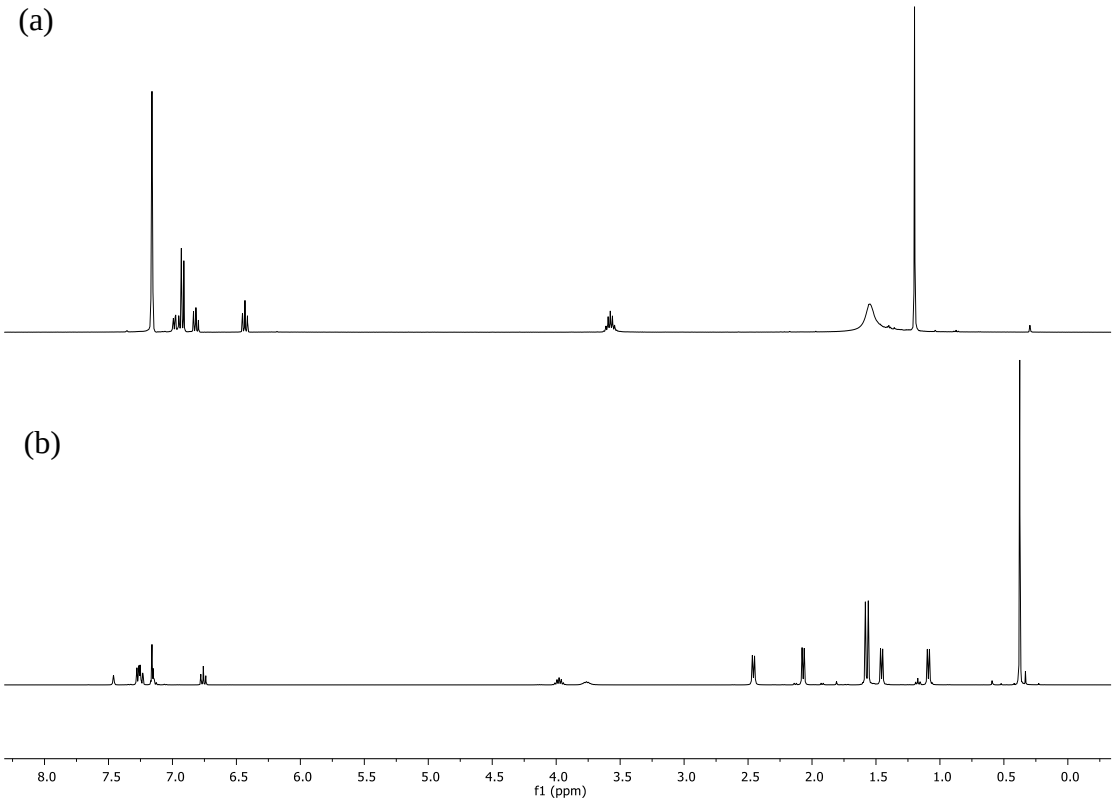

Figure 3.14 ^{1}H NMR (399.9 MHz, C_6D_6, 298 K) spectra of Xanth(CN)(C(NH)N^{i}Pr$_2$) (**31**, a) and Xanth(CN)(N(SiMe$_3$)CN^{i}Pr$_2$) (**32**, b).

3.5.2 Metal complex synthesis

Compounds **31** and **32** were reacted with Cp*TiMe$_3$ and Cp*TiCl$_3$ to give Xanth(CN)({NCN^{i}Pr$_2$}{Cp*TiMe$_2$}) (**33**) and Xanth(CN)({NCN^{i}Pr$_2$}{Cp*TiCl$_2$}) (**34**), respectively (Equation 3.7). Complexes **33** and **34** were isolated in 69 and 68% yields and fully characterised.

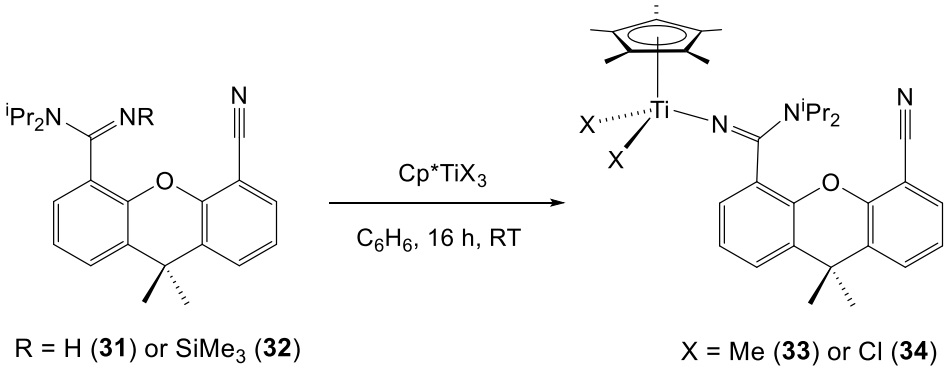

Equation 3.7

The room temperature ^{1}H NMR spectra showed similar features to that of **32**, with distinct resonance for the isopropyl groups and inequivalent xanthene-bound methyl groups. A small chemical shift separation is again observed, which suggests that the backbone is not puckered and that the different chemical shifts are only a result of the differing groups on each face of the xanthene and limited bond rotation. Again strong ν(C≡N) (2227 and 2225 cm^{-1}) and ν(C=N) (1559 and 1529 cm^{-1}) stretches in the IR spectra are observed. The limited shift in stretching frequency within the nitrile group between **31-34** suggests there is minimal electronic communication across the xanthene ring, presumably as a result of the allylic-type-π-system within the κ^{1}-amidinate moiety lying perpendicular to the aromatic ring.

Diffraction-quality crystals of **33** were grown from a hexane solution at room temperature, and of **34** *via* slow cooling of a hot toluene solution. The molecular structures are shown in Figure 3.15 and selected bond lengths and angles of **33** and **34** are compared in Table 3.4.

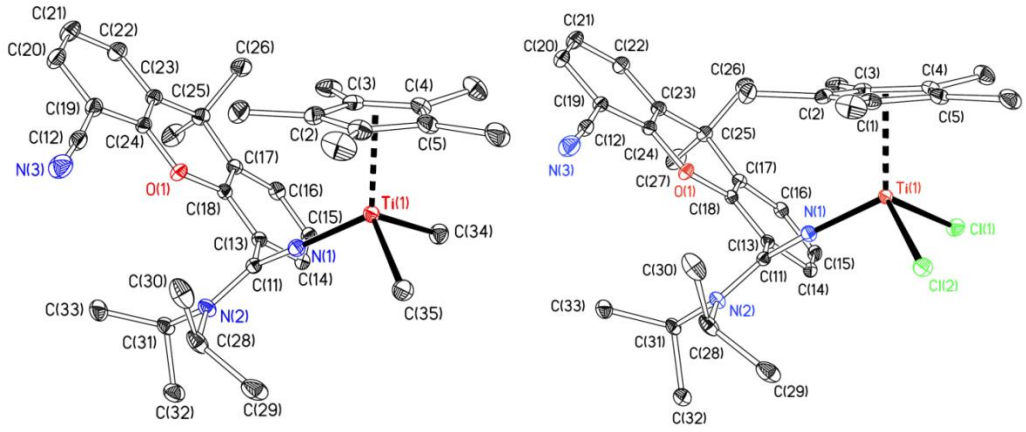

Figure 3.15 Displacement ellipsoid plots of Xanth(CN)({NCN^{i}Pr$_2$}{Cp*TiMe$_2$}) (**33**) and Xanth(CN)({NCN^{i}Pr$_2$}{Cp*TiCl$_2$}) (**34**) (20% probability, H atoms omitted).

Table 3.4 Selected bond lengths (Å) and angles (°) for Xanth(CN)({NCN^{i}Pr$_2$}{Cp*TiMe$_2$}) (**33**) and Xanth(CN)({NCN^{i}Pr$_2$}{Cp*TiCl$_2$}) (**34**). Cp$^*_{cent}$ is the computed Cp* ring carbon centroid.

Parameter	**33**	**34**
Ti(1)-Cp$^*_{cent}$	2.06	2.05
Ti(1)-N(1)	1.8337(16)	1.8032(19)
N(1)-C(11)	1.290(2)	1.308(3)
N(2)-C(11)	1.349(3)	1.336(3)
C(11)-C(13)	1.512(3)	1.504(3)
C(12)-N(3)	1.150(3)	1.153(4)
C(12)-C(19)	1.438(4)	1.439(4)
Ti(1)-Me(1)/Cl(1)	2.122(2)	2.2918(7)
Ti(1)-Me(2)/Cl(2)	2.156(2)	2.3238(7)
Cp$^*_{cent}$-Ti(1)-N(1)	120.7	117.2
Cp$^*_{cent}$-Ti(1)- Me(1)/Cl(1)	112.9	114.2
Cp$^*_{cent}$-Ti(1)- Me(2)/Cl(2)	114.7	114.8
C(11)-N(1)-Ti(1)	164.92(16)	164.80(17)

The molecular structures of **33** and **34** are both isostructural and isomorphous with the titanium centres residing in a *pseudo*-tetrahedral three-legged piano stool arrangement. The same trend in bond lengths on changing substituents from a chloride to a methyl group is observed here, as was discussed in Chapter Two, and neither **33** nor **34** show any significant differences from that of their phenyl substituted counterparts **2.06** and **2.07**. There are no differences between the nitrile groups of **33** or **34,** again indicating a limited electronic communication through the xanthene ring.

3.5.3 Activation studies

Previous work in the Mountford group has shown that activation of monometallic amidinate and imido titanium complexes with nitriles formed the Lewis base adducts followed by migratory insertion, as seen previously for metallocenium systems.[29-31] Reaction of **2.07** with TBF$_{20}$ in the presence of two equivalents of either MeCN or PhCN resulted in the immediate formation of [Cp*Ti{NC(Ph)N^{i}Pr$_2$}{NC(Me)R}(NCR)][BF$_{20}$] (R = Me (**3.16**) or Ph (**3.17**)) (Equation 3.8).[32]

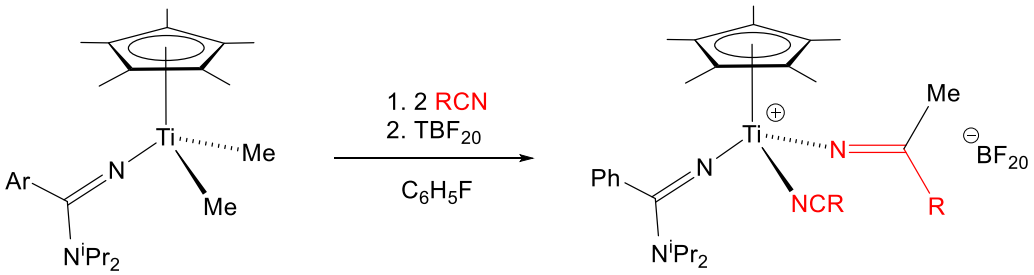

R = Me (**3.16**) or Ph (**3.17**)

Equation 3.8

In Section 3.4.2, and literature complexes discussed therein, it is evident that xanthene based systems of this form have the capacity to form pincer complexes. In light of the previous activation studies of titanium complexes in the presence of nitriles, it was proposed that activation of **33** could result in an intramolecular migratory insertion product. NMR tube scale reaction of **33** with TBF_{20} in C_6D_5Br resulted in an immediate formation of a deep red solution. The room temperature ^1H NMR spectrum displayed quantitative evidence of CPh_3Me formation indicating successful abstraction. A resonance corresponding to the unabstracted methyl environment at a significantly upfield shift of 0.4 ppm was observed, this is indicative that no migratory insertion has occurred and that the methyl remains coordinated to a cationic titanium centre. Within 1 h a dark oil had formed in the reaction mixture, this oil was isolated and a strong ν(C≡N) stretch at 2225 cm^{-1} in the IR spectrum indicated that this is not a polymeric product formed through an attack at the nitrile moiety. This stretching frequency is very similar to that of **33**, which again suggests a minimal electronic interaction. The same reaction was carried out in the presence of 1 equiv. of THF, but again no evidence of the migratory insertion product was observed.

An NMR tube scale reaction of **33** with TBF_{20} in the presence of 2 equiv. of PhCN was carried out. In this case the migratory insertion product does form as is indicated by an unabstracted methyl resonance at 2.20 ppm. The second equivalent of benzonitrile is believed to coordinate to the titanium centre, but due to a large number of resonances in the aromatic region this was unable to be confirmed.

3.6 Synthesis and characterisation of a ferrocenyl bridged cyclopentadienyl-amidinate bimetallic complex

In Chapter Two the monometallic complex $Cp^{*}Ti\{NC(Ar^{Fc})N^{i}Pr_2\}Me_2$ (**15**) was introduced. This ferrocenyl tether gave the opportunity for a bimetallic complex to be formed with a novel linking moiety.

3.6.1 Ligand synthesis

Knapp and Rehahn introduced the arylation of ferrocene derivatives using a Suzuki coupled reaction.[33] Ferrocene-1,1′-diboronic acid (**3.18**) was reacted with a range of halogen-substituted aromatics in the presence of a palladium catalyst and this same procedure was invoked for the synthesis of $Fc'(CN)_2$ (**35**) (where Fc′ = 1,1′-bis(1,4-phenyl)ferrocenyl). Reaction of **3.18** under refluxing conditions with 4-bromobenzonitrile in the presence of $PdCl_2$(DPPF) in DME for 6 days resulted in the desired product in a yield of 73% after recrystallisation. Compound **35** was fully characterised and onward reaction with 2 equiv. of the *in situ* generated amide, $^{i}Pr_2NMgBr$, resulted in formation of $Fc'\{C(NH)N^{i}Pr_2\}_2$ (**36**) initially as an HBr salt in 52% yield (Scheme 3.3).

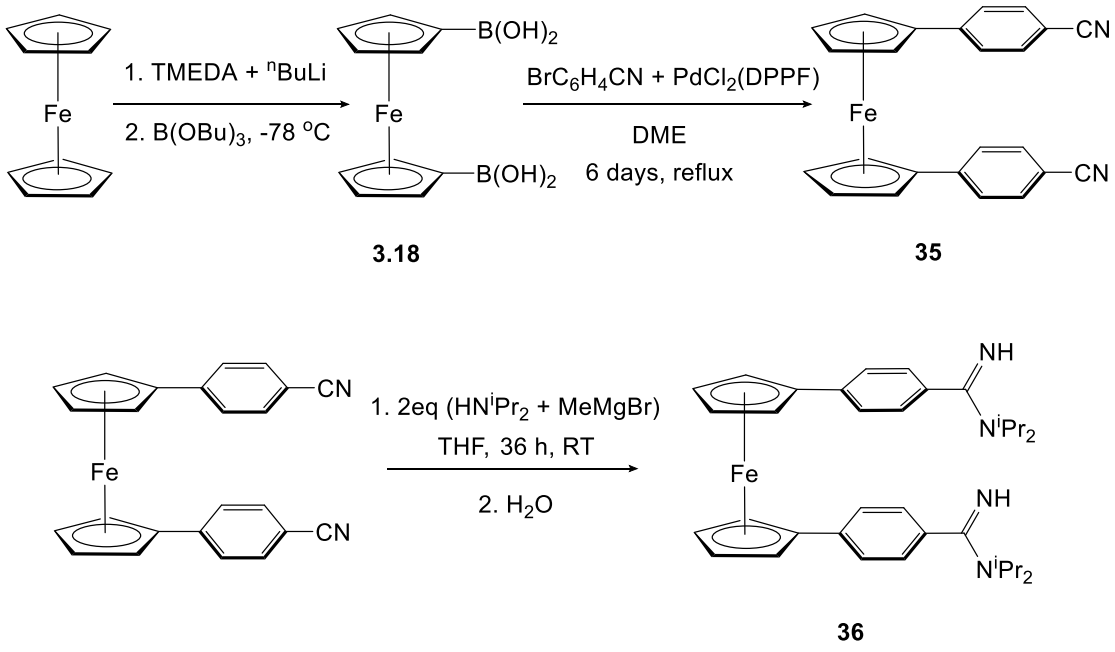

Scheme 3.3 Synthesis of $Fc'(CN)_2$ (**35**) and $Fc'\{C(NH)N^{i}Pr_2\}_2$ (**36**).

The HBr salt of compound **36** (**36·HBr**) was fully characterised and diffraction-quality crystals were grown from a chloroform solution at room temperature. The

molecular structure is shown in Figure 3.16 and again displays a templating effect with two chloroform molecules, from the solvent of crystallisation, also coordinated to the bromide. This templating effect is also favoured by a weak π-stacking interaction (interplanar separation = 3.780 Å) between the phenylene groups, which arises with mutual orientation of the substituents. A "purposeful" stacking interaction bought upon by an eclipsed ferrocene conformation has been previously observed in the literature for ferrocene with fluorophenyl substituents.[34] Unlike the molecular structure **27·HBr** only one amidine is protonated and this results in different bond lengths for both the N(1)/N(2)–C(23)/C(24) (1.315(3) and 1.294(3) Å) and N(3)/N(4)–C(23)/C(24) (1.334(3) and 1.361(3) Å) bonds of the amidine moieties. The protonated amidine has a longer N(1)–C(24) bond, which correspondingly results in a reduced N(3)–C(24) bond length. This difference is not apparent on the NMR experiment timescale where equivalent resonances are observed due to fast proton exchange processes. The bis(amidine) product was isolated through washing with a concentrated NaOH solution.

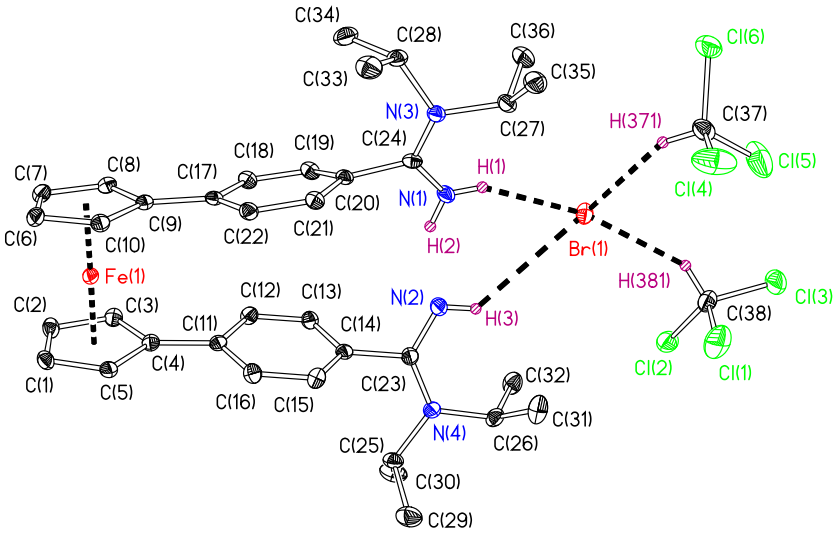

Figure 3.16 Displacement ellipsoid plot of [Fc′{C(NH)N^{i}Pr$_2$}{C(NH$_2$)N^{i}Pr$_2$}]Br (**36·HBr**) (20% probability, C-bound H atoms other than those attached to $CHCl_3$ omitted)

The analogous bis(amidine) ferrocene group without a phenylene spacer, 1,1′-{C(NH)N^{i}Pr$_2$}$_2$ferrocene, was also targeted. 1,1′-dicyanoferrocene (**3.19**) was synthesised according to a modified literature procedure from the reaction of the synthesised 1,1′-diformylferrocene (**3.20**)[35] with 2.6 equiv. of hydroxylamine

hydrochloride in the presence of 2 equiv. of potassium iodide and zinc oxide.[36] This same modified procedure to form **3.19** was later reported by Lang and co-workers.[37] The onwards reaction of **3.19** with either the *in situ* generated amide, $^{i}Pr_2NMgBr$, or the protio amine in the presence of a Lewis acid exclusively generated the mono-substituted product.

3.6.2 Metal complex synthesis

Reaction of **36** with 2 equiv. of $Cp^{*}TiMe_3$ gave the desired bimetallic complex, $Fc'\{NCN^{i}Pr_2\}_2\{Cp^{*}TiMe_2\}_2$ (**37**), in a 64% yield (Equation 3.9).

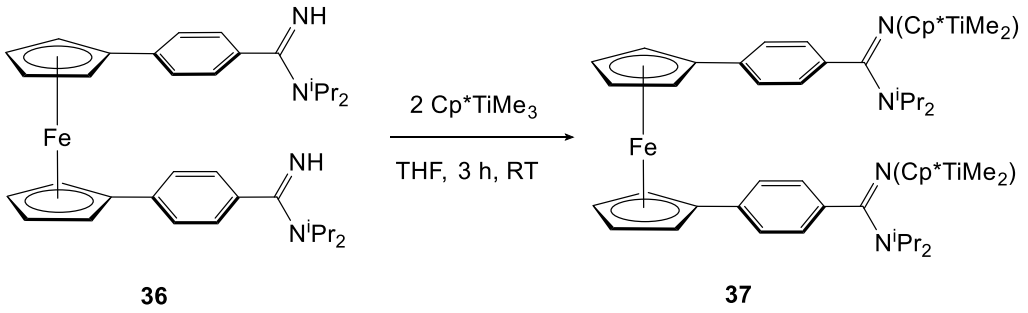

36 **37**

Equation 3.9

The key features of the room temperature ^{1}H NMR spectrum (Figure 3.15) include the Cp^{*} singlet at 1.76 ppm, $TiMe_2$ signal at -0.12 ppm and two apparent triplets at 4.40 and 4.21 ppm for the cyclopentadienyl groups of the ferrocene moiety. The aromatic protons consist of a pair of mutually-coupled doublets (7.33 and 7.16 ppm), as was also observed for complex **15** and discussed in Chapter Two. 2D ^{1}H-^{13}C correlation experiments identified the downfield signal for the cyclopentadienyl group as the protons adjacent to the phenylene substituent and the downfield signal of the aromatic group as those *ortho*- to the cyclopentadienyl substituent; this was confirmed by a ROESY experiment, which showed a through-space correlation (NOE) between these two relatively downfield resonances. The isopropyl resonances appear broad at room temperature, so a variable temperature ^{1}H NMR study was carried out (Figure 3.17). As has been previously observed, the resonances corresponding to the isopropyl group decoalesced into a pair of apparent septets and a pair of doublets for the methine and methyl protons, respectively. Overall the molecule is highly symmetric and the fluxionality of the isopropyl resonances, relative to the more constrained systems previously described in this chapter, suggests that the substituents are orientated away from one another. The complex was characterised at 223 K.

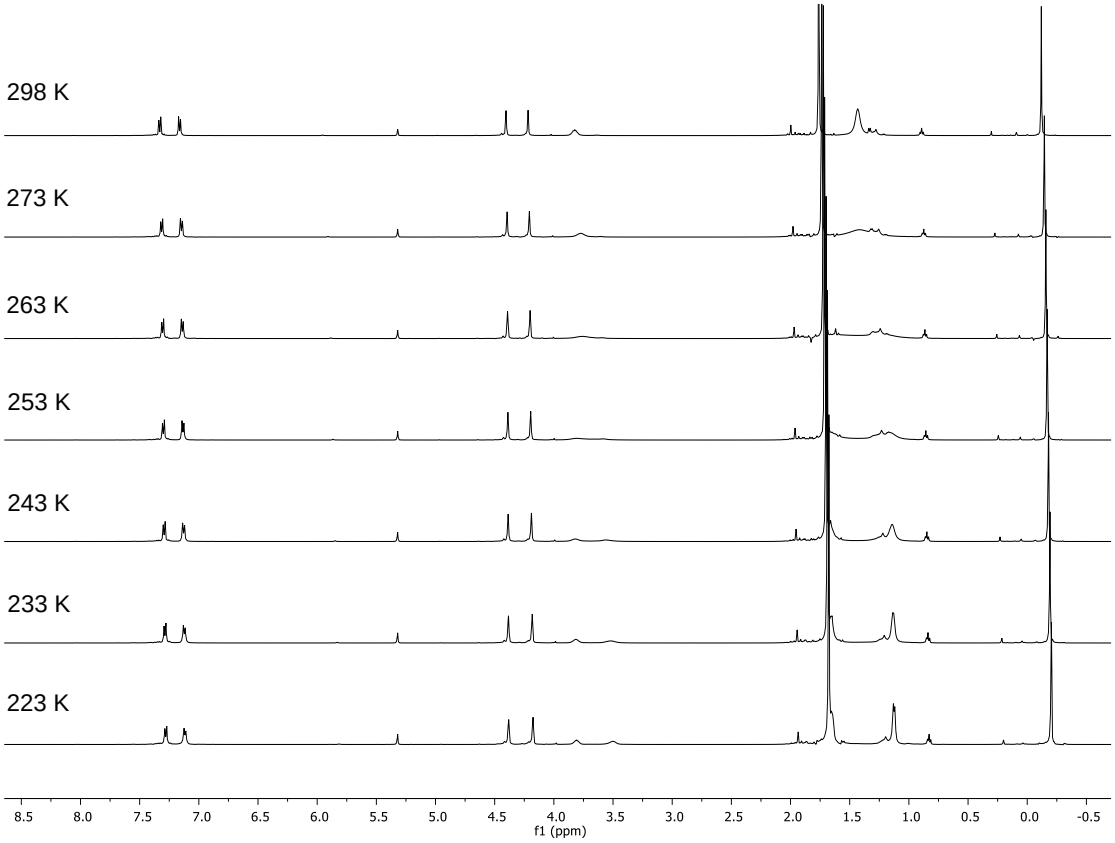

Figure 3.17 Variable temperature ^{1}H NMR (499.9 MHz, CD_2Cl_2) spectra of Fc′{NCN^{i}Pr$_2$}$_2${Cp*TiMe$_2$}$_2$ (**37**).

Diffraction-quality crystals of **37** were formed *via* slow cooling of a hot toluene solution. The molecular structures are shown in Figure 3.18 and selected bond lengths and angles of **37** are displayed in Table 3.5.

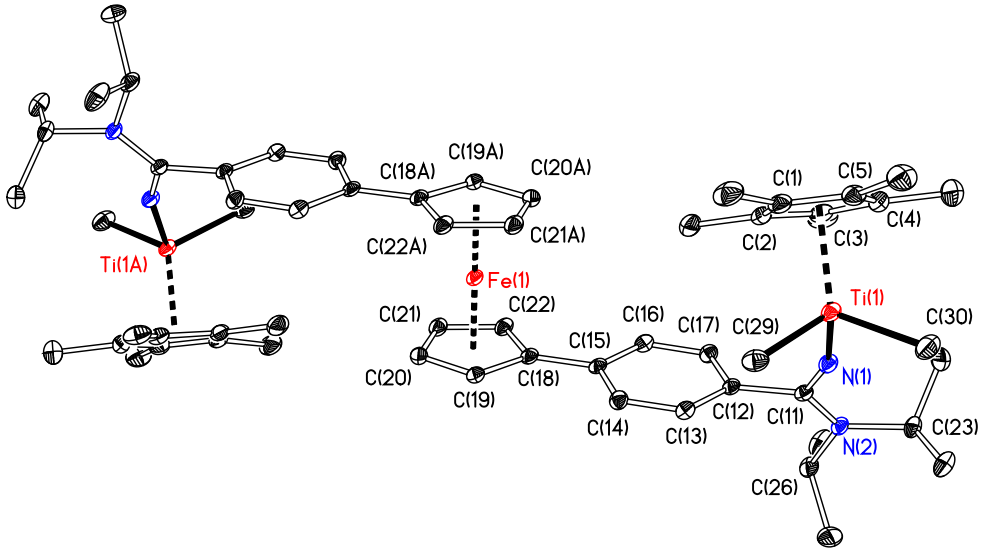

Figure 3.18 Displacement ellipsoid plot Fc′{NCN^{i}Pr$_2$}$_2${Cp*TiMe$_2$}$_2$ (**37**) (20% probability, H atoms omitted). Atoms carrying the suffix 'A' are related to their counterparts by the symmetry operator -x, 1-y, -z

Table 3.5. Selected bond lengths (Å) and angles (°) for Fc′{NCN^{i}Pr$_2$}$_2${Cp*TiMe$_2$}$_2$ (**37**). Cp$^*_{cent}$ and Cp$_{cent}$ are the computed Cp* and Cp ring carbon centroids.

Parameter		Parameter	
Ti(1)-Cp$^*_{cent}$	2.07	Cp$^*_{cent}$-Ti(1)-N(1)	119.5
Ti(1)-N(1)	1.8402(18)	Cp$^*_{cent}$-Ti(1)-Me(1)	115.2
N(1)-C(11)	1.292(3)	Cp$^*_{cent}$-Ti(1)-Me(2)	113.2
N(2)-C(11)	1.354(2)	C(11)-N(1)-Ti(1)	159.31(16)
C(11)-C(12)	1.500(3)		
Ti(1)-Me(1)	2.128(3)		
Ti(1)-Me(2)	2.145(2)		
Fe(1)- Cp$_{cent}$	1.65		

The molecular structure is in good agreement with the low temperature NMR data. The large cyclopentadienyl substituents are orientated in opposing directions, with the phenylene rings remaining planar to the cyclopentadienyl rings and therefore maintaining conjugation. The titanium centres are in a *pseudo*-tetrahedral three-legged piano stool arrangement. There are no significant deviations in bond lengths and angles between this structure and the previously discussed dimethyl molecular structures.

3.7 Cyclic Voltammetry

An electrochemical study was carried out on of HNC(Ar^{Fc})N^{i}Pr$_2$ (**9**), Cp*Ti{NC(Ar^{Fc})N^{i}Pr$_2$}Me$_2$ (**15**), Fc′{C(NH)N^{i}Pr$_2$}$_2$ (**36**) and Fc′{NCN^{i}Pr$_2$}$_2${Cp*TiMe$_2$}$_2$ (**37**) to observe how the coordination of a titanium centre influences the standard reduction potential of the ferrocenyl unit. Substituents can have a large impact on this potential; for example, [FeCp$^*_2$]$^{+/0}$ has a formal potential of -0.48 V while [Fe(η-C$_5$H$_4$COMe)$_2$]$^{+/0}$ occurs significantly higher at +0.49 V (in CH_2Cl_2 and with the ferrocenium/ferrocene couple referenced to 0.0 V).[38]

Cyclic voltammetry measurements were performed on 0.02 mmol compound in 10 mL CH_2Cl_2 solution (0.002 M) with supporting electrolyte 0.2 M ^{n}Bu$_4$NPF$_6$ and a scan rate of 100 mVs^{-1}. Full experimental procedure can be found in Chapter Six. The cyclic voltammograms are shown in Figure 3.19 and the respective potentials are given in Table 3.6. All samples were referenced relative to nickelocene, which was

selected due to the convenient relative position of the redox potential under these conditions.[39]

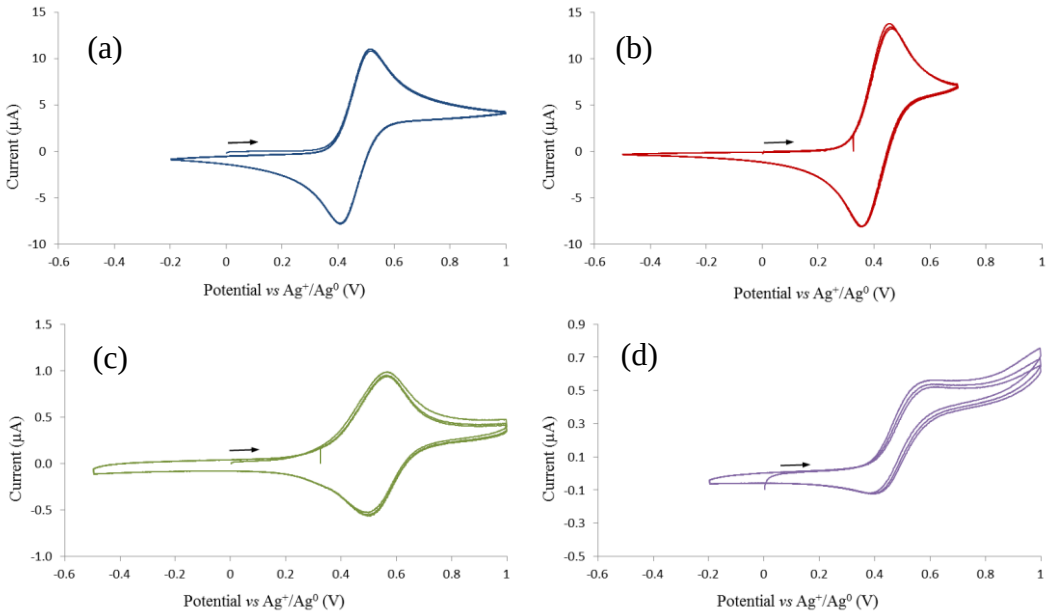

Figure 3.19 Cyclic voltammograms of HNC(Ar^{Fc})N^{i}Pr$_2$ (**9**, a), Cp*Ti{NC(Ar^{Fc})N^{i}Pr$_2$}Me$_2$ (**15**, b), Fc′{C(NH)N^{i}Pr$_2$}$_2$ (**36**, c) and Fc′{NCN^{i}Pr$_2$}$_2${Cp*TiMe$_2$}$_2$ (**37**, d). 3 complete cycles displayed and the first scan is from the rest potential at which it was initiated. The direction of the initial scan is indicated by an arrow

Table 3.6. Cyclic voltammetry data for complexes HNC(Ar^{Fc})N^{i}Pr$_2$ (**9**), Cp*Ti{NC(Ar^{Fc})N^{i}Pr$_2$}Me$_2$ (**15**), Fc′{C(NH)N^{i}Pr$_2$}$_2$ (**36**) and Fc′{NCN^{i}Pr$_2$}$_2${Cp*TiMe$_2$}$_2$ (**37**). Nickelocene used as internal standard ($E_{1/2}$ = -0.46 V *vs.* Fc^{+}/Fc in CH$_2$Cl$_2$/ ^{n}Bu$_4$NPF$_6$).[39]

Compound	E_p^A / V *vs.* Ag$^{+/0}$	E_p^C / V	ΔE / V	$E_{1/2}$ / V *vs.* Fe$^{+/0}$
9	0.58	0.44	0.14	0.01
15	0.65	0.52	0.13	0.01
36	0.72	0.56	0.16	0.01
37	0.66	0.45	0.21	0.03

As can be seen from the plots in Figure 3.19 all complexes show a reversible redox process for the ferrocenyl group. Complex **37** shows the greatest difference in current response between the three consecutive scans, but the rest remain consistent. The

oxidised product is stable on the experimental timescale, as has been confirmed by the peak current for the return potential scan being equal to that of the forward potential scan.[40] The difference in peak potentials varies between 130 to 210 mV which is more than the expected value (58 mV) for a one-electron Nernstian process.[41] This has been regularly reported in the literature and is attributed to the quasi-reversibility rate and some uncompensated solution resistance.[42-44] The difference in peak potentials for the nickelocene reference, a well-known one-electron process, also varied across a similar range.[39] According to the Randles-Sevcik equation the observed peak current (i_p) is proportional to several factors including the square root of the scan rate employed ($\nu^{1/2}$).[45, 46] All complexes were recorded at several scan rates in the range of 0.1 to 1 V and displayed a nearly consistent current factor ($i_p / \nu^{1/2}$), which is again indicative of a reversible process and shows that a constant equilibrium ratio between the oxidised and reduced form is maintained.[40]

The presence of one or two substituents, with or without a metal coordinated, has no significant impact on the redox potential of the ferrocenyl moieties. As discussed in Chapter Two, this suggests the substituents have minimal electronic impact on the ferrocenyl unit. No reduction of the titanium centres in complexes **15** and **37** were observed within the limits of the potential window for solvent (CH_2Cl_2) and electrolyte ($^nBu_4NPF_6$) system. The use of THF as the solvent medium was also attempted, but no oxidative or reductive curve was observed for complex **37**.

3.8 EPDM copolymerisation experiments using 25, 30, 33 and 37

Analogous EPDM copolymerisation experiments to those carried out in Section 2.5 were undertaken using precatalysts DBF{NCN^{i}Pr$_2$}$_2${Cp*TiMe$_2$}$_2$ (**25**), Xanth{NCN^{i}Pr$_2$}$_2${Cp*TiMe$_2$}$_2$ (**30**), Xanth(CN)({NCN^{i}Pr$_2$}{Cp*TiMe$_2$}) (**33**) and Fc′{NCN^{i}Pr$_2$}$_2${Cp*TiMe$_2$}$_2$ (**37**) at LANXESS Elastomers. The results for the active catalysts are summarised in Table 3.7. Higher dosing concentrations (0.28 μmol) were used for precatalysts **25** and **30** due to their poor activity. For these experiments the corresponding MAO and BHT concentrations were not scaled accordingly; this is to avoid high levels of metal residues preventing the analysis of the resultant polymer.

As stated above, **25** and **30** were poorly active catalysts upon MAO activation. Relative to the results observed in Chapter Two, the poor productivity is attributed to the steric congestion invoked by these ligand backbones. The polymer composition

shows low propylene and diene incorporation, which is again presumed to be a response to the more congested complex preventing the approach an binding of these more encumbered monomers. The molecular weights of the polymer produced are considerably lower, and the PDI values higher, than those observed in Chapter Two, which suggests that these systems possess a lower barrier to chain termination versus propagation rate with potentially competing termination pathways. The formation of 6-membered rings through interaction of a Group 4 metal centre with a pendant oxygen atom, and their advantages in polymerisation and oligomerisation experiments has been explored.[47-49] A previous example of the bonding interaction between the donor oxygen in the xanthene backbone and a metal centre was observed in complex **3.11**.[26] It is believed that the metal centres remain orientated away from the xanthene unit and that the oxygen, present on the ligand backbones, remains innocent to the formation of a 6-membered ring with the active metal centres, and also to other interactions with substrates present in the reactor due to the steric congestion and lack of flexibility.

Precatalyst **33** is monometallic, which somewhat relieves the steric strain imposed upon the bimetallic complexes **25** and **30**. However, the presence of the xanthene backbone is still more encumbering than the phenyl group of **2.07**. Precatalyst **33** also proved to be a poorly active relative to the other monometallic species, but showed comparable polymer compositions, molecular weights and PDI value. Complex **33** has a nitrile group in the ligand backbone, which although has been shown to not interact with the active metal centre is presumed to be non-innocent under polymerisation conditions. Several components of the polymerisation mixture could interact with this nitrile group, which would immediately increase the steric imposition around the metal centre and could also cause electrostatic implications.

Unlike the constrained systems, precatalyst **37** gave a moderately active system when compared to the bimetallic catalysts discussed in Chapter Two. The molecular structure indicates that the titanium centres are orientated in opposing directions and the electrochemical study suggests that there is limited electronic influence as a result of the ferrocenyl group. With limited steric congestion or electronic implication of a ferrocenyl group it is unclear as to why the productivity is not as active as those observed for precatalysts **3** or **6** (Table 2.3). The molecular structure of **36·HBr** showed that a freely rotating ferrocenyl group and templating effect is possible, which

would reduce the polymerisation productivity. This relative poor performance is also highlighted with other activating species in Chapter Four. The polymer composition does not deviate from that formed when using the mononuclear analogue, **15**.

Additional studies were carried out to see the effect of the [BHT] and [Al] at different ratios relative to the catalyst, as was carried out on precatalyst **2.07** in Section 2.5. Increasing both the [Al] and [BHT] by a factor of two ([Al]/[BHT] = 0.5, [Al] = 450 µmol) or having equivalent amounts of [Al] and [BHT] at either the same or increased amounts ([Al]/[BHT] = 1, [Al] = 450 or 900 µmol) resulted in minimal variation in either the productivity or resultant polymer product. This is presumably a direct result of the activating and scavenging species being in such a large excess to the active metal centre.

To probe this system further an analogous EPM copolymerisation experiment to that of Section 2.6 was carried out with precatalyst **37**. The productivity (35,830 kg mol^{-1} h^{-1} bar^{-1}) was again considerably lower than other non-constrained bimetallic catalysts and the same propylene and ethylene composition is observed to that of the monometallic species (C_2 = 47.6% ; C_3 = 52.4%). However, this system displays a notably higher molecular weight (Mn = 789 kg mol^{-1}) comparable to the monometallic precatalyst **2.07**. The reduced productivity and comparable molecular weight and composition to precatalyst **2.07** (Entry 1, Table 2.4) suggests there is both a reduction in the rate of propagation and termination. The reduction in rate of propagation could be sterically driven. The templating interaction discussed above could be prevalent and result in a cooperative stabilising interaction or polymer recapture, reducing the rate of termination.

Table 3.7. EPDM polymerisation results for DBF{NCN^{i}Pr$_2$}$_2${Cp*TiMe$_2$}$_2$ (**25**), Xanth{NCN^{i}Pr$_2$}$_2${Cp*TiMe$_2$}$_2$ (**30**), Xanth(CN)({NCN^{i}Pr$_2$}{Cp*TiMe$_2$}) (**33**) and Fc′{NCN^{i}Pr$_2$}$_2${Cp*TiMe$_2$}$_2$ (**37**).

Entry	Precatalyst	Cocatalyst	Productivity[a] (kg mol Ti^{-1} h^{-1} bar^{-1})	C_2 (wt%)	C_3 (wt%)	ENB (wt%)	VNB (wt%)	M_n (kDa)	M_w (kDa)	PDI
1	**25**	MAO	5,600	53.6	45.1	0.85	0.54	126	391	3.1
2[b]	**30**	MAO	3,704	58.1	40.9	0.68	0.37	123	391	3.2
3	**33**	MAO	5,700	48.8	49.8	0.90	0.49	178	397	2.2
4	**37**	MAO	30,690	49.2	49.1	0.98	0.68	211	480	2.3

Polymerisation conditions. T = 90 °C, Pressure: 7 bar, [Cat] = 0.1 µmol (0.28 µmol for entries 1 and 2), [Al] = 450 µmol [Al]:[BHT] = 0.5 ([b] [Al]:[BHT] = 1), 10 minute reaction time. Solvent pentamethylheptane (1 L) C_3/C_2 =400/200 Nl h^{-1}, H_2 flow: 0.35 Nl h^{-1}, ENB: 0.7 mL, VNB: 0.7 mL. [a] Productivity per mol of transition metal centres. *Polymer characterisation.* Polymer molecular weight and molecular weight distributions: the polymers have been analysed with the Freeslate Rapid GPC in 1,2,4 Trichlorobenzene against PS standards. *Average composition:* the polymers have been analysed via transmission IR spectroscopy on a pressed polymer film.

3.9 Summary

This Chapter has described the synthesis and characterisation of novel cyclopentadienyl-amidinate titanium bimetallic catalysts with conformationally constrained and ferrocenyl covalent tethers. This has included a comprehensive discussion of their structures in both the solid state and solution phase through variable temperature NMR studies and where applicable X-ray crystal structure analysis. The synthetic complications in forming the bis(protio-amidine) with a xanthene backbone allowed mono-substituted xanthene complexes to be synthesised and activation experiments with TBF_{20} were performed, which displayed no evidence of "self-trapping". Alongside the ferrocenyl complexes introduced in Chapter One, an electrochemical analysis of all ferrocene based complexes were performed and discussed.

High temperature EPDM, and in select cases EP, copolymerisation experiments were performed in collaboration with LANXESS Elastomers. Overall the xanthene and dibenzofuran catalysts were poorly performing with no evidence of a cooperative interaction. The ferrocenyl based bimetallic complex was an active catalyst and gave no evidence through comonomer incorporation as to advantageous cooperative effects, but an enhanced molecular weight may be synonymous with either a higher barrier to termination or effective polymer recapture.

3.10 References

1. M. Delferro and T. J. Marks, *Chem. Rev.*, 2011, **111**, 2450-2485.
2. M. R. Salata and T. J. Marks, *J. Am. Chem. Soc.*, 2008, **130**, 12-13.
3. M. R. Salata and T. J. Marks, *Macromolecules*, 2009, **42**, 1920-1933.
4. S. H. Lee, C. J. Wu, U. G. Joung, B. Y. Lee and J. Park, *Dalton Trans.*, 2007, 4608-4614.
5. B. J. Ireland, C. A. Wheaton and P. G. Hayes, *Organometallics*, 2010, **29**, 1079-1084.
6. A. Pintado-Alba, H. De la Riva, M. Nieuwhuyzen, D. Bautista, P. R. Raithby, H. A. Sparkes, S. J. Teat, J. M. Lopez-de-Luzuriaga and M. C. Lagunas, *Dalton Trans.*, 2004, 3459-3467.
7. E. M. Vogl, J. Bruckmann, M. Kessler, C. Kruger and M. W. Haenel, *Chem. Ber./Recl.*, 1997, **130**, 1315-1319.

8. K. Ding, D. L. Miller, V. G. Young and C. C. Lu, *Inorg. Chem.*, 2011, **50**, 2545-2552.
9. S. Kanemasa, Y. Oderaotoshi and E. Wada, *J. Am. Chem. Soc.*, 1999, **121**, 8675-8676.
10. U. Iserloh, D. P. Curran and S. Kanemasa, *Tetrahedron: Asymmetry*, 1999, **10**, 2417-2428.
11. M. Hasegawa, F. Ono and S. Kanemasa, *Tetrahedron Lett.*, 2008, **49**, 5220-5223.
12. M. Gomez, S. Jansat, G. Muller, M. A. Maestro and J. Mahia, *Organometallics*, 2002, **21**, 1077-1087.
13. Y. N. Belokon, S. C. Gagieva, T. A. Sukhova, A. B. Dmitriev, K. A. Lyssenko, N. M. Bravaya, B. M. Bulychev and D. Seebach, *Russ. Chem. Bull.*, 2005, **54**, 2348-2353.
14. J. R. Hagadorn, *US20090259085A1*, 2009.
15. M. J. McNevin and J. R. Hagadorn, *Inorg. Chem.*, 2004, **43**, 8547-8554.
16. J. R. Hagadorn, *Chem. Commun.*, 2001, **20**, 2144-2145.
17. K. Y. Tsang, H. Diaz, N. Graciani and J. W. Kelly, *J. Am. Chem. Soc.*, 1994, **116**, 3988-4005.
18. K. McWilliams and J. W. Kelly, *J. Org. Chem.*, 1996, **61**, 7408-7414.
19. G. Besenyei, I. Bitter, L. Párkányi, G. Szalontai, P. Baranyai, É. Kunsági-Máté, F. Faigl, A. Grün and M. Kubinyi, *Polyhedron*, 2013, **55**, 57-66.
20. A. Kivrak and M. Zora, *J. Organomet. Chem.*, 2007, **692**, 2346-2349.
21. P. Vitale, L. Di Nunno and A. Scilimati, *Tetrahedron*, 2011, **67**, 6944-6952.
22. G. H. J. Van Doremaele, M. A. Zuideveld, V. F. Quiroga Norambuena and A. Leblanc, *WO2011054927A1*, 2011.
23. A. Heath, DPhil Thesis, University of Oxford, 2011.
24. A. B. Charette and M. Grenon, *Tetrahedron Lett.*, 2000, **41**, 1677-1680.
25. J. Clayden, A. Lund, L. Vallverdu and M. Helliwell, *Nature*, 2004, **431**, 966-971.
26. R. M. Porter and A. A. Danopoulos, *Polyhedron*, 2006, **25**, 859-863.
27. J. R. Hagadorn and M. J. McNevin, *Organometallics*, 2003, **22**, 609-611.
28. J. R. Hagadorn, M. J. McNevin, G. Wiedenfeld and R. Shoemaker, *Organometallics*, 2003, **22**, 4818-4824.

29. P. D. Bolton, M. Feliz, A. R. Cowley, E. Clot and P. Mountford, *Organometallics*, 2008, **27**, 6096-6110.
30. Y. W. Alelyunas, R. F. Jordan, S. F. Echols, S. L. Borkowsky and P. K. Bradley, *Organometallics*, 1991, **10**, 1406-1416.
31. M. Bochmann, L. M. Wilson, M. B. Hursthouse and M. Motevalli, *Organometallics*, 1988, **7**, 1148-1154.
32. A. F. Russell, DPhil Thesis, University of Oxford, 2014.
33. R. Knapp and M. Rehahn, *J. Organomet. Chem.*, 1993, **452**, 235-240.
34. P. A. Deck, M. J. Lane, J. L. Montgomery, C. Slebodnick and F. R. Fronczek, *Organometallics*, 2000, **19**, 1013-1024.
35. G. G. A. Balavoine, G. Doisneau and T. Fillebeen-Khan, *J. Organomet. Chem.*, 1991, **412**, 381-382.
36. S. Altmannshofer, E. Herdtweck, F. H. Köhler, R. Miller, R. Mölle, E.-W. Scheidt, W. Scherer and C. Train, *Chem. Eur. J.*, 2008, **14**, 8013-8024.
37. F. Strehler, A. Hildebrandt, M. Korb, T. Rueffer and H. Lang, *Organometallics*, 2014, **33**, 4279-4289.
38. N. G. Connelly and W. E. Geiger, *Chem. Rev.*, 1996, **96**, 877-910.
39. D. Chong, J. Slote and W. E. Geiger, *J. Electroanal. Chem.*, 2009, **630**, 28-34.
40. R. G. Compton and C. E. Banks, Understanding Voltammetry, Imperial College Press, 2011.
41. R. S. Nicholson and I. Shain, *Anal. Chem.*, 1964, **36**, 706-723.
42. R. R. Gagne, C. A. Koval and G. C. Lisensky, *Inorg. Chem.*, 1980, **19**, 2854-2855.
43. J. G. Gaudiello, T. C. Wright, R. A. Jones and A. J. Bard, *J. Am. Chem. Soc.*, 1985, **107**, 888-897.
44. M. M. Ghoneim and I. S. El-Hallag, *J. Braz. Chem. Soc.*, 2010, **21**, 7-15.
45. J. E. B. Randles, *Trans. Faraday Soc.*, 1948, **44**, 327-338.
46. A. Sevcik, *Collect. Czech. Chem. Commun.*, 1948, **13**, 349-377.
47. Y. Suzuki, S. Kinoshita, A. Shibahara, S. Ishii, K. Kawamura, Y. Inoue and T. Fujita, *Organometallics*, 2010, **29**, 2394-2396.
48. I. E. Soshnikov, N. V. Semikolenova, J. Ma, K.-Q. Zhao, V. A. Zakharov, K. P. Bryliakov, C. Redshaw and E. P. Talsi, *Organometallics*, 2014, **33**, 1431-1439.

49. A. Sattler, D. G. VanderVelde, J. A. Labinger and J. E. Bercaw, *J. Am. Chem. Soc.*, 2014, **136**, 10790-10800.

Chapter Four

Synthesis, reactivity and polymerisation capabilities of dinuclear cocatalysts

4.1 Overview

The cocatalyst used for the activation of neutral Group 4 dialkyl complexes in olefin polymerisation can have a substantial effect on both the productivity and the properties of the resultant polymer. This Chapter explores the background and synthesis of two different binuclear cocatalysts and their performance in a high temperature EPDM copolymerisation study.

The cationic species will be investigated through abstraction reactions with dimethyl monometallic and bimetallic complexes previously introduced in this Thesis. The Chapter will conclude with an NMR spectroscopic investigation into the intermolecular interaction between activated complexes.

4.2 Introduction to binuclear bis(borane) and bis(borate) cocatalysts

In the polymerisation studies carried out in the previous chapters a large excess of methyl aluminium oxides (MAO) was used as the activating species. This is exceptionally effective at both activating and, with the introduction of BHT, protecting the catalytic species from impurities. Aluminoxane-based activators are still used in the majority of commercial applications.[1] The use of stoichiometric amounts of a strong Lewis acid, such as tris(pentafluorophenyl)borane (BF_{15}), or an alkyl abstraction agent, such as a trityl $[CPh_3]^+$ or ammonium $[PhNHMe_2]^+$ cation, can be employed and have been extensively studied with Group 4 metals in generating the catalytically active species. Advantages over the aluminoxane-based activators were introduced in Chapter One and their utility in investigating the form of the catalytic species is apparent in Chapter Two.

The use of BF_{15} generates an alkyl adduct to the borane, $[RBF_{15}]^-$, and frequently remains partially coordinated. Trityl or ammonium alkyl abstraction agents have been used in conjunction with a variety of anions which remain associated with the catalytic centre upon activation.[2] It is well established that the catalyst will remain as a contact ion-pair and that chain propagation, stereodefect production, chain termination, and catalyst deactivation are all anion-dependent.[3] Concerning these points the anion must be sufficiently labile to be displaced by an unsaturated olefinic monomer and must positively influence the catalytic performance and properties of the resultant polymer. Highly functionalised weakly coordinating borate-, aluminate- and gallate- anions have all been employed in olefin polymerisation studies, with the

most sterically encumbered and charge-dispersed varieties proving to be the most effective under relevant polymerisation conditions.[4-6]

4.2.1 Introduction to the bis(borate) activator, [{B(C$_6$F$_5$)$_3$}$_2$(μ-C$_6$F$_4$)][Ph$_3$C]$_2$ (4.01)

The tetrakis(pentafluorophenyl)borate ([BF$_{20}$]$^-$) anion, introduced in Chapter One, was found to be particularly effective as a thermally stable and non-coordinating species. Its use in a high-temperature EPDM copolymerisation study with the previously introduced precatalysts will be discussed in Section 4.5.1.

The analogous bis(borate) anion, [{B(C$_6$F$_5$)$_3$}$_2$(μ-C$_6$F$_4$)][Ph$_3$C]$_2$ (**4.01**), was first introduced in 1998 in a patent for the heterogeneous polymerisation of olefins[7] and was first reported in a journal article in 2002 by Marks and co-workers, with a rational synthesis that will be discussed in Section 4.3.[8] Marks *et al.* used the cocatalyst **4.01** in polymerisation studies with the assumption that by either bringing two monometallic active centres spatially proximate to one another or by mutually orientating a bimetallic catalyst the dianionic cocatalyst would increase the nuclearity of the catalytic species.[8] This electrostatically induced enhanced nuclearity was studied for beneficial cooperative effects.

The cocatalyst has been employed with both monometallic and bimetallic zirconium CGCs (**1.49 - 1.51**) and their titanium analogues in ethylene and styrene homo- and copolymerisation studies with hexene, pentene or octene as the α-olefin investigated.[8-11] In many cases this cocatalyst has been shown to have a profound effect on the properties of the resultant polymer.[12] For example, when cocatalyst **4.01** is used in conjunction with the mononuclear precatalyst **1.49-Me** the ethylene polymerisation activity is suppressed in comparison to that when activated with TBF$_{20}$ (93 *vs.* 127 kg mol^{-1} h^{-1} bar^{-1}) and the molecular weight remains approximately consistent (630 *vs.* 610 g mol^{-1}), but the number of ethyl branches increases (6.5 *vs* 1.1 units per 1000 C). This is amplified when the dinuclear cocatalyst is used in conjunction with the bimetallic precatalyst **1.51-Me**. In comparison to activation with TBF$_{20}$ the activity is further reduced (63 *vs* 87 kg mol^{-1} h^{-1} bar^{-1}), but the molecular weight (1100 *vs* 760 g mol^{-1}) and number of ethyl branches (12 *vs* 2.7 units per 1000 C) increase.[8] The number of ethyl branches is indicative of the amount of macromonomer reinsertion, as discussed in Chapter One. The same catalytic systems observe an increase in butyl

branches in ethylene/1-hexene copolymerisation studies, which is representative of an increase comonomer incorporation, as discussed in Chapter Two.[8]

All of these polymerisation studies were carried out in a low dielectric constant solvent, such as toluene, and when a polar solvent (C_6H_5Cl) is used then the variations in polymerisation experiments are diminished. This is presumably through a reduction of the catalyst-cocatalyst ion pairing and indicates the significance of the catalytic nuclearity induced by the cocatalyst.[11]

An important example of electrostatic spatial confinement induced by **4.01** was displayed in a heterobimetallic olefin enchainment process for the synthesis of LLDPE. Monometallic titanium and zirconium constrained geometry catalysts, $Me_2Si(^tBuN)(\eta^5$-3-ethylindenyl)-$ZrMe_2$ (**1.49-Me**) and $Me_2Si(^tBuN)(\eta^5$-$C_5Me_4)TiMe_2$ (**4.02**), were used in the same reaction feed. Complex **4.02** is very active and generates high-molecular weight polymers in the homopolymerisation of ethylene, whereas **1.49-Me** is less active and produces vinyl-terminated ethylene oligomers under the same conditions. When introduced in an appropriate ratio, according to their activity, a bimodal distribution is observed in the GPC chromatogram upon activation with a mononuclear cocatalyst, indicative of two distinct active sites. However, upon activation with **4.01** a monomodal GPC chromatogram is observed and a subsequent change in the properties of the polymer produced (Figure 4.1). This is a direct result of a binuclear cooperativity brought upon by the metal site proximity, which is electrostatically dictated by the anion used.[13]

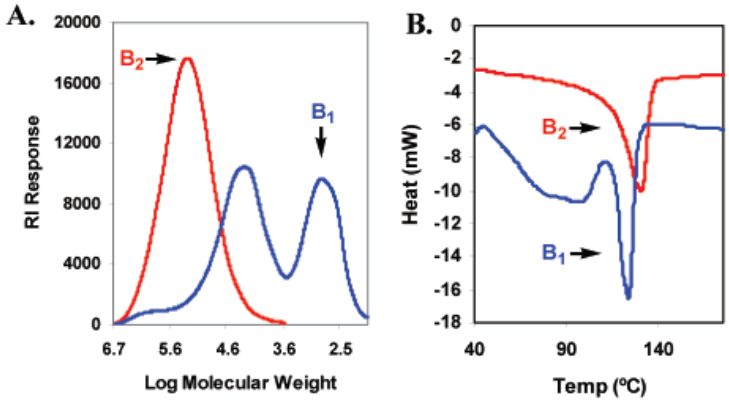

Figure 4.1 GPC (A) and DSC (B) data for ethylene polymerisation with **1.49-Me** and **4.02** (20:1) and with activators "B_1" (TBF_{20}, blue) and "B_2" (**4.01**, red).[13]

Marks *et al*. have reported that on an NMR tube scale reaction **4.01** can rapidly activate the constrained geometry monometallic complexes introduced in Chapter

One (**1.49** and **1.51**). It was reported that a quantitative amount of Ph_3CMe is produced, but that the catalytic species are unstable at room temperature in the absence of ethylene.[8] There have been no examples of isolated activation products using this abstraction agent and corresponding bis(borate) anion.

Aside from the work previously mentioned, the use of **4.01** remains relatively unexplored. The only other reported occurrences are in a patent by LG chemicals[14] and in a study alongside a range of weakly coordinating anions probing their interaction when paired with an iodonium cation.[15]

4.2.2 Introduction to the bis(borane) activator, $\{B(C_6F_5)_2\}_2(\mu\text{-}C_6F_4)$ (4.03)

Lewis acidic species can also be used as cocatalysts in olefin polymerisation, with the most commonly employed being BF_{15}. The binuclear bis(borane) analogue, $\{B(C_6F_5)_2\}_2(\mu\text{-}C_6F_4)$ (**4.03**), was first introduced in several patents at the end of the 20th century[7, 16, 17] and was again reported by Marks and co-workers in a journal article in 2003.[9]

The initial study used **4.03** in conjunction with monometallic and bimetallic titanium CGCs (**2.15** and **2.16)** in the copolymerisation of ethylene and isobutene. The isobutene incorporated increased five-fold when using **2.16** activated with **4.03** in comparison to the mononuclear analogues (**2.15** with BF_{15}), however a decline in molecular weight was found with this binuclear activating species (168 x 10^3 *vs* 577 x 10^3 g mol^{-1}, respectively, for the above combinations).[9] Marks *et al.* later went on to show that using **4.03** as a cocatalyst with a bimetallic catalyst can incorporate large percentages of severely encumbered isoalkenes in comparison to their mononuclear analogues.[18] The isoalkenes investigated include methylenecyclopentane and methyleneclyclohexane, which incorporate in a ring unopened fashion. This gives the polymer unique properties as the unopened rings limit the amount of entanglements by frustrating the ability to coil.[18]

There is only one example of an isolated abstraction product from the reaction of **4.03** with a metal alkyl complex. The reaction of 2 equiv. of Cp_2ZrMe_2 with **4.03** afforded the bimetallic species $[(C_5H_5)_2ZrMe]_2[\{(C_6F_5)_2BMe)_2(\mu\text{-}C_6F_4)]$, which was structurally authenticated (Figure 4.2).[18]

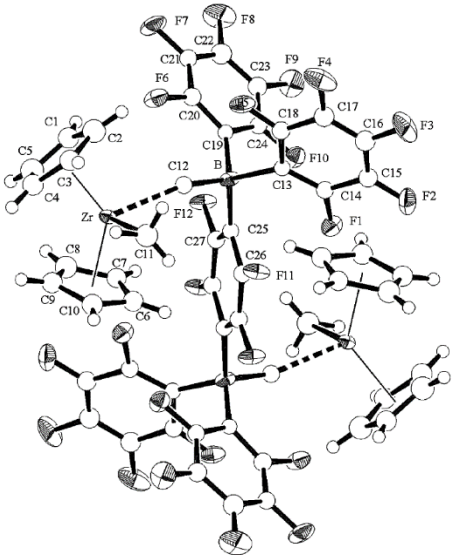

Figure 4.2 Displacement ellipsoid plot of $[(C_5H_5)_2ZrMe]_2[\{(C_6F_5)_2BMe)_2(\mu\text{-}C_6F_4)]$.[18]

Reprinted (adapted) with permission from H. Li, L. Li, D. J. Schwartz, M. V. Metz, T. J. Marks, L. Liable-Sands and A. L. Rheingold, *J. Am. Chem. Soc.*, 2005, **127**, 14756-14768. Copyright 2005 American Chemical Society.

Outside of research into polyolefins, the only other use of **4.03** has been shown in conjunction with sterically encumbered phosphines. The steric congestion prevents generation of a conventional Lewis acid-base adduct and instead a reactive "frustrated Lewis pair" (FLP) is formed, which has been shown to activate dihydrogen and react with nitrous oxide.[19-21] There are no other examples which use **4.03** as a strong Lewis acid. The use of **4.03** in reactions with previously isolated precatalysts will be discussed in Section 4.4.

4.3 Synthesis and reactivity of $[\{B(C_6F_5)_3\}_2(\mu\text{-}C_6F_4)][Ph_3C]_2$ (4.01)

$[\{B(C_6F_5)_3\}_2(\mu\text{-}C_6F_4)][Ph_3C]_2$ (**4.01**) was prepared according to literature procedures (Scheme 4.1). The final product was isolated as a bright red solid whose NMR spectroscopic data, mass ion and elemental analysis were all consistent with those reported in the literature.[8] The ^{19}F NMR spectrum shows a complex series of multiplets, presumably as a result of the steric constraints imposed around the boron centre with the fluorine substituents occupying different chemical environments. Compound **4.01** is sparingly soluble in many conventional organic solvents, namely hexane, benzene and bromobenzene.

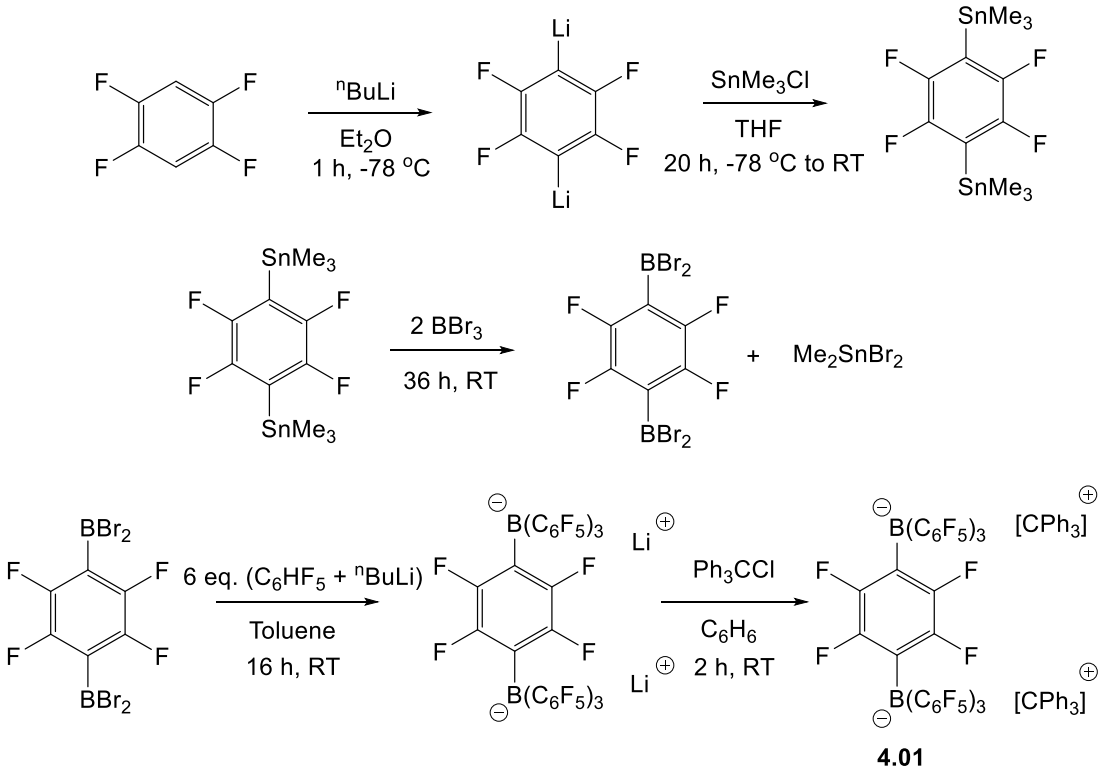

Scheme 4.1 Synthesis of [{B(C$_6$F$_5$)$_3$}$_2$(μ-C$_6$F$_4$)][Ph$_3$C]$_2$ (**4.01**).

In preliminary studies an NMR tube scale reaction between **4.01** and either 1 or 2 equiv. of Cp*Ti{NC(Ph)N^{i}Pr$_2$}Me$_2$ (**2.07**) in C$_6$D$_5$Br resulted in an immediate colour change and formation of a dark oil. An NMR tube scale reaction was subsequently performed using 2 equiv. of **2.07** with **4.01** in the presence of 2 equiv. of *N*,*N*′-diisopropylcarbodiimide. The insertion product, [Cp*Ti{NC(N^{i}Pr$_2$)Ph}{MeC(N^{i}Pr)$_2$}]$_2$[{B(C$_6$F$_5$)$_3$}$_2$(μ-C$_6$F$_4$)] (**38**), formed quantitatively and the NMR spectra were recorded after 5 minutes (Equation 4.1).

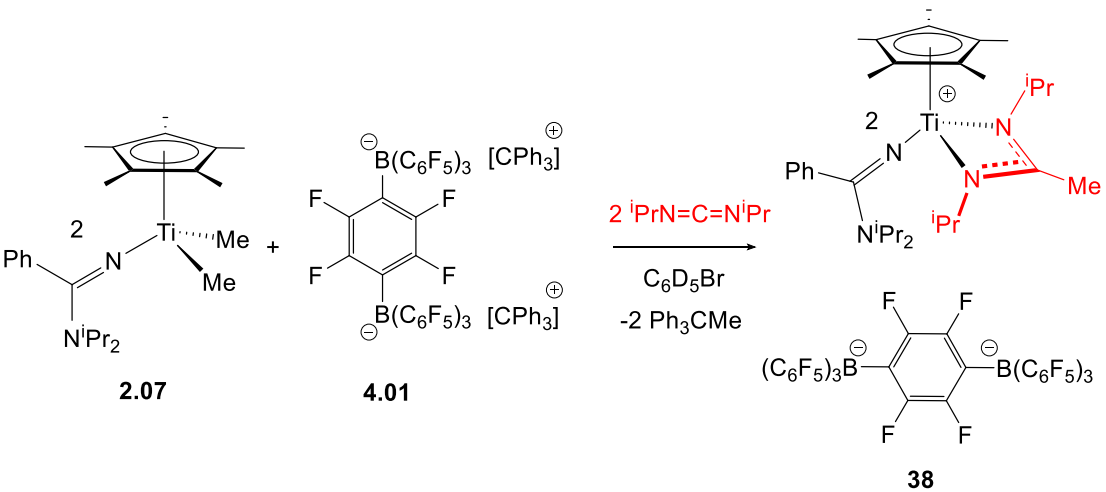

Equation 4.1

A quantitative stoichiometric amount of Ph_3CMe was formed, observed by the distinctive methyl resonance in the ^1H NMR spectrum, suggesting complete abstraction. The product of abstraction with the mononuclear abstraction agent TBF_{20}, namely $[Cp^*Ti\{NC(N^iPr_2)Ph\}\{MeC(N^iPr)_2\}][BF_{20}]$ (**4.04**), has previously been isolated within the Mountford group, and the resonances that correspond to the cation are almost identical to those observed in the room temperature ^1H NMR spectrum of **38**.[22] The key features of this spectrum are the Cp^* signal at 2.02 ppm, the $\underline{Me}C(N^iPr)_2$ signal at 2.20 ppm, the κ^2-$NC\underline{H}Me_2$ signal at 3.59 ppm and the κ^2-$NCH\underline{Me}_2$ resonances at 1.10 and 0.75 ppm. This type of migratory insertion product was discussed in Chapter One. The resonances corresponding to the anion in the ^{19}F NMR spectra remained as a complicated series of multiplets.

4.4 Synthesis and reactivity of $\{B(C_6F_5)_2\}_2(\mu\text{-}C_6F_4)$ (4.03)

$\{B(C_6F_5)_2\}_2(\mu\text{-}C_6F_4)$ (**4.03**) was prepared according to a modified literature procedure (Scheme 4.2).[18] The preparation of $BCl(C_6F_5)_2$ has been reported by both Chivers[23] and Piers.[24] $SnMe_2(C_6F_5)_2$ (**4.05**) was prepared from a reaction of Me_2SnCl_2 and the *in situ* generated LiC_6F_5. A subsequent reaction with boron trichloride in a thick-walled glass bomb produced the desired product.[24] In 2003 it was reported that diarylchloroboranes can be prepared using a heptane solution at 100 °C.[25] This method was employed in this Thesis for simplicity and safety in the synthesis of $BCl(C_6F_5)_2$ (**4.06**). This procedure does not exceed the boiling point of the solvent, removing the need for a high-pressure vessel, and BCl_3 can be purchased as a 1M heptane solution. Purification was achieved *via* a similar method to that reported, and upon completion the reaction was slowly cooled to room temperature affording crystals corresponding to the Me_2SnCl_2, which could be recovered and reused. Removal of the volatiles under reduced pressure resulted in a poor product yield, as **4.06** underwent sublimation under the conditions required to remove the volatiles. Instead, storage of the mixture at -80 °C for 24 h resulted in the product as a white micro-crystalline solid; removal of any residual Me_2SnCl_2 could be achieved by sublimation on to a cold (-78 °C) finger under 1.1 atm. of argon pressure at 35 °C. Using this procedure, **4.06** was achieved in an 80% yield, higher than previously reported, and could be carried out on a multi-gram scale. The NMR spectroscopic data were in good agreement with the literature. Marks and co-workers reported the synthesis of **4.03** by the onward reaction of an excess of **4.06** with 1,4-$C_6F_4(SnMe_3)_2$

in toluene for 72 h. Here 2 equiv. of **4.06** react to give 1,4-$C_6F_4(SnMe_2Cl)_2$, which can then react with an additional equivalent of **4.06** to afford **4.03**.

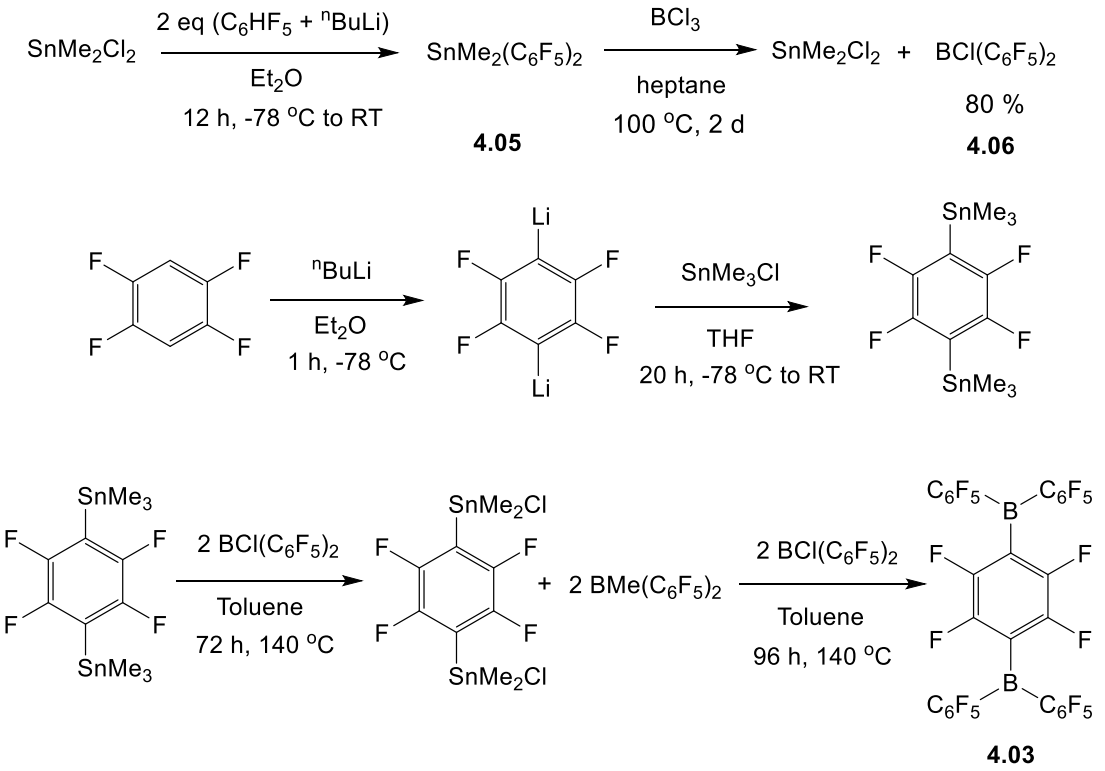

Scheme 4.2 Synthesis of $\{B(C_6F_5)_2\}_2(\mu\text{-}C_6F_4)$ (**4.03**).

An NMR tube scale reaction of **4.03** with 2 equiv. of $Cp^*Ti\{NC(Ph)N^iPr_2\}Me_2$ (**2.07**) in C_6D_5Br resulted in an immediate colour change and quantitative formation of a dark oil before any data could be recorded. However, an NMR tube scale reaction of **4.03** with 1 equiv. of **2.07** in C_6D_6 resulted in a red/brown solution that showed no immediate sign of oil formation. ^1H, ^{19}F and ^{11}B NMR spectroscopy (298 K, C_6D_6) revealed the formation of the mono-substituted bis(borane) product, $[Cp^*Ti\{NC(N^iPr_2)Ph\}Me][\{B(C_6F_5)_2\}(\mu\text{-}C_6F_4)\{BMe(C_6F_5)_2\}]$ (**39**) (Equation 4.2).

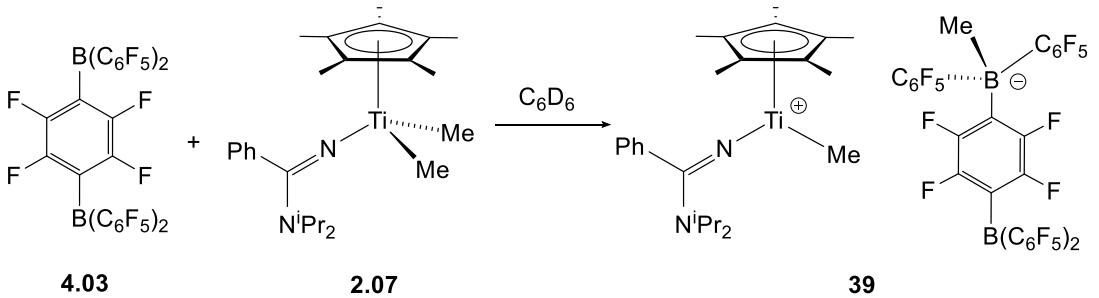

Equation 4.2

The key features of the ^{1}H NMR spectrum (Figure 4.3) are the Cp* signal at 1.55 ppm, TiMe signal at 1.34 ppm and the broad TiMeB signal at 0.78 ppm. The two distinct titanium methyl environments are characteristic of an abstracted bridging methyl and one remaining bound to the now cationic titanium centre. This was observed in the abstraction reactions carried out using the mononuclear BF_{15} in Section 2.8. The ^{11}B NMR spectra gave good evidence as to the formation of **39**, a broad resonance at 72.0 ppm and a sharp resonance at -12.8 ppm indicate the presence of a neutral tri-coordinate borane and anionic tetra-coordinate borate environment corresponding to the unsubstituted and substituted end. In an experiment compensating for the broad background resonance, arising from the glassware used, the peaks were able to be quantitatively integrated and were found in the expected 1:1 ratio. The ^{19}F NMR spectra proved to be very complex as the symmetry was lost and resonances corresponding to several environments observed. A two dimensional ^{19}F-^{19}F COSY experiment identified the resonances at -130.90 and -131.31 ppm correspond to the *ortho* fluorine atoms on the μ-C_6F_4 linkage. After approximately 1 h the ^{1}H NMR spectra became complicated and a precipitate was observed, which prevented additional analysis.

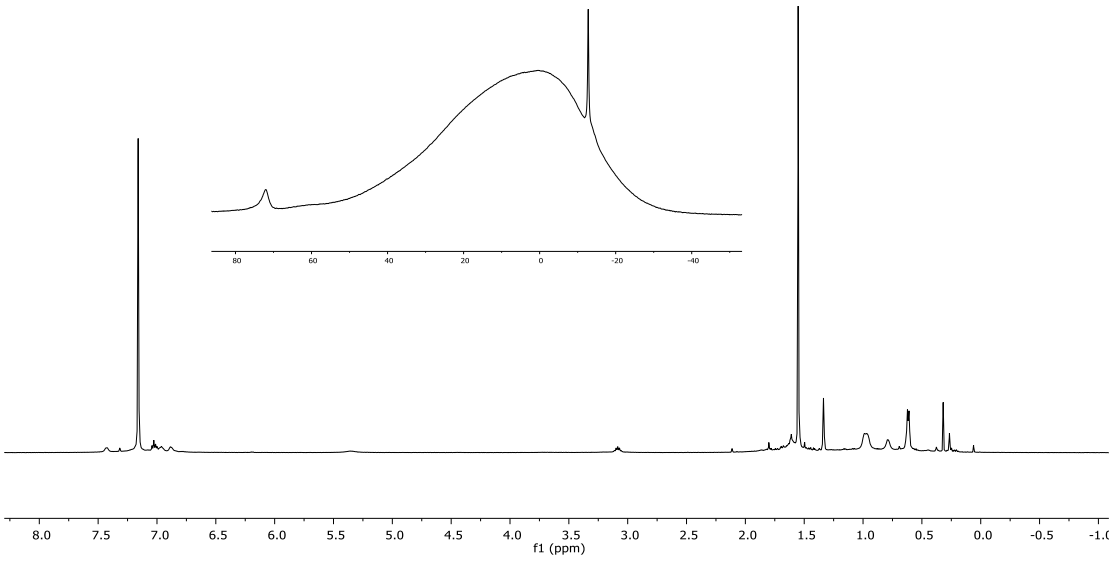

Figure 4.3 ^{1}H and ^{11}B (insert) NMR (499.9 MHz, C_6D_6, 298 K) spectra of [Cp*Ti{NC(N^{i}Pr$_2$)Ph] [{B(C_6F_5)$_2$}(μ-C_6F_4){BMe(C_6F_5)$_2$}] (**39**).

Attempts to form either an insertion or base-stabilised product of the above reaction using stoichiometric amounts of *N,N′*-diisopropylcarbodiimide or THF in C_6D_5Br resulted in what was presumed to be the desired products, but with additional unidentified side-products.

Reaction of **4.03** with 2 equiv. of $Cp^*Ti\{NC(Ph)N^iPr_2\}Me_2$ (**2.07**) in neat THF quantitatively gave the pure product, $[Cp^*Ti\{NC(N^iPr_2)Ph\}Me(THF)]_2[\{(C_6F_5)_2BMe)_2(\mu\text{-}C_6F_4)]$ (**40**), in an NMR tube scale reaction. As was discussed in Chapter Two, cationic complexes of this form can ring-open THF. This was shown to occur after a few hours after almost instantaneous product formation. Complex **40** was isolated on a preparative scale in 55% yield by limiting the reaction time to 15 minutes in THF (Equation 4.3). After the allotted time period a large excess of hexane was added resulting in the formation of an oil, which was isolated and dried *in vacuo* to yield the product as a brown solid.

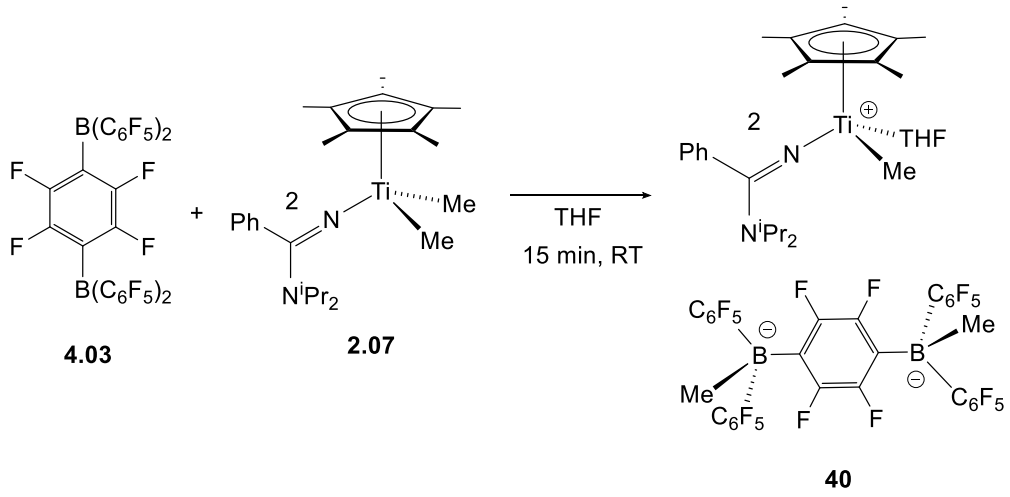

4.03 **2.07** **40**

Equation 4.3

The ^1H NMR spectrum (298 K, C_6D_5Br) shows comparable resonances to the previously reported mononuclear analogue, $[Cp^*Ti\{NC(N^iPr_2)Ph\}Me(THF)][MeBF_{15}]$ (**4.07**).[22] The insertion product $[Cp^*Ti\{NC(N^iPr_2)Ph\}\{MeC(N^iPr)_2\}]_2[\{(C_6F_5)_2BMe)_2(\mu\text{-}C_6F_4)]$ (**41**) was formed in a NMR tube scale reaction by the addition of 2 equiv. of *N,N′*-diisopropylcarbodiimide to **40** in C_6D_5Br, liberating THF (Equation 4.4). Previous work within the Mountford group has shown that the *N,N′*-diisopropylcarbodiimide can displace a THF or pyridine adduct to a κ^1-amidinate supported titanium cation, but cannot displace the very basic $OPPh_3$.[22] The ^1H NMR (298 K, C_6D_5Br) spectrum displays the same resonances as that of **38**, but with an additional broad signal at 1.34 ppm

corresponding to the abstracted methyl group. Identical resonances characteristic of the diborate were displayed in the ^{19}F and ^{11}B NMR spectra for both **40** and **41**, and will be discussed below.

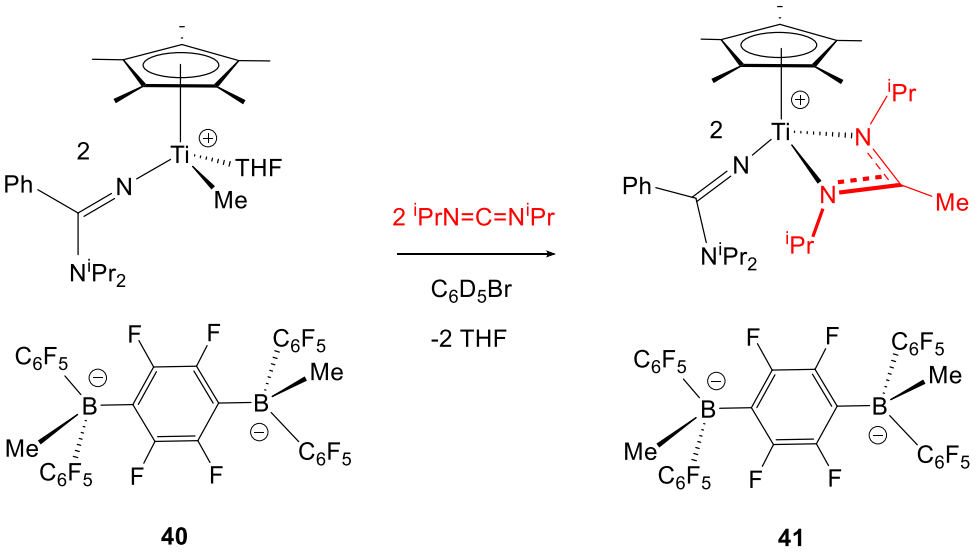

40 **41**

Equation 4.4

An NMR tube scale reaction of **4.03** with 1 equiv. of Cp*Ti{NC(Ph)N^{i}Pr$_2$}Me$_2$ (**2.07**) in THF-d_8 did not form the expected mono-substituted anion product, but instead gave equal amounts of the dianionic methyl substituted diborate and neutral diborane products. The neutral diborane product formed with a THF adduct on both boron centres, {(C$_6$F$_5$)$_2$B(THF)}$_2$(μ-C$_6$F$_4$) (**42**), which was independently synthesised on a preparative scale by addition of THF to **4.03** and was fully characterised by NMR and IR spectroscopy, EI mass spectrometry and elemental analysis.

The ^{11}B NMR shifted significantly downfield to 4.9 ppm upon formation of this adduct and the dianionic diborate compound shows a sharp signal at -14.2 in the ^{11}B NMR spectrum of **40**. The ^{19}F NMR spectra are diagnostic for the symmetric diborane or diborate compounds with the two resonances for the *ortho*-fluorine environments and one signal each for the *meta*- and *para*-fluorine substituents. Figure 4.4 shows the ^{19}F NMR spectrum for **42** (a) and **40** (c), the central spectrum is the result with 1 equiv. of **2.07** and clearly indicates that the mono-substituted mono anion does not form. This is believed to be a result of the enhanced Lewis-acidity of the borane in the mono-substituted product, brought upon by a neighbouring anionic borate, preferentially abstracting a methyl group instead of the neutral diborane. It is

important to note that **40** can also be produced by the reaction of **42** with 2 equiv. of **2.07** in fluorobenzene, circumventing the need to use THF as the solvent.

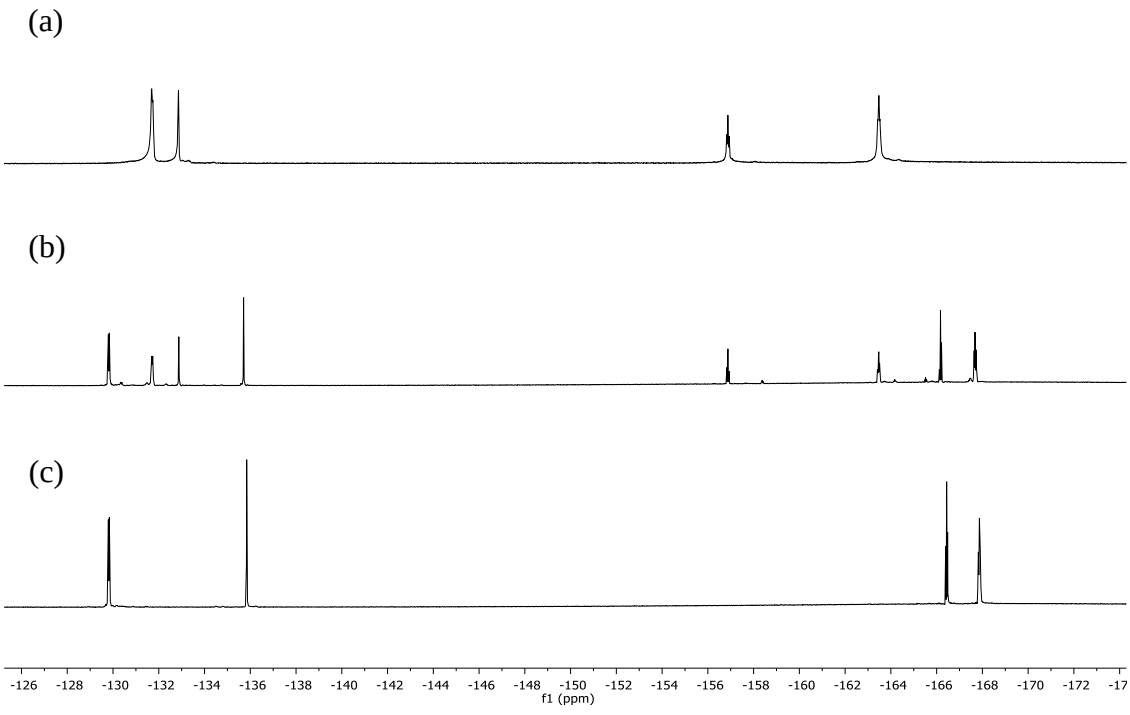

Figure 4.4 ^{19}F NMR (470.4 MHz, THF-d_8, 298 K) spectra of $\{(C_6F_5)_2B(THF)\}_2(\mu\text{-}C_6F_4)$ (**42**, a), **4.03** + 1 equiv. **2.07** (b) and $[Cp^*Ti\{NC(N^iPr_2)Ph\}Me(THF)]_2[\{(C_6F_5)_2BMe\}_2(\mu\text{-}C_6F_4)]$ (**40**, c).

The ^{19}F NMR spectrum (298 K, C_6D_5Br) for **40** includes a doublet at -131.1 ppm for *o*-$C_6\underline{F}_5$, a singlet resonance at -138.0 ppm for μ-$C_6\underline{F}_4$, a triplet resonance at -164.5 ppm for *p*-$C_6\underline{F}_5$ and a multiplet resonance at -166.7 for *m*-$C_6\underline{F}_5$. This assignment is confirmed by the integration, coupling pattern and a 2D ^{19}F-^{19}F COSY experiment. As can be seen in Figure 4.4, formation of the dianionic diborate results in an upfield shift for the μ-$C_6\underline{F}_4$ and a downfield shift for the *o*-$C_6\underline{F}_5$ in comparison to the analogous neutral diborane, with the *meta*- and *para*- shifts following the same upfield shift as observed for the BF_{15} activated product. The difference between the μ-$C_6\underline{F}_4$ and *o*-$C_6\underline{F}_5$ chemical shifts indicate that a large amount of the increased electron density resides on the bridging aromatic group in the dianionic compound. The same trend was observed for $[(C_5H_5)_2ZrMe]_2[\{(C_6F_5)_2BMe\}_2(\mu\text{-}C_6F_4)]$ (Figure 4.2).[18]

1,4-$C_6H_4\{NCN^iPr_2\}_2\{Cp^*TiMe_2\}_2$ (**3**) and **4.03** are both poorly soluble in C_6D_5Br and although a colour change is observed upon addition a large amount of precipitate persists. A reaction stirred in THF resulted in all the solid reacting after a few minutes and a red solution remaining. Addition of an excess of hexanes after 15 minutes generated the desired product, [1,4-$C_6H_4\{NCN^iPr_2\}_2\{Cp^*TiMe(THF)\}_2$] [$\{(C_6F_5)_2BMe\}_2(\mu\text{-}C_6F_4)$] (**43**), as a red precipitate in 68% yield (Equation 4.5).

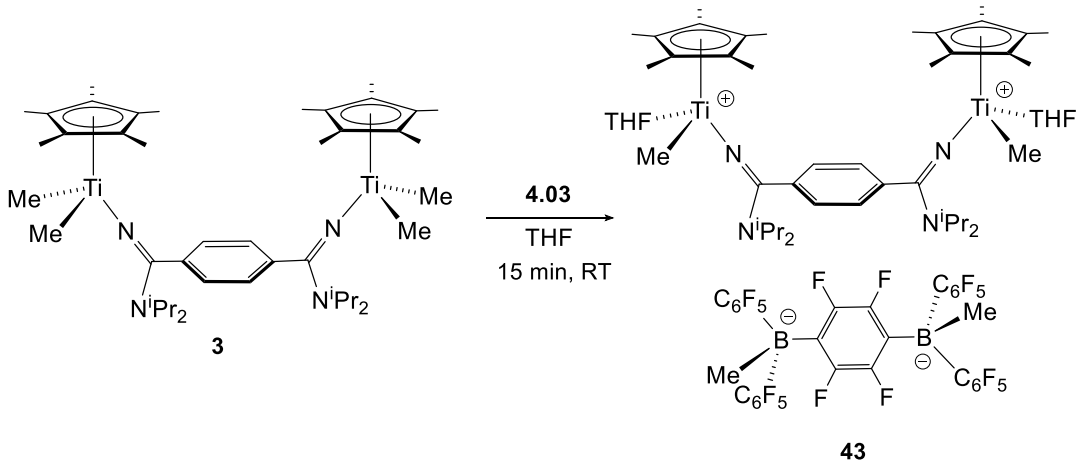

Equation 4.5

Complex **43** was fully characterised. Due its poor solubility in all solvents, the NMR spectroscopic data was recorded in THF-d_8 on a Bruker AVC 500 spectrometer fitted with a cryoprobe. Using this instrument allowed the data to be recorded quickly before ring-opening polymerisation took place. The features of the ^{1}H NMR spectrum are a singlet at 7.42 ppm for the aromatic protons, a signal at 1.78 ppm for Cp^*, a broad signal at 0.60 ppm for Ti<u>Me</u> and at 0.40 ppm for the abstracted B<u>Me</u>. The resonances for NC(N^{i}Pr$_2$)Ph are found at 4.30 (C<u>H</u>Me$_2$), 3.63 (C<u>H</u>Me$_2$), 1.41 (CH<u>Me</u>$_2$) and 1.04 ppm (CH<u>Me</u>$_2$); in both the methine and methyl regions the more downfield resonance is broader. Overall complex **43** has effective C_s symmetry on the NMR timescale, which is indicative of fast rotation around the Ti–N bond. The ^{13}C NMR chemical shift for Ti<u>Me</u> is at 58.2 ppm, this is significantly upfield at 12.1 ppm for the abstracted methyl. The resonances corresponding to the anion observed in the ^{19}F and ^{11}B NMR spectra are identical to those observed for **40**. As was observed for **40**, the addition of 2 equiv. of *N*,*N*′-diisopropylcarbodiimide formed the insertion product [1,4-$C_6H_4\{NCN^iPr_2\}_2\{Cp^*TiMe(MeC(N^iPr)_2\}_2$] [$\{(C_6F_5)_2BMe)_2(\mu\text{-}C_6F_4)$] (**44**), which does not result in the ring opening polymerisation of THF. The resonances in the ^{1}H NMR (298 K, THF-d_8) spectrum that correspond to the cation

are almost identical to those observed for [1,4-$C_6H_4\{NCN^iPr_2\}_2\{Cp^*Ti\{MeC(N^iPr)_2\}_2][BF_{20}]_2$ (**7**), discussed in Chapter Two.

4.5 EPDM copolymerisation experiments using TBF_{20}, BF_{15}, 4.01 and 4.03

EPDM copolymerisation testing of the mononuclear cocatalysts TBF_{20}, BF_{15} and their binuclear counterparts **4.01** and **4.03** with the previously introduced monometallic and bimetallic precatalysts were performed in a small-scale batch reactor under industrially relevant conditions at LANXESS Elastomers, The Netherlands. In all cases an equal number of activators to metal centres were present (B/M = 1). A large excess of triisobutylaluminium (TIBA) and 4-Methyl-2,6-di-tert-butylphenol (BHT) were used ([Al]/[M] = 4500 ; [BHT]/[TIBA] = 1 where [M] is the concentration of titanium metal centres) to scavenge any trace water in the reactor, protecting the catalyst without influencing chain-termination pathways.[26-31] Precatalysts were assessed, unless otherwise stated, using low (0.10 μmol) loadings in order to maintain isothermal conditions (exotherms < 3 °C) and to reduce the possibility of mass-transport limitations. Hydrogen was fed to the reactor together with the ethylene and propylene reactant gases in order to avoid the formation of higher molecular weight polymers, which result in reactor fouling.[32-34] Full experimental details are given in Chapter Six. The composition of the polymers was analysed using FT-IR and the molecular weight and polydispersity index (PDI) were obtained from GPC data.

4.5.1 EPDM copolymerisation experiments using TBF_{20} and 4.01

Tables 4.1 and 4.2 show the results of a high temperature EPDM copolymerisation study with trityl abstraction agents associated with mononuclear or dinuclear borate anions as the respective cocatalysts. The use of TBF_{20} showed a similar trend to that observed in the MAO activated studies discussed in Chapters Two and Three. When used in conjunction with the xanthene-bridged precatalyst **30**, the catalytic species was too inactive to yield sufficient polymer product for analysis. In all active cases for the bimetallic precatalysts comparable polymer compositions (including the enhanced C_3 incorporation for entries 2 and 3), molecular weights and PDIs are observed. This suggests that the same catalytically active metal centre is present in all cases. The productivities are all greater than upon MAO activation and the bimetallic precatalysts **3** and **6** now outperform the un-substituted monometallic analogue **2.07**

(entries 1, 2 and 4), which is presumed to be a result of the strength of the ion-pair interaction.

It has previously been reported that MAO has a stronger contact-ion pair than the perfluorotetraphenyl borate anion. A UV/VIS spectroscopic study on an activated zirconocene catalyst, $Me_2Si(Ind)_2ZrMe_2$, revealed an absorption maximum at a shorter wavelength when activated with MAO compared to TBF_{20}, indicating a higher electron density at the zirconium centre and therefore a stronger coordination.[35] Another study revealed the presence of a bridging methyl group between covalently tethered metal centres upon MAO activation, identified by NMR spectroscopy. This was stated as evidence of a strong anion interaction in providing stabilisation and bringing the metal centres in close proximity.[11] This contact-ion pair will be more pronounced in a bimetallic system, with an increased electrostatic contribution for a dication, and it must be overcome for olefin insertion and a chain-growth propagation pathway to occur.

The improved productivity observed for entries 2 and 4 could be a result of this weaker ion-pair interaction. The same relative increase in productivity is not observed for the more crowded or constrained bimetallic systems, suggesting that the steric limitations in these systems significantly outweigh any electronic advantage a change in cocatalyst may achieve.

The monometallic catalysts **14** - **19** with alternative *para*-substituted end groups also show an increase in productivity both relative to the MAO activated results, discussed in Table 2.9, and to **2.07**. The same general trend in productivities was observed across entries 5-8 as that discussed in Chapter Two. The polymer compositions remain comparable to the MAO activated studies and **2.07** with the exception of precatalyst **19** (entry 8) where a reduced C_3 affinity is observed. This precatalyst differs from the others by containing a π-donating NMe_2 substituent, which could potentially shift the electronic properties of the active titanium centre or independently interact with other components of the polymerisation mixture. Several early transition metal imido complexes (general formula $L_nM{=}NR$) have been synthesised and used in ethylene homopolymerisation. These complexes are good representatives of early metal catalysts with high levels of π-donation and are typically highly active in ethylene homopolymerisation studies and are inactive for C_3 in copolymerisation.[31, 36-39]

It is important to note that the solvent used is a non-polar branched hydrocarbon, pentamethylheptane, in all the batch-polymerisation studies. As previously discussed, it has been reported that the use of a polar solvent in polymerisation studies reduces the differences observed upon counterion variation. A solvent with a high dielectric constant increases the anion solvation rendering the cation freer. The solvent can also compete for coordination to the electrophilic metal centre. The use of pentamethylheptane should not influence the catalytic nuclearity discussed.[11]

Table 4.1 EPDM polymerisation results with TBF_{20}

Entry	Precatalyst	Cocatalyst	Productivity[a] (kg mol Ti^{-1} h^{-1} bar^{-1})	C_2 (wt%)	C_3 (wt%)	ENB (wt%)	VNB (wt%)	M_n (kDa)	M_w (kDa)	PDI
1	**2.07**	TBF_{20}	100,630	53.4	45.1	0.96	0.66	266	535	2.0
2	**3**	TBF_{20}	113,910	43.6	55.3	0.68	0.43	184	399	2.2
3	**4**	TBF_{20}	25,970	45.3	53.7	0.61	0.38	171	374	2.2
4	**6**	TBF_{20}	132,860	50.5	47.8	0.99	0.70	227	483	2.1
5	**14**	TBF_{20}	82,800	51.1	47.1	1.10	0.74	214	454	2.1
6	**15**	TBF_{20}	110,310	51.5	46.8	0.98	0.72	185	421	2.3
7	**18**	TBF_{20}	113,660	49.8	48.3	1.16	0.71	259	574	2.2
8	**19**	TBF_{20}	80,330	54.7	43.7	0.98	0.64	210	476	2.3
9	**25**	TBF_{20}	7,200	57.3	41.1	0.98	0.63	159	346	2.2
10	**30**	TBF_{20}	-	-	-	-	-	-	-	-
11	**33**	TBF_{20}	15,090	54.5	44.2	0.82	0.45	181	394	2.2
12	**37**	TBF_{20}	47,400	50.6	47.7	0.98	0.69	242	440	1.8

Polymerisation conditions. T = 90 °C, Pressure: 7 bar, [Cat] = 0.1 µmol ([Cat] = 0.02 entry 4 [Cat] = 0.05 entries 1, 2, 7, 12 [Cat] = 0.07 entry 8 [Cat] = 0.2 entry 10 [Cat] = 0.28 entry 11) scavenger: [BHT]:[TIBA] (1:1), [Al]:[M] = 4500, [B]:[M] = 1, 10 minute reaction time. Solvent pentamethylheptane (1 L) C_3/C_2 =400/200 Nl h^{-1}, H_2 flow: 0.35 Nl h^{-1}, ENB: 0.7 mL, VNB: 0.7 mL. [a] Productivity per mol of transition metal centres.
Polymer characterisation. Polymer molecular weight and molecular weight distributions*:* the polymers have been analysed with the Freeslate Rapid GPC in 1,2,4 Trichlorobenzene against PS standards. *Average composition:* the polymers have been analysed via transmission IR spectroscopy on a pressed polymer film.

Table 4.2 EPDM polymerisation results with **4.01**

Entry	Precatalyst	Cocatalyst	Productivity[a] (kg mol Ti^{-1} h^{-1} bar^{-1})	C_2 (wt%)	C_3 (wt%)	ENB (wt%)	VNB (wt%)	M_n (kDa)	M_w (kDa)	PDI
1	**2.07**	**4.01**	17,400	50.3	48.0	1.00	0.67	276	601	2.2
2	**3**	**4.01**	7,370	48.7	49.9	0.76	0.50	214	522	2.4
3	**4**	**4.01**	-	-	-	-	-	-	-	-
4	**6**	**4.01**	13,800	51.7	46.7	0.96	0.64	238	477	2.0
5	**14**	**4.01**	39,600	48.8	49.4	1.08	0.75	231	483	2.1
6	**15**	**4.01**	52,290	50.7	47.6	1.02	0.69	238	483	2.0
7	**18**	**4.01**	88,970	52.2	46.1	1.07	0.67	213	497	2.3
8	**19**	**4.01**	48,170	53.5	44.7	1.12	0.71	213	473	2.2
9	**25**	**4.01**	-	-	-	-	-	-	-	-
10	**30**	**4.01**	-	-	-	-	-	-	-	-
11	**33**	**4.01**	-	-	-	-	-	-	-	-
12	**37**	**4.01**	-	-	-	-	-	-	-	-
13	**2.07**	**4.01**	39,000	50.7	47.5	1.03	0.71	275	481	1.8

Polymerisation conditions. T = 90 °C, Pressure: 7 bar, [Cat] = 0.1 µmol ([Cat] = 0.2 entry 4) scavenger: [BHT]:[TIBA] (1:1), [Al]:[M] = 4500, B:M = 1 (B:M = 2 entry 13), 10 minute reaction time. Solvent pentamethylheptane (1 L) C_3/C_2 =400/200 Nl h^{-1}, H_2 flow: 0.35 Nl h^{-1}, ENB: 0.7 mL, VNB: 0.7 mL. [a] Productivity per mol of transition metal centres.

Polymer characterisation. Polymer molecular weight and molecular weight distributions*:* the polymers have been analysed with the Freeslate Rapid GPC in 1,2,4 Trichlorobenzene against PS standards. *Average composition:* the polymers have been analysed via transmission IR spectroscopy on a pressed polymer film.

Table 4.2 displays the polymerisation results using **4.01** as the cocatalyst. When used in conjunction with the precatalysts **4**, **25**, **30**, **33** and **37** the catalytic species were too inactive to yield sufficient polymer product for analysis. The other precatalysts all displayed a significantly lower productivity compared to TBF_{20} activation. This is believed to be a result of the dianionic counterion generating a stronger ion pair interaction, giving the opportunity to form higher aggregates in solution and increasing steric congestion. Two electrostatically tethered monometallic species will have an increase in steric congestion induced by the increased nuclearity. Unlike the results observed in Table 4.1, the bimetallic precatalysts **3** and **6** have a lower activity than **2.07** upon activation with **4.01**. The molecular structure of **3**, discussed in Chapter One, shows that the titanium metal centres are orientated away from one another due to steric constraints, and this is presumed to be the same for complex **6**. The subsequent dianionic diborate zwitterionic complexes are presumed to either orientate the metal centres in the same direction or bridge bimetallic complexes creating multimeric species. This large increase in steric properties is the expected explanation for the large reduction in productivity over the monometallic counterparts. No beneficial cooperative effect is observed for the bimetallic catalysts upon activation with **4.03** as opposed to TBF_{20}. The composition analysis of the resultant polymer displayed in entry 2 shows a reduction in C_3 incorporation in the use of precatalyst **3**. This reduced propylene affinity could be a result of the increased steric congestion. However, a reduction in diene incorporation would also be expected in this case, or a shift in the electronic properties that previously invoked this propylene affinity.

Entries 1 and 4-8 show that the use of this cocatalyst does not influence the polymer produced by the monometallic complexes. The same composition values are observed upon activation with TBF_{20} or **4.01** suggesting that the increased nuclearity does not cooperatively increase the comonomers incorporated; the reduced C_3 affinity for precatalyst **19** is still evident. Narrow PDI values and monomodal GPC chromatograms indicate a single uniform active site is present under these conditions in all cases.

Upon variation of the *para*-substituent across the monometallic complexes an unexpected result is observed; precatalysts **14**, **15**, **18** and **19** all show a greater than two-fold increase in productivity compared to the unsubstituted counterpart, **2.07**.

Notably precatalyst **19** also shows a greater than five-fold increase than with **2.07**. The reason for this increase in productivities is unclear; the increase in non-polar steric bulk incurred by these substituents could help prevent aggregates or bridging species from forming. A synthetic investigation was carried out to see if any differences were observed when **4.01** is reacted with **15**, this is discussed in the following Section.

Bochmann and co-workers reported that an above stoichiometric amount of TBF_{20} could cause an increase in productivity; certain constrained geometry catalysts witnessed an increase by an order of magnitude with a 3:1 TBF_{20} to catalyst ratio as opposed to a stoichiometric amount.[40] This "trityl effect" was not fully understood and was believed to be a result of either more active aggregates forming or caused by an interaction between the excess trityl cations and TIBA, which was introduced as an alkylating and scavenger agent.[40] This effect was still observed when removing the use of TIBA, through the use of a preactivated ion pair complex, and if any reaction were to occur with TIBA it is expected to lead to catalyst deactivation and not an enhanced productivity.[40]

An additional polymerisation study was carried out with **2.07** and **4.01** in a 1:1 ratio (entry 13, Table 4.2), which results in 2 equiv. of trityl cations for every metal centre. The polymer composition and properties remain the same as those observed in entry 1 of Table 4.2, but a greater than two-fold increase in productivity occurs (39,000 kg mol^{-1} h^{-1} bar^{-1}). This productivity increase could be a result of improved catalyst activation. The quantitative formation of complex **38** showed the effectiveness of a stoichiometric amount of **4.01** as an activating species, but the polymerisation conditions contain the catalyst and cocatalyst in much lower concentrations than that of an NMR tube scale reaction. The excess trityl cations could also react with TIBA, as discussed above, but this is assumed not to happen in the presence of BHT.

4.5.2 Activation studies of $Cp^*Ti\{NC(Ar^{Fc})N^iPr_2\}Me_2$ (15)

In Chapter One it was shown that $[Cp^*Ti\{NC(Ar^{Fc})N^iPr_2\}Me][MeBF_{15}]$ (**23**) quantitatively forms from the reaction of $Cp^*Ti\{NC(Ar^{Fc})N^iPr_2\}Me_2$ (**15**) with BF_{15}. As discussed above formation of the base-free zwitterionic complexes formed using **4.01** are not easily observed in solution, an NMR tube scale reaction of **4.01** with 2 equiv. of **15** in the presence of 2 equiv. of *N*,*N*′-diisopropylcarbodiimide quantitatively forms the migratory insertion product $[Cp^*Ti\{NC(Ar^{Fc})\}\{MeC(N^iPr)_2\}]_2[\{MeB(C_6F_5)_3\}_2(\mu\text{-}C_6F_4)]$ (**45**) (Equation 4.6).

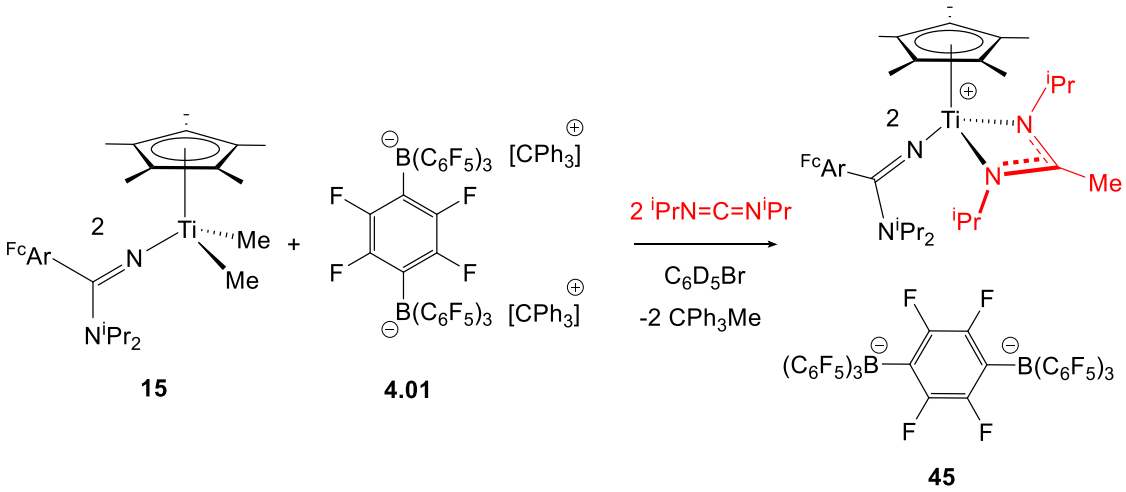

Equation 4.6

A comparable reaction with a stoichiometric amount of TBF_{20} resulted in the quantitative formation of $[Cp^*Ti\{NC(Ar^{Fc})\}\{MeC(N^iPr)_2\}][BF_{20}]$ (**46**). In both reactions a stoichiometrically quantitative amount of Ph_3CMe is observed. Figure 4.5 shows the ^1H NMR spectra (298 K, C_6D_5Br) for **45** and **46**; the only notable difference occurs for the resonance corresponding to the inserted methyl group $\underline{Me}C(N^iPr)_2$ (2.22 and 2.12 ppm for **45** and **46** respectively). The downfield shift for complex **45**, now overlapping with the trityl methyl resonance, is presumed to be the result of this group being in closer proximity to the larger anion.

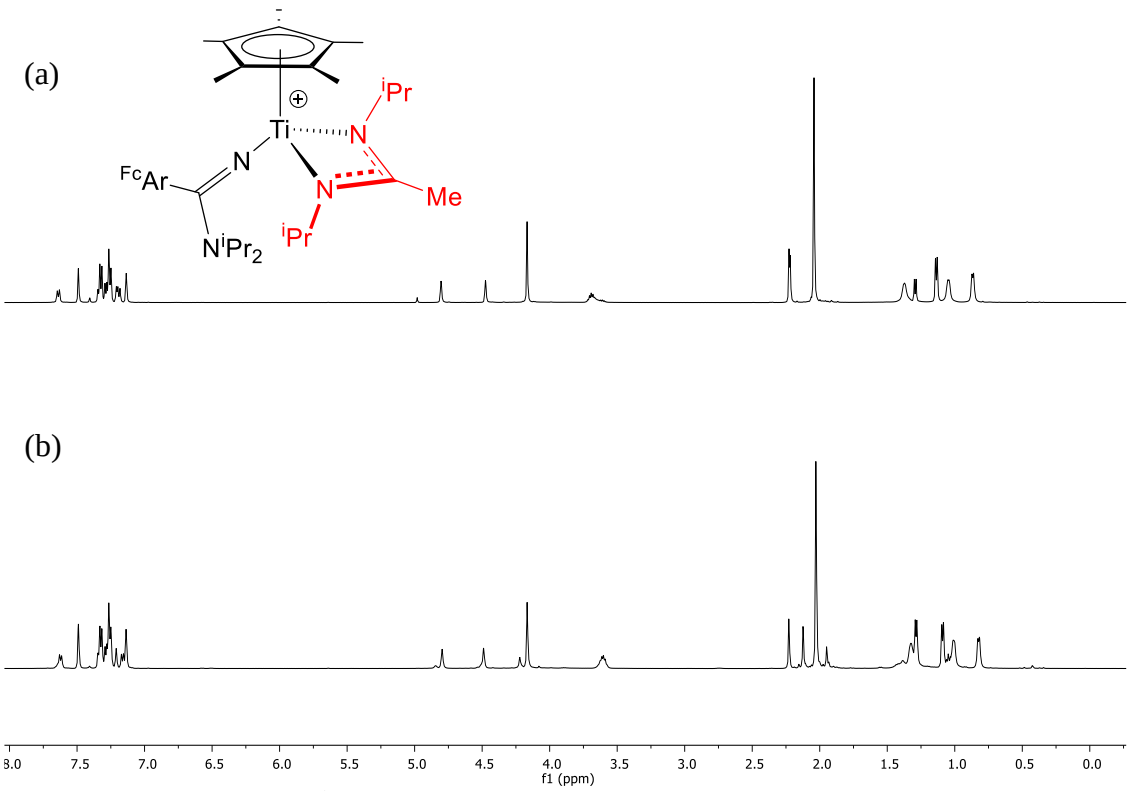

Figure 4.5 ^{1}H NMR (499.9 MHz, C_6D_5Br, 298 K) spectra of $[Cp^{*}Ti\{NC(Ar^{Fc})\}\{MeC(N^{i}Pr)_2\}]_2[\{MeB(C_6F_5)_3\}_2(\mu\text{-}C_6F_4)]$ (**45**, a) and $[Cp^{*}Ti\{NC(Ar^{Fc})\}\{MeC(N^{i}Pr)_2\}][BF_{20}]$ (**46**, b).

The key features of the ^{1}H NMR spectra (298 K, C_6D_5Br) are equivalent to those previously discussed, signals corresponding to κ^1- and κ^2-amidinate, synonymous with a migratory insertion product, are observed and signals appropriate for a ferrocenyl substituent are present in the range 4.17 – 4.80 ppm. The ^{19}F and ^{11}B NMR spectra for **44** give the same resonance for the complexes described in Section 4.3. No obvious differences are observed in the formation of **44** and **45** which would aid in understanding the productivities reported in Table 4.2.

4.5.3 EPDM copolymerisation experiments using BF_{15} and 4.03

Tables 4.3 and 4.4 show the results of a high temperature EPDM copolymerisation study with BF_{15} and **4.03** as the respective cocatalysts. The use of BF_{15} as the cocatalyst follows the same trends in polymer productivity and the resultant properties are as observed when TBF_{20} is employed. The productivities are consistently lower as a result of the stronger contact-ion pair, which can coordinate to the metal centre through the abstracted methyl group, as was introduced in Chapter Two. This suppression in activity results in an inadequate amount of polymer yielded for

analysis in the case of **25**, **30** and **33**. The existence of a bridging methyl group has been extensively studied and verified by both NMR spectroscopy and X-ray crystallography; the first isolable and crystallographically characterised zwitterionic complex of this kind was [{1,2-$(CH_3)_2C_5H_3$}$_2$ZrCH_3][MeBF_{15}] (**1.35**).[41]

As was seen in Section 4.5.1 the use of a binuclear cocatalyst significantly reduces the productivity and several catalysts were unable to produce sufficient polymer for analysis. This reduction can result from the enhanced ion-pair electrostatic attraction, the increased steric congestion and from the potential to form aggregated species; the latter will be investigated further in Section 4.5. Unlike in Table 4.2, the bimetallic complex **6** has a higher productivity than that of some of the monometallic catalysts, the flexible ligand backbone can allow for a less strained conformation unlike the other more restrictive bimetallic catalysts. There are no significant changes in the resultant polymer composition or properties when using this dinuclear cocatalyst, which is again indicative that no beneficial communication is arising between metal centres in the polymerisation mechanism despite the increased nuclearity.

An unexplained trend is observed across the monometallic species; the previously underperforming precatalyst **14** now has the second highest productivity (27,860 kg mol^{-1} h^{-1} bar^{-1}) and precatalyst **18** has the highest (33,685 kg mol^{-1} h^{-1} bar^{-1}), which is approximately double the previous comparable result with precatalyst **15** (16, 110 kg mol^{-1} h^{-1} bar^{-1}). This trend differs from the results concerning the other dinuclear and mononuclear cocatalyst.

An additional study was carried out with **2.07** and **4.03** in a 1:1 ratio (entry 13, Table 4.4), which gives an extra equivalent of the Lewis acidic borane. The polymer composition and properties remain the same as those observed in entry 1 of Table 4.4, but a reduction in productivity occurs (8,490 kg mol^{-1} h^{-1} bar^{-1}). It is known that use of multiple equivalents of BF_{15} lead to an increase in productivity for **2.07**.[42] The presence of an unsubstituted tethered borane proximate to the catalytically active metal centre or a free diborane can be causing a detrimental effect, particularly given the presence of BHT, H_2 and other unsaturated complexes present in the batch reactor.

Table 4.3 EPDM polymerisation results with BF_{15}

Entry	Precatalyst	Cocatalyst	Productivity[a] (kg mol Ti^{-1} h^{-1} bar^{-1})	C_2 (wt%)	C_3 (wt%)	ENB (wt%)	VNB (wt%)	M_n (kDa)	M_w (kDa)	PDI
1	**2.07**	BF_{15}	76,200	51.7	46.5	1.06	0.76	263	529	2.0
2	**3**	BF_{15}	41,310	45.4	53.5	0.66	0.45	226	465	2.1
3	**4**	BF_{15}	11,790	45.6	53.4	0.58	0.37	191	406	2.1
4	**6**	BF_{15}	43,370	52.4	46.0	0.99	0.64	218	469	2.2
5	**14**	BF_{15}	30,170	49.6	48.6	1.07	0.74	253	547	2.2
6	**15**	BF_{15}	57,690	50.3	48.1	0.97	0.69	235	502	2.1
7	**18**	BF_{15}	90,510	51.5	46.9	0.99	0.68	220	497	2.3
8	**19**	BF_{15}	53,660	55.2	42.8	1.18	0.82	251	638	2.5
9	**25**	BF_{15}	-	-	-	-	-	-	-	-
10	**30**	BF_{15}	-	-	-	-	-	-	-	-
11	**33**	BF_{15}	-	-	-	-	-	-	-	-
12	**37**	BF_{15}	18,770	51.5	46.9	0.93	0.67	210	501	2.4

Polymerisation conditions. T = 90 °C, Pressure: 7 bar, [Cat] = 0.1 µmol ([Cat] = 0.05 entry 2) scavenger: [BHT]:[TIBA] (1:1), [Al]:[M] = 4500, [B]:[M] = 1, 10 minute reaction time. Solvent pentamethylheptane (1 L) C_3/C_2 =400/200 Nl h^{-1}, H_2 flow: 0.35 Nl h^{-1}, ENB: 0.7 mL, VNB: 0.7 mL. [a] Productivity per mol of transition metal centres.
Polymer characterisation. *Polymer molecular weight and molecular weight distributions:* the polymers have been analysed with the Freeslate Rapid GPC in 1,2,4 Trichlorobenzene against PS standards. *Average composition:* the polymers have been analysed via transmission IR spectroscopy on a pressed polymer film.

Table 4.4 EPDM polymerisation results with **4.03**

Entry	Precatalyst	Cocatalyst	Productivity[a] (kg mol Ti^{-1} h^{-1} bar^{-1})	C_2 (wt%)	C_3 (wt%)	ENB (wt%)	VNB (wt%)	M_n (kDa)	M_w (kDa)	PDI
1	**2.07**	**4.03**	14,660	51.0	47.4	0.90	0.68	268	539	2.0
2	**3**	**4.03**	10,330	47.0	52.0	0.62	0.40	179	430	2.4
3	**4**	**4.03**	-	-	-	-	-	-	-	-
4	**6**	**4.03**	21,860	47.9	50.6	0.85	0.57	169	387	2.3
5	**14**	**4.03**	27,860	47.8	50.5	1.04	0.67	222	458	2.1
6	**15**	**4.03**	16,110	50.2	48.3	0.88	0.69	261	542	2.1
7	**18**	**4.03**	33,685	50.9	47.3	1.05	0.71	262	598	2.3
8	**19**	**4.03**	23,657	52.2	46.2	0.94	0.71	225	528	2.3
9	**25**	**4.03**	-	-	-	-	-	-	-	-
10	**30**	**4.03**	-	-	-	-	-	-	-	-
11	**33**	**4.03**	-	-	-	-	-	-	-	-
12	**37**	**4.03**	11,910	54.8	46.9	0.93	0.67	210	501	2.4
13	**2.07**	**4.03**	8,490	49.0	48.9	1.29	0.77	280	490	1.8

Polymerisation conditions. T = 90 °C, Pressure: 7 bar, [Cat] = 0.1 µmol ([Cat] = 0.2 entries 5) scavenger: [BHT]:[TIBA] (1:1), [Al]/[M] = 4500, [B]:[M] = 1 ([B]:[M] = 2 entry 13), 10 minute reaction time. Solvent pentamethylheptane (1 L) C_3/C_2 =400/200 Nl h^{-1}, H_2 flow: 0.35 Nl h^{-1}, ENB: 0.7 mL, VNB: 0.7 mL. [a] Productivity per mol of transition metal centres.

Polymer characterisation. *Polymer molecular weight and molecular weight distributions:* the polymers have been analysed with the Freeslate Rapid GPC in 1,2,4 Trichlorobenzene against PS standards. *Average composition:* the polymers have been analysed via transmission IR spectroscopy on a pressed polymer film.

4.6 Diffusion measurement by NMR spectroscopy

The use of dinuclear cocatalysts in polymerisation studies using monometallic and bimetallic cyclopentadienyl titanium κ^1-amidinate complexes has the potential to form highly aggregated species in solution and limit the productivity, as was reflected in Section 4.5. The diffusion coefficients of various cations and anions can be determined by using a technique called Pulsed Gradient Spin Echo (PGSE) NMR, or so-called Diffusion Ordered Spectroscopy (DOSY). This diffusion coefficient will be investigated in this section, for both the mononuclear and dinuclear activating species, to give an insight into the relative size of the species in solution as well as the counterion association.

Interpretation of the diffusion coefficients of $[(C_5H_5)_2ZrMe][BF_{20}]$ led Geyer and co-workers to report the formation of ion quadrupoles in non-polar solutions. This was justified using comparisons to independently established binuclear structures and to inner-sphere ion pairs.[43] This has received criticism through the significantly higher concentration in the PGSE NMR study as opposed to under polymerisation conditions and a lack of consideration of the equilibrium constants.[44] In 2003, Marks and co-workers followed up this study with a range of isolated group 4 metallocenium inner-sphere ion-pairs, with $[MeBF_{15}]^-$ as the anion. It was shown that there was no evidence of significant aggregation and the experimental data were in good agreement with that of an non-aggregated ion-pair.[45] The same group later went on to show that the tendency to form aggregates is dramatically increased when the counterion is displaced from the first coordination sphere, such as in the case of the $[BF_{20}]^-$ anion. However, by investigating the concentration dependence it was argued that the effect that aggregation will have on polymerisation is minimal.[46]

To complement the report of the "trityl effect" discussed above Bochmann *et al*. investigated the diffusion coefficients of two outer-sphere ion pairs with a constrained geometry catalysts, $[(rac\text{-}Me_2Si(1\text{-indenyl}_2)ZrCH_2SiMe_3][BF_{20}]$ (**4.08**) and $[(Me_2C(C_5H_4)(9\text{-fluorenyl})ZrCH_2SiMe_3][BF_{20}]$ (**4.09**), with and without an excess of TBF_{20}. It was found that without an excess of TBF_{20} both species existed predominantly as ion-quadrupoles with identical translation diffusion coefficients for both the anion and cation. An excess of TBF_{20} resulted in an increase in aggregation, supporting the theory that mixed-ion aggregates form.[47, 48] PGSE NMR has been used

to detect a variety of aggregated species and the reader is referred to a relevant review article for a complete description.[49]

A recent study of specific note to this project is the work carried out by Macchioni and co-workers, which tried to investigate all the components of a MAO-activated polymerisation study including the precatalyst, cocatalyst and scavenging species.[50] This work quantitatively highlighted the large self-aggregates MAO can form and that an $AlMe_3$ scavenging system can enhance this aggregation; this is intrinsically linked to the aggregation occurring at the catalytic metal centre.[50] In 2016, work to identify heterometallic metallocene-aluminium species as intermediates in a global MAO-activated polymerisation mechanism identified the reaction of *ansa*-bis(indenyl)zirconocenes with $AlMe_3$ as an inner-sphere ion-pair with no aggregation.[51] No previous study has probed the role of dinuclear cocatalysts in the formation of aggregated species.

Molecular diffusion is a result of the Brownian motion of a molecule through the surrounding media and the diffusion coefficient (D) gives a qualitative value for this as the rate of mean square of molecular displacement. The diffusion coefficient can be obtained by applying pulsed field gradient of different strengths across a sample and measuring the relative loss of intensity after a certain time interval (*ca.* 100 ms). The signal intensity can be related to the gradient strength using the Stejskal-Tanner equation and analysis of the subsequent Gaussian profile can generate D. If the molecule is assumed to be spherical then the hydrodynamic radius is related to the diffusion coefficient by the Stokes-Einstein equation (Equation 4.7, where D is the diffusion coefficient, k is Boltzmann's constant, T is temperature, η is viscosity, r is the hydrodynamic radius, V is volume and c is a numerical factor that depends on the size and shape of the solute and the hydrodynamic behaviour of the solute-solvent system).[52, 53]

$$D = \frac{kT}{c\pi r\eta} = \frac{kT}{c\pi\eta\left(\frac{3V}{4\pi}\right)^{\frac{1}{3}}}$$

Equation 4.7

Modifications on this equation have been reported to account for the fact that the investigated molecules are not spherical or infinitely larger than the molecules that make up the solvent media. However, in this Thesis the ratio of the volumes will be

used to compare species which will negate any significant variations in solvent viscosity or the numerical factor c. The ratio of diffusion coefficients have been successfully used in previous studies for a size comparison.[48, 54-57]

This study will calculate the diffusion coefficients of the isolated complexes: $Cp^*Ti\{NC(Ph)N^iPr_2\}Me_2$ (**2.07**), $[Cp^*Ti\{NC(N^iPr_2)Ph\}Me(THF)][MeBF_{15}]$ (**4.07**) and $[Cp^*Ti\{NC(N^iPr_2)Ph\}Me(THF)]_2[\{(C_6F_5)_2BMe\}_2(\mu\text{-}C_6F_4)]$ (**40**). All samples were prepared as 0.01 M solutions in C_6D_5Br and the residual protio solvent present was used as a reference standard and was consistent in all cases. Signal attenuation was recorded over 16 experiments with gradients strengths ranging from 2-95% of the maximum (Figure 4.6). The results presented in Table 4.5 show the diffusion coefficient of both the anion and cation as well as (given the absence of crystal structure data) the theoretical value obtained by assuming the volume required for a molecule in a crystal structure is *ca.* 18 $Å^3$ per non-hydrogen atom.[58, 59] The bimetallic complex $[1,4\text{-}C_6H_4\{NCN^iPr_2\}_2\{Cp^*TiMe(THF)\}_2][\{(C_6F_5)_2BMe\}_2(\mu\text{-}C_6F_4)]$ (**43**) could not be included in this study due to poor solubility in solvents with low polarity.

To probe for unaccounted motion due to convection, duplicate studies were run for all samples using diffusion times of 100 and 200 ms, and in all cases the diffusion coefficient remained unchanged. An accurate uncertainty error cannot be quoted for the diffusion coefficients, but it is worth noting that it is usually lower than 5 %. It is reported that the error on the derived hydrodynamic radius ranges from 9 to 32 % when a numerical value of 6 is applied for the numerical constant in the Stokes-Einstein equation.[60]

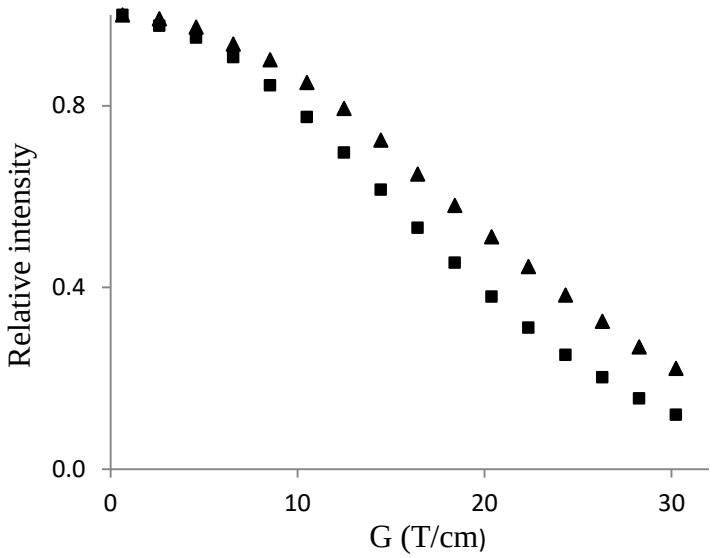

Figure 4.6 Diffusion decay curves for $[Cp^{*}Ti\{NC(N^{i}Pr_2)Ph\}Me(THF)][MeBF_{15}]$ (**4.07**, ■) and $[Cp^{*}Ti\{NC(N^{i}Pr_2)Ph\}Me(THF)]_2[\{(C_6F_5)_2BMe)_2(\mu\text{-}C_6F_4)]$ (**40**, ▲).

Table 4.5 Diffusion coefficients (m^2s^{-1}), NMR volumes ($Å^3$) and theoretical volumes calculated using the "18 $Å^3$ rule" ($Å^3$) for $Cp^{*}Ti\{NC(Ph)N^{i}Pr_2\}Me_2$ (**2.07**), $[Cp^{*}Ti\{NC(N^{i}Pr_2)Ph\}Me(THF)][MeBF_{15}]$ (**4.07**) and $[Cp^{*}Ti\{NC(N^{i}Pr_2)Ph\}Me(THF)]_2[\{(C_6F_5)_2BMe\}_2(\mu\text{-}C_6F_4)]$ (**40**). Theoretical values are calculated using the joint anion and cation values.

Complex	D metal species (x 10^{-10} m^2s^{-1})	NMR Volume metal species ($Å^3$)	D anion (x 10^{-10} m^2s^{-1})	NMR Volume anion ($Å^3$)	Calculated volume ($Å^3$)
2.07	5.22	218	-	-	504
4.07	3.35	825	3.32	845	1,210
40	2.35	2,380	2.34	2,440	2,200

For complexes **4.07** and **40** the values of D are almost identical for the anion and cation pair in each complex. This implies that the zwitterionic complex remains associated in solution as has been previously observed in comparable PGSE NMR experiments described above.[47] This association has also been shown to persist under polymerisation conditions *via* kinetic investigations,[61] and as a result it is well documented that changes in the anion or solvent have a large impact on the catalytic system.[2] The ratio of NMR volumes of **4.07**:**40** is 1:2.9 and the expected ratio

according to the "18 $Å^3$ rule" is 1:1.8. This suggests that there is a greater degree of aggregation for complex **40**, which is unsurprising given the greater degree of electrostatic contributions available from an associated dinuclear counterion. It has been previously shown that the THF will occupy the vacant coordination site at the cationic metal centre in preference to the bridging methyl of a contact ion-pair.[22] The ^{19}F NMR spectra of $[Cp^{*}Ti\{NC(N^{i}Pr_2)Ph\}Me(THF)][MeBF_{15}]$ (**4.07**) gave a $\Delta(m,p)$ value of 2.55 ppm, which is indicative of an uncoordinated $[MeBF_{15}]^{-}$ anion.[62] It is therefore assumed that the anion exists in the outer-sphere, which allows for the greater degree of aggregation observed and is therefore not completely reflective of polymerisation conditions.

In comparison to the neutral monometallic analogue **2.07**, both **4.07** and **40** show a greater NMR volume than anticipated, **2.07**:**4.07** is 1:3.8 and **2.07**:**40** is 1:10.9 (expected values according to the "18 $Å^3$ rule" of 1:2.4 and 1:4.4, respectively). It has previously been reported within the Mountford group that the comparable monometallic complex $[Cp^{*}Ti\{NC(N^{i}Pr_2)Ar^{F_2}\}(OPPh_3)Me][BF_{20}]$ (**4.10**) (where Ar^{F_2} = 2,6-$C_6H_3F_2$) is unaggregated from evidence that it has a smaller NMR volume than an isolated dimeric species.[22] Complex **4.10** includes a triphenyl phosphine as a strong and sterically congested adduct which will prevent aggregation, but the smaller and weaker bound THF adduct in **4.07** could allow for partial aggregation and a subsequent increase in NMR volume. The greater than two-fold increase in volume of **40** relative to the theoretical value is again synonymous with a quadrupole or other aggregated species forming in the solution-phase and complements the reduced productivity observed in the polymerisation studies.

4.7 Summary

This Chapter has described the use of borane and borate mononuclear and dinuclear cocatalysts and their reactions with previously introduced neutral Group 4 dialkyl complexes. This includes the first successful reactions of the trityl bis(borate) as an alkyl abstraction reagent and the first isolated bimetallic complex activated using a bis(borane) compound.

Extensive high temperature EPDM copolymerisation experiments were performed in collaboration with LANXESS Elastomers. Overall these studies showed no evidence of cooperativity invoked from enhanced nuclearity using dincuelar cocatalysts.

This chapter concluded with a PGSE NMR study, which highlighted the propensity for dinuclear cocatalysts to undergo greater aggregation formation in comparison to their mononuclear and neutral dialkyl counterparts.

4.8 References

1. M. C. Baier, M. Zuideveld and S. Mecking, *Angew. Chem. Int. Ed.*, 2014, **53**, 9722-9744.
2. R. A. Collins, A. F. Russell and P. Mountford, *Appl. Petrochem. Res.*, 2015, **5**, 153-171.
3. E. Y.-X. Chen and T. J. Marks, *Chem. Rev.*, 2000, **100**, 1391-1434.
4. M.-C. Chen, J. A. S. Roberts and T. J. Marks, *Organometallics*, 2004, **23**, 932-935.
5. M.-C. Chen, J. A. S. Roberts, A. M. Seyam, L. Li, C. Zuccaccia, N. G. Stahl and T. J. Marks, *Organometallics*, 2006, **25**, 2833-2850.
6. J. A. S. Roberts, M.-C. Chen, A. M. Seyam, L. Li, C. Zuccaccia, N. G. Stahl and T. J. Marks, *J. Am. Chem. Soc.*, 2007, **129**, 12713-12733.
7. C. Fritze, F. Kuber and H. Bohnen, *EP824112A1*, 1998.
8. L. Li, M. V. Metz, H. Li, M.-C. Chen, T. J. Marks, L. Liable-Sands and A. L. Rheingold, *J. Am. Chem. Soc.*, 2002, **124**, 12725-12741.
9. H. Li, L. Li, T. J. Marks, L. Liable-Sands and A. L. Rheingold, *J. Am. Chem. Soc.*, 2003, **125**, 10788-10789.
10. N. Guo, L. Li and T. J. Marks, *J. Am. Chem. Soc.*, 2004, **126**, 6542-6543.
11. H. Li, C. L. Stern and T. J. Marks, *Macromolecules*, 2005, **38**, 9015-9027.
12. M. Delferro and T. J. Marks, *Chem. Rev.*, 2011, **111**, 2450-2485.
13. G. P. Abramo, L. Li and T. J. Marks, *J. Am. Chem. Soc.*, 2002, **124**, 13966-13967.
14. Y.-C. Won, S.-H. Chun, D.-S. Choi, D.-W. Yoo and B.-Y. Lee, *WO2011021805A2*, 2011.
15. K. Ren, J. H. Malpert, H. Li, H. Gu and D. C. Neckers, *Macromolecules*, 2002, **35**, 1632-1637.
16. J. T. Patton, T. J. Marks and L. Li, *WO9914222A1*, 1999.
17. C. Fritze, F. Kueber and H. Bohnen, *DE19632557A1*, 1998.
18. H. Li, L. Li, D. J. Schwartz, M. V. Metz, T. J. Marks, L. Liable-Sands and A. L. Rheingold, *J. Am. Chem. Soc.*, 2005, **127**, 14756-14768.

19. R. C. Neu, E. Y. Ouyang, S. J. Geier, X. Zhao, A. Ramos and D. W. Stephan, *Dalton Trans.*, 2010, **39**, 4285-4294.
20. R. C. Neu, E. Otten, A. Lough and D. W. Stephan, *Chem. Sci.*, 2011, **2**, 170-176.
21. H. Boehrer, N. Trapp, D. Himmel, M. Schleep and I. Krossing, *Dalton Trans.*, 2015, **44**, 7489-7499.
22. A. F. Russell, DPhil Thesis, University of Oxford, 2014.
23. R. D. Chambers and T. Chivers, *J. Chem. Soc.*, 1965, 3933-3939.
24. D. J. Parks, W. E. Piers and G. P. A. Yap, *Organometallics*, 1998, **17**, 5492-5503.
25. J. C. Thomas and J. C. Peters, *Inorg. Chem.*, 2003, **42**, 5055-5073.
26. V. C. Williams, C. Dai, Z. Li, S. Collins, W. E. Piers, W. Clegg, M. R. J. Elsegood and T. B. Marder, *Angew. Chem. Int. Ed.*, 1999, **38**, 3695-3698.
27. V. C. Williams, G. J. Irvine, W. E. Piers, Z. Li, S. Collins, W. Clegg, M. R. J. Elsegood and T. B. Marder, *Organometallics*, 2000, **19**, 1619-1621.
28. R. Vollmerhaus, M. Rahim, R. Tomaszewski, S. Xin, N. J. Taylor and S. Collins, *Organometallics*, 2000, **19**, 2161-2169.
29. R. A. Metcalfe, D. I. Kreller, J. Tian, H. Kim, N. J. Taylor, J. F. Corrigan and S. Collins, *Organometallics*, 2002, **21**, 1719-1726.
30. V. Busico, R. Cipullo, F. Cutillo, N. Friederichs, S. Ronca and B. Wang, *J. Am. Chem. Soc.*, 2003, **125**, 12402-12403.
31. N. Adams, H. J. Arts, P. D. Bolton, D. Cowell, S. R. Dubberley, N. Friederichs, C. M. Grant, M. Kranenburg, A. J. Sealey, B. Wang, P. J. Wilson, M. Zuideveld, A. J. Blake, M. Schroeder and P. Mountford, *Organometallics*, 2006, **25**, 3888-3903.
32. S. W. Ewart, M. A. Parent and M. C. Baird, *J. Polym. Sci., Part A: Polym. Chem.*, 1999, **37**, 4386-4389.
33. Y. V. Kissin, R. I. Mink, T. E. Nowlin and A. J. Brandolini, *J. Polym. Sci., Part A: Polym. Chem.*, 1999, **37**, 4281-4294.
34. P. J. Flory, Principles of Polymer Chemistry, Cornell University Press, 1992.
35. U. Wieser and H.-H. Brintzinger, UV/VIS Studies on the Activation of Zirconocene-Based Olefin-Polymerization Catalysts, Springer Berlin Heidelberg, 2001.

36. C. T. Owen, P. D. Bolton, A. R. Cowley and P. Mountford, *Organometallics*, 2007, **26**, 83-92.
37. M. Said, D. L. Hughes and M. Bochmann, *Dalton Trans.*, 2004, 359-360.
38. D. A. Pennington, P. N. Horton, M. B. Hursthouse, M. Bochmann and S. J. Lancaster, *Polyhedron*, 2005, **24**, 151-156.
39. G. J. Hayday, C. Wang, N. H. Rees and P. Mountford, *Dalton Trans.*, 2008, 3301-3310.
40. F. Song, R. D. Cannon, S. J. Lancaster and M. Bochmann, *J. Mol. Catal. A: Chem.*, 2004, **218**, 21-28.
41. X. Yang, C. L. Stern and T. J. Marks, *J. Am. Chem. Soc.*, 1991, **113**, 3623-3625.
42. R. Scott, DPhil Thesis, University of Oxford, 2013.
43. S. Beck, A. Geyer and H.-H. Brintzinger, *Chem. Commun.*, 1999, 2477-2478.
44. M. Bochmann, *J. Organomet. Chem.*, 2004, **689**, 3982-3998.
45. N. G. Stahl, C. Zuccaccia, T. R. Jensen and T. J. Marks, *J. Am. Chem. Soc.*, 2003, **125**, 5256-5257.
46. C. Zuccaccia, N. G. Stahl, A. Macchioni, M.-C. Chen, J. A. Roberts and T. J. Marks, *J. Am. Chem. Soc.*, 2004, **126**, 1448-1464.
47. C. Alonso-Moreno, S. J. Lancaster, C. Zuccaccia, A. Macchioni and M. Bochmann, *J. Am. Chem. Soc.*, 2007, **129**, 9282-9283.
48. C. Alonso-Moreno, S. J. Lancaster, J. A. Wright, D. L. Hughes, C. Zuccaccia, A. Correa, A. Macchioni, L. Cavallo and M. Bochmann, *Organometallics*, 2008, **27**, 5474-5487.
49. G. Bellachioma, G. Ciancaleoni, C. Zuccaccia, D. Zuccaccia and A. Macchioni, *Coord. Chem. Rev.*, 2008, **252**, 2224-2238.
50. L. Rocchigiani, V. Busico, A. Pastore and A. Macchioni, *Dalton Trans.*, 2013, **42**, 9104-9111.
51. G. Theurkauff, M. Bader, N. Marquet, A. Bondon, T. Roisnel, J.-P. Guegan, A. Amar, A. Boucekkine, J.-F. Carpentier and E. Kirillov, *Organometallics*, 2016, **35**, 258-276.
52. A. Macchioni, G. Ciancaleoni, C. Zuccaccia and D. Zuccaccia, *Chem. Soc. Rev.*, 2008, **37**, 479-489.
53. T. D. W. Claridge, High-resolution NMR Techniques in Organic Chemistry, Elsevier, 2009.

54. A. Moreno, P. S. Pregosin, L. F. Veiros, A. Albinati and S. Rizzato, *Chem. Eur. J.*, 2009, **15**, 6848-6862.
55. D. Sirbu, G. Consiglio, B. Milani, P. G. A. Kumar, P. S. Pregosin and S. Gischig, *J. Organomet. Chem.*, 2005, **690**, 2254-2262.
56. P. G. A. Kumar, P. S. Pregosin, M. Vallet, G. Bernardinelli, R. F. Jazzar, F. Viton and E. P. Kündig, *Organometallics*, 2004, **23**, 5410-5418.
57. A. Macchioni, *Chem. Rev.*, 2005, **105**, 2039-2074.
58. W. Clegg, Crystal Structure determination, Oxford University Press, 1998.
59. C. J. E. Kempster and H. Lipson, *Acta Crystallogr. Sect. B: Struct. Sci.*, 1972, **28**, 3674.
60. D. Zuccaccia and A. Macchioni, *Organometallics*, 2005, **24**, 3476-3486.
61. F. Song, M. D. Hannant, R. D. Cannon and M. Bochmann, *Macromol. Symp.*, 2004, **213**, 173-186.
62. A. D. Horton, J. de With, A. J. van der Linden and H. van de Weg, *Organometallics*, 1996, **15**, 2672-2674.

Chapter Five

Synthesis of a bimetallic zirconium complex and a high-throughput polymerisation study

5.1 Overview

Heterobimetallic catalysts were introduced in Chapter One and were shown to act with a homogeneous cooperative interaction. This Chapter looks to synthesise a Group 4 heterobimetallic complex. This will build upon previous work in the Mountford group that has investigated a congeneric series of monometallic Group 4 cyclopentadienyl amidinate complexes.

The synthesis of a bimetallic zirconium analogue to a titanium complex described in Chapter Two is discussed, along with characterisation by X-ray crystallography and a variable temperature NMR study. The attempted synthesis of a heterobimetallic complex is discussed and in light of these synthetic findings a parallel polymerisation reactor (PPR) experiment on *in situ* generated precatalysts is discussed. This Chapter concludes with synthetic and polymerisation experiments to help understand the results observed in the PPR study.

5.2 Introduction

In Chapter One a Group 4 heterobimetallic CGC with an ethyl tether (**1.61**) was introduced and the complex was shown to act as a single-site catalyst in the production of long-chain branch polyethylene.[1] In Chapter Four the use of a dinuclear cocatalyst with different Group 4 monometallic precatalysts to give a single-site species was discussed.[2] Heterobimetallic species benefit from utilising the advantages of two mechanistically dissimilar metal centres held in close proximity and is often termed "tandem catalysis".[3]

Previous work in the Mountford group introduced a congeneric series of monometallic Group 4 cyclopentadienyl amidinate complexes. The previously described routes to dichloride complexes, namely reaction of Cp^*MCl_3 with an amidine in the presence of excess NEt_3 or a silylated amidine, proved unsuccessful. Instead a transmetallation reaction with the *in situ* formed magnesiated amidinate gave the zirconium (**5.01**) and hafnium (**5.02**) dichloride complexes in good yields (83 and 77%, respectively). These could be alkylated to the dimethyl or dibenzyl complexes *via* a salt metathesis reaction (Scheme 5.1).[4]

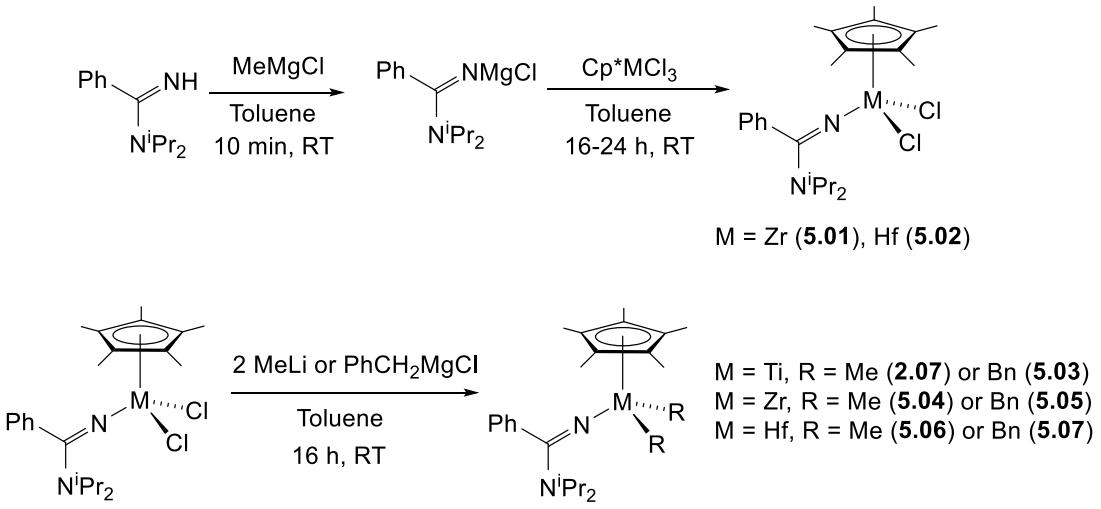

Scheme 5.1 Synthesis of a congeneric series of monometallic Group 4 cyclopentadienyl amidinate complexes.

An extensive structural comparison and complimentary DFT study was carried out across this series. It was evident that the molecular orbitals of complexes **2.07** and **5.04** are very similar, which suggests that the destabilising effect associated with the poorer energy match between the zirconium 4d orbitals and the amidinate moiety is countered by improved orbital overlap due to greater radial extensions. The higher energy metal orbitals of zirconium are reflected in the significantly higher metal based LUMO and the greater difference in atomic charges of the metal and N^{i}Pr$_2$C(Ph)N. The structural differences will be discussed further in Section 5.3.

A high temperature (90 °C) TBF$_{20}$ activated ethylene homopolymerisation study revealed a reduction in activity (62,000, 3,900 and 1,300 kg mol^{-1} h^{-1} bar^{-1} for **2.07**, **5.04** and **5.06** respectively) and molecular weight (770 and 13 kg mol^{-1} for **2.07** and **5.04** respectively **5.06** did not produce sufficient polymer product for analysis) as the group is descended. A corresponding increase in PDI values (2.2 and 8.7 for **2.07** and **5.04**, respectively) is observed on descending the group and the GPC chromatograms revealed a multimodal distribution. A similar trend is observed for the dibenzyl counterparts and in an ethylene/propylene copolymerisation study. This was proposed to be a result of a less sterically protected metal centre and potential formation of dormant amidinate-bridged species.[4] No polymer composition difference was observed across the series in this copolymerisation study. These trends have been observed for other half-sandwich complexes[5] as well as CGCs.[6]

5.3 Synthesis of 1,4-$C_6H_4\{NCN^iPr_2\}_2\{Cp^*ZrBn_2\}_2$ (47)

Chapter Two introduced the synthesis of a κ^1-amidinate supported titanium bimetallic complexes *via* a protonolysis pathway. In this project the same pathway was introduced for the synthesis of the zirconium analogues. Cp^*ZrBn_3 (where Bn = CH_2Ph) was synthesised according to literature procedures[7] and an NMR tube scale reaction with the amidine $HNC(Ph)N^iPr_2$ (**2.08**) quantitatively formed the previously reported complex $Cp^*Zr\{NC(Ph)N^iPr_2\}Bn_2$ (**5.05**) with the extrusion of one equiv. of toluene. The same pathway was invoked for the synthesis of the 1,4-$C_6H_4\{NCN^iPr_2\}_2\{Cp^*ZrBn_2\}_2$ (**47**) from the reaction of two equiv. of Cp^*ZrBn_3 and one equiv. of 1,4-$C_6H_4\{C(NH)N^iPr_2\}_2$ (**1**) (Equation 5.1).

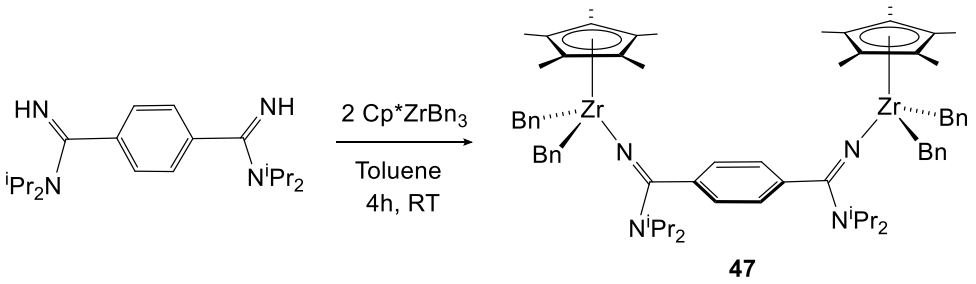

Equation 5.1

Complex **47** was isolated in a 43% yield and fully characterised. The room temperature ^1H NMR spectrum (298 K, Tol-d_8) is shown in Figure 5.1. The features of this spectrum are the Cp^* signal at 1.75 ppm, a pair of doublets as an AB quartet for the C$\underline{H}_2$Ph environment (1.83 and 1.91 ppm) and aromatic resonances corresponding to both the phenylene spacer (6.83 ppm) and benzyl substituents (7.17 – 6.85 ppm). The methylene protons for the benzyl substituent appear as an AB quartet as the phenyl groups prevent free rotation, this causes two different environments for the methylene protons that couple to one another ($^2J_{H\text{-}H}$ = 10.9 Hz). As has been extensively discussed in Chapter Two for complexes 1,4-$C_6H_4\{NCN^iPr_2\}_2\{Cp^*TiMe_2\}_2$ (**3**) and 1,3-$C_6H_4\{NCN^iPr_2\}_2\{Cp^*TiMe_2\}_2$ (**4**) the methyl (1.13 ppm) and methine (3.70 ppm) appear broad at room temperature due to partially restricted rotation around the C–N^iPr_2 and C–phenyl bond. A variable temperature ^1H NMR study was carried out on complex **47** (Figure 5.1). At low temperature the isopropyl group resonances decoalesces into two resonances each for the methyl and methine environments. This complex was fully characterised at 223 K. The $^{13}C\{^1H\}$ NMR spectrum (223 K, Tol-d_8) displayed the methylene carbon for the

benzyl substituent at 63.7 ppm and the diagnostic central carbon of the amidinate moiety at 162.0 ppm.

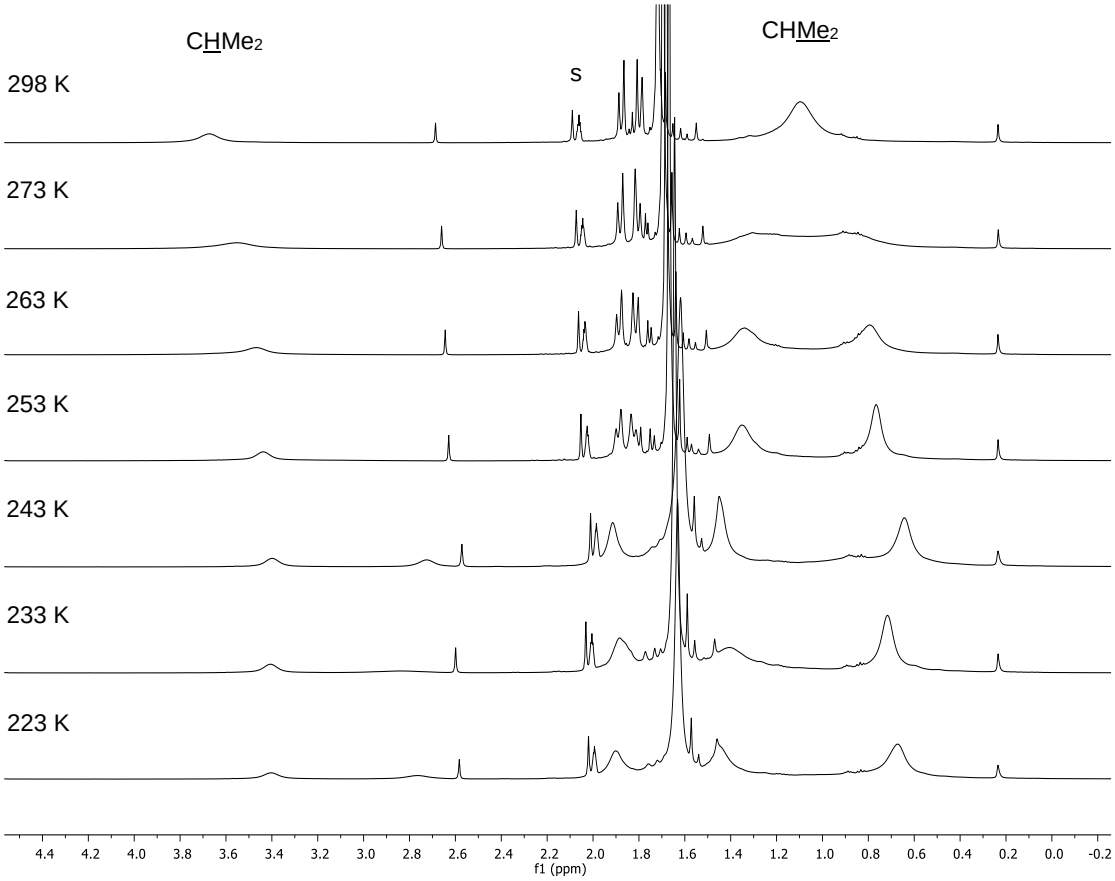

Figure 5.1 Variable temperature ^{1}H NMR (499.9 MHz, Tol-d_8) sub-spectra of 1,4-$C_6H_4\{NCN^iPr_2\}_2\{Cp^*ZrBn_2\}_2$ (**47**). 's' denotes residual protio-solvent.

Diffraction-quality crystals of **47** were grown at -30 °C from a toluene solution. The molecular structure is displayed in Figure 5.2 along with the mononuclear analogue $Cp^*Zr\{NC(Ph)N^iPr_2\}Bn_2$ (**5.05**). Selected bond lengths and angles of complexes **47** and **5.05** are compared in Table 5.1.

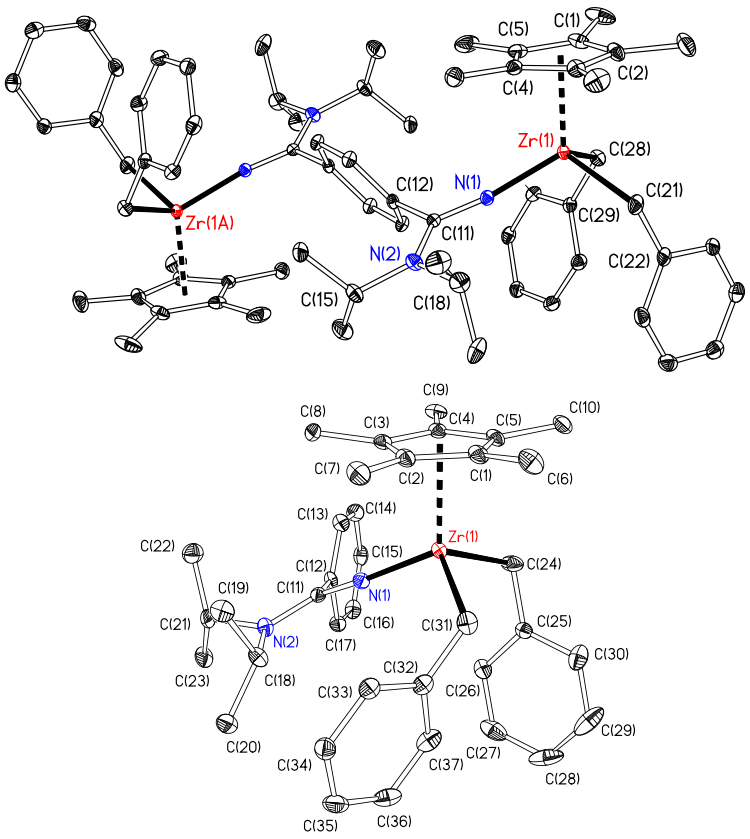

Figure 5.2 Displacement ellipsoid plots of 1,4-$C_6H_4\{NCN^iPr_2\}_2\{Cp^*ZrBn_2\}_2$ (**47**, top) and $Cp^*Zr\{NC(Ph)N^iPr_2\}Bn_2$ (**5.05**, bottom) (20% probability, C-bound H atoms omitted). For compound **47** atoms carrying the suffix 'A' are related to their counterparts by the symmetry operator 1-x, 1-y, 1-z.

Table 5.1 Selected bond lengths (Å) and angles (°) for 1,4-$C_6H_4\{NCN^iPr_2\}_2\{Cp^*ZrBn_2\}_2$ **47** and $Cp^*Zr\{NC(Ph)N^iPr_2\}Bn_2$ **5.05**. Cp^*_{cent} is the computed Cp^* ring carbon centroid.

Parameter	**47**	**5.05**
Zr(1)-Cp^*_{cent}	2.22	2.23
Zr(1)-N(1)	1.9734(13)	1.976(3)
N(1)-C(11)	1.2856(19)	1.297(5)
N(2)-C(11)	1.3547(19)	1.364(5)
C(11)-C(12)	1.5090(19)	1.504(5)
Zr(1)-CH_2(1)	2.2974(16)	2.290(5)
Zr(1)-CH_2(2)	2.3296(17)	2.307(4)
Cp^*_{cent}-Zr(1)-N(1)	115.9	116.7
C(11)-N(1)-Zr(1)	172.21(11)	168.7(3)
Zr(1)-CH_2(1)-C_{phenyl}	111.21(11)	105.1(3)
Zr(1)-CH_2(2)-C_{phenyl}	113.46(11)	118.8(3)

As was previously observed for the titanium complexes, the zirconium metal centre of complex **47** resides in a *pseudo*-tetrahedral three-legged piano stool arrangement. The κ^1-amidinate is again orientated in a near linear fashion to the metal centre (172.21(11)°). There is no difference in the internal amidinate bond lengths either between the titanium and zirconium analogues or the monometallic and bimetallic complexes, which suggests a similar degree of π-donation. A significantly longer bond length is observed for both the Zr(1)–Cp^*_{cent} and Zr(1)–N(1) of both **47** and **5.05** compared to their titanium analogues, which is reflective of a larger ionic radii of zirconium.

The angle between a plane defined by the central three atoms of the amidinate moiety and the phenyl group of the amidinate moiety is 77.86 and 61.58° for **47** and **5.05**, respectively. This larger angle for **47** is the result the steric imposition of the second metal centre has on the crystal packing structure. The reduced angle for **5.05** results in a smaller steric imposition on the benzyl substituents and, unlike complex **47**, this allows one benzyl group to have a more acute Zr(1)–CH_2–C_{phenyl} angle (105.1 *vs* 118.8(3)°). This was proposed to provide a stabilising *ipso* interaction. This *ipso* interaction could still be present for complex **47** in solution as the methylene resonance in the ^{1}H NMR spectrum is shown to broaden at lower temperatures. This *ipso* interaction has been reported for many similar compounds, in particular as a stabilising interaction for Group 4 cations as discussed in Chapter One.[8, 9]

5.4 Attempted synthesis of a Group 4 heterobimetallic complex

There is a large difference in activity between the titanium and zirconium κ^1-amidinate supported monometallic catalyst, *vide supra*. If a complex of the form $Cp^*TiR_2\{1,4\text{-}C_6H_4(NCN^iPr_2)_2\}Cp^*ZrR_2$ could be synthesised it would either provide an excellent mimic of $1,4\text{-}C_6H_4\{NCN^iPr_2\}_2\{Cp^*TiMe_2\}_2$ (**3**), as was attempted through the introduction of alternative *para* substituents in Chapter Two, or result in alternative polymer properties through a cooperative interaction under relevant polymerisation conditions.

The addition of one equiv. of Cp^*TiMe_3 to the bis(amidine) $1,4\text{-}C_6H_4\{C(NH)N^iPr_2\}_2$ (**1**) resulted in almost exclusive formation of complex **3** precipitating out of a benzene solution with a corresponding half an equiv. of compound **1** remaining in solution. The same result was observed for the use of Cp^*ZrBn_3. Variation in temperature,

solvent and slow dropwise addition to ensure an excess of amidine is present and all species remain in solution were attempted, but always resulted in the remaining presence of compound **1**. Attempts to either mono-silylate compound **1** and isolate the product or singly-deprotonate compound **1** *in situ* and react this onwards with a metal complex only resulted in a complicated distribution of products that could not be separated.

A different result is observed for the reaction of one equiv. of Cp^*TiMe_3 with the bis(amidines) 1,3-$C_6H_4\{C(NH)N^iPr_2\}_2$ (**2**) and CH_2-1,4-$(C_6H_4)_2\{C(NH)N^iPr_2\}_2$ (**5**). In these cases a mixture of the bimetallic, monometallic and bis(amidine) is observed, this is in a 75:25 (monometallic:bimetallic) ratio in both cases.

The addition of one equiv. of a metal centre has been a familiar route into many of the heterobimetallic complexes described in Chapter One. The reason for this not being possible with the bis(amidines) is at present unclear.

5.5 Parallel Polymerisation Reactor studies

LANXESS Elastomers have recently installed and explored the use of a Parallel Polymerisation Reactor (PPR) as a high-throughput small scale replicate of an industrially relevant polyolefin batch reactor. This can be used in conjunction with an automated high-throughput chemical (Core Module 3, CM3) platform, which can allow for rapid screening of *in situ* generated precatalysts in olefin polymerisation. The protonolysis pathway previously introduced is highly appropriate for this setup with complexes formed in quantitative yields and only methane or toluene as side products. As a result a preliminary study was carried out using LANXESS Elastomers' equipment.

The CM3 platform was loaded with two equiv. of Cp^*TiMe_3 or Cp^*TiBn_3 and either one or two equiv. of a bis(amidine) in different vessels. Compounds **2**, **5**, **24** and **36** were investigated with Cp*$TiMe_3$ and the vessels were stirred for 24 h at room temperature in toluene. Compounds **2**, **24** and **36** were also investigated with Cp^*TiBn_3, based on NMR tube scale reactions an additional hour with heating at 90 °C was employed for guaranteed reaction completion. The solutions were used as precatalysts in the PPR after which the volatiles were removed and a ^1H NMR spectrum recorded in order to verify the *in situ* generated precatalyst. The cells with one equiv. of the bis(amidine) all successfully formed the bimetallic catalysts, based

on the spectroscopic data in comparison to the isolated complexes. Those with two equiv. gave a mixture of monometallic, bimetallic and bis(amidine) species, the ratios were calculated *via* ^{1}H NMR spectroscopy and are highlighted in Table 5.2.

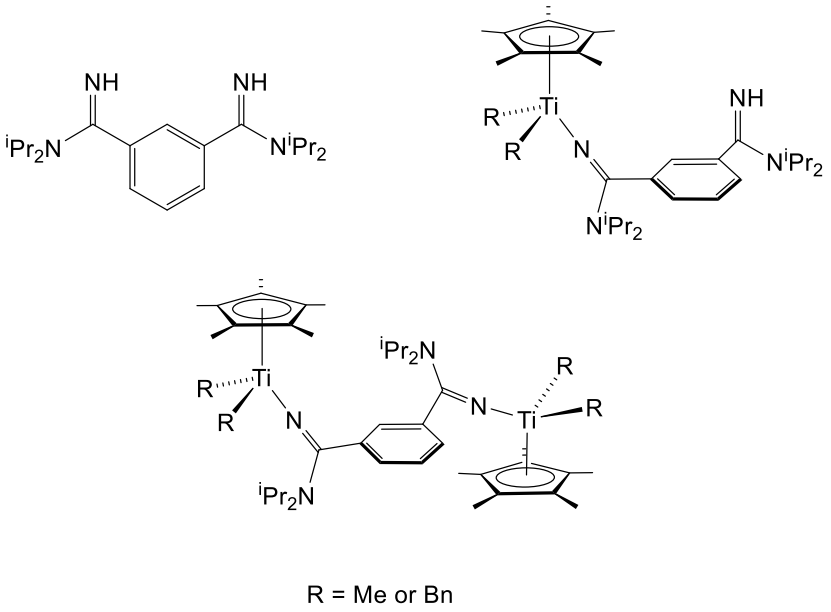

Figure 5.3 Example of a bis(amidine), monometallic complex and bimetallic complex formed *in situ.*

The EPDM copolymerisation study was carried out in the PPR and full experimental details for this can be found in Chapter Six. The cell is initially charged with toluene and ENB, which is then heated to 40 °C along with 50 psi of propylene. Heating this mixture to 90 °C results in an end pressure of 110 psi and ethylene is subsequently added as a 20 psi overpressure. This results in an initial molar ratio in the liquid phase of $C_2/C_3 = 0.025$. During the polymerisation the pressure (total 9 bar) is maintained from an ethylene gas line and maintained at a temperature of 90 °C. Activation of the dimethyl precatalysts was achieved using TBF_{20} ([B]/[M] = 2) and MMAO/BHT was used as a scavenger system in a large excess ([Al] = 10 µmol). The polymerisation was quenched after 300 seconds with a N_2/O_2 mixture (2%v/v O_2) at 3.4 bar (50 psi) overpressure. The composition of the polymers was analysed using FT-IR and the molecular weight and polydispersity index (PDI) were obtained from GPC measurements.

Each precatalyst was run in duplicate, or where possible triplicate, and a series of cells dedicated to a reference precatalyst is included to achieve consistency between studies. Unlike the batch reactors, the multiple runs allow for error calculations,

however given the limited number of cells and typically low polymer yield these errors are very large. The results for the active catalysts with Cp^*TiMe_3 are summarised in Table 5.2. The study with Cp^*TiBn_3 are not discussed, but displayed comparable trends, monometallic percentage formation, productivities and resultant polymer compositions. It is important to note that in this table, due to the presence of mixtures, the productivity and loading concentration is stated per metal centre not per catalyst.

Table 5.2. EPDM polymerisation results for *in situ* generated precatalysts with Cp^*TiMe_3

Entry	Bis(amidine)	Equivalents of Ligand	Monometallic (%)	Productivity[a] (kg mol Ti^{-1} h^{-1} bar^{-1})	C_2 (wt%)	C_3 (wt%)	ENB (wt%)	M_n (kDa)	M_w (kDa)	PDI
1	**2**	1	75	3,270(1,600)	32.3(1.4)	65.2(1.4)	2.5(0.2)	255(14)	484(26)	1.9
2	**2**	0.5	0	21,160(1,500)	32.8(0.9)	64.8(0.9)	2.5(0.1)	133(15)	244(13)	1.8
3	**5**	1	75	6,900(2,100)	33.4(2.1)	63.3(2.0)	3.3(0.2)	300(33)	756(75)	2.3
4	**5**	0.5	0	23,910(1,700)	33.0(1.2)	63.6(1.3)	3.4(0.1)	197(14)	420(25)	2.1
5	**24**	1	80	3,270(400)	38.0(0.6)	58.5(0.9)	3.6(0.7)	272(35)	484(44)	1.8
6	**24**	0.5	0	10,830(1,500)	36.8(0.4)	59.9(0.6)	3.99(1.0)	223(18)	389(19)	1.8
7	**36**	1	0	34,400(14,400)	36.2(3.7)	60.2(4.3)	3.6(0.6)	232(20)	426(46)	1.8
8	**36**	0.5	0	54,100(3,000)	31.4(0.1)	65.0(0.1)	3.6(0.1)	178(12)	305(12)	1.7

Polymerisation conditions. T = 90 °C, Pressure: 9 bar, [M] = 0.02 µmol, (Entry 2 and 6: [Cat] = 0.012 µmol; Entry 3 and 4: [Cat] = 0.008 µmol; Entry 7 and 8: [Cat] = 0.004 µmol) scavenger: BHT/MMAO-3A ([Al] = 10 µmol, BHT:Al = 0.5), 300 seconds reaction time. Solvent toluene (4.1 mL). C_2/C_3 (liquid phase) = 0.025 molar ratio, ENB: 185 µmol. [a] Productivity per mol of transition metal centres.
Polymer characterisation. Polymer molecular weight and molecular weight distributions: the polymers have been analysed with the Freeslate Rapid GPC in 1,2,4 Trichlorobenzene against PS standards. *Average composition:* the polymers have been analysed *via* transmission IR spectroscopy on a pressed polymer film.

In each case that the monometallic species forms in the majority and that catalytic mixture is used the productivity is significantly decreased in comparison to the exclusive formation of their bimetallic counterpart. Due to the insolubility of the bis(amidine) **36** only the bimetallic species forms in both cases, as a result the average productivities show a minimal difference. A small proportion of the catalysts for entries 1, 3 and 5 contain the bimetallic catalysts, which are known to be active as shown by entries 2, 4 and 6. The presence of the bimetallic catalyst can account for some or potentially the entire polymer yield. This is reflected in the polymer composition data, which shows no deviation in each case between using half or one ligand equiv. suggesting the same active species is present. The monometallic species can therefore be assumed to be very poorly active relative to the bimetallic. This could be the result of the tethered unsubstituted amidine having a large detrimental effect. This amidine could be interacting with many of the substrates present, in particular the scavenger system introduced. A synthetic example of this interaction will be discussed in Section 5.6.

Unexpectedly the molecular weight capacity is reduced on forming the bimetallic as opposed to the monometallic mixture for the compounds **2** and **5** (Entries1-4), the remainder do not change within error. This is reminiscent of the EPM and EPDM copolymerisation results discussed in previous Chapters, in which the bimetallic catalysts had a reduced molecular weight in comparison to their monometallic counterparts. This improved molecular weight capacity could be a result of the tethered amidine in the monometallic species behaving as an aluminium alkyl scavenging system that is proximate to the metal centre.

An advantage of using the PPR is the ability to maintain the amount of ethylene that is added to the cell throughout the course of the polymerisation. This addition is in order to maintain the total pressure, but the uptake traces can indicate the rate of consumption and display features such as catalyst deactivation or poor initiation. Example uptake curves for entries 1 and 2 are displayed in Figure 5.4. A large initial uptake is always observed as there is dissolution of the gaseous monomers into the solution injected. As can be seen the ethylene uptake for the bimetallic catalyst is very consistent across the course of the experiment and without a large discrepancy between the cells. The cells containing a majority of the monometallic catalyst all display a wider variation between cells. This could be a result of catalyst

decomposition or alternatively the role of the non-innocent tethered amidine. The same differences between monometallic and bimetallic C_2 traces are observed for all complexes.

The addition of one equiv. of bis(amidine)s **2**, **5** and **24** to Cp^*TiMe_3 not only produce a mixture of the bimetallic and monometallic complexes, but unreacted bis(amidine) will also remain. To investigate whether this unreacted amidine had an impact on the polymerisation study a separate polymerisation experiment was carried out. Utilising the PPR polymerisation a study with complexes **2.07** and **3** were carried out with and without one additional equiv. of their respective protio-ligands (**2.08** and **1**). The productivities are not significantly different when using precatalyst **2.07** without an equiv. of compound **2.08** (28,000(6,500) kg mol^{-1} h^{-1} bar^{-1}) or with one equiv. (21,340(1,000) kg mol^{-1} h^{-1} bar^{-1}). The same lack of impact is observed for precatalyst **3** (16,000(1,700) and 13,900(2,100) kg mol^{-1} h^{-1} bar^{-1}). The polymer composition and molecular weight capacity also display no differences. This data suggests the unreacted bis(amidine), of which there is less than one equiv. in all cases excluding entry 7, has no impact on the polymerisation.

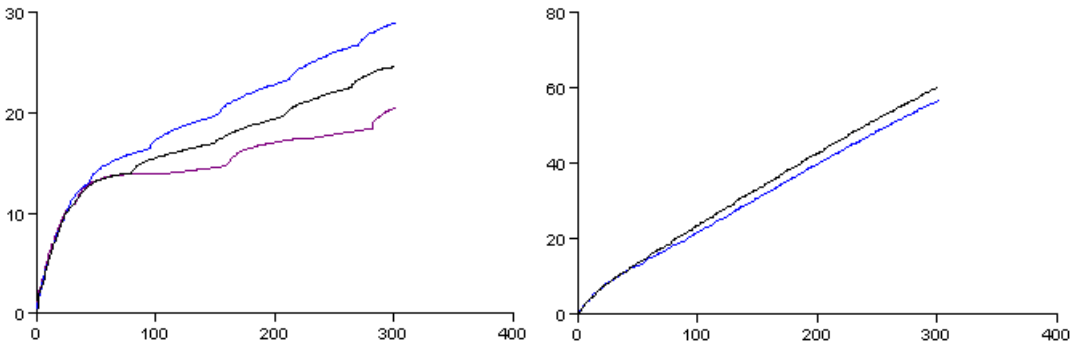

Figure 5.4 Example ethylene uptake curves (C_2 pressure (psi) *vs* time (sec)) for entries 1 (left) and 2 (right) in Table 5.2 over the period of the polymerisation. The different coloured lines refer to different runs with the same catalyst.

Reassuringly, the bimetallic catalysts performed with a comparable trend to the results on the 1 L batch reactor, with the exception that the bimetallic formed from the bis(amidine) **5** gave a lower than expected productivity. The consistent ethylene uptake over the time-frame is indicative that no catalyst death occurs, which can therefore also be assumed to be the case for the polymerisations using the 1 L batch reactor previously reported. Further optimisations and studies are underway at

LANXESS Elastomers and this operation will be used for future studies in the ongoing industrial collaboration with the Mountford Group.

5.6 Synthesis of 1,3-$C_6H_4\{C(NH)N^iPr_2\}_2(AlMe_3)_2$ (48)

As discussed above, an unsubstituted amidine has the potential to interact with many of the substrates in a polymerisation cell. To demonstrate this a reaction between a bis(amidine) and an aluminium alkyl was carried out.

The addition of two equiv. of $AlMe_3$, either neat or as a solution in hexane, to a -30 °C toluene solution of compound **2** resulted in the immediate formation of 1,3-$C_6H_4\{C(NH)N^iPr_2\}_2(AlMe_3)_2$ (**48**) (Equation 5.2).

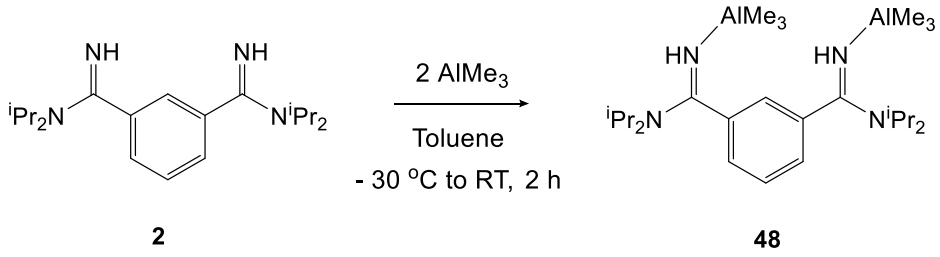

2 **48**

Equation 5.2

Complex **48** is an adduct formed from the donation of $N^iPr_2C\underline{N}H$ lone-pair, as opposed to a covalent bond with the extrusion of methane which has commonly been observed for primary and secondary amine groups.[10, 11] This adduct formation has routinely been observed for nitrogen Lewis base donors, such as triethylamine or pyridine,[12] as well as many other amines.[13-16] Complex **48** was isolated in an 85% yield and was fully characterised. The ^{1}H NMR spectrum (298 K, C_6D_6) of complex **48** is shown in Figure 5.5. The features are an upfield singlet for the aluminium methyl groups (-0.60 ppm), four doublets (0.58 – 1.03 ppm) and two septets (2.98 and 3.78 ppm) for the methyl and methine resonances of the isopropyl groups, a resonance for N$\underline{H}$ (6.01 ppm) and signals corresponding to the bridging phenylene (7.04 (overlapping) and 7.56 ppm). The distinct isopropyl resonances are reminiscent of the low temperature ^{1}H NMR spectrum for 1,3-$C_6H_4\{NCN^iPr_2\}_2\{Cp^*TiMe_2\}_2$ (**4**). An increased donation arises from the C$\underline{N}^iPr_2$, which increases the electron density at C$\underline{N}$H and stabilises the formation of this adduct, this results in more double bond character and a subsequent higher barrier to rotation in the C–N^{i}Pr$_2$ bond. The prevalence of this resonance stabilisation is presumed to be the origin of the preferential formation of this adduct.

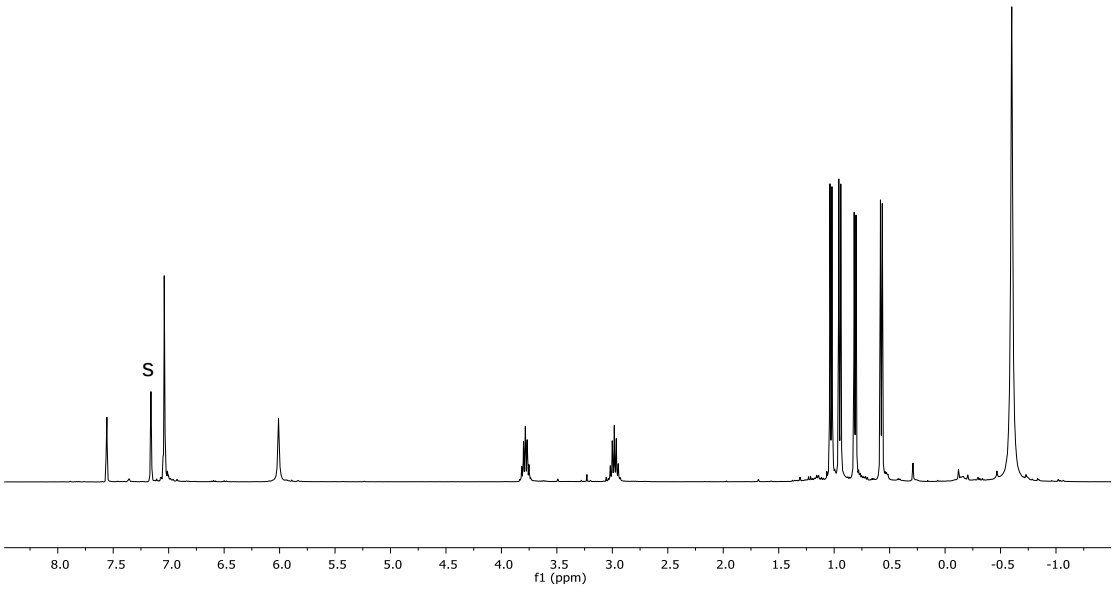

Figure 5.5 ^{1}H NMR (399.9 MHz, C_6D_6, 298 K) spectrum of 1,3-$C_6H_4\{C(NH)N^iPr_2\}_2(AlMe_3)_2$ (**48**). 's' denotes residual protio-solvent.

Diffraction-quality crystals of **48** were grown at -30 °C from a toluene solution. The molecular structure is displayed in Figure 5.6 and is in good agreement with the NMR data previously discussed. The aluminium metal centre resides in a tetrahedral coordination environment with the same bond lengths to the three methyl environments and nitrogen substituent (*avg.* 1.979 Å). The amidinate moiety retains the coplanarity, which is appropriate for the resonance stabilisation discussed. The increased C<u>N</u>^{i}Pr$_2$ donation is reflected by the bond lengths of the amidinate moiety in comparison to 1,3-$C_6H_4\{C(NH)N^iPr_2\}_2$ (**2**). C–NH bond length is increased from compound **2** (1.288(2) Å) to **48** (1.306(2) Å) and the C–N^{i}Pr$_2$ bond length reduced from **2** (1.370(2) Å) to **48** (1.336(2) Å).

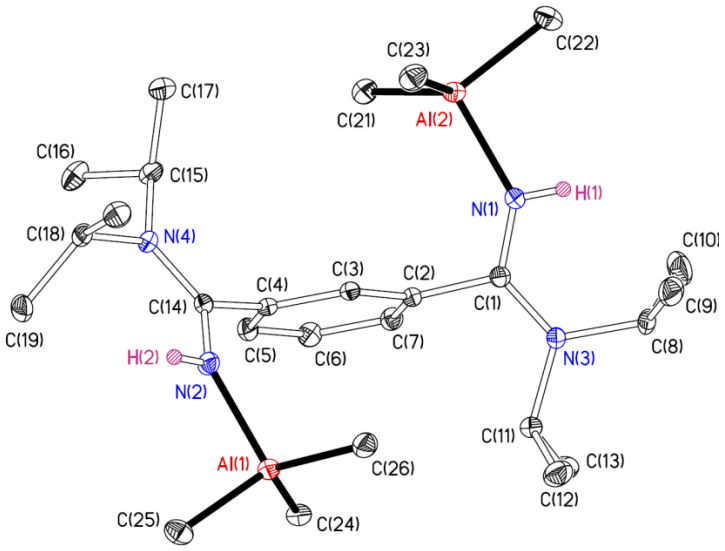

Figure 5.6 Displacement ellipsoid plot of 1,3-$C_6H_4\{C(NH)N^iPr_2\}_2(AlMe_3)_2$ (**48**) (20% probability, C-bound H atoms omitted).

No change was observed upon heating complex **48** to 90 °C in a toluene solution for 10 mins, twice the length of time of the polymerisation experiment. The synthesis of complex **48** highlights the non-innocent nature of an amidine in the polymerisation study described.

5.7 Summary

This Chapter has described the synthesis and characterisation of a cyclopentadienyl-amidinate zirconium bimetallic complex. This included both a solid state analysis using the X-ray crystal structure and solution phase analysis with a variable temperature NMR study.

Utilisation of LANXESS Elastomers' PPR and high-throughput synthetic platform allowed for a fast screening of *in situ* generated monometallic and bimetallic precatalysts for EPDM copolymerisation. The results demonstrated the poor productivity of a monometallic species with a tethered protio-amidine substituent and additional polymerisation and synthetic studies were carried out to help probe this. The limitations to synthesising a heterobimetallic complex were also introduced. The use of this equipment as a high-throughput replicate of catalysts under industrial conditions will be important for future studies and experimental understanding.

5.8 References

1. J. Wang, H. Li, N. Guo, L. Li, C. L. Stern and T. J. Marks, *Organometallics*, 2004, **23**, 5112-5114.
2. G. P. Abramo, L. Li and T. J. Marks, *J. Am. Chem. Soc.*, 2002, **124**, 13966-13967.
3. J. P. McInnis, M. Delferro and T. J. Marks, *Acc. Chem. Res.*, 2014, **47**, 2545-2557.
4. R. Scott, DPhil Thesis, University of Oxford, 2013.
5. K. Itagaki, S. Hasumi, M. Fujiki and K. Nomura, *J. Mol. Catal. A: Chem.*, 2009, **303**, 102-109.
6. J. C. Stevens, in Stud. Surf. Sci. Catal., Elsevier, 1996, vol. 101, pp. 11-20.
7. P. T. Wolczanski and J. E. Bercaw, *Organometallics*, 1982, **1**, 793-799.
8. M. Bochmann and S. J. Lancaster, *Organometallics*, 1993, **12**, 633-640.
9. R. F. Jordan, R. E. LaPointe, N. Baenziger and G. D. Hinch, *Organometallics*, 1990, **9**, 1539-1545.
10. C. Doering and R. Kempe, *Eur. J. Inorg. Chem.*, 2009, 412-418.
11. W. P. Kretschmer, B. Hessen, A. Noor, N. M. Scott and R. Kempe, *J. Organomet. Chem.*, 2007, **692**, 4569-4579.
12. K. Hatada and H. Yuki, *Tetrahedron Lett.*, 1968, 213-217.
13. C. L. Aitken and A. R. Barron, *J. Chem. Crystallogr.*, 1996, **26**, 297-300.
14. J. Liu and H. Ma, *Dalton Trans.*, 2014, **43**, 9098-9110.
15. J.-P. Bezombes, B. Gehrhus, P. B. Hitchcock, M. F. Lappert and P. G. Merle, *Dalton Trans.*, 2003, 1821-1829.
16. A. J. Mountford, S. J. Lancaster, S. J. Coles, P. N. Horton, D. L. Hughes, M. B. Hursthouse and M. E. Light, *Inorg. Chem.*, 2005, **44**, 5921-5933.

Chapter Six

Experimental details and characterising data

6.1 General methods and instrumentation

All manipulations were carried out using standard Schlenk line or dry-box techniques under an atmosphere of argon or dinitrogen. Solvents were degassed by sparging with dinitrogen and dried by passing through a column of the appropriate drying agent[1] or refluxed over sodium (toluene, xylene), potassium (THF), Na/K (Et_2O) or P_2O_5 (fluorobenzene) and distilled. Deuterated solvents were dried over sodium (C_6D_6 and toluene-d_8), potassium (THF-d_8), P_2O_5 ($CDCl_3$ and CD_2Cl_2) or CaH_2 (C_6D_5Br) distilled under reduced pressure and stored under argon in Teflon valve ampoules. NMR samples were prepared under dinitrogen in 5 mm Wilmad 507-PP tubes fitted with J. Young Teflon valves. ^{1}H, ^{13}C-{^{1}H} ,^{11}B, ^{19}F NMR spectra were recorded on Varian Mercury-VX 300, Bruker Avance III HD nanobay 400, Bruker Avance III 500 NMR or on a Bruker AVC 500 spectrometer fitted with a ^{13}C cryoprobe. Spectra are referenced internally to residual protio-solvent (^{1}H) or solvent (^{13}C) resonances, and are reported relative to tetramethylsilane (δ = 0 ppm). ^{19}F spectra were referenced externally to $CFCl_3$ and ^{11}B spectra were referenced externally to $Et_2O{\cdot}BF_3$. Assignments were confirmed using two dimensional ^{1}H-^{1}H and ^{13}C-^{1}H NMR correlation experiments. Chemical shifts are quoted in δ (ppm) and coupling constants in Hz. Mass spectra were recorded by the mass spectrometry service of the University of Oxford. IR spectra were recorded on a Thermo Scientific Nicolet iS5 FTIR spectrometer. Samples were prepared in a dry-box as Nujol mulls between NaCl plates or as a thin film, and the data are quoted in wavenumbers (cm^{-1}) within the range 4000−400 cm^{-1}. Elemental analyses were carried out by the Elemental Analysis Service at the London Metropolitan University.

6.2 Literature preparations and reagent purification

$Cp^{*}TiMe_3$,[2] $CH_2\{1,4\text{-}C_6H_4CN\}_2$,[3] 1,4-cyanophenylferrocene,[4] [1,4-$C_6H_4(CN)(NMe_3)$][I],[5] $DBF(CN)_2$,[6] $Xanth(I)_2$,[7] ferrocene-1,1′-diboronic acid,[8] $\{(C_6F_5)_2B\}_2(\mu\text{-}C_6F_4)$,[9] $[\{B(C_6F_5)_3\}_2(\mu\text{-}C_6F_4)][Ph_3C]_2$,[10] and $Cp^{*}ZrBn_3$[11] were prepared according to or adapted from literature procedures. $HNC(N^{i}Pr_2)Ph$ and $Cp^{*}Ti\{NC(N^{i}Pr_2)Ph\}Me_2$ were prepared in an analogous manner to that described in a previous DPhil Thesis.[12] All other reagents required for the isolation of the novel compounds described below were purchased directly from Alfa Aesar or Sigma-Aldrich or kindly donated from LANXESS Elastomers and used directly or dried as appropriate before use.

6.3 X-ray data collection and processing parameters

Crystals were mounted on glass fibers using perfluoropolyether oil and cooled rapidly in a stream of cold N_2 using an Oxford Cryosystems Cryostream unit. Diffraction data were measured using either an Enraf-Nonius KappaCCD or Agilent Technologies Supernova diffractometer using Mo-K_α or Cu-K_α radiation, respectively. As appropriate, absorption and decay corrections were applied to the data and equivalent reflections merged.[13] The structures were solved with SIR92[14] or Superflip,[15] and further refinements and all other crystallographic calculations were performed using the CRYSTALS program suite.[16] Other details of the structure solution and refinements are given in the Supporting Information (CIF data – see CD Appendix).

6.4 General polymerisation procedure

Polymerisation testing was carried out at LANXESS Elastomers, The Netherlands, by Mr John van de Moosdijk, Mr. Hans Leduc, Dr Richard Scott and Dr Raffaelle Bernardo under the supervision of Dr Alexandra Berthoud. The analytics were carried out by Mr Sander Niessen at LANXESS Elastomers and at DSM Resolve, Geleen.

6.4.1 General polymerisation reagents

Methylaluminoxane (MAO) was purchased from Chemtura as a 10 wt.% Aluminium solution in toluene and was dosed as a 0.10 M or 1.0 M Aluminium solution in toluene. Triisobutylaluminium (TIBA, 10 wt.% Al hexane solution) was purchased from Akzo Nobel and dosed as 0.10 M (Al based) solutions in hexane. 4-Methyl-2,6-di-tert-butylphenol (BHT, +99.0%) was purchased from Sigma-Aldrich and dosed as a 0.20 M solution in hexane. The catalyst precursor solutions were dosed as 1.0 mM solutions in toluene or hexane. Trityl tetrakis(pentafluorophenyl)borate ($[CPh_3][BF_{20}]$) was dosed as a 2.0 mM solution in toluene. Tris(pentafluorophenyl)borane (BF_{15}) was dosed as a 2.0 mM solution in toluene or hexane. The feed streams (ethylene, propylene, hydrogen, nitrogen) were purified by contacting with various absorption media to remove catalyst killing impurities such as water, oxygen and polar compounds (Molsieves 4Å (Merck, nitrogen, ethylene, hydrogen), Molsieves 13-X (Merck, propene, PMH), Cu-catalyst BTS R311 (BASF, nitrogen, ethylene, propylene, nitrogen)). 2,2,4,6,6-Pentamethylheptane (PMH) solvent was additionally stripped with nitrogen. 5-ethylidenebicyclo[2.2.1]hept-2-ene and vinylbicyclo[2.2.1]hept-2-ene were purchased from Ineos and dosed to the reactor

as liquids after stripping with nitrogen. After opening the reactor, the reactor was dried using 450 μmol L^{-1} triisobutylaluminium. In order to avoid mass transfer limitation problems, the total polymer yield in each polymerization was limited to approximately 10 g after a total polymerization time of 10 minutes. The total aluminium (i.e. scavenger) concentration in the reactor was kept above 0.45 mM to ensure efficient scavenging.

6.4.2 Ethylene-Propylene copolymerisation

Ethylene-propylene batch copolymerisation reactions were carried out in a 2 L autoclave equipped with a double intermig stirrer and baffles. The reaction temperature was set to 90 °C and regulated by a Lauda LTH303 Thermostat. Ethylene and propylene monomers were continuously fed to the gas cap of the reactor during the conditioning period and the polymerisation time. The total monomer flow was kept constant during each experiment (either 600 NL h^{-1}). The pressure of the reactor was kept constant by a back-pressure valve. In an inert atmosphere of nitrogen (1.8 bar), the reactor was filled with 950 ml of PMH solvent, BHT and MAO (Chapter Two and Three). The reactor was heated to 90 °C, while stirring at 1350 rpm. The reactor was pressurised to 7 bar by feeding ethylene and propylene and the reactor was conditioned applying a fixed ratio of ethylene and propylene for 15 minutes. Then, the catalyst components were added as PMH solutions to the reactor and the catalyst vessel was rinsed with an additional 50 mL of PMH. After 10 minutes of polymerisation time, the monomer flow was stopped, and the solution was carefully transferred in a 2 L Erlenmeyer flask, containing a solution of Irganox-1076 in isopropanol and dried over night at 100 °C under reduced pressure (< 20 mbar).

6.4.3 Ethylene-Propylene-ENB-VNB (EPDM) copolymerisation

The same procedure was used as for the ethylene-propylene copolymerisation reactions and in addition:

1. 0.70 mL of ENB and 0.70 mL of VNB were added before heating the reactor to 90 °C.
2. 0.35 NL h^{-1} of hydrogen was fed to the reactor together with the ethylene/propylene feed. This was done to avoid the formation of too high molecular weight polymers and reactor fouling.

3. In Chapter Four, TIBA was used in place of MAO as the scavenging system and the cocatalyst was added directly after the catalyst precursor was added.

6.4.4 Parallel Polymerisation Reactor (PPR) procedure

Polymerisation experiments were carried out with a high throughput parallel reactor setup (PPR48 available from Freeslate), with six reactor modules each containing eight reaction cells (5 mL working volume per cell). The whole system is housed in a glovebox maintaining a pure nitrogen atmosphere. The monomer gas and quench gas lines are plumbed directly into the reactors and controlled by automatic valves; ethylene or propylene is fed after purification by passing through columns containing a BASF/Molecular sieves mixed bed. Liquid reagents are robotically added to individual cells by syringes. Solvents are previously purified in an MBraun SPS unit. The cells are fitted with a pre-weighed glass vial insert and a disposable stirring paddle. The reactor is then closed, and 4.1 mL of toluene/scavenger mixture are fed (10 μmol of scavenger, i.e. MMAO-3A from Akzo Nobel, 7 wt.% Al in hexane conditioned with 2,6-ditertbutyl,4-me-phenol, [Al]:[BHT] = 2) are injected into each cell through a valve. The reactors are pressurised with propene at 50 psi at 800 rpm for 30 mins. Afterward the modules are thermostated at 90 °C, and the cells are over pressurised with ethene (Propene and Ethene from Praxair) at 1.4 bar. The precatalyst and activator (activator TBF_{20}, [B]:[Ti] = 2.0) are injected sequentially in to the cells, allowing no mixing via a nitrogen bubble of 50 μL. The polymerization is run at constant temperature and monomer partial pressure for 5 minutes, then quenched with N_2/O_2 mixture (2%v/v O_2) at 50 psi (3.4 bar) overpressure. The reactors are cooled, vented and purged with dinitrogen, in order to prevent the glove box pollution with air from the quenching. After purging with inert gas, the reactors are opened and the glass inserts are unloaded from the cells, transferred to a centrifuge/vacuum drying station (Genevac EZ-2 Plus) for overnight treatment. The polymer samples are recovered and weighed on a Freeslate Weighting station unit, the polymer yields are automatically stored for polymer analysis.

6.5 Electrochemical experiment procedure

Cyclic voltammetry studies were carried out using a PAR AMETEK VersaSTAT 3 potentiostat under computer control. CV experiments were performed in an N_2 glovebox using a three-electrode configuration with a platinum working electrode,

Ag/AgCl as the quasi-reference electrodes and platinum wire as the auxiliary electrode. Sample solutions were prepared by dissolving the analyte in the solvent (10 mL) followed by addition of a supporting 0.2 M electrolyte [^{n}Bu$_4$N][PF$_6$]. The reported mid-peak potentials are referenced internally to that of the $FeCp_2^{+/0}$ redox couple, which was measured by adding nickelocene (*ca.* 1 mg). Nickelocene was selected due to the favourable position of the redox potential under these conditions.[17]

6.6 Experimental details and characterising data for Chapter Two

1,4-C$_6$H$_4${C(NH)N^{i}Pr$_2$}$_2$ (1)

Method A: To a THF (250 mL) solution of diisopropylamine (73 mL, 0.52 mol) at 50 °C was added MeMgBr (140 mL, 3.0 M in diethyl ether, 0.42 mol). Following stirring at 50 °C for 3 h, the solution was cooled to 0 °C and 1,4-dicyanobenzene (5.38 g, 0.042 mol) was added. The solution was allowed to warm to room temperature and was stirred for a further 2 d. The mixture was subsequently cooled to 0 °C and quenched with methanol (50 mL) and then water (100 mL). The organic phase was separated from the aqueous layer which was then back-extracted with dichloromethane (4 x 50 mL). The combined organic phases were washed with aqueous NaOH (4 M, 3 x 30 mL), dried over $MgSO_4$, filtered and the volatiles removed under reduced pressure. The off-white solid was washed with pentane (3 x 15 mL), isolated and dried *in vacuo*. Yield = 5.32 g (38%). Diffraction quality crystals were grown by slow evaporation from a concentrated solution of dichloromethane.

Method B: A small ampoule was loaded with 1,4-dicyanobenzene (1 g, 7.8 mmol), diisopropylamine (7.6 mL, 57.8 mmol) and aluminum chloride (2.19 g, 16.4 mmol). 15 mL of xylene was added and the ampoule was sealed and heated to 120 °C for 48 h. Upon cooling to room temperature the reaction was quenched with icewater (5 mL). The reaction mixture was partitioned between HCl solution (1 M, aqueous 20 mL) and EtOAc (20 mL). The organic phase was extracted with HCl solution (1 M, aqueous 20 mL), the combined aqueous fractions were then basified (NaOH, 4 M, aqueous) and extracted with EtOAc (3 x 20 mL). The combined organic fractions were dried over $MgSO_4$, filtered and volatiles removed under reduced pressure to give a yellow powder. Yield = 2.23 g (86%).

^{1}H NMR ($CDCl_3$, 299.9 MHz, 293 K): 7.21 (4H, s, Ar), 3.59 (4H, sept, ^{3}J = 6.6 Hz, N(C<u>H</u>Me$_2$)$_2$), 1.29 (24H, d, ^{3}J = 6.9 Hz, N(CH<u>Me</u>$_2$)$_2$) ppm (NH not observed). ^{13}C{^{1}H} NMR ($CDCl_3$, 75.4 MHz, 293 K): 167.4 (<u>C</u>N(N^{i}Pr$_2$), 141.9 (Ar <u>C</u>(C(N^{i}Pr$_2$)N)), 126.2 (Ar <u>C</u>HC(C(N^{i}Pr$_2$)N)), 48.5 (N(<u>C</u>HMe$_2$)$_2$), 21.0 (N(CH<u>Me</u>$_2$)$_2$) ppm. IR (NaCl plates, Nujol mull, cm^{-1}): 1576 (m, C=N), 1225 (w), 1085 (w), 813(w), 772(w). ESI^{+}-HRMS: *m/z* = 331.2857 (calcd. For $[C_{20}H_{35}N_4]^{+}$ *m/z* = 331.2856). Anal. found (calcd. for $C_{20}H_{34}N_4$): C, 72.47 (72.68); N, 16.87 (16.95); H, 10.49 (10.37) %.

1,3-C$_6$H$_4${C(NH)N^{i}Pr$_2$}$_2$ (2)

Method A: To a toluene (250 mL) solution of diisopropylamine (73 mL, 0.52 mol) at 50 °C was added MeMgBr (140 mL, 3.0 M in diethyl ether, 0.42 mol). Following stirring at 50 °C for 3 h, the solution was cooled to 0 °C and 1,3-dicyanobenzene (5.38 g, 0.042 mol) was added. The solution was warmed to room temperature before being refluxed for 13 h. The mixture was subsequently cooled to 0 °C, quenched with methanol (50 mL) and then water (100 mL). The organic phase was separated from the aqueous layer which was then back-extracted with dichloromethane (4 x 50 mL). The combined organic phases were washed with aqueous NaOH (4 M, 3 x 30 mL), dried over $MgSO_4$, filtered and the volatiles removed under reduced pressure. Yield = 4.20 g (30%). Diffraction quality crystals were grown from a concentrated pentane solution at -30 °C.

Method B: A small ampoule was loaded with 1,3-dicyanobenzene (1.03 g, 8 mmol), diisopropylamine (8 mL, 57 mmol) and aluminum chloride (2.14 g, 16 mmol). 15 mL of xylene was added and the ampoule was sealed and heated to 120 °C for 24 h. Upon cooling to room temperature the reaction was quenched with icewater (5 mL). The reaction mixture was partitioned between HCl solution (1 M, aqueous 20 mL) and EtOAc (20 mL). The organic phase was extracted with HCl solution (1 M, aqueous 20 mL), the combined aqueous fractions were then basified (NaOH, 4 M, aqueous) and extracted with EtOAc (3 x 20 mL). The combined organic fractions were dried Mg_2SO_4, filtered and volatiles removed under reduced pressure to give a brown oil. Trituration with pentane yielded the product as a brown solid. Yield = 2.2 g (83%).

^{1}H NMR ($CDCl_3$, 299.9 MHz, 293 K): 7.39 (1H, m, Ar C<u>H</u>CHC(C(N^{i}Pr$_2$)N)), 7.28 (2H, m, Ar CHC<u>H</u>C(C(N^{i}Pr$_2$)N)), 7.19 (1H, s, Ar C<u>H</u>(C(C(N^{i}Pr$_2$)N))$_2$), 5.67 (2H, br, N<u>H</u>), 3.65 (4H, sept, ^{3}J = 6.9 Hz, N(C<u>H</u>Me$_2$)$_2$), 1.37 (24H, d, ^{3}J = 6.9 Hz,

N(CH$\underline{Me}_2)_2$)ppm. $^{13}C\{^1H\}$ NMR ($CDCl_3$, 75.4 MHz, 293 K): 167.3 ($\underline{C}N(N^iPr_2)$, 141.5 (Ar $\underline{C}(C(N^iPr_2)N)$), 128.7 (Ar $\underline{C}HCHC(C(N^iPr_2)N)$), 125.5 (Ar $CH\underline{C}HC(C(N^iPr_2)N)$), 123.4 (Ar $\underline{C}H(C(C(N^iPr_2)N))_2$), 48.3 ($N(\underline{C}HMe_2)_2$), 20.8 ($N(CH\underline{Me}_2)_2$) ppm. IR (NaCl plates, Nujol mull, cm^{-1}): 3283 (m, N-H), 1577 (s, C=N), 1363 (m), 1217 (m), 1027 (m), 783 (m). ESI^+-HRMS: *m/z* = 331.2853 (calcd. For $[C_{20}H_{35}N_4]^+$ *m/z* = 331.2856). Anal. found (calcd. for $C_{20}H_{34}N_4$): C, 72.48 (72.68); N, 16.82 (16.95); H, 10.53 (10.37) %.

1,4-$C_6H_4\{NCN^iPr_2\}_2\{Cp^*TiMe_2\}_2$ (3)

To a stirring toluene (15 mL) solution of 1,4-$C_6H_4\{C(NH)N^iPr_2\}_2$ (1.01 g, 3.06 mmol) was added a toluene (10 mL) solution of Cp^*TiMe_3 (1.46 g, 6.40 mmol). The brown solution was stirred for 15 h until a precipitate appeared. After filtration the solid was washed with toluene (3 x 15 mL) to produce a yellow solid, which was isolated and dried *in vacuo*. Yield = 1.18 g (51%). Diffraction quality crystals were grown by slow cooling from a concentrated solution of hot bromobenzene. ^1H NMR ($CDCl_3$, 299.9 MHz, 223 K): 7.13 (4H, s, Ar), 3.71 (2H, sept, ^3J = 6.9 Hz, $N(C\underline{H}Me_2)_2$), 3.51 (2H, br, $N(C\underline{H}Me_2)_2$), 1.67 (12H, d, ^3J = 6.6 Hz, $N(CH\underline{Me}_2)_2$), 1.64 (30H, s, $C_5\underline{Me}_5$), 1.39 (12H, d, ^3J = 6.6 Hz, $N(CH\underline{Me}_2)_2$), -0.19 (12H, s, $Ti\underline{Me}_2$) ppm. $^{13}C\{^1H\}$ NMR ($CDCl_3$, 75.4 MHz, 223 K): 160.6 ($\underline{C}N(N^iPr_2)$, 140.2 (Ar $\underline{C}(C(N^iPr_2)N)$), 125.5 (Ar $\underline{C}HC(C(NMe_2)N)$), 118.9 ($\underline{C}_5Me_5$), 51.8 ($N(\underline{C}HMe_2)_2$), 46.6 ($N(\underline{C}HMe_2)_2$), 45.9 ($Ti\underline{Me}_2$), 20.8 ($N(CH\underline{Me}_2)_2$), 19.9 ($N(CH\underline{Me}_2)_2$), 11.3 ($C_5\underline{Me}_5$) ppm. IR (NaCl plates, Nujol mull, cm^{-1}): 1561 (s, C=N), 1321 (m), 1135 (w), 890 (m), 829 (w). EI-MS: *m/z* = 694 (3%, $[M - 4Me]^+$). Anal. found (calcd. for $C_{44}H_{74}N_4Ti_2$): C, 69.85 (70.01); H, 9.68 (9.88); N, 7.57 (7.42) %.

1,3-$C_6H_4\{NCN^iPr_2\}_2\{Cp^*TiMe_2\}_2$ (4)

To a stirring toluene (15 mL) solution of 1,3-$C_6H_4\{C(NH)N^iPr_2\}_2$ (0.50 g, 1.5 mmol) was a toluene (10 mL) solution of added Cp^*TiMe_3 (0.73 g, 3.2 mmol). The brown solution was stirred for 30 h. The volatiles were removed *in vacuo* to afford a yellow solid which was washed with pentane (3 x 15 mL) and dried *in vacuo*. Yield = 0.52 g (46%). Diffraction quality crystals were grown from a concentrated pentane solution at -30 °C. ^1H NMR ($CDCl_3$, 299.9 MHz, 223 K): 7.24 (1H, t, ^3J = 7.2 Hz, Ar $C\underline{H}CHC(C(N^iPr_2)N)$), 7.12 (1H, s, Ar $C\underline{H}(C(C(N^iPr_2)N))_2$) ,7.07 (2H, d, ^3J = 7.5Hz, Ar $CHC\underline{H}C(C(N^iPr_2)N)$, 3.77 (2H, sept, ^3J = 6.4 Hz, $N(C\underline{H}Me_2)_2$), 3.50 (2H, br,

N(C<u>H</u>Me$_2$)$_2$), 1.73 (6H, d, ^{3}J = 6.4 Hz, N(CH<u>Me</u>$_2$)$_2$), 1.70 (30H, s, C$_5$<u>Me</u>$_5$), 1.56 (6H, d, ^{3}J = 6.4 Hz, N(CH<u>Me</u>$_2$)$_2$), 1.18 (6H, d, ^{3}J = 6.4 Hz, N(CH<u>Me</u>$_2$)$_2$), 1.13 (6H, d, ^{3}J = 6.4 Hz, N(CH<u>Me</u>$_2$)$_2$), -0.11 (6H, s, Ti<u>Me</u>$_2$), -0.21 (6H, s, Ti<u>Me</u>$_2$) ppm. ^{13}C{^{1}H} NMR (CDCl$_3$, 75.4 MHz, 223 K): 160.2 (<u>C</u>N(N^{i}Pr$_2$), 141.5 (Ar <u>C</u>(C(N^{i}Pr$_2$)N)), 127.6 (Ar <u>C</u>HCHC(C(N^{i}Pr$_2$)N)), 124.8 (Ar CH<u>C</u>HC(C(N^{i}Pr$_2$)N)), 123.7 (Ar <u>C</u>H(C(C(N^{i}Pr$_2$)N))$_2$), 119.1 (<u>C</u>$_5$Me$_5$), 51.9 (N(<u>C</u>HMe$_2$)$_2$), 48.1 (Ti<u>Me</u>$_2$), 46.9 (N(<u>C</u>HMe$_2$)$_2$), 45.1 (Ti<u>Me</u>$_2$), 21.7 (N(CH<u>Me</u>$_2$)$_2$), 20.9 (N(CH<u>Me</u>$_2$)$_2$), 20.2 (N(CH<u>Me</u>$_2$)$_2$), 20.0 (N(CH<u>Me</u>$_2$)$_2$) 11.7 (C$_5$<u>Me</u>$_5$) ppm. IR (NaCl plates, Nujol mull, cm^{-1}): 1549 (s, C=N), 1320 (m), 1036 (m), 688 (w). EI-MS: *m/z* = 724 (25%, [M – 2Me]$^+$). Anal. found (calcd. for C$_{44}$H$_{74}$N$_4$Ti$_2$): C, 69.65 (70.01); H, 9.84 (9.88); N, 7.42 (7.42) %.

CH$_2${1,4-C$_6$H$_4$-C(NH)N^{i}Pr$_2$}$_2$ (5)

To a THF (50 mL) solution of diisopropylamine (1.66 mL, 11.8 mmol) at 50 °C was added MeMgBr (3.39 mL, 3.0 M in diethyl ether, 10.2 mmol). Following stirring at 50 °C for 3 h, the solution was cooled to 0 °C and CH$_2${1,4-C$_6$H$_4$CN}$_2$ (0.74 g, 3.4 mmol) was added. The pink solution was slowly warmed to room temperature and stirred for a further 36 h. The mixture was subsequently cooled to 0 °C, quenched with methanol (50 mL) and then water (100 mL). The organic phase was separated from the aqueous layer which was then back-extracted with dichloromethane (4 x 50 mL). The combined organic phases were washed with aqueous NaOH (4 M, 3 x 30 mL), dried over MgSO$_4$, filtered and the volatiles removed under reduced pressure to give a yellow oil. Extraction into pentane (3 x 15 mL) and removal of the volatiles under reduced pressure gave the desired product as a yellow powder. Yield 1.01 g (71%). ^{1}H NMR (C$_6$D$_6$, 400.1 MHZ, 298 K): 7.07 (4H, d, ^{3}J = 8.1 Hz, *o*-C$_6$<u>H</u>$_4$), 6.94 (4H, d, ^{3}J = 8.1 Hz, *m*-C$_6$<u>H</u>$_4$), 3.66 (2H, s, C<u>H</u>$_2$Ph), 3.43 (4H, sept, ^{3}J = 6.8 Hz, N(C<u>H</u>Me$_2$)$_2$), 1.28 (12H, d, ^{3}J = 6.6 Hz, N(CH<u>Me</u>$_2$)$_2$) ppm (NH not observed). ^{13}C – {^{1}H} NMR (C$_6$D$_6$, 100.6 MHz, 298 K): 167.3 (<u>C</u>N(N^{i}Pr$_2$), 140.8 (*i*-<u>C</u>$_6$H$_4$), 140.5 (*p*-<u>C</u>$_6$H$_4$), 129.2 (*m*-<u>C</u>$_6$H$_4$), 126.4 (*o*-<u>C</u>$_6$H$_4$), 48.5 (N(<u>C</u>HMe$_2$)$_2$), 41.7 (<u>C</u>H$_2$Ph$_2$), 20.9 (N(CH<u>Me</u>$_2$)$_2$) ppm. IR (NaCl plates, Nujol mull, cm^{-1}): 1573 (s, C=N), 1223 (s), 1178 (m), 1030 (m), 775 (m). ESI$^+$-HRMS: *m/z* = 421.3323 (calcd. For [C$_{27}$H$_{41}$N$_4$]$^+$ *m/z* = 421.3326). Anal. found (calcd. for C$_{27}$H$_{40}$N$_4$): C, 76.88 (77.10); H, 9.50 (9.59); N, 13.25 (13.32) %.

$CH_2\{1,4\text{-}C_6H_4\text{-}NCN^iPr_2\}_2\{Cp^*TiMe_2\}_2$ (6)

To a stirring benzene (25 mL) solution of Cp^*TiMe_3 (1.08 g, 4.73 mmol) was added a benzene (10 mL) solution of $CH_2\{1,4\text{-}C_6H_4\text{-}C(NH)N^iPr_2\}_2$ (0.99 g, 2.36 mmol). The brown solution was stirred for 22 h. The volatiles were removed under reduced pressure to afford a brown solid which was washed with hexane (3 x 15 mL) and dried *in vacuo.* Concentration of the hexane wash to *ca.* 20 mL and storage at -30 °C for 24 h resulted in an additional amount of the desired compound as a crystalline solid which was subsequently isolated and dried *in vacuo*. Yield = 0.95 g (48%). ^{1}H NMR (Tol-d_8, 499.9 MHz, 233 K): 7.21 (4H, d, ^3J = 7.5 Hz, *o*-$C_6\underline{H}_4$), 6.89 (4H, d, ^3J = 7.6 Hz, *m*-$C_6\underline{H}_4$), 3.67 (2H, br, $N(C\underline{H}Me_2)_2$), 3.61 (2H, s, $C\underline{H}_2Ph_2$), 2.97 (2H, br, $N(C\underline{H}Me_2)_2$), 1.84 (30H, s, $C_5\underline{Me}_5$), 1.72 (12H, br, $N(CH\underline{Me}_2)_2$), 0.69 (12H, br, $N(CH\underline{Me}_2)_2$), 0.52 (12H, s, $Ti\underline{Me}_2$) ppm. ^{13}C – {^{1}H} NMR (Tol-d_8, 125.7 MHz, 233 K): 161.4 ($\underline{C}N(N^iPr_2)$, 141.2 (*i*-$\underline{C}_6H_4$), 140.6 (*p*-$\underline{C}_6H_4$), 129.2 (*m*-$\underline{C}_6H_4$), 127.0 4 (*o*-$\underline{C}_6H_4$), 120.0 ($\underline{C}_5Me_5$), 52.2 ($N(\underline{C}HMe_2)_2$), 48.3 ($Ti\underline{Me}_2$), 47.1 ($N(\underline{C}HMe_2)_2$), 41.8 ($\underline{C}H_2Ph_2$), 20.7 (($N(CH\underline{Me}_2)_2$), 12.3 ($C_5\underline{Me}_5$) ppm. IR (NaCl plates, Nujol mull, cm^{-1}): 1553 (s, C=N), 1322 (s), 1155 (m), 889 (m), 794 (w). EI-MS: *m/z* = 694 (50%, [M – (Me + Cp)]$^+$). Anal. found (calcd. for $C_{51}H_{80}N_4Ti_2$): C, 72.39 (72.50); H, 9.68 (9.54); N, 6.43 (6.63) %.

$[1,4\text{-}C_6H_4\{NCN^iPr_2\}_2\{Cp^*Ti\{MeC(N^iPr)_2\}_2][BF_{20}]_2$ (7)

To a stirring fluorobenzene (10 mL) solution of $1,4\text{-}C_6H_4\{NCN^iPr_2\}_2\{Cp^*TiMe_2\}_2$ (100 mg, 0.13 mmol) and ^{i}PrNCN^{i}Pr (33 mg, 41 μL, 0.26 mmol) was added dropwise a fluorobenzene (5 mL) solution of TBF_{20} (244 mg, 0.26 mmol). After 30 mins pentane (20 mL) was added resulting in the formation of a red oil. The pentane/fluorobenzene was decanted away and the oil washed with pentane (3 x 10 mL). The remaining solid was dried *in vacuo* to yield the desired compound as a red solid. Yield = 187 mg (60%). ^{1}H NMR (THF-d_8, 499.9 MHz, 298 K): 7.56 (4H, s, Ar), 4.15 (2H, κ^1- $NC\underline{H}Me_2$), 3.84 (6H, overlapping sept, κ^1 and κ^2 -$NC\underline{H}Me_2$) 2.40 (6H, s, $\underline{Me}C(N^iPr)_2$), 2.13 (30H, s, $C_5\underline{Me}_5$), 1.47 (12H, br, $NC\underline{H}Me_2$), 1.15 (24H, d, $NC\underline{H}Me_2$, ^3J = 6.2 Hz), 0.92 (12H, d, $NCH\underline{Me}_2$, ^3J = 6.3 Hz) ppm. $^{13}C\{^1H\}$ NMR (THF-d_8, 125.7 MHz, 298 K): 171.5 ($Me\underline{C}(N^iPr)_2$), 167.3 ($\underline{C}N(N^iPr_2)$, 149.35 (br, d, $^1J_{C\text{-}F}$ = 241.5 Hz, *o*-$\underline{C}_6F_5$), 139.3 (br, d, $^1J_{C\text{-}F}$ = 244.2 Hz, *p*-$\underline{C}_6F_5$), 138.7 (Ar $CH\underline{C}(C(NMe_2)N)$), 137.3 (br, d, $^1J_{C\text{-}F}$ = 250.3 Hz, *m*-$\underline{C}_6F_5$), 131.3 ($\underline{C}_5Me_5$), 131.1 (br, d, $^2J_{C\text{-}F}$ = 7.9 Hz, *i*-$\underline{C}_6F_5$), 128.5 (Ar $\underline{C}HC(C(NMe_2)N)$), 52.0 ($\kappa^1$ and κ^2 -$N\underline{C}HMe_2$),

49.8 (κ^2 -N<u>C</u>HMe$_2$), 25.9 (κ^1- NCH<u>Me</u>$_2$), 25.5 (κ^2- NCH<u>Me</u>$_2$), 20.6 (κ^1- NCH<u>Me</u>$_2$), 13.89 (<u>Me</u>C(N^{i}Pr)$_2$), 13.59 (C$_5$<u>Me</u>$_5$) ppm. ^{19}F NMR (THF-d_8, 470.4 MHz, 298 K): -132.7 (br, *o*-C$_6$<u>F</u>$_5$), -164.9 (m, *p*-C$_6$<u>F</u>$_5$), -168.4 (m, *m*-C$_6$<u>F</u>$_5$) ppm. ^{11}B NMR (THF-d_8, 160.4 MHz, 298 K): -16.6 ppm. IR (NaCl plates, Nujol mull, cm^{-1}): 1517 (s, C=N), 980 (m), 774 (w), 682 (w). EI-MS: *m/z* = 694 (100 %, [M-2(MeC(N^{i}Pr)$_2$)]$^+$). Anal. found (calcd. for C$_{104}$H$_{96}$N$_8$F$_{40}$B$_2$Ti$_2$): C, 53.53 (53.49); H, 4.05 (4.14); N, 4.87 (4.80) %.

NMR tube scale synthesis of [1,4-C$_6$H$_4${NCN^{i}Pr$_2$}$_2$[Cp*Ti{MeC(N^{i}Pr)$_2$}$_2$[MeBF$_{15}$]$_2$

1,4-C$_6$H$_4${NCN^{i}Pr$_2$}$_2${Cp*TiMe$_2$}$_2$ (25 mg, 33 μmol) and B(C$_6$F$_5$)$_3$ (34 mg, 66 μmol) were mixed together in THF-d_8 (0.5 mL). The initial slurry went into solution and to this ^{i}PrNCN^{i}Pr (10.4 μL, 66 μmol) was added. The dark red solution transferred to an NMR tube and the NMR spectra recorded. The ^{1}H NMR spectra is identical to **7** with the addition of a resonances at 0.53 (6H, br, <u>Me</u>B(C$_6$F$_5$)$_3$) ppm. ^{19}F NMR (THF-d_8, 470.4 MHz, 298 K): -134.5 (br, *o*-C$_6$<u>F</u>$_5$), -168.5 (m, *p*-C$_6$<u>F</u>$_5$), -170.7 (m, *m*-C$_6$<u>F</u>$_5$) ppm. ^{11}B NMR (THF-d_8, 160.4 MHz, 298 K): -16.8 ppm.

HNC(Ar^{CF3})N^{i}Pr$_2$ (8)

To a THF (50 mL) solution of diisopropylamine (5.6 mL, 40 mmol) at 50 °C was added MeMgBr (11.7 mL, 3.0 M in diethyl ether, 35 mmol). Following stirring at 50 °C for 3 h, the solution was cooled to 0 °C and 4-(Trifluoromethyl)benzonitrile (6 g, 35 mmol) was added. The solution was allowed to warm to room temperature and stirred for a further 17 h. The mixture was subsequently cooled to 0 °C quenched with methanol (50 mL) and then water (100 mL). The organic phase was separated from the aqueous layer which was then back-extracted with dichloromethane (4 x 50 mL). The combined organic phases were washed with aqueous NaOH (4 M, 3 x 30 mL), dried over MgSO$_4$, filtered and the volatiles removed under reduced pressure to give a viscous orange oil. Vacuum distillation (110 °C, 1 x 10^{-1} mbar) yielded a colourless liquid which was extracted into pentane (2 x 10 mL) and dried over CaH$_2$ for 24 h. Following filtration and removal of the pentane *in vacuo* the desired product was achieved as a colourless oil. Yield = 5.2 g (55%). Diffraction quality crystals were grown from slow cooling of the product to 0 °C. ^{1}H NMR (CDCl$_3$, 400.1 MHz, 298 K): 7.62 (2H, d, ^{3}J = 8.0 Hz, *m*-C$_6$<u>H</u>$_4$), 7.37 (2H, d, ^{3}J = 8.0 Hz, *o*-C$_6$<u>H</u>$_4$), 5.75 (1H, br, N<u>H</u>), 3.56 (2H, sept, ^{3}J = 6.8 Hz, N(C<u>H</u>Me$_2$)$_2$), 1.32 (12H, d, ^{3}J = 6.8 Hz,

N(CH$\underline{Me}_2$)$_2$) ppm. ^{13}C – {^{1}H} NMR ($CDCl_3$, 100.6 MHz, 298 K): 166.6 ($\underline{C}$N(N^{i}Pr$_2$), 144.7 (*i*-$\underline{C}_6H_4$), 130.4 (q, $^2J_{C\text{-}F}$ = 32.5 Hz, *p*-$\underline{C}_6H_4$), 126.4 (*o*-$\underline{C}_6H_4$), 125.8 (q, $^3J_{C\text{-}F}$ = 3.8 Hz, *m*-$\underline{C}_6H_4$), 124.0 (q, $^1J_{C\text{-}F}$ = 272.2 Hz, $\underline{C}F_3$), 48.6 (N($\underline{C}$HMe$_2$)$_2$), 20.9 (N(CH$\underline{Me}_2$)$_2$) ppm. ^{19}F NMR ($CDCl_3$, 376.4 MHz, 298 K): -62.7 ppm. IR (NaCl plates, Nujol mull, cm^{-1}): 3316 (m, N-H) 1582 (s, C=N), 1403 (m), 1322 (s), 1220 (m), 1168 (s), 1131 (s), 1106 (s), 850 (m), 829 (m). ESI$^+$-HRMS: *m/z* = 273.1574 (calcd. for $[C_{14}H_{20}N_2F_3]^+$ *m/z* = 273.1573). Anal. found (calcd. for $C_{14}H_{19}N_2F_3$): C, 61.59 (61.75); H, 7.15 (7.03); N, 10.17 (10.29) %.

HNC(Ar^{Fc})N^{i}Pr$_2$ (9)

To a THF (50 mL) solution of diisopropylamine (0.74 mL, 5.3 mmol) at 50 °C was added MeMgBr (1.4 mL, 3.0 M in diethyl ether, 4.2 mmol). Following stirring at 50 °C for 3 h, the solution was cooled to 0 °C and 1,4-cyanophenylferrocene (0.6 g, 2.1 mmol) was added. The solution was allowed to warm to room temperature and stirred for a further 18 h. The mixture was subsequently cooled to 0 °C, quenched with methanol (50 mL) and then water (100 mL). The organic phase was separated from the aqueous layer which was then back-extracted with dichloromethane (4 x 50 mL). The combined organic phases were washed with 4M aqueous NaOH (3 x 30 mL), dried over $MgSO_4$, filtered and the volatiles removed under reduced pressure to afford an orange oil. Extraction into pentane (30 mL) and slow evaporation gave the desired product as a red crystalline solid. Yield = 0.657 g (81%). ^{1}H NMR (C_6D_6, 400.1 MHz, 293 K): 7.30 (2H, d, ^3J = 8.0 Hz, *m*-$C_6\underline{H}_4$), 7.13 (2H, d, ^3J = 8.0 Hz, *o*-$C_6\underline{H}_4$), 6.07 (1H, br, N$\underline{H}$), 4.45 (2H, m, Cp *o*-$C_5\underline{H}_4$), 4.12 (2H, m, Cp *m*-$C_5\underline{H}_4$), 3.88 (5H, s, $C_5\underline{H}_5$FeCp(C_6H_4)), 3.51 (2H, sept, ^3J = 6.5 Hz, N(C$\underline{H}$Me$_2$)$_2$), 1.32 (12H, d, ^3J = 6.6 Hz, N(CH$\underline{Me}_2$)$_2$) ppm. ^{13}C – {^{1}H} NMR (C_6D_6, 100.6 MHz, 293 K): 167.5 (C($\underline{C}$(N^{i}Pr$_2$)N), 139.8 (*p*-$\underline{C}_6H_4$), 139.7 (*i*-$\underline{C}_6H_4$), 126.5 (*m*-$\underline{C}_6H_4$), 126.3 (*o*-$\underline{C}_6H_4$), 85.2 (Cp *i*-$\underline{C}_5H_4$), 70.0 (Cp $\underline{C}_5H_5$FeCpC_6H_4), 69.4 (Cp *m*-$\underline{C}_5H_4$), 67.0 (Cp *o*-$\underline{C}_5H_4$), 48.6 (N($\underline{C}$HMe$_2$)$_2$), 21.0 (N(CH$\underline{Me}_2$)$_2$) ppm. IR (NaCl plates, Nujol mull, cm^{-1}): 1574 (s, C=N), 1220 (m), 1075 (w), 817 (m). ESI$^+$-HRMS: *m/z* = 389.16742 (calcd. For $[C_{23}H_{29}N_2Fe]^+$ *m/z* = 389.16747). Anal. found (calcd. for $C_{25}H_{34}N_2Fe$): C, 71.68 (71.77); H, 8.06 (2.19); N, 6.77 (6.70) %.

HNC(Ar^{tBu})N^{i}Pr$_2$ (10)

To a toluene (30 mL) solution of diisopropylamine (1.75 mL, 13 mmol) at 50 °C was added MeMgBr (3.14 mL, 3.0 M in diethyl ether, 9.4 mmol). Following stirring at 50 °C for 3 h, the solution was cooled to 0 °C and 4-tert-Butylbenzonitrile (1 g, 6.3 mmol) was added. The solution was warmed to room temperature and stirred at for a further 24 h. The mixture was subsequently cooled to 0 °C, quenched with methanol (50 mL) and then water (100 mL). The organic phase was separated from the aqueous layer which was then back-extracted with dichloromethane (4 x 50 mL). The combined organic phases were washed with aqueous NaOH (4 M, 3 x 30 mL), dried over $MgSO_4$, filtered and the volatiles removed under reduced pressure to give a viscous pale yellow oil, which crystallised on standing. Yield = 1.33g (81%). ^{1}H NMR (C_6D_6, 400.1 MHz, 298 K): 6.96 (2H, d, ^{3}J = 8.3 Hz, *m*-$C_6\underline{H}_4$), 6.90 (2H, d, ^{3}J = 8.3 Hz, *o*-$C_6\underline{H}_4$), 5.89 (1H, b, N$\underline{H}$), 3.24 (2H, sept, ^{3}J = 6.7 Hz, N(C$\underline{H}$Me$_2$)$_2$), 1.05 (12H, d, ^{3}J = 6.8 Hz, N(CH$\underline{Me}_2$)$_2$), 0.94 (9H, s, C$\underline{Me}_3$) ppm. ^{13}C – {^{1}H} NMR (C_6D_6, 100.6 MHz, 298 K): 167.6 (N$\underline{C}$N(N^{i}Pr$_2$)), 150.8 (*p*-$\underline{C}_6H_4$), 139.7 (*i*-$\underline{C}_6H_4$), 126.0 (*o*-$\underline{C}_6H_4$), 125.6 (*m*-$\underline{C}_6H_4$), 48.5 (N($\underline{C}$HMe$_2$)$_2$), 34.6 (C$\underline{Me}_3$), 31.5 (C$\underline{Me}_3$), 21.0 (N(CH$\underline{Me}_2$)$_2$) ppm. IR (NaCl plates, Nujol mull, cm^{-1}): 3262 (m, N-H), 2360 (w), 1910 (w), 1581 (s, C=N), 1221 (s), 1180 (m), 116 (m), 870 (w). ESI$^+$-HRMS: *m/z* = 261.23269 (calcd. for $[C_{17}H_{29}N_2]^+$ *m/z* = 261.23253). Anal. found (calcd. for $C_{17}H_{28}N_2$): C, 78.45 (78.41); H, 11.01 (10.84); N, 10.62 (10.76) %.

HNC(Ar^{NMe2})N^{i}Pr$_2$ (11)

To a THF (30 mL) solution of diisopropylamine (5.74 mL, 41 mmol) at 50 °C was added MeMgBr (11.4 mL, 3.0 M in diethyl ether, 34 mmol). Following stirring at 50 °C for 3 h, the solution was cooled to 0 °C and 4–(Dimethylamino)benzonitrile (2 g, 13.6 mmol) was added. The solution was warmed to room temperature and stirred for a further 24 h. The mixture was subsequently cooled to 0 °C, quenched with methanol (50 mL) and then water (100 mL). The organic phase was separated from the aqueous layer which was then back-extracted with dichloromethane (4 x 50 mL). The combined organic phases were washed with aqueous NaOH (4 M, 3 x 30 mL), dried over $MgSO_4$, filtered and the volatiles removed under reduced pressure to give a pale yellow solid. Yield = 2.85 g (84%). ^{1}H NMR ($CDCl_3$, 400.1 MHz, 298 K): 7.14 (2H, d, ^{3}J = 8.6 Hz, *o*-$C_6\underline{H}_4$), 6.66 (2H, d, ^{3}J = 8.6 Hz, *m*-$C_6\underline{H}_4$), 5.87 (1H, br, NH), 3.67 (2H, sept, ^{3}J = 6.8 Hz, N(C$\underline{H}$Me$_2$)$_2$), 2.96 (6H, s, N$\underline{Me}_2$), 1.30 (12H, d, ^{3}J = 6.8

Hz, N(CH<u>Me</u>$_2$)$_2$) ppm. ^{13}C – {^{1}H} NMR ($CDCl_3$, 100.6 MHz, 298 K): 169.1 (<u>C</u>N(N^iPr_2), 150.3 (*p*-<u>C</u>$_6$H$_4$), 129.8 (*i*-<u>C</u>$_6$H$_4$), 127.2 (*o*-<u>C</u>$_6$H$_4$), 111.8 (*m*-<u>C</u>$_6$H$_4$), 48.3 (N(<u>C</u>HMe$_2$)$_2$), 40.5 (N<u>Me</u>$_2$), 21.2 (N(CH<u>Me</u>$_2$)$_2$) ppm. IR (NaCl plates, Nujol mull, cm^{-1}): 3262 (s, N-H), 1581 (s, C=N), 1221 (m), 1201 (w), 1180 (w), 1148 (w), 1132 (w), 841 (m). ESI$^+$-HRMS: *m/z* = 261.23269 (calcd. for $[C_{17}H_{29}N_2]^+$ *m/z* = 261.23253). Anal. found (calcd. for $C_{17}H_{28}N_2$): C, 78.45 (78.41); H, 11.01 (10.84); N, 10.62 (10.76) %.

[1,4-C_6H_4(CN)(NMe_3)][Cl] (12)

To a stirring acetonitrile (50 mL) solution of [1,4-C_6H_4(CN)(NMe_3)][I] (4.69 g, 16 mmol) was added freshly prepared AgCl (2.81 g, 19 mmol) in the absence of light. The solution was stirred for 3 h after which time a large amount of white precipitate was observed. The solution was filtered and distilled water (50 mL) was added to the remaining solid and stirred for a further 1 h. The solid turned a pale yellow colour and the solution filtered. The volatiles were removed under reduced pressure to generate the title compound as a white solid. Yield = 2.4 g (75%). ^{1}H NMR (DMSO-d_6, 400.1 MHz, 298 K): 8.25 (2H, d, ^{3}J = 9.4 Hz, C<u>H</u>CCN), 8.20 (2H, d, ^{3}J = 9.4 Hz, C<u>H</u>CNMe_3), 3.67 (9H, s, N<u>Me</u>$_3$) ppm. ^{13}C{^{1}H} NMR (DMSO-d_6, 100.6 MHz, 298 K): 150.3 (CH<u>C</u>NMe_3), 134.2 (CH<u>C</u>CN), 122.2 (<u>C</u>HCNMe_3), 117.4 (C<u>C</u>N), 113.1 (CH<u>C</u>CN), 56.3 (N<u>Me</u>$_3$) ppm. IR (NaCl plates, Nujol mull, cm^{-1}): 2229 (s, C≡N), 1600 (m), 1501 (m), 1421 (s), 1290 (w), 962 (w), 940 (w). ESI$^+$-HRMS: *m/z* = 161.10735 (calcd. for $[C_{10}H_{13}N_2]^+$ *m/z* = 161.10732). Anal. found (calcd. for $C_{10}H_{13}N_2Cl_1$): C, 60.84 (61.07); H, 6.71 (6.66); N, 14.17 (14.24) %.

[1,4-C_6H_4(CN)(NMe_3)][BF_{20}] (13)

To a stirring acetonitrile (100 mL) solution of [1,4-C_6H_4(CN)(NMe_3)][Cl] (1.26 g, 6.4 mmol) was added TBF_{20} (6.57 g, 7.1 mmol). The pale yellow solution was stirred for 1 h after which time solution was filtered and the volatiles were removed under reduced pressure. The solid was washed with dichloromethane (4 x 20 mL) and extracted into acetone (2 x 10 mL). The volatiles were removed under reduced pressure to give the title compound as a white crystalline powder. Yield = 4.52 g (83 %). ^{1}H NMR (acetone-d_6, 400.1 MHz, 298 K): 8.39, 2H, d, ^{3}J = 9.1 Hz, C<u>H</u>CNMe_3), 8.17 (2H, d, ^{3}J = 9.1 Hz, C<u>H</u>CCN), 4.03 (9H, s, N<u>Me</u>$_3$) ppm. ^{13}C{^{1}H} NMR (acetone-d_6, 100.6 MHz, 298 K): 151.2 (CH<u>C</u>NMe_3), 149.1 (br, d, $^1J_{C-F}$ = 237.8

Hz, *o*-$\underline{C}_6F_5$), 139.1 (br, d, $^1J_{C-F}$ = 245.4 Hz, *p*-$\underline{C}_6F_5$), 137.1 (br, d, $^1J_{C-F}$ = 250.5 Hz, *m*-$\underline{C}_6F_5$), 135.3 ($\underline{C}$HCCN), 122.9 ($\underline{C}$HCNMe$_3$), 117.6 ($\underline{C}$N), 115.6 (CH$\underline{C}$CN), 58.0 (N$\underline{Me}_3$) ppm. *i*-$\underline{C}_6F_5$ could not be observed. ^{19}F NMR (acetone-d_6, 376.4 MHz, 298 K): -133.1 (br, *o*-$C_6\underline{F}_5$), -164.4 (m, *p*-$C_6\underline{F}_5$), -168.4 (br, , *m*-$C_6\underline{F}_5$) ppm. ^{11}B NMR ($(CD_3)_2CO$, 128 MHz, 298 K): -16.7 ppm. IR (NaCl plates, Nujol mull, cm^{-1}): 2360 (w), 2236 (m, C≡N), 1698 (m), 1515 (s), 979 (s). ESI$^+$-HRMS: *m/z* = 161.10737 (calcd. for $[C_{10}H_{13}N_2]^+$ *m/z* = 161.10732). ESI$^-$-HRMS: *m/z* = 678.9779 (calcd. for $[C_{24}F_{20}B]^-$ *m/z* = 678.9779). Anal. found (calcd. for $C_{34}H_{13}N_2B_1F_{20}$): C, 48.74 (48.60); H, 1.38 (1.56); N, 3.21 (3.33) %.

Cp*Ti{NC(Ar^{CF3})N^{i}Pr$_2$}Me$_2$ (14)

To a stirring benzene (25 mL) solution of Cp*TiMe$_3$ (0.419 g, 1.84 mmol) was added a benzene (10 mL) solution of HNC(Ar^{CF3})N^{i}Pr$_2$ (0.5 g, 1.84 mmol). The brown solution was stirred for 17 h. The volatiles were removed *in vacuo* to afford a brown oil which was cooled to -78 °C, washed with hexane (3 x 15 mL) and dried *in vacuo* to yield the desired compound as a brown solid. Yield = 0.35 g (40%).^{1}H NMR (Tol-d_8, 499.9 MHz, 233 K): 7.20 (2H, br, *m*-$C_6\underline{H}_4$), 7.06 (2H, br, *o*-$C_6\underline{H}_4$), 3.33 (2H, br, N($C\underline{H}Me_2)_2$), 2.93 (1H, br, N($C\underline{H}Me_2)_2$), 1.73 (15H, s, $C_5\underline{Me}_5$), 1.65 (6H, br, N($CH\underline{Me}_2)_2$), 0.64 (6H, br, N($CH\underline{Me}_2)_2$), 0.43 (6H, s, Ti$\underline{Me}_2$) ppm. ^{13}C – {^{1}H} NMR (Tol-d_8, 125.7 MHz, 233 K): 159.4 ($\underline{C}$N(N^{i}Pr$_2$), 145.3 (*i*-$\underline{C}_6H_4$), 129.6 (q, $^2J_{C-F}$ = 32.4 Hz, *p*-$\underline{C}_6H_4$), 126.9 (*o*-$\underline{C}_6H_4$), 125.7 (br overlapping, *m*-$\underline{C}_6H_4$), 125.2 (q, $^1J_{C-F}$ = 272.0 Hz, $\underline{C}F_3$), 119.9 ($\underline{C}_5Me_5$), 52.3 (N($\underline{C}HMe_2)_2$), 49.2 (Ti$\underline{Me}_2$), 47.2 (N($\underline{C}HMe_2)_2$), 20.5 (br overlapping, N($CH\underline{Me}_2)_2$), 12.1 ($C_5\underline{Me}_5$) ppm. ^{19}F NMR (Tol-d_8, 470.4 MHz, 233 K): -61.8 ppm. IR (NaCl plates, Nujol mull, cm^{-1}): 1567 (s, C=N), 1322 (s), 1320 (s), 1168 (m), 1132 (m), 890 (w), 839 (w). EI-MS: *m/z* = 469 (100 %, [M – Me]$^+$), 454 (100 %, [M – 2Me]$^+$) Anal. found (calcd. for $C_{26}H_{39}N_2F_3Ti$): C, 64.60 (64.46); H, 8.17 (8.11); N, 5.90 (5.78) %.

Cp*Ti{NC(Ar^{Fc})N^{i}Pr$_2$}Me$_2$ (15)

To a benzene (25 mL) solution of Cp*TiMe$_3$ (0.25 g, 1.1 mmol) was added a benzene (10 mL) solution of {1,4-C_6H_4-C(NH)N^{i}Pr$_2$}ferrocene (0.42 g, 1.1 mmol). The red solution was stirred for 16 h. The volatiles were removed *in vacuo* to afford a solid which was washed with hexane (3 x 15 mL) and dried *in vacuo* to yield the desired compound as an orange solid. Yield = 0.46 g (64%). Diffraction quality crystals were

grown from a toluene solution at 0 °C. ^{1}H NMR (THF-d_8, 499.9 MHz, 223 K): 7.51 (2H, d, ^{3}J = 8.1 Hz, *m*-$C_6\underline{H}_4$), 7.20 (2H, d, ^{3}J = 7.9 Hz, *o*-$C_6\underline{H}_4$), 4.78 (2H, br, Cp *o*-$C_5\underline{H}_4$), 4.33 (2H, br, Cp *m*-$C_5\underline{H}_4$), 4.01 (5H, s, $C_5\underline{H}_5FeCp(C_6H_4)$), 3.90 (1H, br, $N(C\underline{H}Me_2)_2$), 3.64 (1H, br, $N(C\underline{H}Me_2)_2$), 1.73 (6H, br, $N(CH\underline{Me}_2)_2$), 1.69 (15H, s, $C_5\underline{Me}_5$), 1.20 (6H, br, $N(CH\underline{Me}_2)_2$), -0.14 (6H, s, $Ti\underline{Me}_2$) ppm. ^{13}C – {^{1}H} NMR (THF-d_8, 499.9 MHz, 223 K): 162.5 ($C(\underline{C}(N^iPr_2)N$), 140.0 (*i*-$\underline{C}_6H_4$), 139.7 (*p*-$\underline{C}_6H_4$), 127.1 (*o*-$\underline{C}_6H_4$), 126.2 (*m*-$\underline{C}_6H_4$), 119.2 ($\underline{C}_5Me_5$), 85.1 (Cp *i*-$\underline{C}_5H_4$), 70.4 (Cp $\underline{C}_5H_5FeCpC_6H_4$), 70.1 (Cp *m*-$\underline{C}_5H_4$), 67.1 (Cp *o*-$\underline{C}_5H_4$), 53.0 ($N(\underline{C}HMe_2)_2$), 47.4 ($N(\underline{C}HMe_2)_2$), 46.5 ($Ti\underline{Me}_2$), 20.1 ($N(CH\underline{Me}_2)_2$), 20.5 ($N(CH\underline{Me}_2)_2$), 12.0 ($C_5\underline{Me}_5$) ppm. IR (NaCl plates, Nujol mull, cm^{-1}): 1566 (s, C=N), 1324 (m), 1032 (m), 885 (w), 832 (w). EI-MS: 261 (25 % $[FeCp_2Ph]^+$). Anal. found (calcd. for $C_{35}H_{48}N_2FeTi$): C, 69.93 (70.01); H, 8.16 (8.06); N, 4.52 (4.67) %.

$Cp^*Ti\{NC(Ar^{tBu})N^iPr_2\}Cl_2$ (16)

To a stirring benzene (20 mL) suspension of Cp^*TiCl_3 (1.04 g, 3.6 mmol) and $HNC(Ar^{tBu})N^iPr_2$ (0.94 g, 3.6 mmol) was added an excess of triethylamine (3 mL, 21 mmol). The orange/red mixture was stirred for 20 h after which time the volatiles were removed *in vacuo* to result in a deep red solid. The solid was extracted into benzene (3 x 10 mL) and the volatiles removed *in vacuo* to give the desired compound. Yield = 1.54 g (83%). Diffraction quality crystals were grown from an hexane solution at 0 °C. ^{1}H NMR (CD_2Cl_2, 499.9 MHz, 243 K): 7.39 (2H, d, ^{3}J = 8.3 Hz, *m*-$C_6\underline{H}_4$), 7.30 (2H, d, ^{3}J = 8.2 Hz, *o*-$C_6\underline{H}_4$), 3.91 (2H, br, $N(C\underline{H}Me_2)_2$), 3.58 (1H, br, $N(C\underline{H}Me_2)_2$), 1.76 (15H, s, $C_5\underline{Me}_5$), 1.58 (6H, d, ^{3}J = 6.4 Hz, $N(CH\underline{Me}_2)_2$), 1.28 (9H, s, $C\underline{Me}_3$), 1.14 (6H, d, ^{3}J = 6.5 Hz, $N(CH\underline{Me}_2)_2$) ppm. ^{13}C – {^{1}H} NMR (CD_2Cl_2, 125.7 MHz, 243 K): 166.2 ($C(\underline{C}(N^iPr_2)N$), 152.3 (*p*-$\underline{C}_6H_4$), 135.1 (*i*-$\underline{C}_6H_4$), 126.8 (*o*-$\underline{C}_6H_4$), 126.7 ($\underline{C}_5Me_5$), 125.4 (*m*-$\underline{C}_6H_4$), 53.3 ($N(\underline{C}HMe_2)_2$), 48.0 ($N(\underline{C}HMe_2)_2$), 34.9 ($\underline{C}Me_3$), 31.1 ($C\underline{Me}_3$), 20.7 ($N(CH\underline{Me}_2)_2$), 19.9 ($N(CH\underline{Me}_2)_2$), 12.4 ($C_5\underline{Me}_5$) ppm. IR (NaCl plates, Nujol mull, cm^{-1}): 2360 (w), 1525 (s, C=N), 1338 (w), 982 (s), 874 (s). EI-MS: *m/z* = 477 (100 %, $[M - Cl]^+$). Anal. found (calcd. for $Ti_1\ Cl_2\ N_2\ C_{27}H_{42}$): C, 63.31 (63.16); H, 8.19 (8.25); N, 5.48 (5.46) %.

$Cp^{*}Ti\{NC(Ar^{NMe2})N^{i}Pr_2\}Cl_2$ (17)

To a stirring benzene (20 mL) suspension of $CpTiCl_3$ (0.99 g, 3.6 mmol) and $HNC(Ar^{NMe2})N^{i}Pr_2$ (0.85 g, 3.6 mmol) was added an excess of triethylamine (2.4 mL, 21 mmol). The orange/red mixture was stirred for 20 h after which time the volatiles were removed under reduced pressure and the solid extracted into benzene (3 x 10 mL). The volatiles were removed under reduced pressure and the solid was washed with hexane (3 x 10 mL) and dried *in vacuo* affording the desired compound as a red solid. Yield = 1.35 g (79%). Diffraction quality crystals were grown from an hexane solution at -30 °C. ^{1}H NMR (CD_2Cl_2, 499.9 MHz, 213 K): 7.23 (2H, d, ^{3}J = 8.3 Hz, *o*-$C_6\underline{H}_4$), 6.61 (2H, d, ^{3}J = 8.4 Hz, *m*-$C_6\underline{H}_4$), 3.98 (2H, m, $N(C\underline{H}Me_2)_2$), 3.50 (1H, m, $N(C\underline{H}Me_2)_2$), 2.94 (6H, s, $N\underline{Me}_2$), 1.76 (15H, s, $C_5\underline{Me}_5$), 1.55 (6H, d, ^{3}J = 6.1 Hz, $N(CH\underline{Me}_2)_2$), 1.11 (6H, d, ^{3}J = 6.4 Hz, $N(CH\underline{Me}_2)_2$) ppm. $^{13}C - \{^{1}H\}$ NMR (CD_2Cl_2, 125.7 MHz, 213 K): 167.1 ($\underline{C}N(N^{i}Pr_2)$, 150.3 (*p*-$\underline{C}_6H_4$), 128.5 (*o*-$\underline{C}_6H_4$), 126.0 ($\underline{C}_5Me_5$), 124.8 (*i*-$\underline{C}_6H_4$), 110.7 (*m*-$\underline{C}_6H_4$), 53.2 ($N(\underline{C}HMe_2)_2$), 47.6 ($N(\underline{C}HMe_2)_2$), 40.3 ($N\underline{Me}_2$), 20.5 ($N(CH\underline{Me}_2)_2$), 19.6 ($N(CH\underline{Me}_2)_2$), 12.3 ($C_5\underline{Me}_5$) ppm. IR (NaCl plates, Nujol mull, cm^{-1}): 1608 (m), 1508 (s, C=N), 1340 (m), 1200 (w), 1156 (w), 894 (m). EI-MS: *m/z* = 464 (50 %, $[M - Cl]^{+}$), 399 (100 %, $[M - N^{i}Pr_2]^{+}$). Anal. found (calcd. for $Ti_1Cl_2N_3C_{25}H_{39}$): C, 59.83 (60.01); H, 7.87 (7.86); N, 8.27 (8.40) %.

$Cp^{*}Ti\{NC(Ar^{tBu})N^{i}Pr_2\}Me_2$ (18)

To a stirring toluene (15 mL) solution of $Cp^{*}Ti\{NC(Ar^{tBu})N^{i}Pr_2\}Cl_2$ (0.49 g, 0.94 mmol) was added dropwise MeLi (1.2 mL, 1.6 M in diethyl ether, 1.87 mmol) and an immediate colour change of red to yellow was observed. The resulting solution was stirred for 16 h after which time the volatiles were removed *in vacuo*. The yellow solid was then extracted into hexane (2 x 15 mL) and the volatiles removed *in vacuo* to yield the desired compound as a yellow solid. Yield = 0.23 mg (48%). Diffraction quality crystals were grown from a hexane solution at 0 °C. ^{1}H NMR (Tol-d_8, 499.9 MHz, 223 K): 7.25 (2H, d, ^{3}J = 8.0 Hz, *o*-$C_6\underline{H}_4$), 7.10 (2H, d, ^{3}J = 8.2 Hz, *m*-$C_6\underline{H}_4$), 3.75 (2H, br, $N(C\underline{H}Me_2)_2$), 2.93 (1H, br, $N(C\underline{H}Me_2)_2$), 1.84 (15H, s, $C_5\underline{Me}_5$), 1.77 (6H, br, $N(CH\underline{Me}_2)_2$), 1.18 (9H, s, $C\underline{Me}_3$), 0.68 (6H, br, $N(CH\underline{Me}_2)_2$), 0.59 (6H, s, $Ti\underline{Me}_2$) ppm. $^{13}C - \{^{1}H\}$ NMR (Tol-d_8, 125.7 MHz, 223 K): 161.9 ($C(\underline{C}(N^{i}Pr_2)N$), 150.9 (*p*-$\underline{C}_6H_4$), 140.2 (*i*-$\underline{C}_6H_4$), 126.6 (*o*-$\underline{C}_6H_4$), 125.9 (*m*-$\underline{C}_6H_4$), 119.4 ($\underline{C}_5Me_5$), 52.3 ($N(\underline{C}HMe_2)_2$), 48.0 ($Ti\underline{Me}_2$), 47.2 ($N(\underline{C}HMe_2)_2$), 35.0 ($\underline{C}Me_3$), 31.6 ($C\underline{Me}_3$), 20.7 ($N(CH\underline{Me}_2)_2$), 20.5 ($N(CH\underline{Me}_2)_2$), 12.2 ($C_5\underline{Me}_5$) ppm. IR (NaCl plates, Nujol mull,

cm^{-1}): 1549 (s, C=N), 1327 (m), 1156 (w), 889 (w), 830 (w). EI-MS: *m/z* = 457 (10 %, $[M - Me]^+$). Anal. found (calcd. for Ti_1 N_2 $C_{29}H_{48}$): C, 73.43 (73.71); H, 10.41 (10.24); N, 5.81 (5.93) %.

$Cp^*Ti\{NC(Ar^{NMe2})N^iPr_2\}Me_2$ (19)

To a stirring benzene (25 mL) solution of $Cp^*Ti\{NC(Ar^{NMe2})N^iPr_2\}Cl_2$ (0.6 g, 1.19 mmol) was added dropwise MeLi (1.5 mL, 1.6 M in diethyl ether, 2.4 mmol) and an immediate colour change of red to yellow was observed. The resulting solution was stirred for 16 h after which time the volatiles were removed *in vacuo*. The yellow solid was extracted into hexane (2 x 15 mL) and concentrated to *ca.* 15 mL, storage at -30 °C for 24 h resulted in crystallisation of the desired compound as yellow crystals which were isolated and dried *in vacuo*. Yield = 0.32 mg (58%). ^{1}H NMR (Tol-d_8, 499.9 MHz, 213 K): 7.33 (2H, d, ^3J = 8.2 Hz, *o*-$C_6\underline{H}_4$), 6.38 (2H, d, ^3J = 8.2 Hz, *m*-$C_6\underline{H}_4$), 3.99 (2H, br, $N(C\underline{H}Me_2)_2$), 2.94 (1H, br, $N(C\underline{H}Me_2)_2$), 2.98 (6H, s, $N\underline{Me}_2$), 1.92 (15H, s, $C_5\underline{Me}_5$), 1.81 (6H, br, $N(CH\underline{Me}_2)_2$), 0.78 (6H, br, $N(CH\underline{Me}_2)_2$), 0.66 (6H, s, $Ti\underline{Me}_2$) ppm. ^{13}C – {^{1}H} NMR (Tol-d_8, 125.7 MHz, 213 K): 163.0 ($\underline{C}N(N^iPr_2)$, 150.3 (*p*-$\underline{C}_6H_4$), 130.7 (*i*-$\underline{C}_6H_4$), 128.4 (*o*-$\underline{C}_6H_4$), 119.2 ($\underline{C}_5Me_5$), 111.5 (*m*-$\underline{C}_6H_4$), 52.4 ($N(\underline{C}HMe_2)_2$), 47.1 ($Ti\underline{Me}_2$), 47.1 (overlapping, $N(\underline{C}HMe_2)_2$), 40.3 ($N\underline{Me}_2$), 21.0 ($N(CH\underline{Me}_2)_2$), 20.8 ($N(CH\underline{Me}_2)_2$), 12.4 ($C_5\underline{Me}_5$) ppm. IR (NaCl plates, Nujol mull, cm^{-1}): 1610 (m), 1558 (m), 1541 (s, C=N), 1327 (m), 1201 (w), 1156 (m), 890 (w). EI-MS: *m/z* = 120 (10 %, $[PhNMe_2]^+$). Anal. found (calcd. for Ti_1 N_3 C_{27} H_{45}): C, 70.36 (70.57); H, 10.01 (9.87); N, 8.96 (9.14) %.

NMR tube scale synthesis of $[Cp^*Ti\{NC(Ar^{CF3})\}\{MeC(N^iPr)_2\}][MeB(C_6F_5)_3]$ (20)

To a solution of $Cp^*Ti\{NC(Ar^{CF3})N^iPr_2\}Me_2$ (29 mg, 60 μmol) and ^{i}PrNCN^{i}Pr (9.4 μL, 60 μmol) in C_6D_5Br (0.5 mL) was added $B(C_6F_5)_3$ (31 mg, 60 μmol) resulting in the formation of a dark red solution. The solution was transferred to an NMR tube and the NMR spectra recorded after 5 mins. ^{1}H NMR (C_6D_5Br, 499.9 MHz, 298 K): 7.71 (2H, br, $C_6\underline{H}_4$), 7.33 (2H, br, $C_6\underline{H}_4$), 3.50 (4H, m, $NC\underline{H}Me_2$), 2.10 (3H, s, $\underline{Me}C(N^iPr)_2$), 1.99 (15H, s, $C_5\underline{Me}_5$), 1.32 ($\underline{Me}B(C_6F_5)_3$), 1.30 (6H, br, $NCH\underline{Me}_2$), 1.01 (6H, br, $NCH\underline{Me}_2$), 0.95 (6H, br, $NCH\underline{Me}_2$) 0.59 (6H, br, $NCH\underline{Me}_2$) ppm. ^{19}F NMR (C_6D_5Br, 470.4 MHz, 298 K): -62.13 (s, CF_3), -131.39 (m, *o*-$C_6\underline{F}_5$), -163.82 (m, *p*-$C_6\underline{F}_5$), -166.28 (m, *m*-$C_6\underline{F}_5$) ppm. ^{11}B NMR (C_6D_5Br, 160.4 MHz, 298 K): -14.2 ppm.

NMR tube scale synthesis of [Cp*Ti{NC(Ar^{NMe2})}{MeC(N^{i}Pr)$_2$}][MeB(C$_6$F$_5$)$_3$] (21)

To a solution of Cp*Ti{NC(Ar^{NMe2})N^{i}Pr$_2$}Me$_2$ (8 mg, 17 μmol) and ^{i}PrNCN^{i}Pr (2.7 μL, 17 μmol) in C$_6$D$_5$Br (0.5 mL) was added B(C$_6$F$_5$)$_3$ (8.9 mg, 17 μmol) resulting in the formation of a dark red solution. The solution was transferred to an NMR tube and the NMR spectra recorded after 5 mins. ^{1}H NMR (C$_6$D$_5$Br, 499.9 MHz, 298 K): 7.09 (2H, d, ^{3}J = 6.5 Hz, C$_6$H$_4$), 7.33 (2H, d, ^{3}J = 7.2 Hz, C$_6$H$_4$), 3.58 (4H, m, NCHMe$_2$), 2.86 (6H, s, NMe$_2$), 2.10 (3H, s, MeC(N^{i}Pr)$_2$), 2.00 (15H, s, C$_5$Me$_5$), 1.36 (3H, br, MeB(C$_6$F$_5$)$_3$), 1.28 (12H, br, NCHMe$_2$), 1.08 (6H, br, NCHMe$_2$), 0.81 (6H, br, NCHMe$_2$) ppm. ^{19}F NMR (C$_6$D$_5$Br, 470.4 MHz, 298 K): -131.40 (m, *o*-C$_6$F$_5$), -163.94 (m, *p*-C$_6$F$_5$), -166.34 (m, *m*-C$_6$F$_5$) ppm. ^{11}B NMR (C$_6$D$_5$Br, 160.4 MHz, 298 K): -14.2 ppm.

NMR tube scale synthesis of [Cp*Ti{NC(Ar^{Fc})N^{i}Pr$_2$}Me][MeBF$_{15}$] (22)

Cp*Ti{NC(Ar^{Fc})N^{i}Pr$_2$}Me$_2$ (9.7 mg, 16.2 μmol) and B(C$_6$F$_5$)$_3$ (8.3 mg, 16.2 μmol) were mixed together in C$_6$D$_5$Br (0.5 mL) resulting in a dark red solution. The solution was transferred to an NMR tube and the NMR spectra recorded after 5 mins. ^{1}H NMR (C$_6$D$_5$Br, 499.9 MHz, 298 K): 7.58 (2H, d, ^{3}J = 8.3 Hz, *m*-C$_6$H$_4$), 7.07 (2H, br, *o*-C$_6$H$_4$), 4.79 (2H, br, CpFeC$_5$H$_4$(C$_6$H$_4$)), 4.45 (2H, br, CpFeC$_5$H$_4$(C$_6$H$_4$)), 4.19 (5H, br, C$_5$H$_5$FeCp(C$_6$H$_4$)), 3.85 (2H, m, NCHMe$_2$), 3.76 (2H, br, NCHMe$_2$), 1.82 (15H, s, C$_5$Me$_5$), 1.53 (6H, br, NCHMe$_2$), 1.12 (3H, TiMe), 1.05 (6H, br, NCHMe$_2$), 0.73 (3H, br, MeB(C$_6$F$_5$)$_3$) ppm. ^{19}F NMR (C$_6$D$_5$Br, 470.4 MHz, 298 K): -131.99 (br, *o*-C$_6$F$_5$), -159.32 (br, *p*-C$_6$F$_5$), -164.02 (br, *m*-C$_6$F$_5$) ppm. ^{11}B NMR (C$_6$D$_5$Br, 160.4 MHz, 298 K): -13.7 ppm.

NMR tube scale synthesis of [Cp*Ti{NC(Ar^{tBu})N^{i}Pr$_2$}Me][MeBF$_{15}$] (23)

Cp*Ti{NC(Ar^{tBu})N^{i}Pr$_2$}Me$_2$ (10 mg, 21.2 μmol) and B(C$_6$F$_5$)$_3$ (10.8 mg, 21.2 μmol) were mixed together in C$_6$D$_5$Br (0.5 mL) resulting in the formation of a dark red solution. The solution was transferred to an NMR tube and the NMR spectra recorded after 5 mins. ^{1}H NMR (C$_6$D$_5$Br, 499.9 MHz, 298 K): 7.48 (2H, d, ^{3}J = 6.9 Hz, *m*-C$_6$H$_4$), 7.10 (2H, br, *o*-C$_6$H$_4$), 3.87 (2H, m, NCHMe$_2$), 3.65 (2H, br, NCHMe$_2$), 1.77 (15H, s, C$_5$Me$_5$), 1.67 (6H, br, NCHMe$_2$), 1.43 (9H, s, CMe$_3$), 1.11(3H, TiMe), 1.00 (6H, d, ^{3}J = 6.2 Hz NCHMe$_2$), 0.68 (3H, br, MeB(C$_6$F$_5$)$_3$) ppm. ^{19}F NMR (C$_6$D$_5$Br,

470.4 MHz, 298 K): -131.93 (br, *o*-$C_6\underline{F}_5$), -159.34 (br, *p*-$C_6\underline{F}_5$), -164.02 (br, *m*-$C_6\underline{F}_5$) ppm. ^{11}B NMR (C_6D_5Br, 160.4 MHz, 298 K): -13.8 ppm.

6.7 Experimental details and characterising data for Chapter Three

6.7.1 Ligand numbering system for Chapter Three

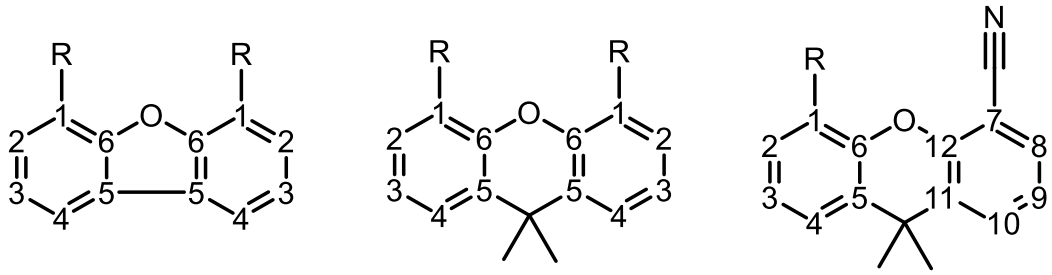

6.7.2 Experimental details and characterising data for Chapter Three

DBF(C(NH)N^{i}Pr$_2$)$_2$ (24)

To a THF (50 mL) solution of diisopropylamine (7 mL, 50 mmol) at 50 °C was added MeMgBr (15.2 mL, 3.0 M in diethyl ether, 45.6 mmol). Following stirring at 50 °C for 3 h, the solution was cooled to 0 °C and $DBF(CN)_2$ (1 g, 4.6 mmol) was added. The solution was allowed to warm to room temperature and stirred for a further 3 h. The mixture was subsequently cooled to 0 °C, quenched with methanol (50 mL) and then water (100 mL). The organic phase was separated from the aqueous layer which was then back-extracted with dichloromethane (4 x 50 mL). The combined organic phases were washed with aqueous NaOH (4 M, 3 x 30 mL), dried over $MgSO_4$, filtered and the volatiles removed under reduced pressure. Yield = 1.56 g (81%). Diffraction quality crystals were grown from a concentrated pentane solution at room temperature. ^{1}H NMR (C_6D_6, 299.9 MHz, 293 K): 7.53 (2H, dd, Ar-4, ^{3}J = 7.7 Hz, ^{3}J = 1.3 Hz), 7.21 (2H, dd, Ar-2, ^{3}J = 7.5 Hz, ^{3}J = 1.3 Hz), 7.02 (2H, t, Ar-3 , ^{3}J = 7.6 Hz), 3.49 (4H, sept, N(C$\underline{H}$Me$_2$)$_2$, ^{3}J = 7.0 Hz), 1.42 (24H, d, N(CH$\underline{Me}_2$)$_2$, ^{3}J = 6.0 Hz) ppm (NH not observed). ^{13}C{^{1}H} NMR (C_6D_6, 75.4 MHz, 293 K): 161.8 ($\underline{C}$N(N^{i}Pr$_2$), 151.7 (Ar-6), 126.9 (Ar-1), 125.8 (Ar-2), 124.5(Ar-5), 123.8(Ar-3), 120.3(Ar-4,), 49.0 (N($\underline{C}$HMe$_2$)$_2$), 20.8 (N(CH$\underline{Me}_2$)$_2$) ppm. IR (NaCl plates, Nujol mull, cm^{-1}): 3314 (m, N-H), 1577 (s, C=N), 1231 (m), 1033 (m), 802 (s), 772 (s). ESI$^+$-HRMS: *m/z* = 421.2946 (calcd. For $[C_{26}H_{37}N_4O]^+$ *m/z* = 421.2962). Anal. found (calcd. for C_{26}-$H_{36}N_4$): C, 74.19 (74.25); H, 8.77 (8.63); N, 13.27 (13.32) %.

DBF{NCN^{i}Pr$_2$}$_2${Cp*TiMe$_2$}$_2$ (25)

To a THF (15 mL) solution of Cp*TiMe$_3$ (0.277 g, 1.2 mmol) was added a THF (10 mL) solution of DBF(C(NH)N^{i}Pr$_2$)$_2$ (0.232 g, 0.55 mmol). The yellow solution was stirred for 12 h. The volatiles were removed *in vacuo* to afford a solid which was washed with pentane (3 x 15 mL) and dried *in vacuo* to yield the desired compound as a yellow solid. Yield = 0.246 g (53%). ^{1}H NMR (CD_2Cl_2, 299.9 MHz, 293 K): 7.84 (2H, dd, ^{3}J = 6.6 Hz, ^{4}J = 2.4 Hz, Ar-4), 7.32 (2H, overlapping m, Ar-2), 7.29 (2H, overlapping m, Ar-3), 3.93 (4H, m, N(C<u>H</u>Me$_2$)$_2$), 1.82 (6H, overlapping d, N(CH<u>Me</u>$_2$)$_2$), 1.80 (6H, overlapping d, N(CH<u>Me</u>$_2$)$_2$), 1.75 (30H, s, C$_5$<u>Me</u>$_5$), 1.46 (6H, d, ^{3}J = 6.9 Hz, N(CH<u>Me</u>$_2$)$_2$), 1.10(6H, d, ^{3}J = 6.7 Hz, N(CH<u>Me</u>$_2$)$_2$), -0.14 (6H, s, Ti<u>Me</u>$_2$), -0.66 (6H, s, Ti<u>Me</u>$_2$) ppm. ^{13}C{^{1}H} NMR (CD_2Cl_2, 75.4 MHz, 293 K): 156.2 (<u>C</u>N(N^{i}Pr$_2$), 151.0 (Ar-6), 127.4 (Ar-2), 126.7 (Ar-1), 124.4 (Ar-5), 123.5 (Ar-3), 120.0 (Ar-4), 119.7 (<u>C</u>$_5$Me$_5$), 52.8 (N(<u>C</u>HMe$_2$)$_2$), 47.6 (Ti<u>Me</u>$_2$), 47.4 (N(<u>C</u>HMe$_2$)$_2$), 46.3 (Ti<u>Me</u>$_2$), 22.6 (N(CH<u>Me</u>$_2$)$_2$), 22.0 (N(CH<u>Me</u>$_2$)$_2$), 21.4 (N(CH<u>Me</u>$_2$)$_2$), 21.0 (N(CH<u>Me</u>$_2$)$_2$), 12.0 (C$_5$<u>Me</u>$_5$) ppm. IR (NaCL plates, Nujol mull, cm^{-1}): 1561 (s, C=N), 1329 (m), 1179 (w), 1159 (w), 899 (m), 733 (m). EI-MS: 829 (5 % [M - Me]$^+$). A satisfactory elemental analysis could not be obtained.

Xanth(CN)$_2$ (26)

A dry 250 mL round bottomed flask was charged with Xanth(I)$_2$ (5.815 g, 12.6 mmol), copper (I) cyanide (4.508 g, 50 mmol) and DMF (60 mL). The reaction mixture was heated at reflux for 3 h after which time the solution had turned dark brown. The reaction was cooled to room temperature and ammonium hydroxide (400 mL) was added and left to stir for 30 mins. After 30 mins 100 mL of dichloromethane was added and the organic phase separated from the aqueous layer which was then back-extracted with dichloromethane (4 x 50 mL). The combined organic phases were dried over MgSO$_4$, filtered and the volatiles removed under reduced pressure to give a brown solid. The solid was extracted into dichloromethane (30 mL) and Concentrated to *ca.* 20 mL, storage at -30 °C for 24 h resulted in crystallisation of the desired compound which was subsequently isolated and dried *in vacuo*. Yield = 2.65 g (80%). Diffraction quality crystals were grown from a chloroform solution at room temperature. ^{1}H NMR ($CDCl_3$, 400.1 MHz, 293 K): 7.67 (2H, d, , ^{3}J = 8.0 Hz Ar-4), 7.56 (2H, d, ^{3}J = 7.6 Hz, Ar-2), 7.24 (2H, t, ^{3}J = 7.8 Hz, Ar-2), 1.66 (6H, s, C<u>Me</u>$_2$) ppm. ^{13}C{^{1}H} NMR ($CDCl_3$, 100.6 MHz, 293 K): 150.5 (Ar-6), 132.1 (Ar-2), 131.1

(Ar-4), 130.8 (Ar-5), 124.5 (Ar-3), 114.9 (Ar-1), 101.9 (CN), 34.3 ($C\underline{Me}_2$), 32.5 ($C\underline{Me}_2$) ppm. IR (Thin film, cm^{-1}): 2230 (s, C≡N), 1433 (s), 1265 (m), 1180 (w), 883 (m). ESI^+-HRMS: *m/z* = 283.0846 (calcd. For $[C_{17}H_{12}N_2O]^+$ *m/z* = 283.0842). Anal. found (calcd. for $C_{17}H_{12}N_2O$): C, 78.62 (78.44); H, 4.59 (4.65); N, 10.67 (10.76).

Xanth(C(NH)N^{i}Pr$_2$)$_2$ (27)

To a toluene (30 mL) solution of diisopropylamine (1.49 mL, 10.7 mmol) at 50 °C was added MeMgBr (2.87 mL, 3.0 M in diethyl ether, 8.6 mmol). Following stirring at 50 °C for 3 h, the solution was cooled to room temperature and the volatiles removed *in vacuo*. Xanth(CN)$_2$ (1.11 g, 4.3 mmol) was added and the mixture charged with 50 mL of toluene. The solution was stirred at room tempereature for 16 h and then at 100 °C for 3 h. The solution was subsequently then cooled to 0 °C, quenched with methanol (50 mL) and then water (100 mL). The organic phase was separated from the aqueous layer which was then back-extracted with dichloromethane (4 x 50 mL). The combined organic phases were concentrated to *ca.* 10 mL and stirred with 4M aqueous NaOH (70 mL) for 48 h. The organic phase was separated from the aqueous layer which was then back-extracted with dichloromethane (4 x 50 mL), dried over $MgSO_4$, filtered and the volatiles removed under reduced pressure to give a yellow oil. Trituration using pentane gave the desired compound as a pale yellow solid. Yield 1.23 g (62%). ^{1}H NMR (CD_2Cl_2, 400.1 MHz, 298 K): 7.41(2H, dd, J = 7.8, 1.7 Hz, Ar-2), 7.06 (2H, t, ^{3}J = 7.7 Hz, Ar-3), 6.99 (2H, dd, J = 7.4, 1.7 Hz, Ar-4), 5.88 (2H, br, N$\underline{H}$), 3.60 (4H, sept, ^{3}J = 6.4 Hz, N($C\underline{H}Me_2$)$_2$), 1.64 (6H, s, $C\underline{Me}_2$), 1.29 (24H, d, ^{3}J = 6.4 Hz, N($CH\underline{Me}_2$)$_2$) ppm. $^{13}C\{^1H\}$ NMR (CD_2Cl_2, 100.6 MHz, 298 K): 163.8 ($\underline{C}N(N^iPr_2)$, 146.5 (Ar-6), 131.1 (Ar-1), 129.9 (Ar-5), 127.0 (Ar-2), 126.1 (Ar-4), 123.3 (Ar-3), 48.5 (N($\underline{C}HMe_2$)$_2$), 34.8 ($\underline{C}Me_2$), 32.9 ($C\underline{Me}_2$), 21.4 (N($CH\underline{Me}_2$)$_2$) ppm. IR (NaCl plates, Nujol mull, cm^{-1}): 1738 (s), 1584(s, C=N), 1429 (m), 1366 (m), 1217 (w). ESI^+-HRMS: *m/z* = 463.3443 (calcd. For $[C_{29}H_{43}N_4O]^+$ *m/z* = 463.3431). Anal. found (calcd. for $C_{29}H_{42}N_4O$): C, 75.14 (75.28); H, 8.96 (9.15); N, 11.96 (12.11).

Xanth(C(NSiMe$_3$)N^{i}Pr$_2$)$_2$ (28)

To a toluene (30 mL) solution of diisopropylamine (0.55 mL, 3.9 mmol) at 50 °C was added MeMgBr (1.02 mL, 3.0 M in diethyl ether, 3.1 mmol). Following stirring at 50 °C for 3 h, the solution was cooled to room temperature and the volatiles removed

in vacuo. Xanth$(CN)_2$ (0.4 g, 1.5 mmol) was added and the mixture charged with 50 mL of toluene. The solution was stirred at room temperature for 16 h and then at 100 °C for 3 h. The solution was allowed to cool to room temperature and filtered. Trimethylsilyl chloride (5 mL) was added and the solution stirred for 17 h whereupon a white precipitate formed. A few drops of dioxane were added to further precipitate MgBrCl and the mixture stirred for a further 30 mins, the mixture was subsequently filtered and the volatiles removed *in vacuo*. The pale yellow solid was extracted into hexane (3 x 10 mL) and concentrated to *ca.* 10 mL, storage at -30 °C for 24 h resulted in crystallisation of the desired compound which was subsequently isolated and dried *in vacuo*. Yield 0.15 g (16%). ^{1}H NMR (C_6D_6, 400.1 MHz, 298 K): 7.03 (2H, dd, ^{3}J = 7.7 Hz, ^{4}J = 1.8 Hz, Ar-4), 6.82 (2H, t, ^{3}J = 7.5 Hz, Ar-3), 6.76 (2H, dd, ^{3}J = 7.3 Hz, ^{4}J = 1.8 Hz, Ar-2), 3.83 (2H, sept, ^{3}J = 6.7 Hz, N(C<u>H</u>Me$_2$)$_2$), 3.40 (2H, sept, ^{3}J = 6.7 Hz, N(C<u>H</u>Me$_2$)$_2$), 1.83 (6H, d, ^{3}J = 6.8 Hz, N(CH<u>Me</u>$_2$)$_2$), 1.62 (6H, d, ^{3}J = 6.7 Hz, N(CH<u>Me</u>$_2$)$_2$), 1.50 (6H, s, C<u>Me</u>$_2$), 1.29 (6H, d, ^{3}J = 6.8 Hz, N(CH<u>Me</u>$_2$)$_2$), 0.77 (6H, d, ^{3}J = 6.6 Hz, N(CH<u>Me</u>$_2$)$_2$), 0.03 (18H, s, Si<u>Me</u>$_3$) ppm. ^{13}C{^{1}H} NMR (C_6D_6, 100.6 MHz, 298 K) 157.8 (<u>C</u>N(N^{i}Pr$_2$)), 145.6 (Ar-6), 130.2 (Ar-1), 130.0 (Ar-5), 127.2 (Ar-2), 126.7 (Ar-4), 123.2 (Ar-3), 51.0 (N(<u>C</u>HMe$_2$)$_2$), 46.3 (N(<u>C</u>HMe$_2$)$_2$), 35.0 (C<u>Me</u>$_2$), 34.3 (<u>C</u>Me$_2$), 23.1 (N(CH<u>Me</u>$_2$)$_2$), 22.8 (N(CH<u>Me</u>$_2$)$_2$), 20.6 (N(CH<u>Me</u>$_2$)$_2$), 20.5 (N(CH<u>Me</u>$_2$)$_2$), 2.0 (Si<u>Me</u>$_3$) ppm. IR (NaCl plates, Nujol mull, cm^{-1}): 1613 (s, C=N), 1423 (m), 1329 (m), 1245 (m), 911 (w), 743 (w). EI-MS: *m/z* = 591 (50 %, [M-Me]$^+$), 506 (100 %, [M-N^{i}Pr$_2$]$^+$), 73 (100 %, [SiMe$_3$]$^+$). Anal. found (calcd. for $C_{35}H_{58}N_4Si_2O$): C, 69.28 (69.25); H, 9.70 (9.63); N, 9.27 (9.23) %.

Xanth{NCN^{i}Pr$_2$}$_2${Cp*TiCl} (29)

To a mixture of Xanth(C(NSiMe$_3$)N^{i}Pr$_2$)$_2$ (231 mg, 0.38 mmol) and Cp*TiCl$_3$ (110 mg, 0.38 mmol) was added toluene (15 mL). The solution was heated to 95 °C for 50 h after which the volatiles removed under reduced pressure to afford a crude solid. The solid was cooled to -50 °C, washed with hexane (3 x 10 mL) and dried *in vacuo* to give the desired compound as a red solid. Yield = 102 mg (40%). Diffraction quality crystals were grown from a hexane solution at -30 °C. ^{1}H NMR (C_6D_5Br, 499.9 MHz, 273 K): 7.42 (2H, d, ^{3}J = 7.4 Hz, Ar-4), 7.24 (2H, t, ^{3}J = 7.4 Hz, Ar-3), 7.18 (2H, d, ^{3}J = 7.2 Hz, Ar-2), 3.99 (2H, br, N(C<u>H</u>Me$_2$)$_2$), 3.83 (2H, m, N(C<u>H</u>Me$_2$)$_2$), 1.88 (3H, s, C<u>Me</u>$_2$ in aromatic plane), 1.86 (6H, br, N(CH<u>Me</u>$_2$)$_2$), 1.81 (15H, s, C$_5$<u>Me</u>$_5$), 1.76 (6H, br, N(CH<u>Me</u>$_2$)$_2$), 1.50 (3H, s, C<u>Me</u>$_2$ perpendicular to aromatic

plane), 1.11 (12H, m, N(CH$\underline{Me}_2)_2$) ppm. $^{13}C\{^1H\}$ NMR (C_6D_5Br, 125.7 MHz, 273 K): 154.3 ($\underline{C}N(N^iPr_2)$), 150.5 (Ar-6), 134.5 (Ar-5), 128.5 (Ar-1), 126.2 (Ar-2), 123.4 (Ar-4), 123.1 (Ar-3), 119.4 ($\underline{C}_5Me_5$), 50.3 (N($\underline{C}HMe_2)_2$), 47.2 (N($\underline{C}HMe_2)_2$), 35.7 ($\underline{C}Me_2$), 32.9 ($C\underline{Me}_2$ perpendicular to aromatic plane), 23.6 ($C\underline{Me}_2$ parallel to aromatic plane), 22.9 (N(CH$\underline{Me}_2)_2$), 21.2 (N(CH$\underline{Me}_2)_2$), 21.0 (N(CH$\underline{Me}_2)_2$), 20.0 (N(CH$\underline{Me}_2)_2$), 12.0 ($C_5\underline{Me}_5$) ppm. IR (NaCl plates, Nujol mull, cm^{-1}): 1583 (s, C=N), 1531 (m). EI-MS: *m/z* = 643 (10 %, $[M\text{-}Cl]^+$), 578 (100 %, $[M\text{-}N^iPr_2]^+$), 478 (100 %, $[M\text{-}2(N^iPr_2)]^+$). Anal. found (calcd. for $C_{39}H_{55}N_4Cl_1Ti_1O_1$): C, 68.86 (68.97); H, 8.17 (8.16); N, 8.22 (8.25) %.

Xanth{NCN^{i}Pr$_2$}$_2${Cp*TiMe$_2$}$_2$ (30)

To a benzene (15 mL) solution of Cp^*TiMe_3 (0.38 g, 1.67 mmol) at 60 °C was added dropwise a benzene (10 mL) solution of Xanth(C(NH)N^{i}Pr$_2$)$_2$ (0.35 g, 0.76 mmol) over 5 h. The brown solution was stirred for an additional 72 h at 60 °C. The solution was subsequently cooled to room temperature and the volatiles were removed under reduced to afford a solid. The solid was washed with hexane (3 x 10 mL) and dried *in vacuo* to yield the desired compound as a pale brown solid. Yield = 0.18 g (27%). Diffraction quality crystals were grown from a benzene solution at room temperature ^1H NMR (C_6D_5Br, 400.1 MHz, 298 K): 7.24 (2H, d, ^3J = 7.3 Hz, Ar-4), 7.04 (2H, d, ^3J = 6.7 Hz, Ar-2), 7.00 (2H, overlapping m, Ar-3), 4.39 (2H, m, N($C\underline{H}Me_2)_2$), 3.93 (2H, br, N($C\underline{H}Me_2)_2$), 2.17 (6H, d, ^3J = 6.4 Hz, N(CH$\underline{Me}_2)_2$), 1.89 (15H, s, $C_5\underline{Me}_5$), 1.80 (6H, d, ^3J = 6.6 Hz, N(CH$\underline{Me}_2)_2$), 1.75 (6H, s, $C\underline{Me}_2$), 1.69 (6H, d, ^3J = 6.5 Hz, N(CH$\underline{Me}_2)_2$), 1.20 (6H, d, ^3J = 6.4 Hz, N(CH$\underline{Me}_2)_2$), 0.37 (6H, s, Ti$\underline{Me}_2$), 0.03 (6H, s, Ti$\underline{Me}_2$) ppm. $^{13}C\{^1H\}$ NMR (C_6D_5Br, 100.6 MHz, 298 K): 157.2 ($\underline{C}N(N^iPr_2)$), 145.3 (Ar-6), 130.4 (Ar-5), 130.2 (Ar-1), 126.5 (Ar-2), 125.9 (Ar-4), 122.2 (Ar-3), 119.1 ($\underline{C}_5Me_5$), 52.5 (N($\underline{C}HMe_2)_2$), 48.5 (Ti$\underline{Me}_2$), 47.1 (N($\underline{C}HMe_2)_2$), 46.9 (Ti$\underline{Me}_2$), 34.4($\underline{C}Me_2$), 34.3 ($C\underline{Me}_2$), 32.3 ($C\underline{Me}_2$), 23.9 (N(CH$\underline{Me}_2)_2$), 22.1 (N(CH$\underline{Me}_2)_2$), 20.9 (N(CH$\underline{Me}_2)_2$), 20.7 (N(CH$\underline{Me}_2)_2$), 12.0 ($C_5\underline{Me}_5$) ppm. IR (NaCl plates, Nujol mull, cm^{-1}): 1551 (s, C=N), 1420 (m). Anal. found (calcd. for $C_{53}H_{84}N_4Ti_2O_1$): C, 71.48 (71.61); H, 9.46 (9.52); N, 6.17 (6.30) %.

Xanth(CN)(C(NH)N^{i}Pr$_2$) (31)

To a THF (50 mL) solution of diisopropylamine (1.34 mL, 9.6 mmol) at 50 °C was added MeMgBr (2.56 mL, 3.0 M in diethyl ether, 7.7 mmol). Following stirring at

50 °C for 3 h, the solution was cooled to 0 °C and Xanth(CN)$_2$ (1 g, 3.8 mmol) was added. The solution was allowed to warm to room temperature and was stirred for 24 h. The mixture was subsequently cooled to 0 °C and quenched with methanol (50 mL) and then water (100 mL). The organic phase separated from the aqueous layer which was then back-extracted with dichloromethane (4 x 50 mL). The combined organic phases were washed with 4M aqueous NaOH (3 x 30 mL), dried over $MgSO_4$, filtered and the volatiles removed under reduced pressure to afford a brown oil. Trituration in pentane gave the desired product as a brown solid. Yield = 0.95 g (68%). ^{1}H NMR (CD_2Cl_2, 400.1 MHz, 298 K): 7.67 (1H, d, ^{3}J = 7.7 Hz, Ar-10), 7.51 (1H, d, ^{3}J = 7.4 Hz, Ar-8), 7.43 (1H, d, ^{3}J = 7.3 Hz, Ar-4), 7.16 (2H, overlapping m, Ar-9 and Ar-3), 7.09 (1H, d, ^{3}J = 7.3 Hz, Ar-2), 3.60 (2H, sept, ^{3}J = 6.6 Hz, N(C<u>H</u>Me$_2$)$_2$), 1.64 (6H, s, C<u>Me</u>$_2$), 1.38 (12H, br, N(CH<u>Me</u>$_2$)$_2$) ppm (NH not observed). ^{13}C{^{1}H} NMR (CD_2Cl_2, 100.6 MHz, 298 K): 163.0 (<u>C</u>N(N^{i}Pr$_2$)), 152.0 (Ar-12), 144.9 (Ar-6), 132.6 (Ar-8), 131.9 (Ar-11), 131.8 (Ar-10), 130.3 (Ar-5), 130.1 (Ar-1), 126.8 (Ar-2), 126.3 (Ar-4), 124.8 (Ar-3), 123.9 (Ar-9), 116.3 (Ar-7), 101.4 (Ph<u>C</u>N), 49.0 (N(<u>C</u>HMe$_2$)$_2$), 34.8 (C<u>Me</u>$_2$), 32.8 (C<u>Me</u>$_2$), 21.0 (N(CH<u>Me</u>$_2$)$_2$) ppm. IR (NaCl plates, Nujol mull, cm^{-1}): 2231 (m, C≡N), 1575 (s, C=N), 1430 (m), 1227 (m), 1170 (m), 804 (w). ESI$^+$-HRMS: *m/z* = 362.2224 (calcd. For [$C_{23}H_{28}N_3O$]$^+$ *m/z* = 362.2227). Anal. found (calcd. for $C_{23}H_{28}N_3O$): C, 76.28 (76.42): H, 7.65 (7.53); N, 11.62 (11.62).

Xanth(CN)(N(SiMe$_3$)CN^{i}Pr$_2$) (32)

To a THF (50 mL) solution of diisopropylamine (0.55 mL, 3.9 mmol) at 50 °C was added MeMgBr (1.02 mL, 3.0 M in diethyl ether, 3.1 mmol). Following stirring at 50 °C for 3 h, the solution was cooled to 0 °C and Xanth(CN)$_2$ (0.4 g, 1.54 mmol) was added. The solution was warmed to room temperature and stirred for a further 24 h. Trimethylsilyl chloride (5 mL) was added and the solution stirred for 17 h whereupon a white precipitate formed. A few drops of dioxane were added to further precipitate MgBrCl and the mixture stirred for a further 30 mins, the solution was subsequently filtered and the volatiles removed *in vacuo*. The solid was extracted into hexane (3 x 10 mL) and concentrated to *ca.* 10 mL, storage at -30 °C for 24 h resulted in crystallisation of the desired compound which was subsequently isolated and dried *in vacuo.* Yield = 0.39 mg (59%). ^{1}H NMR ($CDCl_3$, 400.1 MHz, 298 K): 7.64 (1H, dd, ^{3}J = 7.9 Hz, ^{4}J = 1.5 Hz, Ar-10), 7.51 (1H, dd, ^{3}J = 7.6 Hz, ^{4}J = 1.5 Hz, Ar-8), 7.34 (1H, dd, ^{3}J = 7.8 Hz, ^{4}J = 1.5 Hz, Ar-4), 7.14 (1H, t, ^{3}J = 7.3 Hz, Ar-9), 7.11 (1H, t, ^{3}J

= 7.6 Hz, Ar-3), 6.94 (1H, dd, ^{3}J = 7.4 Hz, ^{4}J = 1.5 Hz, Ar-2), 3.67 – 3.50 (2H, overlapping m, N(C<u>H</u>Me$_2$)$_2$), 1.78 (3H, d, ^{3}J = 6.8 Hz, N(CH<u>Me</u>$_2$)$_2$), 1.69 (3H, s, C<u>Me</u>$_2$), 1.62 (3H, s, C<u>Me</u>$_2$), 1.59 (3H, d, ^{3}J = 6.7 Hz, N(CH<u>Me</u>$_2$)$_2$), 1.19 (3H, d, ^{3}J = 6.7 Hz, N(CH<u>Me</u>$_2$)$_2$), 1.02 (3H, d, ^{3}J = 6.6 Hz, N(CH<u>Me</u>$_2$)$_2$), 0.29 (9H, s, Si<u>Me</u>$_3$) ppm. ^{13}C – {^{1}H} NMR (CDCl$_3$, 100.6 MHz, 298 K): 154.0 8 (<u>C</u>N(N^{i}Pr$_2$)), 151.6 (Ar-12), 144.6 (Ar-6), 132.4 (Ar-8), 131.4 (Ar-11), 131.1 (Ar-10), 129.7 (Ar-1), 129.4 (Ar-5), 126.2 (Ar-2), 124.8 (Ar-4), 124.2 (Ar-3), 123.2 (Ar-9), 115.6 (Ar-7), 101.2 (Ph<u>C</u>N), 50.4 (N(<u>C</u>HMe$_2$)$_2$), 46.1 (N(<u>C</u>HMe$_2$)$_2$), 34.3 (<u>C</u>Me$_2$), 33.3 (C<u>Me</u>$_2$), 32.2 (C<u>Me</u>$_2$), 21.4 (N(CH<u>Me</u>$_2$)$_2$), 21.1 (N(CH<u>Me</u>$_2$)$_2$), 20.8 (N(CH<u>Me</u>$_2$)$_2$), 20.6 (N(CH<u>Me</u>$_2$)$_2$), 1.2 (Si<u>Me</u>$_3$) ppm. IR (NaCl plates, Nujol mull, cm^{-1}): 2235 (m, C≡N), 1616 (s, C=N), 1428 (s), 1331 (m), 1240 (m). 901 (m), 832 (s). EI-MS: 434 (100 %, [M]$^{+}$). Anal. found (calcd. for C$_{26}$H$_{35}$N$_3$OSi): C, 72.19 (72.01); H, 8.23 (8.14); N, 9.65 (9.69) %.

Xanth(CN)({NCN^{i}Pr$_2$}{Cp*TiMe$_2$}) (33)

To a stirring benzene (15 mL) solution of Cp*TiMe$_3$ (0.19 g, 0.83 mmol) was added a benzene (10 mL) solution of Xanth(CN)(C(NH)N^{i}Pr$_2$) (0.3 g, 0.83 mmol). The orange solution was stirred for 16 h. The volatiles were removed *in vacuo* to afford a brown solid and the solid was extracted into *hexane* (3 x 10 mL). Concentration to *ca.* 10 mL, resulted in the crystallisation of the desired compound upon standing at room temperature which was subsequently isolated and dried *in vacuo*. Yield = 0.33 g (69%). ^{1}H NMR (C$_6$D$_6$, 400.1 MHz, 298 K): 7.22 (1H, dd, ^{3}J = 7.0 Hz, ^{4}J = 2.0 Hz, Ar-8), 6.98 (1H, dd, ^{3}J = 7.7 Hz, ^{4}J = 1.6 Hz, Ar-2), 6.96 (1H, dd, ^{3}J = 7.5 Hz, ^{4}J = 1.6 Hz, Ar-4), 6.91 (1H, dd, ^{3}J = 7.9 Hz, ^{4}J = 1.6 Hz, Ar-10), 6.87 (1H, m, Ar-9), 6.45 (1H, t, ^{3}J = 7.8 Hz, Ar-3), 3.73 (1H, sept, ^{3}J = 6.7 Hz, N(C<u>H</u>Me$_2$)$_2$), 3.63 (1H, br, N(C<u>H</u>Me$_2$)$_2$), 2.07 (3H, d, ^{3}J = 6.8 Hz, N(CH<u>Me</u>$_2$)$_2$), 1.94 (3H, d, ^{3}J = 6.8 Hz, N(CH<u>Me</u>$_2$)$_2$), 1.91(15H, s, C$_5$<u>Me</u>$_5$), 1.30 (3H, s, C<u>Me</u>$_2$), 1.28 (3H, s, C<u>Me</u>$_2$), 1.24 (3H, d, ^{3}J = 6.7 Hz, N(CH<u>Me</u>$_2$)$_2$), 0.78 (3H, d, ^{3}J = 6.7 Hz, N(CH<u>Me</u>$_2$)$_2$), 0.53 (3H, s, Ti<u>Me</u>$_2$), 0.37 (3H, s, Ti<u>Me</u>$_2$) ppm. ^{13}C{^{1}H} NMR (C$_6$D$_6$, 100.6 MHz, 298 K): 155.8 (<u>C</u>N(N^{i}Pr$_2$)), 151.3 (Ar-6), 143.9 (Ar-12), 132.4 (Ar-4), 131.2 (Ar-2), 130.2 (Ar-5), 129.0 (Ar-11), 128.6 (Ar-7), 127.5 (Ar-8), 125.1 (Ar-10), 124.4 (Ar-9), 120.0 (Ar-3), 116.0 (<u>C</u>$_5$Me$_5$), 101.8 (Ar-1), 101.8 (Ph<u>C</u>N), 51.7 (N(<u>C</u>HMe$_2$)$_2$), 49.5 (Ti<u>Me</u>$_2$), 47.4 (Ti<u>Me</u>$_2$), 47.3 (N(<u>C</u>HMe$_2$)$_2$), 34.1(<u>C</u>Me$_2$) , 33.7 (C<u>Me</u>$_2$), 32.3 (C<u>Me</u>$_2$), 21.1 (N(CH<u>Me</u>$_2$)$_2$), 21.0 (N(CH<u>Me</u>$_2$)$_2$), 20.8 (N(CH<u>Me</u>$_2$)$_2$), 20.6 (N(CH<u>Me</u>$_2$)$_2$), 11.9 (C$_5$<u>Me</u>$_5$) ppm. IR (NaCl plates, Nujol mull, cm^{-1}): 2227 (m, C≡N), 1559 (s, C=N),

1329 (m), 1156 (w), 742 (w), 668 (m). EI-MS: *m/z* = 598 (50 %, $[M - Me]^+$), 543 (100 %, $[M - 2Me]^+$). Anal. found (calcd. for $C_{35}H_{47}N_3OTi$): C, 73.12 (73.28); H, 8.40 (8.26); N, 7.21 (7.33) %.

Xanth(CN)({NCN^{i}Pr$_2$}{Cp*TiCl$_2$}) (34)

To a stirring benzene (15 mL) solution of Cp^*TiCl_3 (0.29 g, 1.14 mmol) was added a benzene (10 mL0 solution of Xanth(CN)(N($SiMe_3$)CN^{i}Pr$_2$) (0.434 g, 1.14 mmol). The red solution was stirred for 16 h after which time the volatiles were removed *in vacuo*. The solid was washed with pentane (3 x 10 mL), isolated and dried *in vacuo* to yield the desired compound as an orange solid. Yield = 0.37 g (68%). Diffraction quality crystals were grown from slow cooling of a hot toluene solution. ^{1}H NMR (CD_2Cl_2, 400.1 MHz, 298 K): 7.73 (1H, dd, ^3J = 7.9 Hz, ^4J = 1.6 Hz, Ar-4), 7.59 (1H, dd, ^3J = 7.6 Hz, ^4J = 1.6 Hz, Ar-2), 7.46 (1H, dd, ^3J = 7.9 Hz, ^4J = 1.6 Hz, Ar-10), 7.36 (1H, dd, ^3J = 7.6 Hz, ^4J = 1.6 Hz, Ar-8), 7.24 (1H, t, ^3J = 7.8 Hz, Ar-3), 7.19 (1H, t, ^3J = 7.7 Hz, Ar-9), 3.81 (1H, br, N(C<u>H</u>Me$_2$)$_2$), 3.71 (1H, sept, ^3J = 6.7 Hz, N(C<u>H</u>Me$_2$)$_2$), 1.91 (C_5<u>Me</u>$_5$), 1.73 (3H, d, ^3J = 6.9 Hz, N(CH<u>Me</u>$_2$)$_2$), 1.71 (3H, s, C<u>Me</u>$_2$), 1.69 (3H, d, ^3J = 7.0 Hz, N(CH<u>Me</u>$_2$)$_2$), 1.67 (3H, s, C<u>Me</u>$_2$), 1.34 (3H, d, ^3J = 6.7 Hz, N(CH<u>Me</u>$_2$)$_2$), 1.07 (3H, d, ^3J = 6.7 Hz, N(CH<u>Me</u>$_2$)$_2$) ppm. ^{13}C{^{1}H} NMR (CD_2Cl_2, 100.6 MHz, 298 K): 161.2 (<u>C</u>N(N^{i}Pr$_2$)), 151.1 (Ar-6), 143.75 (Ar-12), 133.1(Ar-2), 132.5 (Ar-4), 131.6 (Ar-5), 129.5 (Ar-11), 129.0 (Ar-8), 127.5 (<u>C</u>$_5$Me$_5$), 127.4 (Ar-10), 126.0 (Ar-7), 125.1 (Ar-9), 124.3 (Ar-3), 116.6 (Ar-1), 101.3 (Ph<u>C</u>N), 53.3 (N(<u>C</u>HMe$_2$)$_2$), 48.9 (N(<u>C</u>HMe$_2$)$_2$), 34.6 (<u>C</u>Me$_2$), 34.0 (C<u>Me</u>$_2$), 33.3(C<u>Me</u>$_2$), 21.4 (N(CH<u>Me</u>$_2$)$_2$), 21.0(N(CH<u>Me</u>$_2$)$_2$), 20.7 (N(CH<u>Me</u>$_2$)$_2$), 20.3(N(CH<u>Me</u>$_2$)$_2$), 12.9 (C_5<u>Me</u>$_5$) ppm. IR (NaCl plates, Nujol mull, cm^{-1}): 2225 (m, C≡N), 1529 (s, C=N), 1346 (m), 1290 (w), 682 (m). EI-MS: *m/z* = 613 (100 %, $[M]^+$). Anal. found (calcd. for $C_{33}H_{41}N_3Cl_2OTi$): C, 64.43 (64.50); H, 6.79 (6.73); N, 6.81 (6.84) %.

Fc′(CN)$_2$ (35)

A mixture of ferrocene-1,1′-diboronic acid (2.5 g, 9.13 mmol), 4-bromobenzonitrile (3.47 g, 19.1 mmol), DME (70 mL), [1,1′-Bis(diphenylphosphino)ferrocene] dichloropalladium(II) (136 mg, 186 mmol) and 3 M aqueous NaOH (13.5 mL) was refluxed for 6 d. The mixture was cooled to room temperature and chloroform (200 mL) and water (50 mL) were added. The organic phase was separated from the aqueous layer which was then back-extracted with chloroform (4 x 50 mL). The

combined organic phases were dried over $MgSO_4$, filtered and the volatiles removed under reduced pressure. The resulting red solid was extracted into THF (3 x 20 mL). Concentration of the solution to *ca.* 20 mL and storage at -30 °C for 24 h resulted in crystallisation of the desired compound which was subsequently isolated and dried *in vacuo*. Yield = 2.6 g (73%). ^{1}H NMR ($CDCl_3$, 499.9 MHz, 293 K): 7.48 (4H, d, ^{3}J = 7.7 Hz, Ar C<u>H</u>C(CN)), 7.31 (4H, d, ^{3}J = 7.7 Hz, Ar C<u>H</u>CHC(CN)), 4.57 (4H, m, Cp C<u>H</u>CC_6H_4), 4.38 (4H, m, Cp C<u>H</u>CHCC_6H_4) ppm. ^{13}C{^{1}H} NMR ($CDCl_3$, 125.7 MHz, 293 K): 143.6 (Ar CH<u>C</u>Cp), 132.3 (Ar <u>C</u>HC(CN)), 126.1 (Ar <u>C</u>HCHC(CN)), 119.2 (Ar CH<u>C</u>(CN)), 109.3 (C_6H_4<u>C</u>N), 83.7 (Cp CHCH<u>C</u>C_6H_4), 72.0 (Cp <u>C</u>HCHCC_6H_4), 68.5 (Cp CH<u>C</u>HCC_6H_4) ppm. IR (Thin film, cm^{-1}): 2227 (s, C≡N), 1608 (s), 1524 (m), 1183 (m), 1039 (m), 820 (m), 820 (m). ESI$^+$-HRMS: *m/z* = 411.0550 (calcd. For $[C_{24}H_{16}N_2FeNa]^+$ *m/z* = 411.0555). Anal. found (calcd. for $C_{24}H_{16}N_2Fe$): C, 74.11 (74.25); H, 3.96 (4.15); N, 7.36 (7.22) %.

Fc′{C(NH)N^{i}Pr$_2$}$_2$ (36)

To a THF (50 mL) solution of diisopropylamine (3.96 mL, 28 mmol) at 50 °C was added MeMgBr (8.6 mL, 3.0 M in diethyl ether, 26 mmol). Following stirring at 50 °C for 3 h, the solution was cooled to 0 °C and Fc′$(CN)_2$ (1 g, 2.5 mmol) was added. The solution was allowed to warm to room temperature and stirred for a further 36 h. the mixture was subsequently cooled to 0 °C, quenched with methanol (50 mL) and then water (100 mL). The organic phase was separated from the aqueous layer which was then back-extracted with dichloromethane (4 x 50 mL). The combined organic phases were dried over $MgSO_4$, filtered and the volatiles removed under reduced pressure. The orange solid was washed with pentane (3 x 15mL), isolated and dried *in vacuo* to give the HBr salt of the desired product. Yield = 0.9 g (52%). Diffraction quality crystals were grown from a concentrated chloroform solution at room temperature**.** ^{1}H NMR ($CDCl_3$, 499.9 MHz, 293 K): 7.12 (4H, d, ^{3}J = 7.8 Hz, Ar C<u>H</u>CHC(C(N^{i}Pr$_2$)N)), 7.01 (4H, d, ^{3}J = 7.8 Hz, Ar C<u>H</u>C(C(N^{i}Pr$_2$)N)), 4.59 (4H, s, Cp C<u>H</u>CC_6H_4), 4.33 (4H, s, Cp C<u>H</u>CHCC_6H_4), 3.65 (4H, sept, ^{3}J = 6.4 Hz, N(C<u>H</u>Me$_2$)$_2$), 1.35 (24H, d, ^{3}J = 6.4 Hz, N(CH<u>Me</u>$_2$)$_2$) ppm (NH not observed). ^{13}C{^{1}H} NMR ($CDCl_3$, 125.7 MHz, 293 K): 164.4 (<u>C</u>N(N^{i}Pr$_2$)), 138.3 (Ar CH<u>C</u>(C(N^{i}Pr$_2$)N), 133.8 (Ar CH<u>C</u>Cp), 126.6 (Ar <u>C</u>HC(C(N^{i}Pr$_2$)N)), 126.0 (Ar <u>C</u>HCCp), 85.2 (Cp CHCH<u>C</u>C_6H_4), 70.5 (Cp <u>C</u>HCHCC_6H_4), 67.5 (Cp CH<u>C</u>HCC_6H_4), 49.5 (N(<u>C</u>HMe$_2$)$_2$), 20.7 (N(CH<u>Me</u>$_2$)$_2$) ppm. IR (Thin film, cm^{-1}): 1574 (s, C=N),

1559 (w), 1368 (m), 847 (m), 821 (w). ESI$^+$-HRMS: *m/z* = 591.3162 (calcd. For $[C_{36}H_{47}N_4Fe]^+$ *m/z* = 591.3145). Anal. found (calcd. for $C_{36}H_{47}N_4FeBr$): C, 64.47 (64.39); H, 7.09 (7.05); N, 8.23 (8.34) %.

1,1′-{1,4-C_6H_4-C(NH)N^{i}Pr$_2$}$_2$ferrocene.HBr was extracted into dichloromethane (50 mL) and washed with 4M aqueous NaOH (3 x 30 mL), dried over $MgSO_4$ and the volatiles removed under reduced pressure. Yield = 0.63 g (76%). ^{1}H NMR ($CDCl_3$, 400.1 MHz, 293 K): 7.31 (4H, d, ^{3}J = 8.1 Hz, Ar C<u>H</u>CHC(C(N^{i}Pr$_2$)N)), 7.14 (4H, d, ^{3}J = 8.1 Hz, Ar CHC(C(N^{i}Pr$_2$)N)), 4.45 (4H, s, Cp C<u>H</u>CC$_6$H$_4$), 4.23 (4H, s, Cp C<u>H</u>CHCC$_6$H$_4$), 3.66 (4H, sept, ^{3}J = 6.8 Hz, N(C<u>H</u>Me$_2$)$_2$), 1.33 (24H, d, ^{3}J = 6.8 Hz, N(CH<u>Me</u>$_2$)$_2$) ppm. ^{13}C{^{1}H} NMR ($CDCl_3$, 100.6 MHz, 293 K): 168.0 (<u>C</u>N(N^{i}Pr$_2$)), 138.9 (Ar CH<u>C</u>(C(N^{i}Pr$_2$)N), 138.8 (Ar CH<u>C</u>Cp), 126.1 (Ar <u>C</u>HC(C(N^{i}Pr$_2$)N)), 126.0 (Ar <u>C</u>HCCp), 85.3 (Cp CHCH<u>C</u>C$_6$H$_4$), 71.1 (Cp <u>C</u>HCHCC$_6$H$_4$), 68.3 (Cp CH<u>C</u>HCC$_6$H$_4$) , 48.4 (N(<u>C</u>HMe$_2$)$_2$), 21.1 (N(CH<u>Me</u>$_2$)$_2$) ppm (NH not observed). IR (Thin film, cm^{-1}): 2963 (w, N-H), 1572 s, C=N), 1551 (m), 1384 (m), 1224 (m), 1029 (w), 844 (m). ESI$^+$-HRMS: *m/z* = 591.3131 (calcd. For $[C_{36}H_{47}N_4Fe]^+$ *m/z* = 591.3145).

Fc′{NCN^{i}Pr$_2$}$_2${Cp*TiMe$_2$}$_2$ (37)

To a THF (15 mL) solution of Cp*TiMe$_3$ (0.51 g, 2.2 mmol) was added a THF (10 mL) solution of Fc′{C(NH)N^{i}Pr$_2$}$_2$ (0.44 g, 0.75 mmol). The red solution was stirred for 3 h after which time volatiles were removed *in vacuo* to afford a deep red solid. Recrystallisation from slow cooling of a hot toluene solution (10 mL) afforded the desired compound as red crystals which were isolated and dried *in vacuo.* Yield = 0.48 g (64%). ^{1}H NMR (CD_2Cl_2, 499.9 MHz, 223 K): 7.28 (4H, d, ^{3}J = 8.0 Hz, Ar C<u>H</u>CHC(C(N^{i}Pr$_2$)N)), 7.12 (4H, d, ^{3}J = 8.0 Hz, Ar C<u>H</u>C(C(N^{i}Pr$_2$)N)), 4.38 (4H, s, Cp C<u>H</u>CC$_6$H$_4$), 4.18 (4H, s, Cp C<u>H</u>CHCC$_6$H$_4$), 3.81 (4H, br, N(C<u>H</u>Me$_2$)$_2$), 3.50 (4H, br, N(C<u>H</u>Me$_2$)$_2$), 1.68 (30H, s, C$_5$<u>Me</u>$_5$), 1.64 (12H, d, N(CH<u>Me</u>$_2$)$_2$, ^{3}J = 5.8 Hz), 1.13 (12H, d, N(CH<u>Me</u>$_2$)$_2$ cis to phenyl, ^{3}J = 5.8 Hz), -0.20 (12H, d, Ti<u>Me</u>$_2$) ppm. ^{13}C{^{1}H} NMR (CD_2Cl_2, 499.9 MHz, 223 K): 161.4 (<u>C</u>N(N^{i}Pr$_2$), 138.8 (Ar CH<u>C</u>Cp), 137.8 (Ar CH<u>C</u>(C(N^{i}Pr$_2$)N), 126.2 (Ar <u>C</u>HC(C(N^{i}Pr$_2$)N)), 125.2 0 (Ar <u>C</u>HCCp), 118.8 (<u>C</u>$_5$Me$_5$), 84.8 (Cp CHCH<u>C</u>C$_6$H$_4$), 71.1 (Cp <u>C</u>HCHCC$_6$H$_4$), 68.0 (Cp CH<u>C</u>HCC$_6$H$_4$), 52.0 (N(<u>C</u>HMe$_2$)$_2$ cis to phenyl), 46.6 (N(<u>C</u>HMe$_2$)$_2$), 45.3 (Ti<u>Me</u>$_2$), 20.7 (N(CH<u>Me</u>$_2$)$_2$ cis to phenyl), 19.8 (N(CH<u>Me</u>$_2$)$_2$), 11.5 (C$_5$<u>Me</u>$_5$) ppm. IR (NaCl plates, Nujol mull, cm^{-1}): 1566 (s, C=N), 1031 (w), 798 (w). ESI$^+$-HRMS: *m/z* = 771 (80%, [M – 2Me –

$Cp^*TiMe2]^+$). Anal. found (calcd. for $C_{60}H_{86}N_4Fe_1Ti_2$): C, 71.17 (71.00); H, 8.61 (8.54); N, 5.38 (5.52) %.

6.8 Experimental details and characterising data for Chapter Four

NMR tube scale synthesis of $[Cp^*Ti\{NC(N^iPr_2)Ph\}\{MeC(N^iPr)_2\}]_2[\{B(C_6F_5)_3\}_2(\mu\text{-}C_6F_4)]$ (38)

To a solution of $Cp^*Ti\{NC(N^iPr_2)Ph\}Me_2$ (5 mg, 12 μmol) and $^iPrNCN^iPr$ (1.9 μL, 12 μmol) in C_6D_5Br (0.5 mL) was added $[\{B(C_6F_5)_3\}_2(\mu\text{-}C_6F_4)][Ph_3C]_2$ (10 mg, 6 μmol) resulting in the formation of a dark red solution. The solution was transferred to an NMR tube and the NMR spectra recorded after 5 mins. ^{1}H NMR (C_6D_5Br, 499.9 MHz, 298 K) 7.45-7.25 (10H, m, $NC(N^iPr_2)\underline{Ph}$), 3.82 (2H, br, κ^1-$NC\underline{H}Me_2$), 3.59 (6H, overlapping m, κ^1 and κ^2-$NC\underline{H}Me_2$) 2.20 (6H, s, $\underline{Me}C(N^iPr)_2$), 2.02 (30H, s, $C_5\underline{Me}_5$), 1.37 (12H, br, κ^1-$NC\underline{H}Me_2$), 1.10 (12H, d, ^3J = 6.3 Hz, κ^2-$NC\underline{H}Me_2$), 0.99 (12H, d, ^3J = 6.7 Hz, κ^1-$NC\underline{H}Me_2$), 0.75 (12H, d, ^3J = 6.2 Hz, κ^2-$NC\underline{H}Me_2$) ppm. ^{19}F NMR (C_6D_5Br, 470.4 MHz, 298 K): -129.2 - -131.5 (m, *o*-$C_6\underline{F}_5$), -136.1 (s, *o*-$C_6\underline{F}_4$), -163.4 - -163.6 (m, *p*-$C_6\underline{F}_5$), -166.3 - -166.8 (m, *m*-$C_6\underline{F}_5$) ppm. ^{11}B NMR (C_6D_5Br, 160.4 MHz, 298 K): -15.83 ppm.

NMR tube scale synthesis of $[Cp^*Ti\{NC(N^iPr_2)Ph\}Me][\{B(C_6F_5)_2\}(\mu\text{-}C_6F_4)\{BMe(C_6F_5)_2\}]$ (39)

$Cp^*Ti\{NCN^iPr_2Ph\}Me_2$ (3 mg, 7.2 μmol) and $\{(C_6F_5)_2B(THF)\}_2(\mu\text{-}C_6F_4)$ (6 mg, 7.2 μmol) were mixed together in C_6D_6 (0.5 mL) resulting in a dark red solution. The solution was transferred to an NMR tube and the NMR spectra recorded after 5 mins. ^{1}H NMR (C_6D_6, 499.9 MHz, 298 K): 6.90-7.10 (5H, overlapping multiplets, aromatic), 3.06 (2H, br, $NC\underline{H}Me_2$), 1.55 (15H, s, $C_5\underline{Me}_5$), 1.34 (3H, s, $Ti\underline{Me}$), 0.99 (6H, br, $NCH\underline{Me}_2$), 0.78 (3H, br, $\underline{Me}B(C_6F_5)_3$), 0.62 (6H, br, $NCH\underline{Me}_2$) ppm. ^{19}F NMR (C_6D_6, 470.4 MHz, 298 K): -127.8 – 132.2 (overlapping multiplets, *o*-$C_6\underline{F}_5$ and *o*-$C_6\underline{F}_4$), -140.0 - -146.7 (overlapping multiplets, *p*-$C_6\underline{F}_5$), -159.5 – 161.3 (m, *m*-$C_6\underline{F}_5$ and *p*-$C_6\underline{F}_5$) ppm. ^{11}B NMR (C_6D_6, 160.4 MHz, 298 K): 72.01($\underline{B}(C_6F_5)_2(\mu\text{-}C_6F_4)BMe(C_6F_5)_2$), -12.8 ($B(C_6F_5)_2\}(\mu\text{-}C_6F_4)$ $\underline{B}Me(C_6F_5)_2$) ppm.

$[Cp^*Ti\{NC(N^iPr_2)Ph\}Me(THF)]_2[\{(C_6F_5)_2BMe)_2(\mu\text{-}C_6F_4)]$ (40)

A THF (10 mL) solution of $\{(C_6F_5)_2B(THF)\}_2(\mu\text{-}C_6F_4)$ (0.07 g, 0.08 mmol) was added dropwise to a stirred THF solution (5 mL) of $Cp^*Ti\{NC(N^iPr_2)Ph\}Me_2$ (0.1 g,

0.24 mmol). After 15 mins pentane (20 mL) was added resulting in the formation of a brown oil. The pentane/THF was decanted away and the oil washed further with pentane (10 mL). The remaining solvent was removed *in vacuo* to yield the desired compound as a brown solid. Yield = 0.08 g (55%). ^{1}H NMR (C_6D_5Br, 499.9 MHz, 298 K): 7.45 – 7.20 (5H, m, NC(N^{i}Pr$_2$)Ph), 3.72 (2H. br, N(CHMe$_2$)$_2$), 3.62 (10H, overlapping br, N(CHMe$_2$)$_2$ and CH_2CH_2O), 1.82 (30H, s, C_5Me_5), 1.74 (8H, br, CH_2CH_2O), 1.55 (6H, br, N(CHMe$_2$)$_2$), 1.41(6H, br, N(CHMe$_2$)$_2$), 1.25 (6H, br, BMe), 1.01 (12H, m, N(CHMe$_2$)$_2$), 0.80 (6H, s, TiMe) ppm. ^{13}C{^{1}H} NMR (C_6D_5Br, 125.7 MHz, 298 K): 167.5 (CN(N^{i}Pr$_2$)), 149.03 (br overlapping d, *o*-C_6F_5 and *o*-C_6F_4), 137.8 (*i*-NC(N^{i}Pr$_2$)Ph), 137.6 (br d, ^{1}J = 237.9 Hz, *p*-C_6F_5), 136.7 (br d, ^{1}J = 240.6 Hz, *m*-C_6F_5), 128.9 (*o*-NC(N^{i}Pr$_2$)Ph), 128.4 (*m*-NC(N^{i}Pr$_2$)Ph), 126.1 (*p*-NC(N^{i}Pr$_2$)Ph), 125.4 (C_5Me_5), 68.3 (OCH_2CH_2), 58.4 (TiMe), 52.2 (N(CHMe$_2$)$_2$), 48.5 (N(CHMe$_2$)$_2$), 25.5 (OCH_2CH_2), 21.4 (N(CHMe$_2$)$_2$), 20.9 (N(CHMe$_2$)$_2$), 20.4 (N(CHMe$_2$)$_2$), 19.8 (N(CHMe$_2$)$_2$), 12.0 (BMe), 11.7 (C_5Me_2) ppm. ^{19}F NMR (C_6D_5Br, 470.4 MHz, 298 K): -131.1 (d, *o*-C_6F_5), -138.0 (s, *o*-C_6F_4), -164.5 (t, *p*-C_6F_5), -166.7 (m, *m*-C_6F_5) ppm. ^{11}B NMR (C_6D_5Br, 160.4 MHz, 298 K): -14.17 ppm. IR (NaCl plates, Nujol mull, cm^{-1}): 1543 (m, C=N), 1508 (m), 668 (w). Anal. found (calcd. for $C_{88}H_{96}B_2F_{24}N_4O_2Ti_2$): C, 57.97 (58.23); H, 5.12 (5.33); N, 3.12 (3.09) %.

NMR tube scale synthesis of [Cp*Ti{NC(N^{i}Pr$_2$)Ph}{MeC(N^{i}Pr)$_2$}]$_2$[{(C_6F_5)$_2$BMe)$_2$(μ-C_6F_4)] (41)

[Cp*Ti{NC(N^{i}Pr$_2$)Ph}Me{THF}]$_2$[{(C_6F_5)$_2$BMe)$_2$(μ-C_6F_4)] (30.5 mg, 0.017 mmol) was dissolved in C_6D_5Br (0.5 mL) and ^{i}PrNCN^{i}Pr (5.26 μL, 0.034 mmol). The solution was transferred to an NMR tube and the NMR spectra recorded after 5 mins. ^{1}H NMR (C_6D_5Br, 499.9 MHz, 298 K) 7.45-7.25 (5H, m, NC(N^{i}Pr$_2$)Ph), 3.72-3.50 (4H, br, N(CHMe$_2$)$_2$), 2.17 (3H, s, MeC(N^{i}Pr)$_2$), 2.01 (15H, s, C_5Me_5), 1.34 (6H, br, BMe), 1.30 (6H, br, NCHMe$_2$), 1.09 (6H, br, NCHMe$_2$), 0.98 (6H, br, NCHMe$_2$), 0.71 (6H, br, NCHMe$_2$) ppm. ^{19}F NMR (C_6D_5Br, 470.4 MHz, 298 K) -130.8 (m, *o*-C_6F_5), -137.5 (s, *o*-C_6F_4), -165.0 (m, *p*-C_6F_5), -167.0 (m, *m*-C_6F_5) ppm. ^{11}B NMR (C_6D_5Br, 160.4 MHz, 298 K) -14.51 ppm.

{(C_6F_5)$_2$B(THF)}$_2$(μ-C_6F_4) (42)

THF (10 mL) was charged into a vessel containing {(C_6F_5)$_2$B(THF)}$_2$(μ-C_6F_4) (0.1 g, 0.12 mmol) and left to stir for 20 mins at room temperature. The volatiles were

subsequently removed *in vacuo* and washed with pentane (3 x 10 mL) and dried to give *in vacuo* to yield the desired compound as a white solid. Yield = 0.1 g (85%). ^{1}H NMR (C_6D_5Br, 499.9 MHz, 298 K): 4.00 (8H, br, $CH_2C\underline{H}_2O$), 1.65 (8H, br, $C\underline{H}_2CH_2O$) ppm. ^{19}F NMR (C_6D_5Br, 470.4 MHz, 298 K) -132.07 (*o*-C_6F_5), -133.00 (-*o*-C_6F_4), -154.50 (*p*-C_6F_5), -161.82 (*m*-C_6F_5) ppm. ^{11}B NMR (C_6D_5Br, 160.4 MHz, 298 K) 4.86 ppm. A satisfactory ^{13}C NMR spectrum could not be obtained for this compound due to the insoluble nature of the material in common organic solvents. IR (NaCl plates, Nujol mull, cm^{-1}): 1646 (w), 1517 (m), 1293 (w), 679 (m). EI-MS: *m/z* = 837 (100 %, [M - 2THF]$^+$). Anal. found (calcd. for $C_{36}H_{16}B_2F_{24}O_2$): C, 46.54 (46.47); H, 1.55 (1.64); N, 0 (0) %.

[1,4-C_6H_4{NCN^{i}Pr$_2$}$_2${Cp*TiMe(THF)}$_2$][{(C_6F_5)$_2$BMe}$_2$(μ-C_6F_4)] (43)

To a stirred THF (10 mL) suspension of 1,4-C_6H_4{NCN^{i}Pr$_2$}$_2$[Cp*TiMe$_2$]$_2$ (0.08 g, 0.11 mmol) was added a THF (5 mL) solution of {(C_6F_5)$_2$B(THF)}$_2$(μ-C_6F_4) (0.07 g, 0.11 mmol). After 10 mins all the solid had gone in solution and pentane (20 mL) was added resulting in the formation of a red oil. The pentane/THF was decanted away and the oil washed further with pentane (10 mL). The remaining solvent was removed *in vacuo* to yield the desired compound as a red solid. Yield = 0.13 g (68%). ^{1}H NMR (THF-d_8, 499.9 MHz, 298 K): 7.42 (4H, s, Ar), 4.30 (2H, br, N($C\underline{H}Me_2$)$_2$), 3.63 (2H, br, N($C\underline{H}Me_2$)$_2$), 1.78 (30H, s, $C_5\underline{Me}_5$), 1.41 (12H, br, N($CH\underline{Me}_2$)$_2$), 1.04 (12H, br, N($CH\underline{Me}_2$)$_2$), 0.60 (6H, s, Ti$\underline{Me}$) 0.40 (6H, br, B$\underline{Me}$) ppm. ^{13}C{^{1}H} NMR (THF-d_8, 125.8 MHz, 298 K): 167.5 ($\underline{C}$N(N^{i}Pr$_2$)), 149.6 (br d, ^{1}J = 236.4 Hz, *o*-$\underline{C}_6F_5$), 149.3 (br d, ^{1}J = 236.0 Hz, *o*-$\underline{C}_6F_4$), 139.7 (Ar CH$\underline{C}$(C(NMe$_2$)N)), 138.1 (br d, ^{1}J = 242.4 Hz, *p*-$\underline{C}_6F_5$), 137.0 (br d, ^{1}J = 244.7 Hz, *m*-$\underline{C}_6F_5$), 132.5 (br, *i*-$\underline{C}_6F_4$), 128.3 (br, *i*-$\underline{C}_6F_5$), 126.4 ($\underline{C}_5Me_5$), 123.9 (Ar $\underline{C}$HC(C(NMe$_2$)N)), 58.2 (Ti$\underline{Me}$), 50.20 (N($\underline{C}HMe_2$)$_2$), 21.9 (N($CH\underline{Me}_2$)$_2$), 20.4 (N($CH\underline{Me}_2$)$_2$), 12.1 (B$\underline{Me}$), 12.0 (C5$\underline{Me}_5$) ppm. The resonances for the bound THF could not be observed. ^{19}F NMR (THF-d_8, 470.4 MHz, 298 K): -131.2 (m, *o*-$C_6\underline{F}_5$), -137.5 (s, *o*-$C_6\underline{F}_4$), -167.8 (m, *p*-$C_6\underline{F}_5$), -169.4 (m, *m*-$C_6\underline{F}_5$) ppm. ^{11}B NMR (THF-d_8, 160.4 MHz, 298 K): -14.99 ppm. IR (NaCl plates, Nujol mull^{-1}) 1508 (s, C=N), 1211 (m), 958 (w), 831 (m). EI-MS: *m/z* = 135 (40 %, [Cp*]$^+$). Anal. found (calcd. for $C_{82}H_{90}B_2F_{24}N_4O_2Ti_2$): C, 56.51 (56.70); H, 4.95 (5.22); N, 3.14 (3.23) %.

NMR tube scale synthesis of [1,4-C_6H_4{NCN^iPr_2}$_2${Cp^*Ti{$MeC(N^iPr)_2$}$_2$}$_2$] [{$(C_6F_5)_2BMe$}$_2$(μ-C_6F_4)] (44)

[1,4-C_6H_4{NCN^iPr_2}$_2${$Cp^*TiMe(THF)$}$_2$][{$(C_6F_5)_2BMe$}$_2$(μ-C_6F_4)] (5.6 mg, 3.2 μmol) was dissolved in THF-d_8 (0.5 mL) and ^{i}PrNCN^{i}Pr (1 μL, 6.4 μmol) was added. The solution was transferred to an NMR tube and The NMR spectra recorded after 5 mins. ^{1}H NMR (THF-d_8, 400.1 MHz, 298 K): 7.56(4H, s, Ar), 3.85 (4H, br, κ^1 -NC<u>H</u>Me_2), 3.62 (4H, m, κ^2 -NC<u>H</u>Me_2), 2.35 (6H, s, <u>Me</u>C(N^iPr)$_2$), 2.13 (30H, s, C_5<u>Me</u>$_5$), 1.46 (12H, br, NCH<u>Me</u>$_2$), 1.15 (12H, br, NCH<u>Me</u>$_2$), 0.87 (12H, br, NCH<u>Me</u>$_2$), 0.57(6H, s, B<u>Me</u>) ppm. ^{19}F NMR (THF-d_8, 376.4 MHz, 298 K): -131.7 (m, *o*-C_6<u>F</u>$_5$), -137.5 (s, *o*-C_6<u>F</u>$_4$), -168.0 (m, *p*-C_6<u>F</u>$_5$), -169.5 (m, *m*-C_6<u>F</u>$_5$) ppm. ^{11}B NMR (THF-d_8, 128.4 MHz, 298 K): -15.12 ppm.

NMR tube scale synthesis of [Cp^*Ti{$NC(Ar^{Fc})$}{$MeC(N^iPr)_2$}$]_2$[[{$MeB(C_6F_5)_3$}$_2$(μ-C_6F_4)] (45)

To a solution of Cp^*Ti{$NC(Ar^{Fc})N^iPr_2$}Me_2 (10 mg, 16.6 μmol) and ^{i}PrNCN^{i}Pr (2.6 μL, 16.6 μmol) in C_6D_5Br (0.5 mL) was added [{$B(C_6F_5)_3$}$_2$(μ-C_6F_4)][Ph_3C]$_2$ (13.8 mg, 8.3 μmol) resulting in the formation of a dark red solution. The solution was transferred to an NMR tube and the NMR spectra recorded after 5 mins. ^{1}H NMR (C_6D_5Br, 499.9 MHz, 298 K): 7.64 (2H, d, C_6<u>H</u>$_4$, ^{3}J = 7.6 Hz), 7.20 (2H, br, C_6<u>H</u>$_4$, ^{3}J = 7.5 Hz), 4.80 (2H, br, CpFeC_5<u>H</u>$_4$(C_6H_4)), 4.48 (2H, br, CpFeC_5<u>H</u>$_4$(C_6H_4)), 4.17 (5H, br, C_5<u>H</u>$_5$FeCp(C_6H_4)), 3.69 (4H, m, NC<u>H</u>Me_2), 2.22 (3H, s, <u>Me</u>C(N^iPr)$_2$), 2.04 (15H, s, C_5<u>Me</u>$_5$), 1.37 (6H, br, NCH<u>Me</u>$_2$), 1.14 (6H, d, NCH<u>Me</u>$_2$, ^{3}J = 6.2 Hz), 1.05 (6H, br, NCH<u>Me</u>$_2$) 0.87 (6H, br, NCH<u>Me</u>$_2$) ppm. ^{19}F NMR (C_6D_5Br, 470.4 MHz, 298 K): -129.2 - -131.4 (m, *o*-C_6<u>F</u>$_5$), -136.1 (s, *o*-C_6<u>F</u>$_4$), -163.4 - -163.6 (m, *p*-C_6<u>F</u>$_5$), -166.3 - -166.8 (m, *m*-C_6<u>F</u>$_5$) ppm. ^{11}B NMR (C_6D_5Br, 160.4 MHz, 298 K): -15.7 ppm.

NMR tube scale synthesis of [Cp^*Ti{$NC(Ar^{Fc})$}{$MeC(N^iPr)_2$}][BF_{20}] (46)

To a solution of Cp^*Ti{$NC(Ar^{Fc})N^iPr_2$}Me_2 (8 mg, 13.3 μmol) and ^{i}PrNCN^{i}Pr (2 μL, 13.3 μmol) in C_6D_5Br (0.5 mL) was added TBF_{20} (12.3 mg, 13.3 μmol) resulting in the formation of a dark red solution. The solution was transferred to an NMR tube and the NMR spectra recorded after 5 mins. ^{1}H NMR (C_6D_5Br, 499.9 MHz, 298 K): 7.62 (2H, d, C_6<u>H</u>$_4$, ^{3}J = 7.6 Hz), 7.16 (2H, br, C_6<u>H</u>$_4$, ^{3}J = 7.5 Hz), 4.80 (2H, br, CpFeC_5<u>H</u>$_4$(C_6H_4)), 4.49 (2H, br, CpFeC_5<u>H</u>$_4$(C_6H_4)), 4.17 (5H, br, C_5<u>H</u>$_5$FeCp(C_6H_4)),

3.60 (4H, m, NC<u>H</u>Me$_2$), 2.12 (3H, s, <u>Me</u>C(N^{i}Pr)$_2$), 2.03 (15H, s, C$_5$<u>Me</u>$_5$), 1.32 (6H, br, NCH<u>Me</u>$_2$), 1.09 (6H, d, NCH<u>Me</u>$_2$, ^{3}J = 6.1 Hz), 1.01 (6H, br, NCH<u>Me</u>$_2$) 0.83 (6H, br, NCH<u>Me</u>$_2$) ppm. ^{19}F NMR (C$_6$D$_5$Br, 470.4 MHz, 298 K): -131.37 (br, *o*-C$_6$<u>F</u>$_5$), -161.88 (br, *p*-C$_6$<u>F</u>$_5$), -165.67 (br, *m*-C$_6$<u>F</u>$_5$) ppm. ^{11}B NMR (C$_6$D$_5$Br, 160.4 MHz, 298 K): -15.9 ppm.

Alternative synthesis of BCl(C$_6$F$_5$)$_2$

To a stirring heptane (50 mL) solution of Me$_2$Sn(C$_6$F$_5$)$_2$ (12.49 g, 25.9 mmol) in a thick walled ampoule was added BCl$_3$ (25.86 mL, 1.0 M in heptane, 25.9 mmol). The vessel was sealed, stirred at room temperature form 30 mins and then at 100 °C for 48 h. The solution was subsequently allowed to slowly cool to room temperature, which formed crystals of Me$_2$SnCl$_2$, and filtered. The filtrate was stored at -80 °C for 24 h to generate a white solid, which was isolated and dried *in vacuo* at 0 °C. If any Me$_2$SnCl$_2$ was observed it was removed by sublimation under an atmosphere of argon at 35 °C. Yield = 7.8 g (79 %). The NMR data was in good agreement with the literature.[9]

6.9 Experimental details and characterising data for Chapter Five

1,4-C$_6$H$_4${NCN^{i}Pr$_2$}$_2${CpZrBn$_2$}$_2$ (47)

To a stirring toluene (15 mL) solution of Cp*ZrBn$_3$ (0.32 g, 0.64 mmol) was added a toluene (10 mL) solution of 1,4-C$_6$H$_4${C(NH)N^{i}Pr$_2$}$_2$ (0.1 g, 0.3 mmol). The yellow solution was stirred at room temperature for 4 h. The volatiles were removed *in vacuo* to afford a yellow solid which was washed with hexane (3 x 15 mL) and dried *in vacuo.* Yield = 150 mg (43%). Diffraction quality crystals were grown from a toluene solution at -30 °C. ^{1}H NMR (Tol-*d*$_8$, 499.9 MHz, 223 K): 7.24 (8H, m, *o*-C$_6$H$_5$ of CH$_2$Ph), 7.12 (8H, m, *m*-C$_6$H$_5$ of CH$_2$Ph), 6.95 (4H, m, *p*-C$_6$H$_5$ of CH$_2$Ph), 6.74 (4H, s, C$_6$<u>H</u>$_4$), 3.47 (2H, br, N(C<u>H</u>Me$_2$)$_2$), 2.85 (2H, br, N(C<u>H</u>Me$_2$)$_2$), 1.97 (8H, br, C<u>H</u>$_2$Ph), 1.70 (30H, s, C$_5$<u>Me</u>$_5$), 1.53 (12H, br, N(CH<u>Me</u>$_2$)$_2$), 0.72 (12H, br, N(CH<u>Me</u>$_2$)$_2$) ppm. ^{13}C{^{1}H} NMR (Tol-*d*$_8$, 125.7 MHz, 223 K): 162.0 (<u>C</u>N(N^{i}Pr$_2$), 149.5 (*i*-C$_6$H$_5$ of CH$_2$Ph), 141.8 (Ar CH<u>C</u>(C(NMe$_2$)N)), 128.9 (*o*-C$_6$H$_5$ of CH$_2$Ph), 127.3(*m*-C$_6$H$_5$ of CH$_2$Ph), 126.0 (Ar <u>C</u>HC(C(NMe$_2$)N)), 121.4 (*p*-C$_6$H$_5$ of CH$_2$Ph), 118.0 (<u>C</u>$_5$Me$_5$), 63.7 (<u>C</u>H$_2$Ph), 52.1 (N(<u>C</u>HMe$_2$)$_2$), 45.2 (N(<u>C</u>HMe$_2$)$_2$), 21.3(N(CH<u>Me</u>$_2$)$_2$), 20.4(N(CH<u>Me</u>$_2$)$_2$), 11.5 (C$_5$<u>Me</u>$_5$) ppm. IR (NaCl, Nujol mull, cm^{-1}): 1541 (s, C=N), 1322 (s), 1208 (m), 886 (m), 744 (s). EI-MS: *m/z* = 91.05 (100 %, [CH$_2$Ph]$^+$), 1051.5

(50 %, $[M\text{-}CH_2Ph]^+$). Anal. found (calcd. for $C_{68}H_{90}N_4Zr_2$): C, 71.26 (71.27); H, 7.71 (7.92); N, 4.72 (4.89) %.

1,3-C_6H_4{$C(NH)N^iPr_2$}$_2(AlMe_3)_2$ (48)

To a stirring toluene (40 mL) solution of 1,3-C_6H_4{$C(NH)N^iPr_2$}$_2$ (0.4 g, 1.2 mmol) was added dropwise $AlMe_3$ (1.21 ml, 2M in hexane, 2.4 mmol) at -78 °C. The solution was stirred for 1 h at -78 °C before being allowed to warm to room temperature and stirred for a further 1 h. Concentration to *ca.* 20 mL and storage at -30 °C for 24 h resulted in crystallisation of the desired compound which was subsequently isolated and dried *in vacuo*. Yield = 0.49 g (85%). ^{1}H NMR (C_6D_6, 400.1 MHZ, 298 K): 7.55 (1H, br, C<u>H</u>CHC), 7.04 (3H, overlapping br, C<u>H</u>(C(C(N^iPr_2)N))$_2$ and CHC<u>H</u>C(C(N^iPr_2)N), 6.01 (2H, br, N<u>H</u>), 3.91 (2H, sept, ^3J = 6.6 Hz, N(C<u>H</u>Me_2)$_2$), 3.10 (2H, sept, ^3J = 7.2 Hz, N(C<u>H</u>Me_2)$_2$), 1.15 (6H, d, , ^3J = 7.2 Hz, N(CH<u>Me</u>$_2$)$_2$), 1.07 (6H, d, ^3J = 7.2 Hz, N(CH<u>Me</u>$_2$)$_2$), 0.93 (6H, d, , ^3J = 6.6 Hz, N(CH<u>Me</u>$_2$)$_2$), 0.70 (6H, d, ^3J = 6.6 Hz, N(CH<u>Me</u>$_2$)$_2$), 0.48 (18H, s, Al<u>Me</u>$_3$) ppm. ^{13}C{^{1}H} NMR (C_6D_6, 100.6 MHz, 298 K): 166.3 (<u>C</u>N(N^iPr_2)), 135.5 (<u>C</u>(C(N^iPr_2)N)), 129.2 (CH<u>C</u>HC(C(N^iPr_2)N)), 129.0 (<u>C</u>H(C(C(N^iPr_2)N))$_2$), 127.7 (<u>C</u>HCHC(C(N^iPr_2)N)), 53.3 (N(<u>C</u>HMe_2)$_2$), 45.2 (N(<u>C</u>HMe_2)$_2$), 20.8 (N(CH<u>Me</u>$_2$)$_2$), 20.3 (N(CH<u>Me</u>$_2$)$_2$), 20.0 (N(CH<u>Me</u>$_2$)$_2$), 19.3 (N(CH<u>Me</u>$_2$)$_2$), -6.6 (Al<u>Me</u>$_3$) ppm. IR (NaCl plates, Nujol mull, cm^{-1}): 3382 (m, N-H), 1575 (s, C=N), 1499 (m), 1182 (m), 688 (m). EI-MS: *m/z* = 473 (50%, $[M - H]^+$), 459 (100 %, $[M - Me]^+$). Anal. found (calcd. for $C_{26}H_{52}N_4Al_2$): C, 65.58 (65.79); H, 10.85 (11.04); N, 11.61 (11.80) %.

6.10 References

1. A. B. Pangborn, M. A. Giardello, R. H. Grubbs, R. K. Rosen and F. J. Timmers, *Organometallics*, 1996, **15**, 1518-1520.
2. M. Mena, P. Royo, R. Serrano, M. A. Pellinghelli and A. Tiripicchio, *Organometallics*, 1989, **8**, 476-482.
3. J. Doiron, A. H. Soultan, R. Richard, M. M. Touré, N. Picot, R. Richard, M. Čuperlović-Culf, G. A. Robichaud and M. Touaibia, *Eur. J. Med. Chem.*, 2011, **46**, 4010-4024.
4. B. J. Coe, C. J. Jones, J. A. McCleverty, D. Bloor and G. Cross, *J. Organomet. Chem.*, 1994, **464**, 225-232.
5. L.-G. Xie and Z.-X. Wang, *Angew. Chem. Int. Ed.*, 2011, **50**, 4901-4904.

6. K. Y. Tsang, H. Diaz, N. Graciani and J. W. Kelly, *J. Am. Chem. Soc.*, 1994, **116**, 3988-4005.
7. K. McWilliams and J. W. Kelly, *J. Org. Chem.*, 1996, **61**, 7408-7414.
8. R. Knapp and M. Rehahn, *J. Organomet. Chem.*, 1993, **452**, 235-240.
9. H. Li, L. Li, D. J. Schwartz, M. V. Metz, T. J. Marks, L. Liable-Sands and A. L. Rheingold, *J. Am. Chem. Soc.*, 2005, **127**, 14756-14768.
10. L. Li, M. V. Metz, H. Li, M.-C. Chen, T. J. Marks, L. Liable-Sands and A. L. Rheingold, *J. Am. Chem. Soc.*, 2002, **124**, 12725-12741.
11. P. T. Wolczanski and J. E. Bercaw, *Organometallics*, 1982, **1**, 793-799.
12. R. Scott, DPhil Thesis, University of Oxford, 2013.
13. Z. Otwinowski and W. Minor, Processing of X-ray Diffraction Data Collected in Oscillation Mode, Academic Press, New York, 1997.
14. A. Altomare, G. Cascarano, C. Giacovazzo and A. Guagliardi, *J. Appl. Crystallogr.*, 1994, **27**, 1045-1050.
15. L. Palatinus and G. Chapuis, *J. Appl. Crystallogr.*, 2007, **40**, 786-790.
16. P. W. Betteridge, J. R. Carruthers, R. I. Cooper, K. Prout and D. J. Watkin, *J. Appl. Crystallogr.*, 2003, **36**, 1487.
17. D. Chong, J. Slote and W. E. Geiger, *J. Electroanal. Chem.*, 2009, **630**, 28-34.